UNIVERSITÀ
POLITECNICA
DELLE MARCHE

Università Politecnica delle Marche

DIPARTIMENTO DI INGEGNERIA INDUSTRIALE E SCIENZE MATEMATICHE
Corso di Dottorato di Ricerca in Ingegneria Industriale – Curriculum Ingegneria Energetica

Ph.D. Thesis

Thermophysical properties of environmentally friendly refrigerants and their blends: a theoretical and experimental study

Advisor:
Prof. Giovanni Di Nicola

Ph.D. Dissertation of:
Sebastiano Tomassetti

Curriculum Supervisor:
Prof. Giovanni Di Nicola

XVIII Edition – New Series

To Marta

Contents

List of Figures

List of Tables

Abstract

In the last years, the interest in low global warming potential refrigerants as replacements of conventional refrigerants has been increasing to reduce their environmental impact. In this context, the thermophysical properties of these alternative refrigerants and their blends are needed to accurately evaluate their potential performance in HVAC&R applications. Thus, the focus of this study is a theoretical and experimental analysis of some of main thermophysical properties of these alternative working fluids.

For the theoretical part, some of the most well-known models to estimate different thermodynamic and transport properties have been investigated. In particular, the vapor pressure of 9 alternative refrigerants and the vapor-liquid equilibrium of 25 binary systems containing these refrigerants were calculated using different cubic equations of state. After an in-depth comparison between the experimental and calculated data, it was found that a cubic equation proposed by Stryjek provided slightly better results.

The experimental surface tension data for 14 halogenated alkene refrigerants and 5 binary systems were analyzed with some of the most reliable semi-empirical correlation models designed for pure refrigerants and blends. The experimental data were collected from the literature and databases. Moreover, a scaled correlation based on the corresponding states principle developed for the surface tension of other kinds of fluids was re-fitted and tested for the studied fluids. The deviations of the new re-fitted equation for the studied pure refrigerants are in agreement with the values of the correlations existing in the literature. Instead, the proposed equation for the binary systems gave a considerable improvement respect to available models.

An empirically modified Kardos equation specifically oriented to both liquid and vapor thermal conductivity of refrigerants was developed. The modified scaled correlation is much simpler than its original form. The final equations provided very accurate results for the liquid and vapor thermal conductivity of the studied refrigerants.

As concern the experimental work, the Pressure - Specific Volume - Temperature - Composition ($PvTz$) properties for different compositions of three binary systems containing different hydrofluoroolefins and a traditional refrigerant (i.e. R32 + R1234yf, R32 + R1234ze(E), and R32 + R1234ze(Z)) were measured both in the two-phase and superheated vapor regions with an isochoric apparatus. Moreover, the vapor-phase $PvTz$ measurements for R1234yf + R600a, R1234ze(E) + R600a, R600a + R1233zd(E), R600a + R1234ze(Z), R1225ye(Z) + R600a, R1243zf + R600a binary systems were performed with the same setup. From the measurements in the two-phase region, an accurate vapor-liquid equilibrium behavior of the measured binary systems was derived by applying the flash method with different equations of state. The vapor-phase data were correlated through different equations of state.

Moreover, the solid-liquid equilibrium of the R32 + R1234ze(E) binary pair was measured with an experimental setup in the temperature range from 168.2 K to 132.0 K. The studied binary pair showed an eutectic point that was estimated at the

temperature of 132.00 K. In order to test the validity of the experimental setup, the triple point temperatures of the components of the binary system and four well-described refrigerants (R125, R152a, R143a, and R41) were measured. The experimental results for the pure refrigerants agreed with reliable values available in the literature.

Sommario

Negli ultimi anni è aumentato l'interesse verso i refrigeranti a basso potenziale di riscaldamento globale come sostituti dei refrigeranti convenzionali in modo da ridurre il loro impatto ambientale. In questo contesto, le proprietà termofisiche dei refrigeranti alternativi e delle loro miscele sono necessarie per valutare le loro prestazioni nelle applicazioni HVAC&R. Di conseguenza, lo scopo del presente lavoro di tesi è l'analisi teorica e sperimentale di alcune delle principali proprietà termofisiche di questi fluidi alternativi.

Riguardo la parte teorica, sono stati testati alcuni dei più conosciuti modelli per determinare differenti proprietà termodinamiche e di trasposto. Nello specifico, la pressione di vapore di 9 refrigeranti alternativi e l'equilibrio liquido-vapore di 25 sistemi binari contenenti questi refrigeranti sono state calcolati mediante diverse equazioni di stato cubiche. Dopo un approfondito confronto tra i dati calcolati e sperimentali è stato trovato che un'equazione di stato cubica proposta da Stryjek ha dato i migliori risultati.

I dati di tensione superficiale di 14 refrigeranti alogenati alcheni e 5 sistemi binari sono stati analizzati con alcune correlazioni semi-empiriche specifiche per refrigeranti e miscele. I dati sperimentali sono stati raccolti dalla letteratura e da database. Inoltre, una correlazione scalata basata sul principio degli stati corrispondenti sviluppata per la tensione superficiale di altri fluidi è stata testata per i fluidi studiati. Le deviazioni tra i dati sperimentali e quelli calcolati con l'equazione proposta per i refrigeranti puri sono in accordo con i valori dati delle correlazioni esistenti. Invece, l'equazione proposta per i sistemi binari contenenti refrigeranti alternativi ha dato un notevole miglioramento rispetto ai modelli esistenti.

È stata sviluppata una versione modificata dell'equazione di Kardos specifica per la conducibilità termica di refrigeranti allo stato liquido e allo stato vapore. La versione modificata è più semplice della forma originale e ha dato risultati accurati per la conducibilità termica dei refrigeranti studiati.

Riguardo la parte sperimentale, le proprietà pressione – volume specifico – temperatura – composizione ($PvTz$) di diverse composizioni di tre sistemi binari contenenti differenti idrofluoroolefine e un refrigerante tradizionale (R32 + R1234yf, R32 + R1234ze(E), and R32 + R1234ze(Z)) sono state misurate sia nella regione liquido-vapore che in quella di vapore surriscaldato mediante un apparato isocorico. Inoltre, le misurazioni delle proprietà $PvTz$ per i sistemi binari R1234yf + R600a, R1234ze(E) + R600a, R600a + R1233zd(E), R600a + R1234ze(Z), R1225ye(Z) + R600a, R1243zf + R600a sono state realizzate nella zona del vapore surriscaldato con lo stesso apparato. Dalle misure realizzate nella regione liquido-vapore, è stata derivata una rappresen-

tazione accurata dell'equilibrio liquido-vapore dei sistemi binari studiati per mezzo del flash method e diverse equazioni di stato. I dati misurati nella regione del vapore surriscaldato sono stati elaborati mediante diverse equazioni di stato.

L'equilibrio solido-liquido del sistema R32 + R1234ze(E) è stato misurato con un apparato sperimentale nel range di temperature da 168.2 K fino a 132.0 K. Questo sistema binario ha mostrato il punto eutettico, che è stato stimato alla temperatura di 132.0 K. Per testare la validità dell'apparato sperimentale, sono state misurate le temperature dei punti tripli dei componenti della miscela studiata e di altri quattro noti refrigeranti (R125, R152a, R143a, e R41). I dati misurati per i refrigeranti puri sono in accordo con i valori disponibili in letteratura.

Acknowledgments

Firstly, I would like to thank Prof. Giovanni Di Nicola for believing in me and for his support during my doctoral studies. I would like to express my gratitude to Prof. Claudio Zilio and Prof. Antonio Rosato for the time and efforts dedicated in the revision of my thesis. My thanks also go to my colleagues Dr. Gianluca Coccia and Dr. Mariano Pierantozzi for their precious suggestions and their time dedicated to me.

I am grateful to Dr. Giulio Santori and Prof. Chieko Kondou for having allowed me to live two significant life experiences in their universities.

Besides, my thanks go to Ms. Ivana Cooke for helping me to improve my English language skills.

I am extremely thankful to Marta for her support and patience during my doctoral studies, especially during difficult times. I am where I am because of you.

And last but not least, I am grateful to my parents and my brother Matteo for their continuous support and assistance, despite our many vicissitudes.

Ancona, Novemeber 2019 S. T.

Introduction

Recently, the Heating, Ventilation, Air Conditioning, and Refrigeration (HVAC&R) industry is seeking suitable low Global Warming Potential (GWP) refrigerants as alternatives to conventional working fluids to reduce their contribution to climate change. The research of these environmentally friendly refrigerants is mainly driven by the environmental regulations and legislation which impose reductions on the emissions of fluorinated greenhouse gasses, such as several conventional refrigerants, in the coming years. However, at present, only a limited number of low GWP fluids were found to possess the combination of environmental, thermodynamic, and safety properties needed for different HVAC&R applications. Different potential alternative working fluids result flammable or toxic or they do not have suitable thermodynamic properties. To balance the drawbacks of these potential alternatives and the environmental problems of traditional refrigerants, the interest in blends of the former and the latter refrigerants is increasing.

The thermophysical properties of low GWP potential refrigerants and their blends, both experimentally-determined and/or estimated from reliable models, are necessary to accurately evaluate their potential performance in HVAC&R applications. However, only a limited number of studies present their properties. Further investigations of their thermophysical properties are needed to find suitable alternatives.

For this reason, this thesis is focused on the thermodynamic and transport properties of different potential low GWP refrigerants and their blends. In particular, the experimental Pressure - Specific Volume - Temperature - Composition ($PvTz$) data of nine binary systems containing low GWP refrigerants (R1234yf + R600a, R1234ze(E) + R600a, R600a + R1233zd(E), R600a + R1234ze(Z), R1225ye(Z) + R600a, R1243zf + R600a, R32 + R1234yf, R32 + R1234ze(E), and R32 + R1234ze(Z)) are reported in this thesis. Moreover, the Solid-Liquid Equilibrium (SLE) measurements of R32 + R1234ze(E) binary pair are presented. As shown in List of publications, most of these experimental data were already reported in papers published in international journals. The proposed measurements can also be used for developing accurate models (e.g., Equations of State (EoSs)) for the thermodynamic description of the binary systems. In addition, the prediction capability of several models was investigated to estimate different thermophysical properties of alternative working fluids.

The manuscript is divided into five chapters. Chapter 1 presents an overview of the progression of refrigerants during the years. As explained, this progression was mainly driven by different regulations and international agreements proposed to reduce the environmental problems of refrigerants. The recent developments in the research of low GWP working fluids are discussed. Finally, details about the importance of experimentally-determined thermophysical properties of the refrigerants and the models proposed for their estimation are given.

In Chapter 2, models available in the literature for the estimation of different

thermodynamic properties of refrigerants and their blends are presented and tested to describe the properties of low GWP working fluids. Firstly, different EoSs mainly used to describe the PvT properties of refrigerants are described. Moreover, mixing rules for extending these EoSs to estimate the $PvTz$ behaviors of refrigerant blends are reported. Some of these EoSs, called Cubic Equations of State (CESs), are used to estimate the vapor pressure and the Vapor-Liquid Equilibrium (VLE) of low GWP refrigerants and their binary systems, respectively. A method based on EoSs to estimate the VLE of binary systems of refrigerants from their isochoric $PvTz$ measurements, called flash method, is described. Then, the Schröder equation is introduced. This equation often provides a sufficient accurate description of the Solid-Liquid Equilibrium (SLE) of refrigerant binary systems.

In Chapter 3, different models to estimate the surface tension and the thermal conductivity of refrigerants and their blends are studied. The results obtained by comparing the experimental surface tension data of low GWP refrigerants and their binary systems collected from the literature and the values calculated from literature correlations to estimate this property of refrigerants are reported. Moreover, a recent scaled correlation based on the corresponding states principle and developed for other kinds of fluids was re-fitted and tested for the selected fluids. The estimated surface tension values provided by these equations are compared with the selected experimental data. Then, an empirically modified version of the Kardos equation for thermal conductivity specifically oriented to refrigerants is presented. The values provided by this equation are compared with the thermal conductivity data of different refrigerant collected from literature and the values estimated from existing correlations for this property.

Chapter 4 presents experimental $PvTz$ properties of the aforementioned binary systems containing six different low GWP refrigerants (R1234yf, R1234ze(E), R1233zd(E), R1234ze(Z), R1225ye(Z), and R1243zf) measured both in the two-phase and superheated vapor regions through an isochoric apparatus. In particular, the VLE behavior for R32 + R1234yf, R32 + R1234ze(E), and R32 + R1234ze(Z) binary pairs derived by their two-phase measurements using the flash method are presented. Instead, the vapor-phase $PvTz$ of R1234yf + R600a, R1234ze(E) + R600a, R600a + R1233zd(E), R600a + R1234ze(Z), R1225ye(Z) + R600a, R1243zf + R600a, R32 + R1234yf, R32 + R1234ze(E), R32 + R1234ze(Z) are correlated with different EoSs and the results are presented. The triple point temperature of R1234ze(E) and the Solid-Liquid Equilibrium (SLE) of R32 + R1234ze(E) binary pair, measured with an experimental apparatus specifically built for this purpose, are reported. The triple point measurement of the pure fluid is compared with the values available in the literature. The measured SLE data are compared with the estimation provided by the Schröder equation.

Finally, some critical conclusions and future developments of the thesis work are presented in Chapter 5.

Appendix A reports the expressions for the fugacity coefficients estimated from the EoSs studied in this work. Instead, all the experimental $PvTz$ data of the studied binary systems measured with the isochoric apparatus are reported in Appendix B. Finally, the nomenclature used in this thesis is showed Appendix C.

Chapter 1

Overview on refrigerants and their thermophysical properties

An overview of the refrigerant progression is presented in this chapter. In particular, the environmental impact of the different refrigerants, the main regulations and international agreements that have driven their progression and the recent developments in the research of environmentally friendly refrigerants are discussed in detail. Finally, the importance of the thermophysical properties of the refrigerants is described, providing details about the experimental values of their properties available in the literature and the models proposed for their estimation.

1.1 Progression of refrigerants

A refrigerant is the working fluid of heat pump and refrigeration systems used to transfer heat from a region at relatively low temperature to a region at a higher temperature. In particular, the refrigerants are used in the vapor-compression refrigeration cycles where the heat transfer takes place through their reversible phase change from liquid to gas and back. Several refrigerants, both naturals and synthetics, and their blends have been studied and adopted throughout the years. The development and selection of these working fluids have been driven by different criteria, such as performance, safety, stability, durability, economic or environmental issues, giving origin to new researches and equipment improvements in terms of safety and efficiency. A standardized safety classification and designation system of the numerous refrigerants and their blends were proposed by the American Society of Heating, Refrigerating and Air-Conditioning Engineers (ASHRAE) [1].

The refrigerants can be classified in four generations [2]. Figure 1.1 shows the refrigerant progression in the four generations which are briefly described below:

- **First generation**. After the invention of the vapor-compression machine by Perkins [3] in the 1830s, the refrigerants used for the first hundred years were available solvents and other volatile fluids, such as ether, ammonia (denoted as R717 in ASHRAE designation [1]), carbon dioxide (R744), sulfur dioxide (R764), water (R718) and Hydrocarbons (HCs). However, most of these early refrigerants were flammable, toxic or also highly reactive; therefore, different accidents occurred in that period.

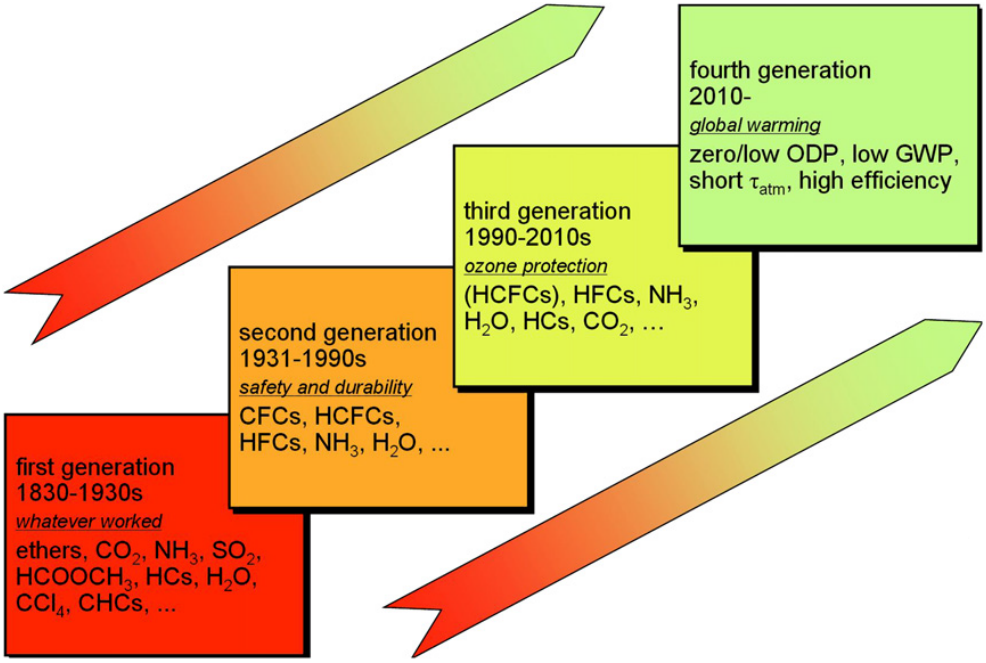

Figure 1.1: Refrigerant progression [2].

- **Second generation**. The second generation was dominated by synthetic Chlorofluorocarbon (CFC) refrigerants for high thermodynamic performance, safety and durability reasons. Their development was based on the research activities of Thomas Midgley and his associates that studied the properties of the elements of the periodic table to find stable, no toxic and no flammable chemicals with desirable boiling points. In particular, these researchers showed how the variation of the chlorination and fluorination of hydrocarbons influences the boiling point, flammability, and toxicity [4]. In the 1930s, the first two non-toxic and non-flammable CFCs, named trichlorofluoromethane (R11) and dichlorodifluoromethane (R12), were produced [5].

  Starting from the 1950s, Hydrochlorofluorocarbons (HCFCs) were also used as refrigerants in residential and small commercial air conditioners and heat pumps. Instead, ammonia was, as is still today, the most popular refrigerant in large industrial refrigeration systems. Although it is toxic, irritating, mildly flammable and presents materials compatibility issues, ammonia remains the main refrigerant used in industrial systems, especially food and beverage processing, because of its thermodynamic properties and performances [2].

- **Third generation**. The third generation of refrigerants was characterized by the need to find alternatives to CFCs which were discovered to cause the depletion of the stratospheric ozone layer. Since they contain halogen atoms, such as chlorine (Cl), these fluids have very high values of Ozone Depletion Potential (ODP). The Montreal Protocol to the Vienna Convention for the Protection of the Ozone Layer [6] and its successive amendments and adjustments forced the abandonment of Ozone-Depleting Substances (ODSs), among which CFCs. In particular, this international agreement, which entered into force in 1989 and

achieved universal ratification in 2009, scheduled the phase-out of CFC refrigerant use and production by 1996 in developed countries and by 2010 in developing countries that are parties of the international environmental agreement.

As alternative refrigerants, the HCFCs for transitional use and the Hydrofluorocarbons (HFCs) for the longer-term use were proposed and commercialized in the 1990s. Moreover, researchers and manufacturers showed renewed interest in natural refrigerants, such as R717, R744, and HCs. However, although their ODP values are low than that of CFCs, the HCFCs impact on stratospheric ozone depletion. Consequently, the Montreal Protocol limited the production and use of HCFCs. In particular, it was scheduled for the global HCFC consumption phase-out by 2040 at a meeting of the parties of the Montreal Protocol [7].

It is worthwhile pointing out that, even if refrigerants constituted only a limited fraction of ODS emission, different CFCs and HCFCs were also used in much more emissive applications, such as solvents, blowing agents, fire extinguishing agents and aerosol propellants [2].

- **Fourth generation**. The main feature of the fourth and current refrigerant generation is the need to to find economically and environmentally sustainable working fluids which do not impact on global warming. It was shown that the global surface temperature is increasing due to Greenhouse Gas (GHG) emissions generated by human activity. This global anthropogenic climate change can result in disastrous consequences, such as an increase in the number of extreme climate events.

  In particular, although they are not ODSs, almost all the HFCs, along with CFCs and HCFCs, are potent GHGs, having high values of Global Warming Potential (GWP). Even if their present contribution to climate change is still small, the consumption of HFCs is rapidly increasing in many applications and their emission will have severe implications on global climate [8]. Therefore, a phase-down of HFCs is underway and is regulated and promoted by international environmental agreements and different national regulations and laws. Some of the most important and recent of them are addressed below.

  In 1997, more than 160 countries negotiated the Kyoto Protocol [9] that, for the first time, imposed GHG (among which HFCs) emission reduction targets for industrialized countries. This protocol entered into force in 2005, after being ratified also by Russia. Moreover, this international agreement is linked to the 1992 United Nations Framework Convention on Climate Change (UNFCCC) which commits its Parties to reduce GHG emissions by setting internationally binding emission reduction targets. The Kyoto Protocol was adopted at the third session of the Conference of Parties to the UNFCCC (COP 3). The COP is the decision-making body responsible for monitoring and reviewing the implementation of the UNFCCC and it meets every year in different locations. All the COPs strengthened the agreement that the global surface temperature is increasing due to anthropogenic greenhouse gas emissions and that, to avoid serious consequences, it is mandatory to keep the rise in temperature below 2 $^{\circ}$C above pre-industrial levels. Among these COPs, the 21st Session of the COP (COP 21) held in Paris in 2015 [10] was one of the most important. The outcome of this conference was the first international climate agreement. This agreement established that the Parties to the Convention have to take action to decrease greenhouse gas emissions with an agreed-upon goal of staying below a global

Table 1.1: Placing on the market prohibitions by the EU Regulation No 517/2014 [14].

Products and equipment	GWP	Date
Domestic refrigerators and freezers	150	2015
Refrigerators and freezers for commercial use (hermetically sealed equipment)	2500	2020
Refrigerators and freezers for commercial use (hermetically sealed equipment)	150	2022
Stationary refrigeration equipment that contains, or whose functioning relies upon, HFCs (except equipment intended for application designed to cool products to temperatures below -50 ° C)	2500	2020
Multipack centralized refrigeration systems for commercial use with a rated capacity $>$ 40 kW that contain, or whose functioning relies upon, fluorinated greenhouse gases (except in the primary refrigerant circuit of cascade systems where fluorinated greenhouse gases with a GWP $<$ 1500 may be used)	150	2022
Movable room air conditioning equipment (hermetically sealed equipment which is movable between rooms by the end user)	150	2020
Single split air conditioning systems containing less than 3 kg of fluorinated greenhouse gases that contain, or whose functioning relies upon, fluorinated greenhouse gases	750	2025

average temperature increase of 2 °C above pre-industrial levels. In particular, the Nations responsible for more than 90 % of global emissions have to come up with their targets. The EU should cut its emissions by 40 %, compared with 1990 levels, by 2030. The US should cut its emissions by 26 % to 28 %, compared with 2005 levels, by 2025. China should agree that its emissions will peak by 2030.

In the European Union (EU), the first step to reduce the HFC use was placed with the Directive 2006/40/EC [11]. This directive banned the use of refrigerant with GWP greater than 150 in automobile air conditioners. This limit value is below the GWP of 1,1,1,2-tetrafluoroethane (R134a) (equal to 1430), which was the HFC refrigerant most commonly used in Europe in this application. Moreover, the Regulation (EC) No. 842/2006 [12] has been issued to stabilize the GHG concentrations in the atmosphere at a level that prevents dangerous anthropogenic interference with the climate system. Then, the EU Regulation No. 517/2014 [13] (F - gas Regulation) replaced the previous directive [11] and extended the GWP limit of 150 to the refrigerant used in most of the refrigeration and air conditioning systems. Moreover, this regulation aimed to decrease at least two-thirds of the 2010 emissions of fluorinated greenhouse gases by 2030 in the EU. The main limitations imposed by the F - gas Regulation are reported in Table 1.1.

Recently, the European Commission [15] adopted a proposal to ratify the Kigali amendment to the Montreal Protocol [16] that established a global phase-down of the HFC production and use. In particular, it was stated that a reduction of the consumption of HFCs would potentially help to maintain global temperature rise well below 2 °C by 2100.

Therefore, the replacement of HFCs with low GWP alternative refrigerants, both naturals, synthetics and, their blends, with suitable properties for different Heating, Ventilating, Air Conditioning & Refrigeration (HVAC&R) applications is the main aim of the last refrigerant generation to fight the global climate change. Besides, the HFC phase-down can also be considered an opportunity to

redesign the existing refrigerating and air conditioning equipment to improve their energy efficiency, similar to that achieved during CFC and HCFC phase-out [17].

1.1.1 Environmental impact of refrigerants

Different measures can be used to evaluate the environmental impact of refrigerants. In particular, the ones used to define their direct environmental impact are the Ozone Depletion Potential (ODP) and the Global Warming Potential (GWP). However, a refrigerant has also an indirect effect on the environment due to the equivalent amount of carbon dioxide (CO_2) produced from its manufacturing, transporting, recycling, etc. and from powering the refrigeration system. Measures that attempt to capture both their direct and indirect environmental impact are Total Equivalent Warming Impact (TEWI) and Life-Cycle Climate Performance (LCCP). The values of the measures of the direct environmental impact for the refrigerants studied in this thesis are reported in Table 2.1 of Chapter 2. A brief description of these measures is provided below:

- **Ozone Depletion Potential (ODP)**

  Since halogen atoms are known to react with ozone, altering the natural chain of reactions that occurs between oxygen and ozone in the stratosphere, the ODP was defined to evaluate the destructive effect of ODSs containing these atoms to the ozone layer. The ODP of a compound provides a relative measure of its overall impact on the stratospheric ozone destruction over long term. It is defined as the ratio of the global loss of stratospheric ozone (i.e. integrated over latitude, altitude and time) from the compound at steady-state per unit mass emitted relative to the loss of ozone due to emission of a unit mass of a reference compound, usually taken as R11 [18]. Since the time scale for contribution to ozone depletion is not the same for all the compounds, their ODPs can change with time [18]. Among the different models proposed to derive the ODPs, a reliable semi-empirical model was developed by Solomon et al. [19, 20] for the estimation of time-depending ODPs on both short and long time scales. The ODP of a compound X is calculated from the following equation:

$$\mathrm{ODP}(t) = \frac{F_{\mathrm{X}}}{F_{\mathrm{R11}}} \frac{M_{\mathrm{R11}}}{M_{\mathrm{X}}} \frac{n_{\mathrm{hal,X}}}{3} \alpha^{*} \frac{\int_{t_{\mathrm{s}}}^{t} e^{-(t-t_{\mathrm{s}})/\tau_{\mathrm{X}}}\, dt}{\int_{t_{\mathrm{s}}}^{t} e^{-(t-t_{\mathrm{s}})/\tau_{\mathrm{R11}}}\, dt} \tag{1.1}$$

  where the ratio $F_{\mathrm{X}}/F_{\mathrm{R11}}$ is the fraction of the compound X that has been dissociated in the stratosphere compared to that of R11, M is the molar mass of each compound, $n_{\mathrm{hal,X}}$ is the number of chlorine, bromine or iodine atoms of X (3 at denominator represents the three chlorine atoms in R11), α^{*} is an enhancement factor that reflects the relative efficiency of ozone destruction by bromine, t_{s} is the time for a molecule to be transported from the surface to the stratosphere region, t is the total time ($(t - t_{\mathrm{s}})$ represents the total time in the stratosphere available for conversion into active forms of chlorine) and τ is the total atmospheric lifetimes of each compound. τ is defined as the time required for a pulse emitted into the atmosphere to decay to $1/e$ of its initial value [18]. It is possible to calculate the global, steady-state ODPs from Eq. (1.1) at $t \to \infty$. However, a combination of the time-dependent and global ODPs can be used to evaluate the impact of refrigerants to stratospheric ozone depletion on both short and long time scales [18]. Another approach to determine the ODP values is the

use of programs that calculate impacts by employing three-dimensional models and are based on decomposing paths, rates, atmospheric conditions and the influence of additional ozone-depleting substances [21]. The ODPs of blends are estimated as the mass-weighted averages of the ODPs of their components [21]. Currently, the ODPs of the refrigerants and their blends as to be equal to zero or near-zero, as stated by Montreal Protocol [6] and its successive amendments and adjustments.

- **Global Warming Potential (GWP)**

  The GWP of a compound compares its global warming impact in relation to the impact due to the emission of similar amount of a reference compound, usually taken as CO_2 [22, 23]. This impact is estimated during a time horizon that is usually assumed equal to 100 years. In particular, the GWP results from the combination of the cumulative radiative forcing, both direct and indirect effects, and atmospheric lifetime of a compound (trace gas), together with the time horizon for evaluation [24]. The radiative forcing is the change in net irradiance at the tropopause due to the change in atmospheric concentration of a trace gas resulting from a pulse release of that gas. In particular, the The Intergovernmental Panel on Climate Change (IPCC) developed the following equation to calculate the GWP of a compound X [23, 25]:

$$\mathrm{GWP} = \frac{\int_0^{n^*} a_{\mathrm{X}}^* \, c_{\mathrm{X}}^* \, dt}{\int_0^{n^*} a_{\mathrm{CO_2}}^* \, c_{\mathrm{CO_2}}^* \, dt} \tag{1.2}$$

  where a_{X}^* and $a_{\mathrm{CO_2}}^*$ are the radiative forcing per unit mass increase in atmospheric abundance of the compound X and CO_2, respectively, c_{X}^* and $c_{\mathrm{CO_2}}^*$ are the concentration of the compound X and CO_2, respectively, remaining at time t after their release and n^* is the number of years over which the calculation is performed ($n^* = 100$). Although the concept of GWP has different weaknesses, such as that it neglects the effect of reaction products resulting from breakdown and the assumption of a global mean concentration [24], this index is an easy and most commonly used environmental metric. The GWPs of blends are estimated as the mass-weighted averages of components' GWPs [21]. The United Nations Environment Programme (UNEP) [26] proposed a classification scheme, distinguishing between very low (or ultra-low) ($<$ ~30), very low ($<$ ~100), low ($<$ ~300), moderate ($<$ ~1000), high ($<$ ~3000), very high ($<$ ~10000) and ultra-high ($>$ ~10000) GWP fluids. However, at present, a demarcation value for the acceptability of refrigerants and their blends for many refrigeration and air conditioning applications is GWP relative to CO_2 for 100-year integration equal to 150 or less, as stated by the European F-gas Regulation [13].

- **Total Equivalent Warming Impact (TEWI)**

  The TEWI accounts for both the direct global warming impact of a refrigerant due to its release during the lifetime of the equipment and the indirect impact of CO_2 emissions produced from powering the equipment throughout its lifetime. Therefore, this index is sensible to the energy performance of a system [22]. The TEWI can be calculated with the following equation proposed by Makhnatch & Khodabandeh [22]:

$$\mathrm{TEWI} = (\mathrm{GWP}\, L\, N^{**}) + (E^a\, \beta^{**}\, n^{**}) \tag{1.3}$$

where L is the annual leakage rate in the system, N^{**} is the life of the system, n^{**} is the system running time, E^a is the energy consumption per year and β^{**} is the CO_2 emission factor. Even if the TEWI can be considered a more complete index than GWP in the selection of environmentally friendly refrigerants [22], its calculation is more complex than that of the GWP.

- **Life-Cycle Climate Performance (LCCP)**

  In addition to the environmental effects already accounted in the TEWI, the LCCP accounts also for all GWP related to the refrigeration system operation, including the environmental impact of substances emitted during the process of refrigerant production and transportation [22]. Although this index can provide a holistic picture of the environmental impact of different refrigerants, in practice, its calculation is more complex than that of the TEWI. Moreover, the contribution of the additional emissions accounted by LCCP compared to the TEWI is negligible [22].

1.1.2 Low global warming potential refrigerants

As described above, the environmental concerns have always been one of the main driven forces in the refrigerant development, as it is the case today with the concern of the contribution of HFCs to anthropogenic global warming [8]. Consequently, researches and manufacturers are looking for alternative low GWP working fluids on the basis of different criteria, such as stability within the refrigeration system, short atmospheric lifetime (which reduce their ODP and GWP), suitable thermodynamic properties for the different applications, low flammability and toxicity and additional practical considerations (including cost and compatibility with the system materials) [27]. However, compounds having too short lifetime would result in high flammability and high contribution to urban smog. Moreover, the decomposition materials would give rise to safety concerns. The most suitable refrigerant depends on many constraints, and the selected refrigerants must be reconsidered when those constraints change [8].

It is important to point out that any alternative that lowers the overall efficiency of the system respect the original working fluid is likely to provide more adverse impact than benefit, considering the net global warming impact (e.g. TEWI and LCCP) [2]. Usually, the alternatives are less efficient than the original refrigerants. In fact, with a few exceptions, the efficiency gains achieved in systems that use the alternative refrigerants derive usually from improvements in equipment design rather than the thermodynamic properties of new working fluids. Moreover, better optimization with the old refrigerants would have yielded even higher efficiency in most cases, and the alternative refrigerants reduce margins for further systems efficiency improvements [28]. Consequently, besides looking for refrigerants that accomplish the GWP limitations, safe fluids that imply low energy consumption in the different systems should be used [2].

In the last years, different low GWP alternatives, both natural and synthetic fluids, have been proposed and studied.

The possibility to use natural refrigerants as alternatives in air conditioning and refrigeration systems was again investigated because of their low GWPs [29]. However, the thermodynamic properties of these refrigerants do not always allow their use in all the applications. For example, R744 is a low-efficiency fluid that works at very high pressures with the need to operate in transcritical cycles when used at high temperatures [30]. Instead, HCs, such as isobutane (R600a) and propane (R290), are

efficient refrigerants and can be considered suitable alternatives to HFCs in several ways. Nevertheless, their main drawback is that they are very flammable fluids [31].

A systematic and complete screening process to find potential long-term alternative low GWP pure fluids suitable for air conditioning and refrigeration applications was performed by McLinden et al. [24, 32] and Domanski et al. [33]. Thermodynamic (high efficiency and high volumetric capacity), environmental (low GWP and zero or near-zero ODP), and safety (low toxicity and low flammability) screening criteria were used to analyze a comprehensive database of possible refrigerants. Only a limited group of pure fluids was found to satisfy the aforementioned criteria and potentially be used for the studied applications. It is important to note that many of the identified potential working fluids are unsaturated halogenated hydrocarbons, such as Hydrofluoroolefins (HFOs) and Hydrochlorofluoroolefins (HCFOs), characterized by the presence of at least one carbon-carbon double bond in the molecules. Because of the carbon-carbon double bond, the unsaturated fluorinated hydrocarbons are highly reactive and rapidly decompose in the lower atmosphere, leading to short atmospheric lifetime, low ODP and low GWP [21]. Moreover, few HCFs, such as difluoromethane (R32) and 1,1-difluoroethane (R152a), were selected in the screening process because of their relatively low GWPs. In particular, because of its low flammability, good thermodynamic properties, and high system performance, R32 has been proposed as a suitable replacement of high GWP refrigerant blend R410A for air conditioning and heat pump applications [34]. However, its main drawback is that it has a GWP of 675. Instead, R152a has been investigated as an option for replacing R134a in mobile vehicle air conditioning applications, but its relatively high flammability poses a major limitation to widespread adoption [35]. This refrigerant might also be a suitable alternative refrigerant in commercial refrigeration applications, chillers, and industrial refrigeration.

Even if their thermodynamic, environmental and safety characteristics have not been thoroughly investigated yet, the main drawbacks of the identified potential alternative refrigerants are that most of them are mildly flammable or do not have suitable thermodynamic properties. For example, the HCFOs ensure similar low GWP values to HFOs with reduced or avoided flammability, but they introduce a trade-off concern with ODP even if it is still very low. In fact, none of these fluids is ideal in all regards and trade-off between thermodynamic, environmental and safety properties is necessary. Consequently, as pointed out by McLinden et al. [24, 32] and Domanski et al. [33], blends containing alternative, conventional and/or natural refrigerants can offer additional possibilities to optimize the thermodynamic, environmental and safety characteristics of the blended working fluid for particular applications.

Since the necessity to study their properties and performances in different applications, several researches about the thermophysical properties [36, 37], system adaptation (compatibility and flammability) [38–40], heat transfer [37, 41, 42] and pressure drop [37, 43] characteristics and vapor compression system performance [35, 44–46] of some of the potential alternative refrigerants selected by McLinden et al. [24, 32] and Domanski et al. [33] and their blends have been performed.

While details about the thermophysical properties of these working fluids are reported in the next section, some of the most recent review works of the manuscripts investigating the possibility to substitute the conventional refrigerants with low-GWP ones and their blends are briefly described below.

On the basis of the GWP limitations imposed by the EU Regulation No. 517/2014 [13] (F - gas Regulation), Mota-Babiloni et al. [47] reviewed and theoretically analyzed different low GWP blends proposed by the air conditioning, heating, and refrigeration

institute to replace the refrigerants currently employed in refrigeration and air conditioning systems (R134a, R404A, and R410A). The studied blends were composed of different HFCs and HFOs (R1234yf and R1234ze(E)). From the theoretical analysis, it was shown that most of the low GWP blends performed under the HFC analyzed (even if some experimental studies showed the contrary) and, in most cases, do not meet the GWP restrictions imposed by F - gas Regulation. Besides, some of the proposed blends would have problems due to their flammability. For these reasons, the studied working fluids were not considered a definitive solution and additional low GWP refrigerants and their blends should be studied.

Recently, the same authors [47] reviewed the works evaluating the performances of low GWP synthetic refrigerants to replace the high GWP refrigerants used for different applications, as air conditioning, stationary and domestic refrigeration, and cascade systems. The authors showed that pure HFOs or their blends have been mainly evaluated to replace conventional HFCs in several studies. However, only two HFOs among the possible alternative refrigerants presented by McLinden et al. [24, 32] and Domanski et al. [33], namely 2,3,3,3-tetrafluoroprop-1-ene (R1234yf) and *trans*-1,3,3,3-tetrafluoroprop-1-ene (R1234ze(E)), were analyzed in the selected studies. In particular, these two refrigerants have already been commercialized because of their thermodynamic properties suitable for low-temperature and medium-temperature refrigeration and air conditioning applications. Therefore, a possible reason for this limitation is that the properties of the other HFOs are still under analysis and they have not been commercialized yet. Moreover, it was shown that R32 is often used in air conditioning systems to substitute R410A. Even if R32 can only be considered a medium-term alternative for this application, different studies showed that no other low GWP blends alternatives to R410A offered new advantages compared to pure R32. Therefore, the authors stated that additional studies using new refrigerants and blends containing low GWP alternative and conventional refrigerants are necessary and expected in the next years.

1.2 Thermophysical properties of refrigerants

Accurate values of the thermodynamic and transport properties of fluids are necessary for the design of industrial processes and products. In particular, the thermophysical properties of refrigerants and their blends are essential to properly design components of refrigeration systems and to evaluate the potential performances of these working fluids in refrigeration and air conditioning applications. During the years, several data for refrigerants and their blends have been experimentally measured, correlated, estimated and collected in different works and databases [48–51]. However, considering the necessity to find suitable low GWP refrigerants or their blends in the next years, there is still the need to determine the unavailable properties of these alternative working fluids.

In addition to directly measuring the properties of the fluids, different models can be used for reliable estimations of the thermophysical properties. It is not practical to obtain all the necessary data from experimental measurements since they can be expensive and time-consuming [52]. Therefore, some of these properties can be estimated from suitable models of varying degrees of complexity which can be based on theories, on correlations of experimental data or a combination of both. Several of the best estimation models are equations based on incomplete theories with empirical correlations for the parameters that are not provided by those theories [52].

Consequently, in many cases, a sufficient amount of experimental data for different properties are necessary to regress reliable parameters of the estimation models.

1.2.1 Experimental measurements of thermophysical properties

Throughout the years, the thermodynamic and transport properties of several refrigerants and their blends have been measured in different thermodynamic conditions and phase regions by using various experimental techniques.

In particular, the main thermodynamic properties measured for evaluating the potential system performances of these working fluids and developing accurate estimation models are:

- the properties along the phase boundaries of the thermodynamic space (i.e. critical point, triple point, vapor pressure, saturation densities for pure refrigerants and critical point, Vapor-Liquid Equilibrium (VLE) and Solid-Liquid Equilibrium (SLE) properties for their blends);
- the Pressure - Specific Volume - Temperature (PvT) and Pressure - Specific Volume - Temperature - Composition ($PvTz$) behaviors of pure and blended working fluids, respectively, in the single-phase regions.

Moreover, the measurements of specific heat capacity and speed of sound are very useful for the developing of predictive models and for checking the thermodynamic consistency of experimental data [36]. Among the transport properties, the values of thermal conductivity, viscosity and surface tension are necessary for accurately designing components, particularly heat exchangers, and optimizing the performances of refrigeration systems.

Several experimental data of the aforementioned properties for various refrigerants and their blends were collected in different works [36, 48] and numerical databases containing thermophysical property data of chemicals. Among the available databases, the DIPPR [51] and the DETHERM [50, 53] databases are some of the most reliable and comprehensive ones. The DIPPR database contains thermophysical property data for thousands of pure compounds, together with references, notes, and quality codes. Therefore, its main advantage is that it collects data from a wide range of sources and evaluates them critically. The DETHERM database provides high quality and checked values, along with references, descriptions, and abstracts for the thermophysical properties of a large set of fluids and blends.

As concerns the low GWP refrigerants and their blends, Bobbo et al. [36] recently presented a review of the state-of-the-art of the thermophysical properties of different synthetic alternative refrigerants and binary systems containing one of these fluids. In particular, the authors surveyed the publicly available literature to evaluate the experimentally-determined data for several important thermodynamic and transport properties of 17 HFO and HCFO refrigerants and their blends. These working fluids are considered the potential alternative for different refrigeration, heat pump, and organic Rankine cycle applications. For the pure alternative refrigerants, it was showed that the thermophysical properties of R1234yf and R1234ze(E) are the most investigated, followed by those of *cis*-1,3,3,3-tetrafluoroprop-1-ene (R1234ze(Z)) and *trans*-1-chloro-3,3,3-trifluoro-1-propene (R1233ze(E)). Instead, fewer (or even none) experimental data of the analyzed properties were found for the other refrigerants. For the binary blends containing low GWP refrigerants, it was found that almost all the investigated blends

contained either R1234yf or R1234ze(E) as one of the components. Only few papers reported binary systems containing others of the investigated low GWP refrigerants. Therefore, the authors pointed out that further experimental measurements of the thermophysical properties of a large number of alternative refrigerants and their blends are needed. Even if new papers reporting additional experimental data for the thermophysical properties of these working fluids have been presented in the last years, this claim is still valid.

For these reasons, the $PvTz$ and SLE properties of different binary systems containing low GWP refrigerants have been measured by our group of work by using different experimental setups. The measured binary systems and the obtained results are presented in Chapter 4, together with an overview of the experimental data for these properties of the studied low GWP blends available in the open literature.

1.2.2 Modeling of thermophysical properties

The physical properties of pure and blended substances are related to molecular structure and the bonds between atoms that determine their intermolecular forces [52, 54]. For example, it was showed that the behavior of the relationships between T, P and v of pure substances and P, T, v and z of blends depends on intermolecular relations [55]. Although the statistical mechanics and intermolecular force theory are continually developing, the molecular theories cannot still provide reliable values of all thermophysical properties of substances needed for the different engineering applications [52]. The present quantitative relations which link the intermolecular forces to macroscopic properties of substances are suitable only for simple and idealized cases [54]. Therefore, several reliable and accurate models to estimate different thermophysical properties based on limited and empirically modified molecular theories were developed [52, 56]. Some of the most used theories and concepts in the development of semi-theoretical property estimation models are group contribution (GC), local composition, corresponding states principle (CSP), solubility parameters, free volumes, mixing and combining rules, and association theories (chemical-like, lattice and perturbation theories) [56]. Among them, two of the most used theories and concepts in the estimating models for the thermophysical properties are:

- **Group contribution (GC)**. The dependence of all macroscopic properties on the molecular behavior and the intermolecular forces suggests that a macroscopic property can be calculated from group contributions [52]. In fact, since the main characteristics of the molecular structure are related to the atoms, atomic groups, bond type, etc, it is possible to divide a molecule into functional groups and to assign weighting factors to them. Then the property is usually determined by an algebraic operation that sums the contributions from the different functional groups of the molecule. In particular, for a multi-functional component in blends, it is assumed that each functional group behaves independently from the molecule in which it appears [54]. Sometimes this approach is not used for the direct calculation of properties but to correct their values calculated by some simplified theories or empirical models [52].

- **Corresponding states principle (CSP)**. Derived by van der Waals in 1873 from his well-known Equation of State (EoS), the classical CSP expresses the generalization that the macroscopic equilibrium PVT properties, which depend on certain intermolecular forces, are related to the critical properties according

to a universal function ($\mathcal{F}$) such that [52, 54]:

$$\mathcal{F}\left(\frac{v}{v_c}, \frac{T}{T_c}, \frac{P}{P_c}\right) = 0 \tag{1.4}$$

where subscript c refers to the critical point. In particular, van der Waals showed that this relationship is theoretically valid for all pure fluids whose PVT properties can be described by a two-parameter EoS.

A molecular form of the CSP bases on mathematical properties of the potential-energy function was proposed by Pitzer [57]. It was shown that a universal function that can be theoretically applied to all pure substances exists if the intermolecular potential function is scaled by two characteristic parameters [52, 54]. Moreover, it was demonstrated that the two-parameter CSP can be derived from statistical mechanics by introducing strict simplifications into the partition function [52]. However, to obtain a more general framework for the development of estimation methods, less strict simplifications can be introduced into statistical mechanics. In fact, fundamental equations for the description of different properties (including transport properties) can be derived from the CSP, provided that an expression for the potential-energy function for molecular interactions is available. Even if this function could be, at least in part, empirical, the fundamental equations for properties are not often affected by details of the potential function from which they result and, in many cases, two-constant potential functions are suitable [52].

However, the aforementioned forms of the CSP characterized by two independent parameters can be applied for the estimation of the properties of fluids containing simple molecules. Considering semi-empirical extensions with an additional parameter, e.g. the acentric factor (ω), reliable results for non-polar (or slightly polar), non-associating and moderate size fluids where molecular orientation is not important (called "normal" fluids) can be obtained from the CSP [52, 54].

Even if it was showed that the estimation models based on theoretical basis usually provide more reliable and accurate results [52], different useful empirical models have been presented. However, their main limitation is that these models must be used only in the narrow range of thermodynamic conditions on which they are based [52].

As concern the refrigerants, very well-known and used models for the description of their PvT behavior and the estimations of different thermodynamic properties in single and multi-phase regions are the Equations of State (EoSs). In general, several semi-theoretical and empirical EoSs characterized by different degrees of complexity have been developed to accurately describe the thermodynamic properties of a great number of fluids over wide ranges of T and P [52, 58]. As will be explained in the Subsection 2.2.1 of Chapter 2, some of the most used EoSs to estimate the values of the thermodynamic properties of several refrigerants are the virial EoS [59, 60], different cubic and generalized van der Waals EoSs [61, 62] and some multi-parameter EoSs [63]. Moreover, the EoSs can describe the $PvTz$ behavior and estimate different thermodynamic properties of multi-component systems when they are extended to these systems through specific mixing and combining rules.

Different EoSs are used in REFerence fluid PROPerties (REFPROP) [63–65] to provide reliable estimated values of different thermodynamic properties of refrigerants and their blends. Developed by the National Institute of Standards and Technology (NIST), REFPROP is one of the most widespread and well-known software to estimate

different thermodynamic and transport properties of industrially important fluids (in particular refrigerants) and their blends. The software is based on some of the most accurate property estimation models currently available for pure fluids and blends. In particular, the last version of the software (REFPROP 10.0 [65]) implements two multiparameter EoSs for the thermodynamic properties of pure fluids: fundamental EoSs explicit in Helmholtz energy [58] specific for each fluid and the modified Benedict-Webb-Rubin EoS [66]. The property calculations for blends are calculated on the basis of the multi-fluid Helmholtz-energy-explicit mixture models [67].

Several additional semi-theoretical models based on the aforementioned theories have been developed for the estimation of different thermodynamic and transport properties of refrigerants and their blends. For example, correlations based on CSP for thermal conductivity [68, 69], viscosity [70] and surface tension [71, 72] of refrigerants and their blends are available in literature. Moreover, different transport and thermodynamic properties of some refrigerants in REFPROP 10.0 [65] are modeled through fluid-specific correlations based on extended CSP.

Among the different empirical models proposed for estimating the thermophysical properties of refrigerants and their blends, the Artificial Neural Networks (ANNs) have been widely used to estimate different properties [73–75]. An ANN is a mathematical model inspired by the functioning of the human brain. This structure is trained respecting to a dataset until it learns the patterns used as inputs and, once trained, new patterns may be presented for prediction [76]. An ANN generally presents three parts: the input of data, the elaboration process, and the output. Referring to the human brain, the inputs correspond to dendrites, the information is elaborated in the nucleus of the neuron, and the output is transmitted by the axon. In particular, an ANN consists of a system of interconnected artificial neurons that interact with one another. The artificial neurons are structured to process multiple inputs, including the unity bias, in a nonlinear way, producing a single output. However, the main drawbacks of this powerful tool are its completely empirical nature and its computational complexity. Since the notable developments in computational techniques, the latter problem is less relevant nowadays.

Since few experimental data are available for low GWP refrigerants and their blends, almost all the available semi-theoretical and empirical models for refrigerants can estimate accurate thermophysical properties for a limited number of these working fluids.

An overview of different models that could be used for estimating the thermophysical properties of refrigerants studied in this thesis is reported in Chapters 2 and 3.

Chapter 2

Modeling of thermodynamic properties

This chapter presents some of the most reliable models available in the literature for the estimation of different thermodynamic properties of refrigerants and their blends. Besides, the capability of some of these models to estimate the properties of low Global Warming Potential (GWP) refrigerants and blends containing these fluids is investigated. In particular, after introducing the refrigerants studied in this work, details about different models to describe Pressure-Specific Volume-Temperature (PvT) and Pressure-Specific Volume-Temperature-Composition ($PvTz$) behaviors, the phase equilibria (vapor pressure, Vapor-Liquid Equilibrium (VLE) and Solid-Liquid Equilibrium (SLE)) are reported.

2.1 Refrigerants studied in this work

All the refrigerants studied in this thesis are reported in Table 2.1, together with their values of the Ozone Depletion Potential (ODP) and GWP. In addition, Table 2.1 presents the following physical properties of the refrigerants needed in the estimation models for the studied thermophysical properties: molar mass (M), normal boiling point temperature (T_b), critical pressure (P_c), critical temperature (T_c), critical molar volume (v_c), acentric factor (ω), dipole moment (μ) and radius of gyration (Gr). The reported ODP and GWP values were collected from WMO 2018 [77]. If not otherwise stated in Table 2.1, the reported physical parameters were collected from the DIPPR database [51]. In general, these physical properties were employed in the studied property estimation models. However, as described below, different physical properties collected from more suitable sources were used for some models. It is worthwhile noting that the unsaturated halogenated hydrocarbon (halogenated alkene) refrigerants reported in Table 2.1 are the low GWP refrigerants which are mainly investigated in this thesis. The selection criteria of these alternative refrigerants were based on the availability of the experimental data for the analyzed properties in open literature and databases. In particular, almost all the studied low GWP fluids were selected by McLinden et al. [24, 32] and Domanski et al. [33] as potential alternative refrigerants. However, even if they could not be suitable for HVAC&R applications, five additional low GWP fluids, namely R1140, R1130, R1113, R1120 and R1233xf, were selected to perform a thorough investigation of this type of refrigerants. The characteristics

of additional synthetic and natural refrigerants studied in this thesis are provided in Table 2.1.

2.2 Pressure, volume, and temperature behavior

The relationship between Temperature (T), Pressure (P) and Specific Volume (v) (or Density (ρ)) due to intermolecular interactions allows to fully determine the thermodynamic equilibrium states of pure fluids [87, 88]. The behavior of the volumetric properties defines the different phase regions characterized by specific values of the thermodynamic properties. In particular, in these regions, a different number of volumetric properties are independent and it is possible to evaluate all the additional thermodynamic properties, such as the derived properties (e.g. internal energy and enthalpy), from the PvT relations. For example, the single-phase regions (i.e. liquid and gas regions) are characterized by two independent volumetric properties. Therefore, if P and T are fixed, the thermodynamic state and the other thermodynamic properties are defined [87, 88]. Consequently, the knowledge of the relationship between the volumetric properties is fundamental for the evaluation of the thermodynamic performances of fluids, such as refrigerants, and the design of engineering systems.

Because of the high number of possible combinations of intermolecular interactions, the molecular behavior of blends of fluids is more complex than that of pure species. Consequently, the thermodynamic properties of blends depend on the nature and amount of each of the blended fluids and their resultant intermolecular interactions. To evaluate the thermodynamic properties of blends in the different thermodynamic states, it is necessary to know the relationships between T, P, v and composition, expressed as mole (z), mass (w) or volume (ϕ) fractions [87, 88].

Different experimental techniques can be used to measure the PvT and $PvTz$ properties of pure fluids and blends, respectively. Some of the ones mainly used to measure these thermodynamic properties of refrigerants and their blends will be mentioned in Section 4.1 of Chapter 4. In addition, several models characterized by different degrees of accuracy, reliability, and complexity were developed for estimating the behaviors of PvT and $PvTz$ properties of pure fluids and their blends, respectively, in different phase regions when a limited number of (or no) experimental data are available [52]. In particular, the most well-known and widespread models are semi-theoretical models based on the Corresponding State Principle (CSP) which require a sufficient amount of experimental data for their development. Many of the estimation models for pure fluids can be extended to blends using specific models, (i.e. mixing rules and combing rules) that take into account the composition dependence in the description of their thermodynamic properties. However, the composition dependence is described by models that complicate the modeling of the thermodynamic properties of blends [52]. Some of the most used and reliable models for the PvT and $PvTz$ estimation of fluids, especially refrigerants, and their blends are the Equations of State (EoSs), which will be described in the following subsections.

2.2.1 Equations of state

An Equation of State (EoS) is an algebraic relation between P, v (or ρ) and T which can describe the PvT behavior of pure substances in different phase regions over different temperature and pressure ranges. In particular, it can be used to estimate different properties of pure substances (e.g. densities of liquid and vapor, vapor pressure,

Table 2.1: Values of the direct environmental impact and physical properties of the refrigerants studied in this work. Notes: Ozone Depletion Potential (ODP) and Global Warming Potential (GWP) values were collected from WMO 2018 [77]. The values of the physical properties were collected from DIPPR database [51]. Footnotes provide references for different sources of the physical properties.

ASHRAE designation [1]	IUPAC name	CAS number	ODP	GWP	M kg kmol^{-1}	T_b K	P_c kPa	T_c K	v_c cm^3 mol^{-1}	ω	μ D	Gr Å
Unsaturated halogenated hydrocarbons (halogenated alkenes)												
R1141	Fluoroethene (vinylfluoride)	75-02-5	0	<1	46.04	200.95	5240	327.80	144.0	0.143	1.430	1.934
R1140	Chloroethylene (vinyl chloride)	75-01-4	-	«1	62.50	259.25	5670	432.00	179.0	0.100	1.451	2.049
R1132a	1,1-difluoroethene	75-38-7	0	<1	64.03	187.50	4460	302.80	154.0	0.136	1.379	2.528
R1123[a]	Trifluoroethylene	359-11-5	0	«1	82.03	214.06	4546[b]	331.73[b]	166.7	0.261	1.720[c]	2.336[d]
R1243zf	3,3,3-trifluoroprop-1-ene	677-21-4	0	<1	96.05	248.15	3609	378.59	211.0	0.265	2.449	3.158
R1130	1,2-dichloroethene	156-60-5	<0.003	«1	96.94	320.85	5510	516.50	224.0	0.223	0.000	2.553
R1234yf	2,3,3,3-Tetrafluoropropene	754-12-1	0	<1	114.04	244.15	3382	367.85	238.6	0.282	2.255	3.215
R1234ze(E)	*trans*-1,3,3,3-Tetrafluoropropene	29118-24-9	0	<1	114.04	254.83	3662	382.51	235.0	0.324	1.124	3.495
R1234ze(Z)[e]	*cis*-1,3,3,3-Tetrafluoropropene	29118-25-0	0	<1	114.04	282.90	3533	423.27	242.3	0.327	3.540[f]	3.249[d]
R1113	1-chloro-1,2,2-trifluoroethene	79-38-9	-	-	116.47	244.80	4053	379.15	212.0	0.244	0.399	3.293
R1233xf[l]	2-chloro-3,3,3-trifluoropropene	2730-62-3	-	-	130.49	-	3322	439.98	-	0.187	-	-
R1233zd(E)[g]	*trans*-1-chloro-3,3,3-trifluoro-1-propene	102687-65-0	<0.0004	4	130.49	291.41[h]	3624	439.60	271.7	0.302	1.143[i]	3.526[d]
R1120	Trichloroethene	79-01-6	<0.004	<1	131.39	360.10	4910	571.00	256.0	0.217	0.770	3.742
R1225ye(Z)[m]	*cis*-1,2,3,3,3-pentafluoroprop-1-ene	5528-43-8	0	<1	132.03	253.15	3529	380.05	255.3	0.326	-	-
R1336mzz(Z)[h]	*cis*-1,1,1,4,4,4-Hexafluoro-2-butene	692-49-9	0	2	164.05	306.53	2901	444.42	348.3	0.387	2.920	-
Halogenated hydrocarbons (halogenated alkanes)												
R41	Fluoromethane	593-53-3	0	116	34.03	194.82	5875	317.42	113.0	0.195	1.856	1.421
R161	Fluoroethane	353-36-6	0	6	48.06	235.45	5028	375.31	159.0	0.218	1.940	2.178
R32	Difluoromethane	75-10-5	0	705	52.02	221.50	5784	351.26	123.0	0.277	1.979	1.950
R152a	1,1-difluoroethane	75-37-6	0	148	66.05	249.13	4520	386.44	179.0	0.275	2.262	2.514
R23	Trifluoromethane	75-46-7	0	12690	70.01	191.09	4816	299.01	132.0	0.264	1.649	2.454
R143a	1,1,1-trifluoroethane	420-46-2	0	5080	84.04	225.81	3764	345.88	195.0	0.261	2.320	2.767
R22	Chlorodifluoromethane	75-45-6	0.034	1780	86.47	232.32	4971	369.30	166.0	0.219	1.458	2.689
R14	Tetrafluoromethane	75-73-0	0	6630	88.00	145.10	3745	227.51	143.0	0.179	0.000	2.582
R134	1,1,2,2-tetrafluoroethane	359-35-3	0	1135	102.03	250.15	4640	391.80	191.0	0.266	0.992	3.118
R134a	1,1,1,2-tetrafluoroethane	811-97-2	0	1360	102.03	247.08	4056	374.18	198.8	0.327	2.058	2.944
R125	Pentafluoroethane	354-33-6	0	3450	120.02	225.04	3620	339.17	211.3	0.305	1.541	3.282
R12	Dichlorodifluoromethane	75-71-8	0.81	10300	120.91	243.36	4125	384.95	217.0	0.180	0.510	3.052
R245cb	1,1,1,2,2-pentafluoropropane	1814-88-6	0	4000	134.05	255.50	3137	380.11	273.2	0.305	2.392	3.399
R245fa	1,1,1,3,3-pentafluoropropane	460-73-1	0	880	134.05	288.45	3640	427.20	259.0	0.375	1.556	3.650
R124	1-Chloro-1,2,2,2-tetrafluoroethane	2837-89-0	0.022	530	136.48	261.05	3660	395.65	243.8	0.288	1.469	3.523
R244bb[m]	2-chloro-1,1,1,2-tetrafluoropropane	421-73-8	0.027	1600	150.50	-	3225	431.49	-	0.264	-	-
R123	2,2-Dichloro-1,1,1-trifluoroethane	306-83-2	0.01	80	152.93	301.05	3676	456.94	278.0	0.282	1.356	3.748
R227ea	1,1,1,2,3,3,3-heptafluoropropane	431-89-0	0	3140	170.03	256.79	2912	374.83	274.0	0.355	1.456	3.882
R218	Octafluoropropane	76-19-7	0	8900	188.02	236.45	2680	345.05	299.0	0.328	0.000	3.999
R13I1	Trifluoroiodomethane	2314-97-8	<0.09	-	195.91	251.35	3953	396.44	225.3	0.176	1.049	2.692
Natural refrigerants												
R50	Methane	74-82-8	0	28	16.0425	111.66	4599	190.564	98.6	0.011548	0.000	1.118
R717	Ammonia	7664-41-7	0	<1	17.03	239.72	11280	405.65	72.5	0.253	1.469	0.853
R728	Nitrogen	7727-37-9	-	-	28.01	77.34	3400	126.20	89.2	0.038	0.000	-
R1150	Ethylene	74-85-1	-	-	28.05	169.41	5041	282.34	131.0	0.086	0.000	1.548
R170	Ethane	74-84-0	-	-	30.069	184.55	4872	305.32	145.5	0.099493	0.000	1.826
R740	Argon	7440-37-1	-	-	39.95	87.28	4898	150.86	74.6	0.000	0.000	0.000
R1270	Propylene	115-07-1	0	«1	42.08	225.45	4600	364.85	185.0	0.138	0.366	2.231
R744	Carbon dioxide	124-38-9	0	1	44.01	194.67	7383	304.21	94.0	0.224	0.000	1.040
R290	Propane	74-98-6	0	<1	44.10	231.11	4248	369.83	200.0	0.152	0.000	2.431
R600a	Isobutane	75-28-5	0	«1	58.12	261.43	3640	407.80	259.0	0.184	0.132	2.948
R600	n-Butane	106-97-8	-	-	58.1222	272.65	3796	425.12	255	0.200164	0.000	2.886

[a] Values given in [78] [b] Value given in [79] [c] Value given in [80] [d] Value given in [81] [e] Values given in [64] [f] Value given in [82] [g] Values given in [83] [h] Values given in [65]
[i] Value given in [84] [l] Values given in [85] [m] Values given in [86]

critical properties, deviations of enthalpy and entropy, etc.) [52, 89]. Currently, no EoS is equally suitable for all the different thermodynamic properties for a high number of substances. However, several EoSs which ensure accurate results for specific cases have been proposed [89].

In the nineteenth century, the observations of Charles and Gay-Lussac were combined with the hypothesis of Avogadro to form the well-known ideal gas law, defined as $Pv = nRT$ where n is the number of moles and R is the universal gas constant [52, 89]. In addition, investigations on mixed gases led to Dalton's law of partial pressures and the Amagat's law [89]. However, these simple relations are only a rough approximation of the behavior of the volumetric properties of real gases and their blends. In particular, the ideal gas law can closely approximate the PvT properties of gasses at low pressures and high temperatures that implies low densities.

Consequently, during the years, hundreds of equations describing deviations from ideal gas behavior and, therefore, the PvT behavior of real fluids have been proposed. Since the sizes, shapes, and structure of molecules determine the intermolecular forces and the PvT behavior of the substances, different EoSs were developed based on the molecular behavior of the substances [89]. For example, the virial EoS was derived from the statistical mechanic, but its range of applicability is limited to represent only the gas behavior of substances. The EoS proposed by van der Waals [89] presents parameters that quantitatively take into account the finite volume occupied by the molecules and forces of attraction and repulsion between molecules, ensuring a qualitative representation of the coexistence of liquid and vapor phases and the critical state. Moreover, as will be described below, this EoS was the basis for several reliable semi-theoretical EoSs which can represent both liquid and vapor behavior over different ranges of T and P for many but not all substances [52].

A great number of empirical EoSs which are applicable on broader ranges of T and P than that of analytic EoSs were developed. However, these non-analytic EoSs require several parameters (also component-specific parameters) fitted to a large amount of experimental data of several properties [52].

Besides, different kinds of mixing rules and models characterized by different degrees of complexity and accuracy have been proposed to include the effects of composition in the EoS parameters to represent the volumetric properties of blends in terms of the composition and the properties of the pure components [52].

In general, the primary differences between the several EoS forms are the computational complexity and quality of the results for liquids, for polar substances, for associating substances and for polymers, especially at high pressure. While EoSs were previously limited to vapor phase properties, they are now commonly used to describe the liquid phase as well. Thus, the most desirable expressions give the PvT behavior of both vapor and liquid phases and also all other pure component properties with extensions to their blends while remaining as simple as possible for computation. However, since not all of these constraints can be satisfied simultaneously, EoSs are still an active field of research and the most suitable model to use has to be carefully chosen among the possibilities for the specific cases [52].

Some of the most well-known and widespread EoSs used for the description of the PvT behavior of refrigerants are described below. Moreover, different mixing rules mainly used to extend the EoSs to blends of refrigerants are presented.

Viral equation of state

The virial equation of state is the only equation of state known with a thoroughly sound theoretical foundation [90]. In fact, although it was originally developed on a purely empirical basis, this EoS was derived from a statistical-mechanical analysis of the forces between molecules [89]. The virial EoS (in Leiden form) shows the deviations from the ideal gas law as an infinite power series in the molar volume, v_m:

$$Z = \frac{Pv_m}{RT} = 1 + \frac{B}{v_m} + \frac{C}{v_m^2} + \frac{D}{v_m^3} + \dots \tag{2.1}$$

where Z is the compressibility factor, B is the second virial coefficient, C is the third virial coefficient, D is the forth virial coefficient, etc. Theoretical expressions for several virial coefficients can be derived from statistical mechanics. The coefficient B corresponds to the interaction between pairs of molecules, C to molecular trio interactions, etc. Thus, the importance of the virial EoS is its theoretical relation with molecular interactions, in particular of the forces between molecules [90]. In theory, these coefficients depend on temperature and the particular gas under consideration and are independent of density and pressure [89]. In particular, B increases with temperature from negative values at sufficiently low temperatures to positive values at high temperature. The temperature at which B is equal to zero is called Boyle temperature (T_{Boyle}) and it is specific for each fluid. Instead, C and higher coefficients are positive, except at very low T where they are of little importance.

Since the virial expansion is not accurate at high pressures, it cannot represent the liquid state and coexistence of liquid and vapor phases. Considering that the infinite series is impracticable for purposes of calculation, the virial EoS is usually truncated at the second or third term and applied only to single-phase gas systems. However, this EoS, when truncated after the second term, gives a proper representation of the PvT behavior of real gases at low and moderate pressure. Even if B can be experimentally measured using different techniques, an accurate estimation of this coefficient is an important task in thermodynamics.

It is possible to estimate B from complicate models based on theoretical interpretations of intermolecular interactions between molecules in the gaseous state. These models produce accurate results for simple molecules, but they usually fail when applied to more complex molecules. To overcome the limitations of the theoretical approaches, several empirical and semi-empirical methods were proposed in the literature for its estimation. Some of those models will be briefly described below.

Tsonopoulos [91] modified the correlation to estimate B proposed by Pitzer & Curl [92], based on CSP, to improve its predictive capability. The full form of the equation is:

$$\frac{BP_c}{RT_c} = f_0 + \omega f_1 + a_1 f_2 + b_1 f_3 \tag{2.2}$$

where T_c is the critical temperature, P_c is the critical pressure, and ω is the acentric factor. For non-polar (or slightly polar), non-associating and moderate size gases, called normal fluids, Tsonopoulos introduced the following terms:

$$f_0 = 0.1445 - 0.330\,T_r^{-1} - 0.1385\,T_r^{-2} - 0.0121\,T_r^{-3} - 0.000607\,T_r^{-8} \tag{2.3}$$

and

$$f_1 = 0.0637 + 0.0331\,T_r^{-2} - 0.423\,T_r^{-3} - 0.008\,T_r^{-8} \tag{2.4}$$

where $T_r = T\,T_c^{-1}$ is the reduced temperature. He also introduced corrective functions to estimate B of polar gases:

$$f_2 = T_r^{-6} \tag{2.5}$$

and

$$f_3 = -T_r^{-8} \tag{2.6}$$

The terms a_1 and b_1, which are evaluated by different equations for each chemical family, are variable functions of the reduced dipole moment, defined as [52]:

$$\mu_r = \frac{0.987\,\mu^2 P_c}{T_c^2} \tag{2.7}$$

where μ is the dipole moment. In summary, the Tsonopoulos' equation (2.2) requires 5 parameters: T_r, T_c, P_c, ω and μ_r.

Weber [93] modified Tsonopoulos' correlation to better describe the temperature dependence of the second virial coefficient. He removed the last term in Tsonopoulos' equation (2.2), and the terms with T_r^{-8} in f_0 and f_1. He also proposed a unique a_1 function for all chemical families, defined as:

$$a_1 = -8.766 \times 10^{-7} \mu_r^2 \tag{2.8}$$

Therefore, the parameters used are the same 5 of Tsonopoulos' correlation: T_r, T_c, P_c, ω and μ_r.

Virendra et al. [94] proposed a simple generalized equation based on the similarity in the shape of the second virial coefficient and vapor pressure curves. The equation is similar to the Antoine's equation for vapor pressure and requires three parameters (T_r, T_c, P_c):

$$\frac{BP_c}{RT_c} = c_1 + \frac{c_2}{T_r + c_3} \tag{2.9}$$

The authors tried to relate c_1, c_2, and c_3 to characteristic properties such as molecular weight or critical properties, but their efforts failed.

Iglesias-Silva & Hall [95] presented an expression that satisfies the known limits of B and does not require addition terms to encompass the effects of polar substances, molecules with association and quantum effects. Their correlation has the following form:

$$\frac{B}{b_0} = \left(\frac{T_{Boyle}}{T}\right)^{0.2}\left[1 - \left(\frac{T_{Boyle}}{T}\right)^{0.8}\right]\left\{\frac{B_C}{b_0}\left[\left(\frac{T_{Boyle}}{T_c}\right)^{0.2} - \left(\frac{T_B}{T_c}\right)\right]\right\}^{\left(\frac{T_c}{T}\right)^n} \tag{2.10}$$

The authors suggest the following correlation for the Boyle temperature:

$$\frac{T_{Boyle}}{T_c} = 2.0525 + 0.6428\exp\left(-3.6167\,\omega\right) \tag{2.11}$$

The terms b_0, B_C, and n are given from the following generalized expressions:

$$\frac{b_0}{v_c} = 0.1368 - 0.4791\,\omega + 13.81\left(\frac{T_B}{T_c}\right)^2 \exp\left(-1.95\frac{T_B}{T_c}\right) \tag{2.12}$$

$$\frac{B_C}{v_c} = -1.1747 - 0.3668\,\omega - 0.00061\,\mu_r \tag{2.13}$$

$$n = 1.4187 + 1.2058\,\omega \tag{2.14}$$

Summarizing, Equation (2.10) requires 5 parameters: T, T_c, v_c, ω and μ_r. In a later work [96], the authors used the Stockmayer potential to obtain a correlation requiring 5 parameters: 2 intermolecular force constants, the dipole moment μ, the experimental temperature T and T_c.

Gharagheizi et al. [97] applied the Gene Expression Programming mathematical algorithm to obtain an expression based on the CSP to estimate the second virial coefficient of 127 chemical compounds, mostly organic. The expression requires 5 parameters (T_r, T_c, P_c, ω and the reduced temperature at the normal boiling point (T_{br})) and has the following form:

$$\frac{BP_c}{RT_c} = \left(\frac{10^5}{T_r}\right)\left[\frac{A - 2.27753\,T_r}{T_r^2} + T_r + T_{br} - 2.69271\right] \tag{2.15}$$

where

$$A = 8.458259\,\omega\left\{\frac{16.382118\,(1 - T_r)(2 - T_r) - 2.27753}{T_c} - (1 - T_r)\right\} \tag{2.16}$$

A semi-empirical scaled correlation for B of refrigerants, based on CSP, was proposed by Di Nicola et al. [60]. The correlation requires 5 parameters (T_r, T_c, P_c, ω and μ_r) and its coefficients were regressed for five refrigerant subgroups, which are representative of the different chemical structures of the studied refrigerants: single halogenated, double halogenated, hydrocarbons, inorganics and elements. In particular, the proposed scaled correlation has the following form:

$$B = \frac{10^6 \mathrm{R} T_c}{P_c}\left(\frac{a\,\log T_r + b\,\omega + c\,\mu_r + d}{T_r^{1.7}}\right) \tag{2.17}$$

where R is the universal gas constant. It is worthwhile to note that, even if a large experimental dataset of B for several refrigerants was used to regress the parameters of the previous equation, only two selected refrigerants, namely R1141 and R1132a, are potential low GWP refrigerants included in the list proposed by McLinden et al. [24, 32] and Domanski et al. [33]. This aspect is likely due to the fact that experimental data of B for the low GWP refrigerants could be not available in the open literature.

A different approach to estimate B is based on Artificial Neural Networks (ANNs). However, only a limited number of literature works reported an ANN for the estimation of B [98, 99]. Oreški [98] presented an ANN for the estimation of second virial coefficients of 20 pure gases. The model has 6 input variables (T_c, P_c, V_c, ω, μ and T) and two hidden-layers with 10 and 4 neurons, respectively. The average ANN estimation error between the experimental and calculated points is low (1.3%), but only few fluids were studied. Recently, an ANN for the estimation of B for 234 organic and inorganic fluids was presented by our research group [100]. The proposed ANN was based on a Multilayer Perceptron (MLP) architecture consisting of one input layer with 5 parameters (T_r, T_c, P_c, ω and μ_r), one output layer with one parameter (B) and 2 hidden layers with 19 neurons each. To determine the number of the ANN inputs, a deep statistical analysis of the selected data was carried out, adopting a factor analysis approach. The proposed architecture of the ANN was built using the back-propagation technique and ensured the smallest deviations between the calculated and experimental values of B. In particular, the experimental points of B of the refrigerants used by Di

Nicola et al. [60] were included in the set of experimental data used to obtain this ANN configuration. Respect to different equations available in the literature, the proposed ANN was usually remarkably better, but its complexity justifies its utilization only if high accuracy is desired. Moreover, the results of the Leverage approach show that the proposed ANN configuration is statistically valid with only few probable outliers in the whole dataset.

A truncated form of the virial EoS was used to correlate the $PvTz$ properties of different binary systems containing low GWP refrigerants measured in the superheated vapor region employing an isochoric setup. The obtained results are reported in Section 4.1 of Chapter 4.

Cubic equations of state

The Cubic Equations of State (CESs) are semi-theoretical expressions derived from the original van der Waals equation of state [89] that are explicit in pressure and cubic in molar volume (v_m). Since they are solvable analytically for v_m (or the compressibility factor (Z)), these models are considered analytical equations of state that describe both the liquid and vapor phases [52]. The ambiguity of multiple roots usually is not a problem [89]. These equations provide one or three real roots depending on the number of phases in the studied system. In the two-phase region, the largest real root corresponds to the vapor phase and the smallest to the liquid phase; the intermediate root has no physical meaning. At the critical point, all three roots are the same [89].

The CESs can be used to estimate the molar volumes of liquid and vapor phases, vapor pressures, fugacities and deviations of thermodynamic properties from ideal values. Since they combine the speed of computation with thermodynamic consistency, the CESs represent a family of classical but still very useful and widely used models in many engineering applications, especially for the representation of properties and phase equilibria of blends of fluids [56, 58]. However, since these EoSs usually lack the needed flexibility in the same phase regions, they are not the most suitable models for the accurate representation of pure-fluid properties.

To enhance the prediction of the vapor pressure and volumetric properties, a large number of CESs for pure fluids with different expression and number of parameters were developed [52, 58]. Among them, same of the most widespread and well-known models for the thermodynamic properties of normal substances are the two-parameter CESs, that have the following general form:

$$P = P_\mathrm{R} + P_\mathrm{A} = \frac{R\,T}{v_\mathrm{m} - b} - \frac{a}{v_\mathrm{m}^2 + u\,b\,v_\mathrm{m} + w\,b^2} \tag{2.18}$$

where P_R express the repulsive contribution to pressure, P_A express the attractive contribution to pressure and u and w are two constants that define a specific two-parameter CES. Since they account for the attraction and repulsion forces between the molecules of the fluid, a is the attraction parameter and b is the repulsive parameter, called covolume.

Several two-parameters CESs characterized by different levels of accuracy have been proposed in the literature by considering different values of u and w which were selected following specific constrains to avoid that the CESs were thermodynamically inconsistent [101]. Two of the most well-known two-parameters CESs are Redlich-Kwong-Soave (RKS) EoS [102] and Peng-Robinson (PR) EoS [103]. In particular, the PR EoS is still one of the most useful and successfully applied models for thermodynamic and volumetric property calculations in both industrial and academic fields [104]. To

obtain more accurate descriptions of specific properties for pure fluids and blends, many modifications of the original CESs were proposed in literature [58]. In this respect, the modified RKS and PR EOSs proposed by Stryjek [105, 106], which guaranteed a better representation of the saturated vapor pressure of blends' components, shown accurate prediction of the Vapor-Liquid Equilibrium (VLE) and critical state for the studied blends. Moreover, the author proposed other CESs, not systematically studied till then, that were also found reliable models.

The u and w values of the RKS, PR and some of the CESs proposed by Stryjek are reported in Table 2.2. The capability of the CESs reported in Table 2.2 to describe the vapor pressure of low GWP refrigerants and VLE of their binary systems was tested and the results will be reported in Sections 2.3 and 2.4. In particular, their description capability for the vapor pressure of the studied refrigerant was studied since an accurate description of this property of the pure fluids over the studied temperature range of concern is an essential requirement for reliable CESs used for multi-component systems. Moreover, some of these CESs were used to correlate the $PvTz$ properties of different binary systems containing low GWP refrigerants measured with an isochoric apparatus and the results are reported in Section 4.1 of Chapter 4.

To estimate the values of the CESs' parameters, different approaches have been used. Probably, the most widespread method is based on the CSP which needs only the knowledge of the critical properties and few additional specific physical properties. In particular, the parameter values were determined from critical-point coordinates by applying the critical-conditions [52, 58]. However, to obtain an enhanced description of specific properties for different fluids, such as vapor pressure, several authors used a combination of CSP and fitting of experimental data to estimate the parameter values [52, 58].

In addition, several expressions based on CSP for the CES parameters were proposed to improve the representation of specific fluid-properties. One of the most important modifications consisted of the addition of a temperature dependent function to the attractive term to improve the vapor pressure prediction of different fluids [58]. In this case, in contrast with the van der Waals parameters a and b which are constant and only function of the critical properties, the parameters a and b in Equation (2.18) are expressed as:

$$a(T) = \Omega_{\mathrm{a}} \frac{R^2 T_{\mathrm{c}}^2}{P_{\mathrm{c}}} \alpha\left(T_{\mathrm{r}}, \omega\right) \tag{2.19}$$

$$b = \Omega_{\mathrm{b}} \frac{R\,T_{\mathrm{c}}}{P_{\mathrm{c}}} \tag{2.20}$$

where $\alpha\left(T_{\mathrm{r}}, \omega\right)$ is a dimensionless function of the reduced temperature (T_{r}) and acentric factor (ω), and Ω_{a} and Ω_{b} are numerical constants which were calculated from the thermodynamic conditions of the critical point. The α function introduced by Soave [102] is one of the most used ones and has the following expression:

$$\alpha\left(T_{\mathrm{r}}, \omega\right) = \left[1 + k\left(1 - T_{\mathrm{r}}\right)^{0.5}\right]^2 \tag{2.21}$$

where usually k is a function of ω. The α function proposed by Soave [102] was used to obtain the results reported in this thesis by considering the following expression of the parameter k:

$$k\left(\omega\right) = c_0 + c_1\,\omega - c_2\,\omega^2 + c_3\,\omega^3 \tag{2.22}$$

where c_0, c_1, c_2 and c_3 are coefficients specific for each CES. The values of the coefficients for the CESs used in this thesis are reported in Table 2.2.

Table 2.2: Names, references to original work and coefficients of different CESs.

CES name	Ref.	u	w	Ω_a	Ω_b	Z_c	c_0	c_1	c_2	c_3
RKS	[102]	1	0	0.4275	0.0866	0.333	0.4800	1.5740	0.1760	0.0000
PR	[103]	2	-1	0.4572	0.0778	0.307	0.3746	1.5423	0.2699	0.0000
PR mod	[105, 106]	2	-1	0.4572	0.0778	0.307	0.3788	1.4895	0.1709	0.0194
CES(A)	[105, 106]	1	-1	0.4638	0.1074	0.333	0.3577	1.4713	0.1665	0.0183

Even if these aspects will not be deeply investigated in this thesis, further modifications of the CES parameters focused on overcoming the limitations in the description of the volumetric properties in the supercritical region and at low reduced temperatures and for large acentric factor were developed [52, 58].

Moreover, it is well known that the two-parameter CESs usually fail in the description of the liquid volumetric properties. Since the functional form of the pressure-volume relationship is important for the representation of the volumetric properties, different CESs with additional parameters were proposed to overcome this drawback. In particular, it was shown that three-parameter CESs with different empirical correction terms applied to the liquid volume provided accurate values of liquid volumes except near the critical point [58]. A group contribution volume translated PR EoS was recently proposed by Bell et al. [107] and was applied to estimate the VLE and single-phase densities of blends containing low GWP refrigerants. The authors showed that the proposed EoS offered better results than the original PR and competitive results with the more complex fundamental EoSs explicit in Helmholtz energy. Therefore, they could be used for the study of alternative refrigerant blends for which insufficient experimental data are available.

Besides, different CESs with four or five parameters were proposed, but they only lead to only small improvements of the accuracy because of the fundamental limitations of the cubic form. Moreover, the issue of which CESs with the same number of parameters provides the best results does not have a universal answer [58]. As stated by Martin [108] in his detailed analysis of the volumetric descriptions of different two-parameter CESs, "no one equation stands clearly above the others". All CESs usually give a poor performance in a relatively wide region near the critical point [58]. Moreover, these models presented limitations in the prediction of properties of polar and associating substances. However, it was showed that CESs with more than three parameters obtained from critical properties and measured liquid volumes and vapor pressures can provide a sufficiently accurate description of the volumetric properties of complex substances [52]. But, they cannot be extrapolated outside the temperature and pressure ranges where the parameters were fitted.

Carnahan-Starling-De Santis equation of state

Even if the original van der Waals EoS and several its modifications, such as the CESs, were developed based on simple molecular concepts, many of these EoSs can be considered nothing more than comprehensive empirical correlations of fluid properties [58]. Although the CESs can provide sufficiently accurate results, their major weakness is that neither their repulsive not their attractive terms reflect the physical reality. Therefore, different researches tried to develop EoSs with clear physical foundations [58].

Some of these EoSs were still based on the van der Waals theory but they had theoretically defined terms to model the effects of repulsive forces. Among them, Carnahan and Starling [109] proposed a famous expression for the repulsion term of

Equation (2.18) (P_{R}), based on the hard-sphere theory. The expression is:

$$P_{\mathrm{R}} = \frac{RT}{v_{\mathrm{m}}} \frac{1 + \eta + \eta^2 - \eta^3}{(1-\eta)^3} \tag{2.23}$$

where $\eta = b\,(4v_{\mathrm{m}})^{-1}$. This expression was combined with several attraction pressure terms, such as the one proposed by De Santis et al. [110] defines as:

$$P_{\mathrm{A}} = -\frac{a}{v_{\mathrm{m}}\,(v_{\mathrm{m}} + b)} \tag{2.24}$$

Therefore, the so-called Carnahan-Starling-De Santis (CSD) EoS was obtained by combining Equations (2.23) and (2.24) and it is defined as follows:

$$P = \frac{RT}{v_{\mathrm{m}}} \frac{1 + \eta + \eta^2 - \eta^3}{(1-\eta)^3} - \frac{a}{v_{\mathrm{m}}\,(v_{\mathrm{m}} + b)} \tag{2.25}$$

Solving Equation (2.25) for v_{m} requires finding the roots of a fifth-degree polynomial equation. In the two-phase region, two of these roots are related to the volume of saturated liquid and vapor. Instead, one of the roots is in the intermediate range between the former two values and the remaining two roots, if real, have no physical meaning [110].

Among the several expressions developed to describe the temperature dependence of a and b coefficients, Morrison & McLinden [111] proposed the following equations expressly oriented to refrigerants and their blends:

$$a = a_0 \exp\left(a_1 T + a_2 T^2\right) \tag{2.26}$$

$$b = b_0 + b_1 T + b_2 T^2 \tag{2.27}$$

The coefficients of the previous equations are determined for a specific refrigerant by fitting them to experimental values of saturation liquid and vapor volumes and the equilibrium vapor pressure. The CSD EoS with aforementioned expressions of the parameters was applied to accurately estimate different thermodynamic properties of pure refrigerants and mixtures [112, 113]. Moreover, as it will be explained in Subection 2.4.2, this EoS was used in the flash method for the VLE assessment for binary systems containing refrigerants from two-phase $PvTz$ data measured with an isochoric apparatus. This method with the CSD EoS was also used for the VLE derivations of the binary systems containing alternative refrigerants reported in this work and the results are provided in Section 4.1 of Chapter 4.

Multiparameter equations of state

Since the complexity of the property behavior of several fluids cannot be represented with high accuracy with the previous described EoSs, several accurate non-analytic EoSs characterized by high levels of complexity and several fitted parameters were proposed [52, 58]. Among them, the multiparameter EoSs are practical empirical models developed for accurately calculating or deriving all the thermodynamic properties of fluids on the basis of specific thermodynamic property formulations. In particular, these equations are empirical, even if virtually all are based upon sound theoretical principles [58]. The development of accurate and thermodynamic consistent multiparameter

EoSs for a pure fluid with optimized functional forms requires that these models are fitted to different suitable and accurate experimental data (e.g. PvT properties, phase-equilibrium data, isobaric heat capacities at gaseous and supercritical states, speeds of sounds, etc.). Moreover, these EoSs can be constrained to exactly represent specific properties at specific thermodynamic states, such as the critical point, by determining their coefficients with a weighted and constrained fitting procedure [58].

Several modern multiparameter EoSs for estimating the properties of fluids are fundamental equations explicit in the Helmholtz energy as a function of density and temperature. By using the fundamental Helmholtz energy EoSs, all the thermodynamic properties may be estimated without additional equations for saturation properties through the use of the Maxwell criterion [58]. However, perhaps the most common form of the multiparameter EoSs in technical applications is the pressure explicit for, such as the Benedict-Webb-Rubin EoS and its modified version [66].

As mentioned in the previous chapter, different multiparameter EoSs are used in REFPROP [63–65] for the calculation of accurate values of different thermodynamic properties of refrigerants and their blends. In particular, the last version of the software (REFPROP 10.0 [65]) uses the fundamental EoSs explicit in Helmholtz energy [58] specific for each fluid and the modified Benedict-Webb-Rubin EoS [66].

Different generalized models can be used to extend the multiparameter EoSs to blends of fluids. Among them, some mixture models use the Helmholtz-Energy EoSs for the pure fluids and an excess function to account for the interaction between different species [58]. In particular, multi-fluid Helmholtz-energy-explicit mixture models are used in REFPROP 10.0 for the property calculations for blends [67].

The values calculated from REFPROP 10.0 were compared with the experimental $PvTz$ data of binary systems containing low GWP refrigerants measured with an isochoric apparatus. The obtained results are reported in Section 4.1 of Chapter 4.

2.2.2 Mixing rules

To use the EoSs for describing the thermodynamic properties and the phase behavior of blends of fluids, a composition dependence for the EoS parameters has to be introduced. In this regard, several mixing and combining rules have been proposed to extend the use of EoSs developed for pure substances to blends. All mixing and combining rules are, at least partially, empirical in nature, since there is no exact statistical mechanical solution relating the properties of dense fluids to their intermolecular potentials, or detailed information available about intermolecular potential functions [58].

However, several mixing rules have been developed on the basis of some thermodynamic boundary conditions [58]. In particular, it was showed from the statistical mechanics that the only composition dependence of the coefficients of virial EoS of Equation (2.1) for blends is given by:

$$B = \sum_i \sum_j x_i \, x_j \, B_{ij}(T) \tag{2.28}$$

$$C = \sum_i \sum_j \sum_k x_i \, x_j \, x_k \, C_{ijk}(T) \text{ and so forth.} \tag{2.29}$$

Since Equations (2.28) and (2.29) are exact, they can be considered low-density boundary conditions that should be satisfied for blends by other EoSs when expanded into the virial form. Although there is no exact high-density boundary condition for

EoSs for blends, another boundary condition that could be imposed is that the excess free energy of mixing calculated from an EoS has to be equal to excess free energy of mixing calculated from an activity coefficient model [58].

It worthwhile pointing out that, although the coefficients of the virial EoS for a blend can be calculated from Equations (2.28) and (2.29) on the basis of the statistical mechanics, different empirical expressions can be used to estimate the virial coefficients of blends. For example, it is possible to assume that the second and third virial coefficients for blends can present the following functional form in T and z_i:

$$B = B_1 \ln T + \frac{B_2}{T} + B_3 z_i^2 + B_4 z_i + B_5 \tag{2.30}$$

$$C = C_1 \ln T + \frac{C_2}{T} + C_3 z_i^2 + C_4 z_i + C_5 \tag{2.31}$$

where the constants B_i and C_i ($i = 1...5$) are determined by minimizing the average absolute relative deviations between the experimental and calculate values. Equations (2.30) and (2.31) were used to correlate the vapor-phase $PvTz$ properties of binary systems containing low GWP refrigerants measured with an isochoric apparatus. The results are reported in Section 4.1 of Chapter 4.

Among the many mixing rules proposed over the years, the van der Waals one-fluid mixing rules have been widely used, and are still used, to extend the two-parameter EoSs based on van der Waals EoS and theory, such as the CESs and the CSD EoS [110], to several hydrocarbon and refrigerant blends [58]. The basic assumption of these mixing rules is that an EoS used for pure fluids can be used for blends if a suitable way is found for obtaining the EoS parameters of the blends. The method for doing this is based the boundary condition of Equation (2.28)[58]. In fact, to satisfy this boundary condition, the composition dependence of the two parameters of the EoSs for blends has to be expressed as follows:

$$a = \sum_i \sum_j x_i x_j a_{ij} \tag{2.32}$$

$$b = \sum_i \sum_j x_i x_j b_{ij} \tag{2.33}$$

Usually, to estimate the cross coefficients a_{ij} and b_{ij} from the pure component parameters, the following combining rules are used:

$$a_{ij} = \left(a_i a_j\right)^{0.5} \left(1 - k_{ij}\right) \tag{2.34}$$

$$b_{ij} = \frac{1}{2} \left(b_i + b_j\right) \left(1 - l_{ij}\right) \tag{2.35}$$

where k_{ij} and l_{ij} are the binary interaction parameters which range between -1 and 1. These parameters are usually obtained by fitting the calculated values to the experimental phase equilibrium and volumetric data [58]. Moreover, they can be constants, functions of T, or functions of the composition. Usually, l_{ij} is set to zero and Equation (2.33) becomes:

$$b = \sum_i x_i b_i \tag{2.36}$$

Equations (2.32) and (2.36) are called the van der Waals one-fluid mixing rules with a single binary interaction parameter, also known as the standard one-binary-parameter mixing rules [58]. In fact, since $k_{ij} = k_{ji}$, the mixing rules have only one binary interaction parameter. As explained below, these mixing rules were used to extend the studied CESs and the CSD EoS [110] to binary systems containing low GWP refrigerants for the estimation of their VLE behaviors.

Even if this aspect is not investigated in this thesis, it is important to point out that the van der Waals one-fluid mixing rules with a single binary interaction parameter are usually not adequate for multi-component systems involving organic chemicals and highly non-ideal blends [58].

An empirical approach to overcome the drawbacks of the van der Waals one-fluid model for the EoSs based on van der Waals EoS and theory was the introduction of more than one binary interaction parameter in the conventional mixing rules [58]. However, also these mixing rules provided inaccurate results for highly nonideal and polar blends of organic compounds [58]. Moreover, these multiparameter mixing rules showed several problems that limit their use for blends containing many compounds, or to blends which contain some species with similar characteristics [58].

Later, to describe the thermodynamic properties and phase equilibria of strong non-ideal blends [58], different mixing rules that combine the activity coefficient (or excess Gibbs free energy) models with the CESs were proposed, such as the Huron-Vidal mixing rules [114] and the Wong-Sandler mixing rules [115]. However, these mixing rules are characterized by high complexity and a high number of parameters [58].

2.3 Vapor pressure

The vapor pressure, or saturation pressure, (P_{sat}) is the pressure of a pure fluid that coexists in liquid and vapor phases at thermodynamic equilibrium in a closed system. This pressure is defined as the unique pressure condition where boiling (bubble) can occur in the liquid and droplets (dew) can occur in the vapor at a specific temperature. The values of the vapor pressure of different substances are particularly important for different engineering applications, such as for designing separation processes [55]. Moreover, as concern pure refrigerants, this property is one of the main thermodynamic properties needed to estimate their potential thermodynamic performances in refrigeration and air conditioning applications.

In addition to the possibility to directly measure this property by using different experimental techniques (e.g. some of the methods used to measure the PvT behavior of fluids), models based on thermodynamic conditions of phase equilibrium were proposed to estimate and correlate P_{sat} of several fluids as a function of the temperature.

In general, a closed multi-phase system is in a state of thermodynamic equilibrium when the thermal equilibrium, the mechanical equilibrium, and the phase equilibrium occur simultaneously [54, 55, 88]. While the first two conditions correspond to the equality of T and P in all phases, the phase equilibrium is expressed as the equality of the Gibbs energy, G, of the pure fluid in the phases [55, 88]. In particular, for a closed system with liquid (L) and vapor (V) phases, the phase equilibrium condition is expressed as:

$$G^{\text{L}} = G^{\text{V}} \tag{2.37}$$

It was demonstrated that, since the fundamental independent variable to define G are T and P, the state of thermodynamic equilibrium implies that$G$ of the pure fluid at constant T and P is minimized at a constant value, equal for all the phases [55, 88].

The conditions for the phase equilibrium of multi-component systems will be explained in more detail in Section 2.4.

By applying the aforementioned conditions for the phase equilibrium to closed liquid-vapor phase systems, the Clapeyron equation for the estimation of P_{sat} of pure fluids was developed [52, 55]. Several of the most well-known and used vapor pressure estimation correlations were obtained from the Clapeyron equation, such as a simple equation to describe the vapor pressure dependence on the temperature at low temperature, called Clausius-Clapeyron equation [52]. An additional well-known equation for the estimation of the vapor pressure of pure fluids as function of the temperature, based on the Clapeyron equation and presenting coefficients regressed on experimental data, is the Antoine equation [52]. Instead, different forms of an empirical equation for the vapor pressure based on an elaborate statistical method, called Wagner equation, are also widespread models for the estimation of this property of several fluids in different temperature and pressure ranges [52].

A more general approach to estimate P_{sat} of pure fluid is based on a proper application of Equation (2.37). In principle, the phase-equilibrium problems of pure fluids could be solved by calculating the Gibbs energy from the PvT properties of fluids [55]. However, an alternative property, called fugacity, f, has been usually applied in phase equilibrium calculations. In fact, f can be directly related to the measurable volumetric properties under the correct conditions and it can be calculated from experimental PvT data or values estimated from correlations or EoSs. Moreover, since its application to blends is a straightforward extension of its application to pure fluids, the fugacity has one advantage over the Gibbs energy. Moreover, this property has some empirical appeal since it is possible to show that the fugacity of an ideal gas equals the pressure and the fugacity of a liquid in equilibrium with an ideal gas equals the vapor pressure under common conditions; in fact, f can be considered a "corrected pressure" of the real fluids [54, 55]. In particular, the fugacity is correlated to the Gibbs energy departure of a fluid at a fixed T and P by the following equation:

$$d(G - G^{ig}) = RT\, d\ln\left(\frac{f}{P}\right) = RT\, d\ln(\phi) \tag{2.38}$$

where $(G - G^{ig})$ is the Gibbs energy departure, G^{ig} is the Gibbs energy of an ideal gas at the same T and P and ϕ is the dimensionless fugacity coefficient which is a measure of non-ideality of fluids [55]. In practice, ϕ is directly evaluated from experimental data or EoSs, and then the fugacity is calculated. For a closed vapor-liquid phase system of a pure fluid, it can be showed that Equation (2.37) can be rewritten in terms of f as follows:

$$f^{L} = f^{V} \tag{2.39}$$

Equation (2.39) is called isofugacity condition. In general, the most common method to estimate the properties of different phase equilibria consists of the calculation of fugacities and equating their values in each phase. In particular, this approach can be also used to estimate P_{sat} of some fluids, such as refrigerants, by iteratively calculating ϕ of liquid and vapor phases from EoSs until the isofugacity condition is fulfilled [55].

The vapor pressures of 9 low GWP refrigerants estimated using an iterative algorithm based on the isofugacity condition and cubic equations of state are presented in this thesis. In particular, the accuracy of different CESs for the vapor pressure of these alternative refrigerants was tested. The obtained results were compared with the experimental data available in the literature. These results have been already presented elsewhere [116].

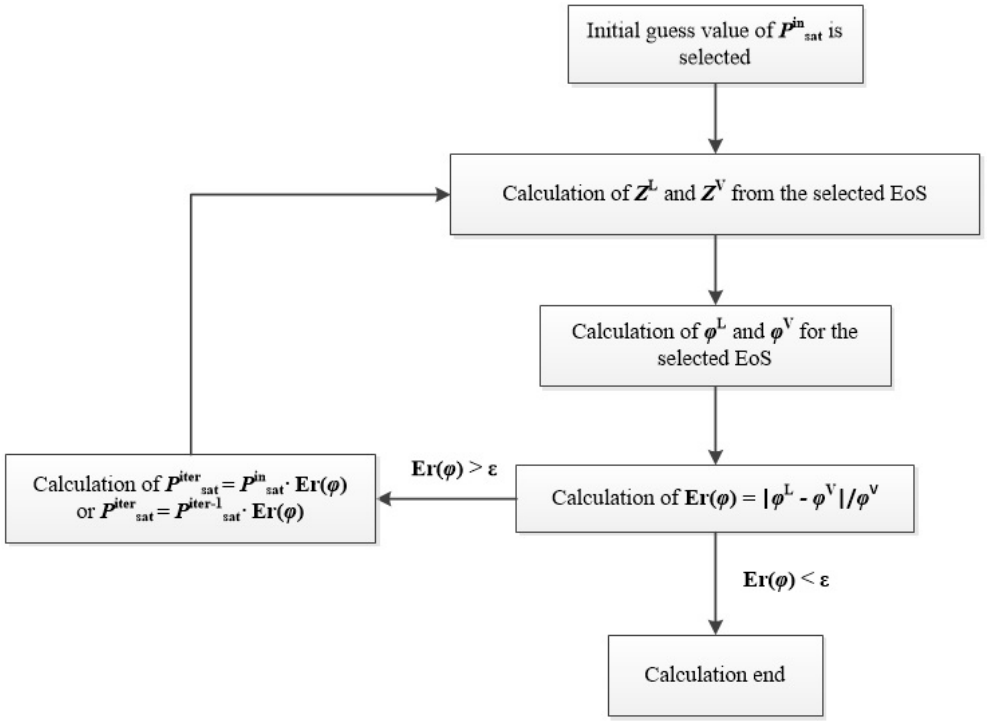

Figure 2.1: Flow chart of the algorithm used to estimate the vapor pressure of pure refrigerants from equations of state.

2.3.1 Vapor pressure of low GWP refrigerants

An iterative algorithm based on the isofugacity condition calculated by using four CESs was tested to estimate P_{sat} for 9 low GWP refrigerants on the basis of the same set of experimental data collected from the literature. The flow chart of the iterative algorithm is showed in Figure 2.1. In the algorithm, the initial guess P_{sat}, called P^{in}_{sat} in Figure 2.1, is randomly selected in a range centered on the experimental P_{sat} at the studied temperature. Instead, the compressibility factor (Z) of the liquid and vapor phases and the P_{sat} calculated in each iteration are called Z^L, Z^V and P^{iter}_{sat} in Figure 2.1. Moreover, the residual value, called ϵ in Figure 2.1, is equal to a suitable small value (usually $\sim 1 \cdot 10^{-10}$).

Table 2.2 presents the characteristics of the CESs used in the algorithm. The well-known Redlich-Kwong-Soave EoS [102] and Peng-Robinson EoS [103], called RKS and PR in Table 2.2, respectively, were studied. Besides, several modified and new equations proposed by Stryjek [105, 106] were tested, but only the results of the most accurate models are given in this work. In the end, the results of a modified PR EoS, called PR mod in Table 2.2, and a CES proposed by Stryjek, not systematically studied till now, called CES(A) in Table 2.2, are presented. The general expression to calculate ϕ of pure fluids with the CESs is reported in Appendix A.

Table 2.3 shows the references to the original sources, the number of experimental points, and the temperature ranges for the selected low GWP refrigerants. In particular, several of these experimental data were measured through an isochoric apparatus used to measure the PvT and $PvTz$ properties of refrigerants and their blends, respectively.

Table 2.3: Vapor pressure experimental data for low GWP refrigerants (updated in January 2018).

Refrigerant (ASHRAE Designation)	Ref.	N. points	T range K
R1123	[79]	13	300 - 331
	[117]	27	277 - 331
R1234yf	[118]	34	224 - 366
	[119]	40	246 - 343
	[120]	30	250 - 320
	[121]	11	310 - 360
R1243zf	[122]	83	234 - 373
	[117]	20	310 - 376
R1234ze(E)	[123]	78	223 - 353
	[124]	10	253 - 293
	[125]	30	261 - 280
	[126]	17	300 - 380
	[127]	7	310 - 380
	[128]	15	303 - 373
R1234ze(Z)	[129]	64	238 - 373
	[130]	19	310 - 420
	[131]	4	353 - 413
	[126]	22	300 - 400
R1225ye(Z)	[86]	95	233 - 366
R1233zd(E)	[132]	16	263 - 353
	[133]	81	234 - 375
	[83]	23	280 - 438
R1336mzz(Z)	[134]	13	324 - 443
R1336mzz(E)	[135]	17	323 - 403

Moreover, Vapor-Liquid Equilibrium (VLE) apparatus and densimeters were used to measure this property of pure refrigerants. The P_{sat} uncertainty of many of the collected data is of the order of ± 1 kPa. Since they were considered suitable for this study, almost all the adopted physical properties of the studied refrigerants were collected from Lemmon et al. [64].

Table 2.4 summarizes the Average Absolute Relative Deviation of the pressure, AARD(ΔP) %, of the four CESs for the selected alternative refrigerants. In particular, AARD(ΔP) % is defined as:

$$\text{AARD}\,(\Delta P)\,\% = \frac{100}{N}\sum_{i=1}^{N}\left|\frac{P_{i,\text{exp}} - P_{i,\text{calc}}}{P_{i,\text{exp}}}\right| \tag{2.40}$$

where N is the number of the experimental data, P_{exp} is the experimental pressure and P_{calc} is the calculated pressure.

As shown in Table 2.4, the results of all the studied CESs are sufficiently accurate and quite similar. In particular, the AARD(ΔP) % obtained through the four models are less than 2 %. However, it is possible to note that CES(A) generally gave lower deviations between the calculated and experimental P_{sat} than the other models while RKS gave slightly higher deviations. The goodness of CES(A) for most of the refrigerants is

Table 2.4: Deviations between experimental and calculated vapor pressures of pure low GWP refrigerants.

Refrigerant	N. points	AARD(ΔP) %			
		RKS	PR	PR mod	CES(A)
R1123	40	0.426	0.524	0.474	0.603
R1234yf	115	1.099	0.286	0.372	0.256
R1243zf	103	1.082	0.313	0.31	0.206
R1234ze(E)	157	0.989	0.274	0.253	0.305
R1234ze(Z)	109	1.423	0.615	0.527	0.461
R1225ye(Z)	95	0.98	1.056	0.885	1.013
R1233zd(E)	120	1.87	1.406	1.202	1.153
R1336mzz(Z)	13	1.058	0.336	0.334	0.335
R1336mzz(E)	17	1.118	0.616	0.617	0.601
Avg.	-	1.191	0.624	0.564	0.549

also visible in Figure 2.2, where the relative deviations of the vapor pressure data, $100\,(P_{\mathrm{sat,exp}} - P_{\mathrm{sat,calc}})/P_{\mathrm{sat,exp}}$, for the studied fluids versus the reduced temperature, T_{r} are shown. Moreover, Figure 2.2 shows that this equation provided accurate results in all the studied reduced temperature range, except below $T_{\mathrm{r}} = 0.6$. Since the CESs with Soave's α function are inaccurate for the vapor pressure calculation at low reduced temperature (less than 0.6) and large acentric factor [58], this behavior could be expected. Moreover, as shown in the next section, the studied CESs were also tested for the description of VLE of binary systems containing low GWP refrigerants. Therefore, to confirm their reliability for the vapor pressure representation of the conventional refrigerant contained in the studied binary systems, deviations for R32 were reported in Figure 2.2 as an example. The experimental P_{sat} for R32 were collected from Fu et al. [136] and Malbrunot et al. [137].

However, as can be noted both in Table 2.4 and in Figure 2.2, CES(A) gives higher deviations for R1225ye(Z) and R1233zd(E) than the ones for the other refrigerants. Since all the studied CESs give poor results for these two fluids, it should be considered that this lack of accuracy is due to shortcomings in the experimental measurements or the reliability of the physical parameters used in the work. As visible in Figure 2.2, the high deviations for the R1233zd(E) could be caused by both the calculated data at $T_{\mathrm{r}} < 0.6$, that are inaccurate,and the scattered point in the T_{r} range from 0.6 to 0.8. After an in-depth evaluation of the results, these less accurate results were obtained from the experimental data reported in Hulse et al. [132]. Moreover, Table 2.4 shows that the modified PR EOS proposed by Stryjek [105, 106], called PR mod in this table, provides a better estimation of the vapor pressure for almost all the refrigerants than the original PR EoS.

2.4 Phase equilibria of multi-component systems

The phase-equilibrium thermodynamic properties of blends of fluids, such as temperatures, pressures, specific volumes and equilibrium compositions of the different phases, are needed for the design of components of several engineering systems, e.g. separation processes, chemical, and biochemical product design [54, 56]. In particular, to evaluate their potential performances in refrigeration and air conditioning

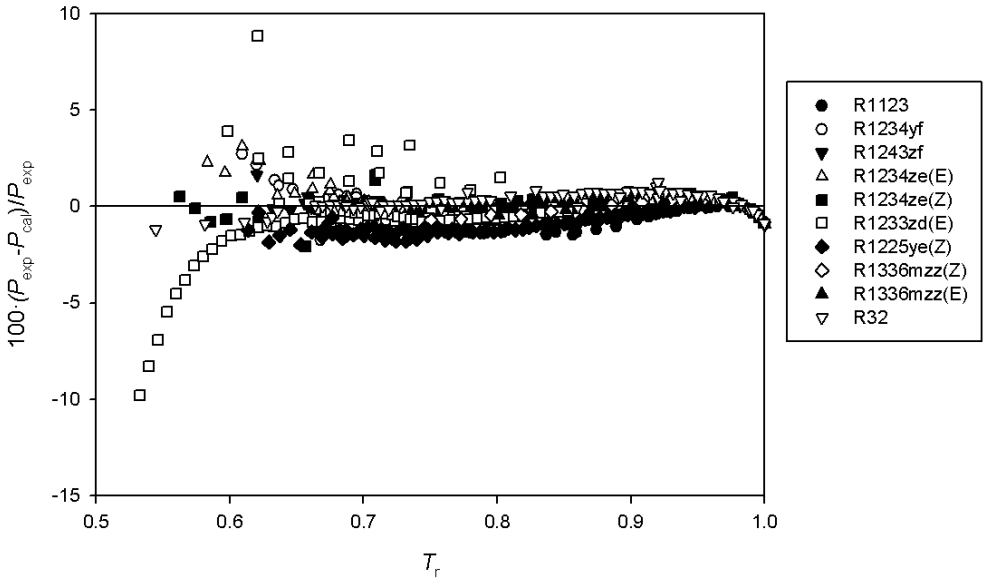

Figure 2.2: Relative deviations of the vapor pressure data, $100 \cdot (P_{\mathrm{sat,exp}} - P_{\mathrm{sat,calc}})/P_{\mathrm{sat,exp}}$, versus the reduced temperature, T_{r}. The data were calculated from CES(A) in Table 2.2.

applications and select the optimal compositions for design and operation purposes, it is necessary to know the phase-equilibrium properties of blends of refrigerants, such as Vapor-Liquid Equilibrium (VLE) and Solid-Liquid Equilibrium (SLE) properties. Consequently, the experimental data for the phase equilibria of multicomponent systems are requested for the aforementioned reasons. However, these data can be scarce and the methods used for their measurements can be laborious and costly even for well-known multi-component systems of industrial importance [56]. Therefore, several models and techniques for the calculation of phase equilibria of different blends have been developed based on the equations that determine the state of thermodynamic equilibrium between all the phases.

The starting point for all the models used for phase equilibrium estimations of multi-component systems is the phase equilibrium criterion. As well as for the pure fluids, the phase equilibrium of a multi-component system occurs when G for each component is minimized at a constant value equal for all the phases. However, this condition of equilibrium for blends is usually expressed in terms of chemical potential, μ. The phase equilibrium of a component i between different phases π occur when the following necessary condition is verified [54]:

$$\mu_i^{\alpha} = \mu_i^{\beta} = ... = \mu_i^{\pi} \tag{2.41}$$

Since μ_i is the partial molar Gibbs energy of the i-th component, it is possible to show that the phase equilibrium condition expressed as equality of Gibbs energy of i-th component between equilibrium phases is equivalent to the condition of Equation (2.43) [54]. However, since the chemical potential of a component does not have a simple relation to physically measurable properties, it is necessary to express the chemical

potential in terms of some auxiliary property that can be directly related to the measurable PvT properties and compositions under the correct conditions [54]. As for the pure component, a useful auxiliary function was found in the concept of fugacity, f. It was showed that the change in the chemical potential for an isothermal change for any component in any system in any phase (solid, liquid or vapor or gas) can be expressed as [54]:

$$\mu_i - \mu_i^0 = RT \ln \frac{f_i}{f_i^0} \tag{2.42}$$

where μ_i^0 and f_i^0 are the chemical potential and fugacity standard states, respectively; even if they are arbitrary, these two values can not be chosen independently [54]. From Equation (2.42), it is possible to show that the necessary conditions for the phase equilibria for all components in a multi-component system can be expressed as the equality of fugacities of the components for all phases. The resulting expression for the i-th component is:

$$f_i^\alpha = f_i^\beta = ... = f_i^\pi \tag{2.43}$$

These conditions are called isofugacity conditions. The fugacity is a "corrected partial pressure" for a component of a blend that take into account the non-idealities that can be interpreted by molecular considerations [54]. In fact, this value for a component of a blend of ideal gasses is equal to the partial pressure of that component. Moreover, the fugacity can be considered as the "tendency" of a molecule to leave from one phase to another; in fact, phase equilibria are dynamic ones [56].

By using Equation (2.43), the mathematical problem for phase equilibria is solved [56]. Considering the degree of freedom (e.g. independent variables) given by the thermodynamic relations or constraints (e.g. the Gibbs-Duhem equation), the models used the isofugacity conditions to estimate the values of some of the equilibrium properties of the multi-component systems by fixing the remaining ones as inputs [54].

It is important to note that Equation (2.43) can be expressed in different forms depending on the type of the phase equilibria studied and also the nature of the thermodynamic models used for the estimations of the properties (e.g. EoSs, activity coefficient models, etc.). In fact, even if they are all derived from Equation (2.43) by considering suitable assumptions, the additional expressions of the phase equilibria are sometimes simpler to use in practical problems than the general one [56]. For example, a simplified expression known as Raoult's law can be used to describe the VLE of ideal liquid systems with an ideal vapor phase; instead, complex equations were proposed for the estimation of SLE of multicomponent systems at high pressures [56].

The VLE of blends of refrigerants is usually described by using the following equation:

$$y_i \, \phi_i^{\mathrm{V}} = x_i \, \phi_i^{\mathrm{L}} \tag{2.44}$$

where the fugacity coefficients of the i-th compound for the vapor and liquid phases are calculated from EoSs by using the equations below:

$$RT \ln \phi_i = RT \ln \frac{f_i}{y_i P} = \int_{v_\mathrm{m}}^{\infty} \left[\left(\frac{\partial P}{\partial n_i} \right)_{T, v_\mathrm{m}, n_\mathrm{j}} - \frac{RT}{v_\mathrm{m}} \right] dv_\mathrm{m} - RT \ln \left(\frac{P v_\mathrm{m}}{RT} \right) \tag{2.45}$$

$$RT \ln \phi_i = RT \ln \frac{f_i}{y_i P} = \int_0^P \left(v_{\mathrm{m},i} - \frac{RT}{P} \right) dP \tag{2.46}$$

Equations (2.45) and (2.46) are suitable for EoSs of the type $P = F(v_\mathrm{m}, T)$ and EoSs of the type $v_\mathrm{m} = F(P, T)$, respectively [56].

It is worthwhile pointing out that, in principle, the approach based on Equation (2.44) and the EoSs, called $\phi - \phi$ approach, is suitable for all types of fluid phases, thermodynamic conditions and any types of multi-component systems. However, this approach is traditionally considered suitable only for describing VLE of rather simple systems, such as mixtures of hydrocarbons, refrigerants, and inorganic gases, at high and moderate pressures [54, 56]. Instead, different equations based on an approach where the activity coefficient models are used for the description of the liquid or solid phases (called $\gamma - \phi$ approach) are traditionally employed for the description of Liquid-Liquid Equilibrium (LLE) and SLE and also the VLE of complex systems at moderate and low pressures [56]. However, the distinction between the two approaches is not of a fundamental character but rather a traditional one due to model and calculation limitations used in the previous century [56]. The $\phi - \phi$ approach can be used with all components at all conditions if more complex EoSs and mixing rules are considered in the elaboration [138].

The models based on the $\phi - \phi$ approach allow us to solve different types of VLE problems of multi-component systems, providing the values of different equilibrium properties by fixing the remaining ones as inputs. For example, for a multi-component vapor-phase system, it is possible to estimate the values of P and mole fractions of vapor phases (y_i) from these models by fixing the values of T and mole fractions of the liquid phases (x_i). This type of VLE problem is one of the most studied and is called the bubble-point P problem [52].

The VLE properties of 25 binary systems containing low GWP refrigerants estimated by using an iterative algorithm based on the $\phi - \phi$ approach are reported below. The CESs reported in Table 2.2 were used in the algorithm. The results were compared with the experimental data available in the literature. These results have been already presented elsewhere [116, 139].

A particular type of VLE problem is estimating the two-phase equilibrium properties when either a liquid of known composition is partially vaporized or a vapor of known composition is partially condensed due to a change in T and/or P. This problem is generically called flash calculation [138]. Although the $\phi - \phi$ approach can be used in these cases, the partial vaporization or partial condensation problems are usually more difficult to solve than the other VLE problems [138]. The equilibrium compositions of liquid and vapor phases are unknown in the flash calculation. Therefore, in addition to the equations of the isofugacity conditions and the composition restrictions, the component mass balance equations have to be used to solve these problems at constant temperature [138]. A more complex calculation is necessary for the flash processes that do not take place at constant temperature; in fact, the energy balance has also to be included in the calculation, which makes the solution much more tedious [138]. As will be explained below, a method based on the flash calculation, so-called flash method, have been proposed to derive the VLE properties of binary systems of refrigerants from two-phase $PvTz$ properties measured by using an isochoric apparatus [140]. This thesis presents the results obtained by applying this approach for the VLE assessment from isochoric measurements of binary systems containing low GWP refrigerants in the two-phase region. These results are reported in Section 4.1 of Chapter 4.

Since the SLE of multi-component systems depends both on the crystals formed in solution and on the properties of the liquid phase, different equations for the SLE description of multi-component systems studied in different temperature and pressure conditions have been proposed [56]. However, it was shown that many organic binary systems, such as several binary systems of refrigerants, present a solid phase formed by pure system components and an eutectic point [141, 142]. The behavior of the

temperatures where the solid crystals begin to form (*liquidus*) of this type of organic systems is well described by the Schröder equation [143]. This simplified equation describes the solubility of the solid solute in the solvent by neglecting the difference between the heat capacity of the subcooled liquid solute and the solid solute, and it has the following form:

$$\ln\left(\gamma^* z^*\right) = -\frac{\Delta h_{\text{fus}}}{RT}\left(1 - \frac{T}{T_{\text{m}}}\right) \tag{2.47}$$

where γ^* is the activity coefficient of the solute, z^* is the mole fraction of the solute, Δh_{fus} is the enthalpy of fusion at the melting point and T_{m} is the temperature at the melting point. As will be shown in Section 4.2 of Chapter 4, the SLE behavior provided by this simplified equation was compared with the experimental SLE data of a binary system containing low GWP refrigerants measured with a specific experimental setup.

2.4.1 VLE of binary systems containing low GWP refrigerants

An iterative algorithm based on the $\phi - \phi$ approach was used to describe the VLE behavior of 25 binary systems containing low GWP refrigerants. The used algorithm allowed to solve the bubble-point P problem for the studied binary systems and its flow chart is reported in Figure 2.3. In the algorithm, the initial guesses for the bubble point pressure, called P^{in} in Figure 2.3, and the distribution factor (or K-factor) for the components of the binary systems (K_i) were calculated through the following expressions:

$$P^{\text{in}} = \sum_i x_i \, P_{\text{sat},i}(T) \tag{2.48}$$

$$K_i = \frac{y_i}{x_i} = \frac{P_{\text{sat},i}(T)}{P} \tag{2.49}$$

Equations (2.48) and (2.49) were obtained by assuming ideal liquid and vapor binary systems. The compressibility factor (Z) of the liquid and vapor phases, the bubble point pressure and vapor phase mole fractions calculated in each iteration are called Z^{L}, Z^{V} P^{iter} and $y_{\text{i}}^{\text{calc}}$ in Figure 2.3, respectively. Moreover, the residual value, called ϵ in Figure 2.3, is equal to a suitable small value (usually $\sim 1 \cdot 10^{-10}$).

To test their accuracy for the VLE description of the selected binary systems, the CESs reported in Table 2.2 were used in the algorithm. The van der Waals one-fluid mixing rules with a single binary interaction parameter (k_{ij}), described in Subsection 2.2.2, was used to extend the CESs to the studied binary systems. In particular, this parameter was regressed by minimizing the deviations between the calculated and experimental pressure for complete datasets and by minimizing the deviations for each isotherm. The Nelder-Mead algorithm [144] was used in addition to the iterative algorithm to obtain k_{ij} by minimizing the AARD(ΔP) % (defined as Equation (4.5)). The expressions to calculate ϕ of the components of the binary systems trough the CESs and the van der Waals one-fluid mixing rules are reported in Appendix A.

Reliable experimental VLE data of the selected binary systems were collected from the literature and compared with the calculated ones. In particular, the collected data were measured employing different Vapor-Liquid Equilibrium (VLE) apparatus and their uncertainties of P, T and mole fractions are usually of the order of $\pm$1 kPa, $\pm$0.005 K and $\pm$0.01, respectively. Since the simple EoSs under analysis are often inaccurate in the description of the properties of asymmetric systems and the deviations between the

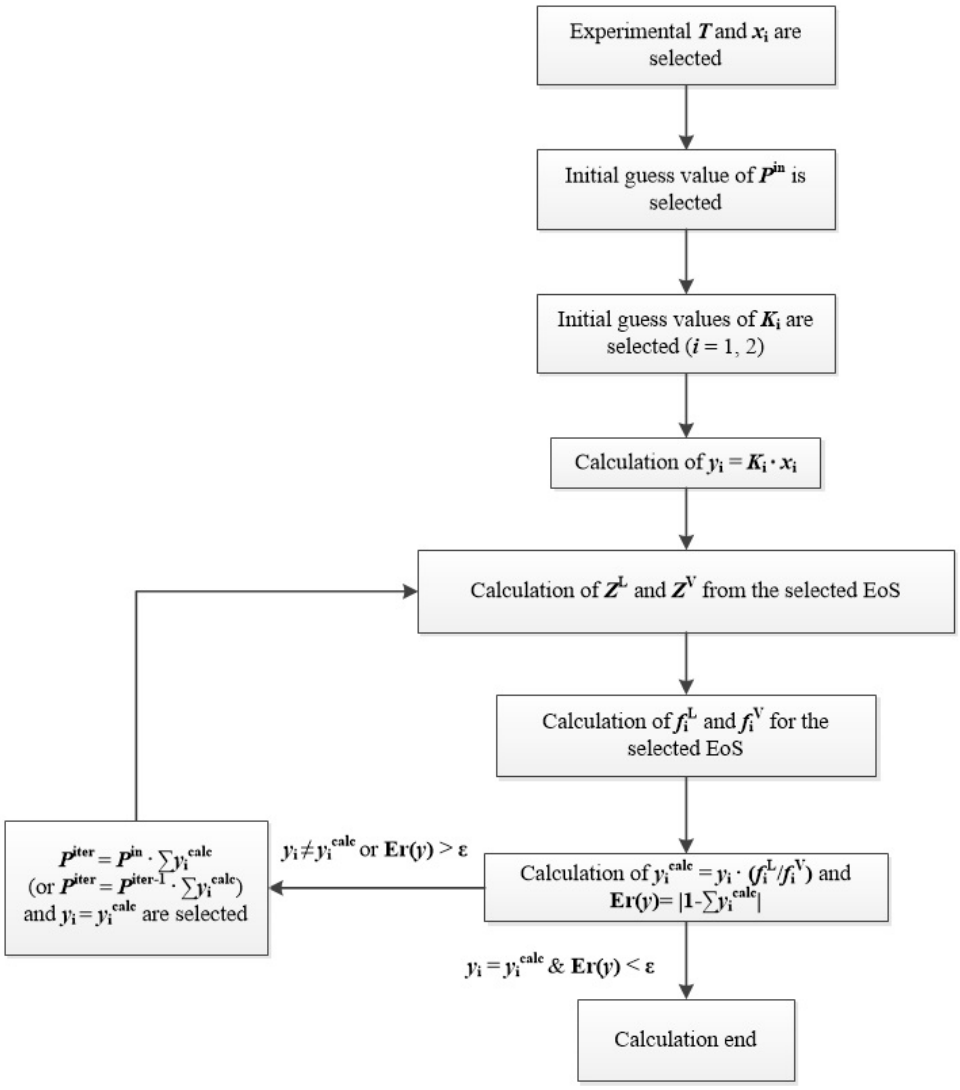

Figure 2.3: Flow chart of the algorithm used to estimate the vapor-liquid equilibrium of binary systems from equations of state.

Table 2.5: Experimental VLE data for low GWP refrigerant binary systems (updated in January 2018).

Binary system	Ref.	N. isotherms (N. points)	T range K
R1233xf + R244bb	[85]	3(30)	323.15 - 303.15
R1234yf + R1233xf	[85]	3(30)	313.15 - 293.15
R1234yf + R152a	[145]	5(60)	323.15 - 283.15
R1234yf + R227ea	[146]	5(50)	323.15 - 283.15
R1234yf + R244bb	[147]	3(30)	313.15 - 293.15
R1234yf + R245cb	[148]	4(44)	313.15 - 283.15
R1234yf + R290	[149]	5(54)	293.15 - 253.15
R1234yf + R600a	[150]	5(60)	323.15 - 283.15
R1234ze(E) + R290	[151]	4(38)	283.15 - 258.15
R1234ze(E) + R600a	[152]	4(40)	288.15 - 258.15
R125 + R1234yf	[153]	7(84)	333.21 - 273.15
R134 + R1234ze(E)	[154]	4(40)	288.15 - 258.15
R134 + R1234ze(Z)	[155]	5(71)	343.15 - 303.15
R134a + R1234yf	[153]	7(63)	333.21 - 273.31
R13I1 + R1234ze(E)	[156]	5(55)	298.15 - 258.15
R143a + R1234yf	[157]	5(45)	323.15 - 283.15
R152a + R1234ze(E)	[158]	4(44)	288.15 - 258.15
R161 + R1234yf	[159]	5(55)	323.15 - 283.15
	[160]	5(60)	323.15 - 283.15
R218 + R1234yf	[161]	2(20)	272.81 - 223.08
R23 + R1234yf	[161]	3(26)	273.25 - 193.19
R290 + R1234ze(Z)	[162]	5(68)	293.15 - 253.15
R32 + R1234yf	[159]	5(55)	323.15 - 283.15
	[153]	7(77)	333.15 - 273.15
R32 + R1234ze(E)	[159]	5(15)	323.15 - 283.15
	[163]	5(65)	323.15 - 283.15
R600a + R1234ze(Z)	[164]	6(69)	353.15 - 303.15
R717 + R1234yf	[165]	4(58)	283.15 - 253.15

experimental and calculated data points are high, the calculation of VLE properties for binary systems containing refrigerants that were studied above their critical point was not considered. To obtain more accurate results for the aforementioned binary systems, more complex EoSs (e.g. three-parameter CESs or non-analytic EoSs) and mixing rules (e.g the Huron-Vidal mixing rules [114] and the Wong-Sandler mixing rules [115]) should be tested. The number of isotherms, the number of points, the references to the original sources and the ranges of temperature for the binary systems under analysis are reported in Table 2.5. As already stated for the calculation of the vapor pressure from CESs, also in this case almost all the adopted physical properties of the studied refrigerants were collected from Lemmon et al. [64].

Table 2.6 shows the AARD(ΔP) % and the Average Absolute Deviation of vapor phase mole fraction of the first component (AAD(Δy_1)) for the studied binary systems considering the binary interaction parameter (k_{ij}) as a constant. In fact, k_{ij} were regressed from the complete datasets of each binary system by minimizing AARD(ΔP)

%. The AAD of vapor phase mole fraction of the first component is defined as:

$$\mathrm{AAD}\,(\Delta y_1) = \sum_{i=1}^{N} \left| \frac{y_{1,i,\mathrm{exp}} - y_{1,i,\mathrm{calc}}}{N} \right| \tag{2.50}$$

AARD(ΔP) % and AAD(Δy_1) for the selected binary systems calculated adopting a temperature dependent binary interaction parameter ($k_{ij}(T)$) for the standard one-binary-parameter mixing rules are reported in Table 2.7. In this case, k_{ij} were regressed by minimizing the AARD(ΔP) % for each isotherm.

Table 2.6 and Table 2.7 show that the CESs generally ensure a good representation of the VLE for almost all the studied systems, adopting both constant k_{ij} and temperature-dependent $k_{ij}(T)$. In the former case, the studied CESs ensured AARD(ΔP) % lower than 2 % and AAD(Δy_1) lower than 0.01 for almost all the selected binary systems. However, as expected, Table 2.7 shows that the CESs with $k_{ij}(T)$ generally provided lower AARD(ΔP) % and AAD(Δy_1) than that of CESs with constantk_{ij}. As example, the enhanced description provided by CES(A) with k_{ij} regressed for each isotherm is shown in Figure 2.4. This figure presents the behaviors of experimental and calculated pressure versus liquid and vapor mole fractions for R134 + R1234ze(Z) binary system at five temperatures considering both constant k_{ij} and $k_{ij}(T)$ for the CES(A). It is important to note that, as evident in Figure 2.5 for the aforementioned binary system, a slight variation of k_{ij} with T guarantees an improved representation of the VLE for the studied binary pairs. However, the CESs provided high values of AARD(ΔP) % and AAD(Δy_1) for R717 + R1234yf in both the cases. As previously mentioned, more complex EoSs and mixing rules should be test to obtain a more accurate representation of the VLE for this binary pair.

2.4.2 Flash method for VLE derivation

As detailed by Di Nicola et al. [140], an approach based on the flash calculation can be used to derive the VLE behavior of binary systems of refrigerants from their two-phase $PvTz$ properties measured by an isochoric apparatus. This method allows to calculate the values of P, x_i and y_i for each isochoric point by simultaneously ensuring the isofugacity conditions (in the form of Equation (2.44)) and the following additional conditions:

1. mass conservation

$$n = n^{\mathrm{L}} + n^{\mathrm{V}} \tag{2.51}$$

where

$$n^{\mathrm{L}} = n\,F_{\mathrm{L}} \tag{2.52}$$

and

$$n^{\mathrm{V}} = n\,(1 - F_{\mathrm{L}}) \tag{2.53}$$

where n is the number of charged moles, n^{L} is the number of moles of the liquid phase, n^{V} is the number of moles of the vapor phase and F_{L} is overall mole fraction of the liquid phase.

2. the balance of isochoric cell volume (V_{iso})

$$V_{\mathrm{iso}} = n^{\mathrm{L}}\,v_{\mathrm{m}}^{\mathrm{L}} + n^{\mathrm{V}}\,v_{\mathrm{m}}^{\mathrm{V}} \tag{2.54}$$

where $v_{\mathrm{m}}^{\mathrm{L}}$ is the molar volume of the liquid phase and $v_{\mathrm{m}}^{\mathrm{V}}$ is the molar volume of the vapor phase.

Table 2.6: Deviations between experimental and calculated VLE data for binary systems of low GWP refrigerants considering constant k_{ij}.

Binary systems	RKS		PR		PR mod		CES(A)	
	AARD (ΔP) %	AAD (Δy_1)	AARD (ΔP) %	AAD (Δy_1)	AARD (ΔP) %	AAD (Δy_1)	AARD (ΔP) %	AAD (Δy_1)
R1233xf (1) + R244bb (2)	0.90	0.0105	0.96	0.0102	1.00	0.0103	1.03	0.0102
R1234yf (1) + R1233xf (2)	1.16	0.0024	1.36	0.0012	1.37	0.0009	1.42	0.0010
R1234yf (1) + R152a (2)	0.62	0.0029	0.24	0.0021	0.24	0.0019	0.20	0.0021
R1234yf (1) + R227ea (2)	0.80	0.0049	0.36	0.0034	0.40	0.0035	0.33	0.0034
R1234yf (1) + R244bb (2)	0.83	0.0028	0.37	0.0031	0.44	0.0033	0.38	0.0036
R1234yf (1) + R245cb (2)	0.80	0.0106	0.38	0.0118	0.38	0.0116	0.32	0.0119
R1234yf (1) + R290 (2)	0.29	0.0016	0.19	0.0027	0.22	0.0020	0.26	0.0024
R1234yf (1) + R600a (2)	1.01	0.0063	0.57	0.0052	0.61	0.0048	0.53	0.0049
R1234ze(E) (1) + R290 (2)	0.34	0.0039	0.34	0.0041	0.32	0.0037	0.34	0.0036
R1234ze(E) (1) + R600a (2)	0.42	0.0040	0.38	0.0028	0.43	0.0030	0.49	0.0027
R125 (1) + R1234yf (2)	0.72	0.0120	0.40	0.0107	0.37	0.0110	0.35	0.0108
R134 (1) + R1234ze(E) (2)	0.37	0.0044	0.15	0.0032	0.18	0.0041	0.26	0.0041
R134 (1) + R1234ze(Z) (2)	3.58	0.0138	3.41	0.0134	3.37	0.0135	3.37	0.0135
R134a (1) + R1234yf (2)	0.81	0.0056	0.38	0.0037	0.34	0.0039	0.28	0.0036
R13I1 (1) + R1234ze(E) (2)	0.53	0.0040	0.27	0.0044	0.21	0.0038	0.23	0.0039
R143a (1) + R1234yf (2)	0.81	0.0027	0.40	0.0015	0.41	0.0014	0.34	0.0017
R152a (1) + R1234ze(E) (2)	0.64	0.0025	0.44	0.0017	0.47	0.0023	0.52	0.0023
R161 (1) + R1234yf (2)	0.84	0.0049	0.37	0.0023	0.41	0.0025	0.33	0.0022
	0.84	0.0047	0.45	0.0036	0.50	0.0037	0.44	0.0036
R218 (1) + R1234yf (2)	0.72	0.0051	0.59	0.0049	0.69	0.0055	0.85	0.0056
R23 (1) + R1234yf (2)	1.94	0.0028	1.06	0.0029	1.19	0.0034	1.18	0.0037
R290 (1) + R1234ze(Z) (2)	1.09	0.0071	1.24	0.0080	1.15	0.0080	1.18	0.0080
R32 (1) + R1234yf (2)	0.89	0.0057	0.63	0.0038	0.65	0.0040	0.61	0.0038
	0.82	0.0098	0.51	0.0091	0.54	0.0093	0.48	0.0092
R32 (1) + R1234ze(E) (2)	0.73	0.0051	0.67	0.0032	0.67	0.0034	0.66	0.0031
	0.85	0.0055	0.59	0.0052	0.60	0.0051	0.58	0.0050
R600a (1) + R1234ze(Z) (2)	0.59	0.0077	0.57	0.0095	0.55	0.0092	0.58	0.0096
R717 (1) + R1234yf (2)	4.37	0.0419	4.19	0.0415	3.99	0.0415	3.93	0.0413
Average	1.06	0.0077	0.81	0.0071	0.81	0.0071	0.79	0.0071

Table 2.7: Deviations between experimental and calculated VLE data for binary systems of low GWP refrigerants considering temperature dependent $k_{ij}(T)$.

Binary systems	RKS		PR		PR mod		CES(A)	
	AARD (ΔP) %	AAD (Δy_1)	AARD (ΔP) %	AAD (Δy_1)	AARD (ΔP) %	AAD (Δy_1)	AARD (ΔP) %	AAD (Δy_1)
R1233xf (1) + R244bb (2)	0.80	0.0108	0.80	0.0108	0.80	0.0108	0.80	0.0107
R1234yf (1) + R1233xf (2)	0.65	0.0031	0.80	0.0029	0.80	0.0025	0.85	0.0026
R1234yf (1) + R152a (2)	0.56	0.0029	0.23	0.0022	0.24	0.0019	0.20	0.0021
R1234yf (1) + R227ea (2)	0.74	0.0049	0.34	0.0035	0.38	0.0035	0.32	0.0034
R1234yf (1) + R244bb (2)	0.60	0.0026	0.22	0.0030	0.30	0.0032	0.29	0.0034
R1234yf (1) + R245cb (2)	0.59	0.0109	0.22	0.0120	0.24	0.0119	0.20	0.0121
R1234yf (1) + R290 (2)	0.23	0.0018	0.14	0.0025	0.14	0.0020	0.14	0.0023
R1234yf (1) + R600a (2)	0.99	0.0063	0.56	0.0052	0.60	0.0049	0.52	0.0049
R1234ze(E) (1) + R290 (2)	0.31	0.0040	0.33	0.0043	0.31	0.0038	0.33	0.0039
R1234ze(E) (1) + R600a (2)	0.40	0.0041	0.28	0.0030	0.34	0.0032	0.34	0.0031
R125 (1) + R1234yf (2)	0.60	0.0116	0.33	0.0104	0.33	0.0108	0.31	0.0106
R134 (1) + R1234ze(E) (2)	0.18	0.0039	0.12	0.0033	0.14	0.0041	0.16	0.0041
R134 (1) + R1234ze(Z) (2)	0.45	0.0055	0.43	0.0062	0.38	0.0059	0.45	0.0061
R134a (1) + R1234yf (2)	0.53	0.0053	0.22	0.0037	0.20	0.0039	0.18	0.0037
R1311 (1) + R1234ze(E) (2)	0.34	0.0041	0.26	0.0044	0.21	0.0038	0.20	0.0038
R143a (1) + R1234yf (2)	0.73	0.0023	0.26	0.0017	0.30	0.0016	0.22	0.0018
R152a (1) + R1234ze(E) (2)	0.53	0.0025	0.41	0.0016	0.43	0.0022	0.43	0.0022
R161 (1) + R1234yf (2)	0.79	0.0048	0.33	0.0022	0.39	0.0025	0.31	0.0021
	0.79	0.0046	0.45	0.0036	0.49	0.0037	0.44	0.0036
R218 (1) + R1234yf (2)	0.66	0.0053	0.45	0.0054	0.55	0.0056	0.62	0.0062
R23 (1) + R1234yf (2)	1.62	0.0038	1.02	0.0029	1.15	0.0033	1.17	0.0037
R290 (1) + R1234ze(Z) (2)	0.94	0.0070	1.05	0.0081	0.95	0.0081	0.97	0.0084
R32 (1) + R1234yf (2)	0.88	0.0056	0.62	0.0039	0.64	0.0041	0.59	0.0039
	0.80	0.0097	0.51	0.0091	0.53	0.0093	0.48	0.0092
R32 (1) + R1234ze(E) (2)	0.68	0.0050	0.60	0.0032	0.60	0.0034	0.58	0.0031
	0.84	0.0055	0.56	0.0052	0.56	0.0051	0.54	0.0051
R600a (1) + R1234ze(Z) (2)	0.54	0.0077	0.51	0.0094	0.48	0.0090	0.50	0.0094
R717 (1) + R1234yf (2)	4.24	0.0413	4.05	0.0415	3.86	0.0411	3.80	0.0411
Average	0.80	0.0072	0.58	0.0068	0.58	0.0068	0.57	0.0068

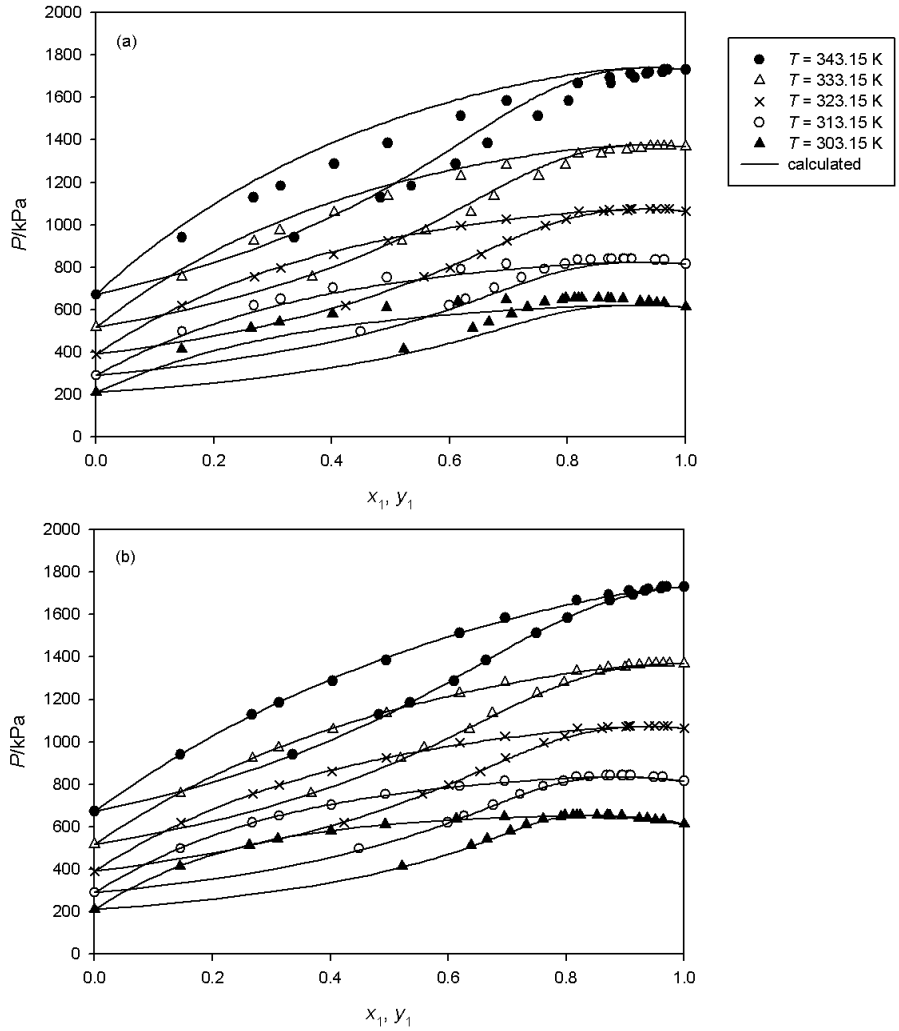

Figure 2.4: Experimental VLE data for R134 (1) + R1234ze(Z) (2) binary system and calculated values by using CES(A) considering both a constant k_{ij} (k_{ij} = 0.1102) (a) and temperature variable $k_{ij}(T)$ (b) at five temperatures.

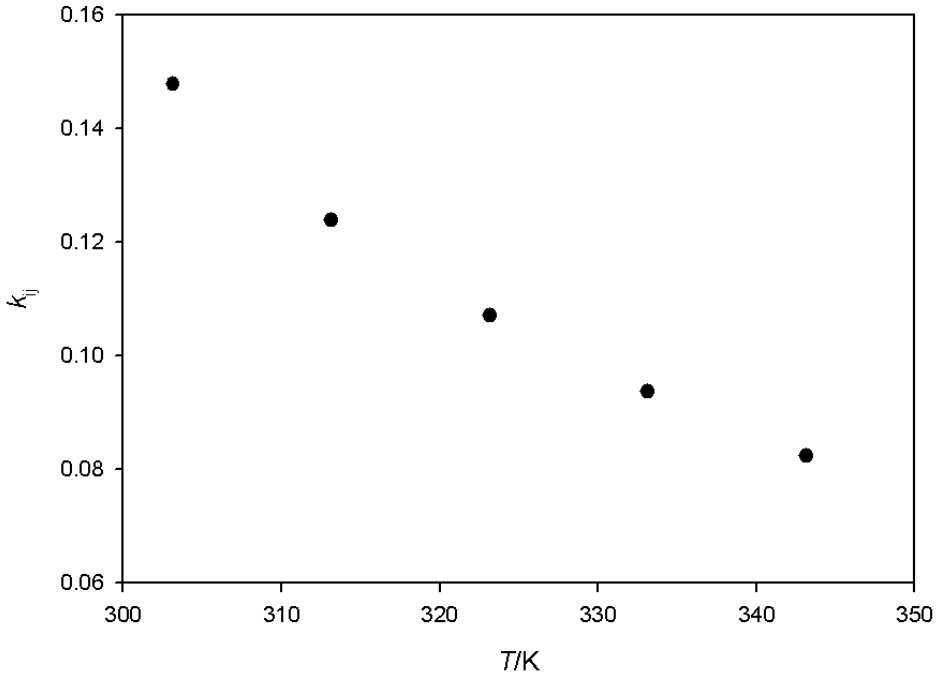

Figure 2.5: $k_{ij}(T)$ of the CES(A) as function of the T for R134 + R1234ze(Z) binary pair.

3. the balance of composition

$$1 - \sum_i x_i < \epsilon \tag{2.55}$$

$$1 - \sum_i y_i < \epsilon \tag{2.56}$$

$$z_i - (F_{\mathrm{L}}\, x_i + (1 - F_{\mathrm{L}})\, y_i) < \epsilon \tag{2.57}$$

where z_i is the overall experimental mole fraction of i-th component and ϵ is a residual value (usually $\sim 1 \cdot 10^{-10}$).

In particular, V^{iso} is a known value. For the volume condition, the flash method needs the values of ϕ_i, $v_{\mathrm{m}}^{\mathrm{L}}$ and $v_{\mathrm{m}}^{\mathrm{V}}$ which are usually calculated from EoSs and mixing rules. Therefore, the accuracy in volumetric property description is essential in this procedure and depends on the predictive ability of the EoSs being used.

In this work, an algorithm based on the flash method was used to derive the VLE properties from two-phase $PvTz$ properties of different binary systems containing low GWP refrigerant measured with an isochoric apparatus. The obtained results are reported in Section 4.1 of Chapter 4. The flow chart of this algorithm is shown in Figure 2.6. In particular, the PR EoS [103], the CES(A) of Table 2.2 and the CSD EoS [110] were used in the flash method algorithm and these EoSs were extended to the binary systems through the van der Waals one-fluid. The expressions to calculate ϕ of the components of the binary systems trough the CSD EoS and the van der Waals one-fluid mixing rules are reported in Appendix A.

In the algorithm of Figure 2.6, Equation (2.49) was used to calculate the initial guesses of the distribution factor (or K-factor) for the components of the binary systems (K_i). Instead, the initial guess for the bubble point pressure, called P^{in} in Figure 2.6, was selected on the basis of the Nelder-Mead algorithm [144] used to minimize the deviation between V_{iso} and the calculated volume, called $Er(V)$ in Figure 2.6. During the fitting procedure, T, z_i and n are kept equal to the experimental values. The compressibility factor (Z) of the liquid and vapor phases, the bubble point pressure, and mole fractions of the liquid and vapor phases calculated with the algorithm are called Z^{L}, Z^{V}, P^{iter} and x_i y_i in Figure 2.3, respectively. The values of k_{ij} were adjusted by minimizing the following objective function by using the the Nelder-Mead algorithm [144]:

$$Q = \sum_{i=1}^{N} \left(\frac{P_{\mathrm{exp},i} - P_{\mathrm{calc},i}}{P_{\mathrm{exp},i}} \right)^2 \tag{2.58}$$

where N is the number of experimental data.

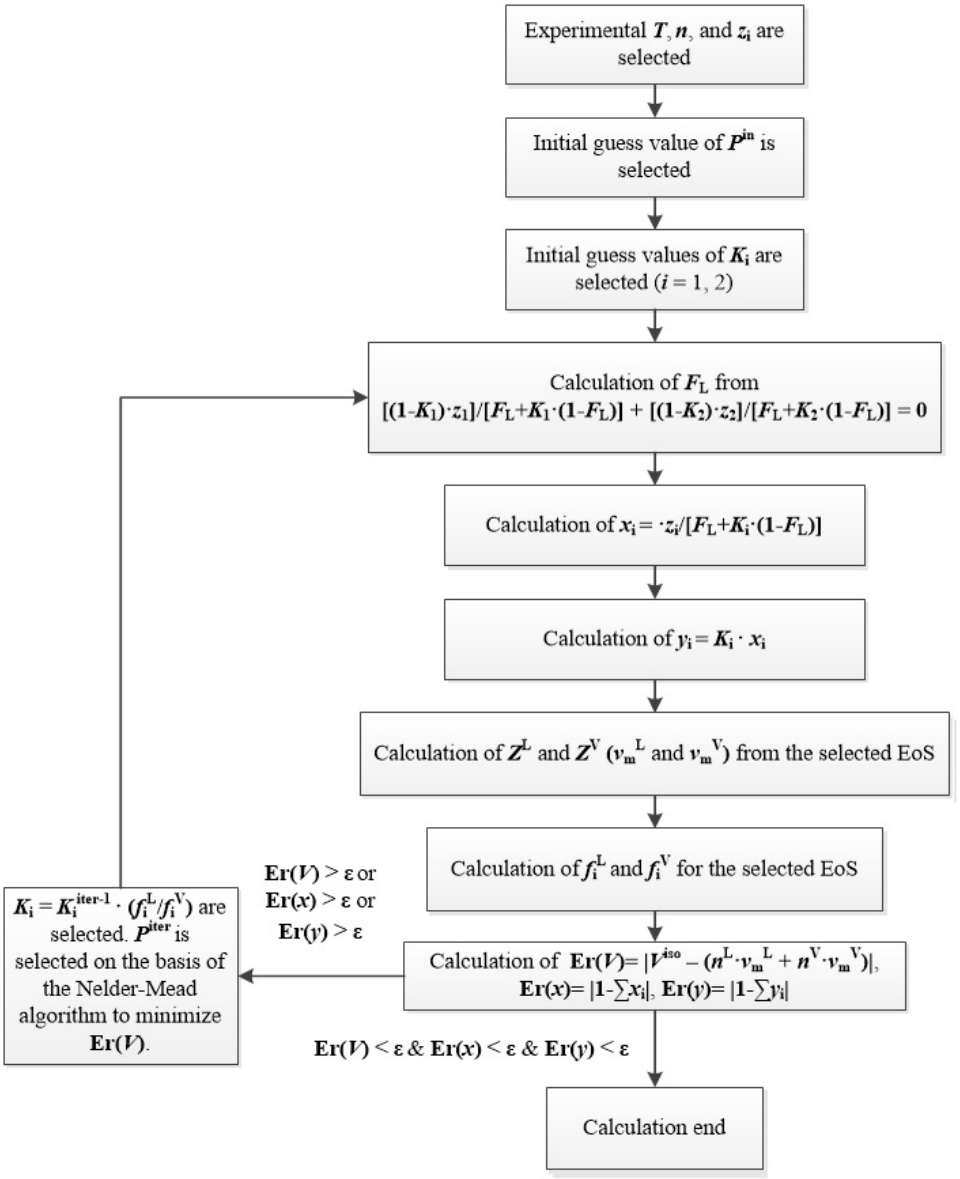

Figure 2.6: Flow chart of the algorithm based on the flash method used to estimate the vapor-liquid equilibrium of binary systems from equations of state.

Chapter 3

Modeling of transport properties

In this chapter, different models available in the literature for the estimation of the surface tension and the thermal conductivity of refrigerants and their blends are studied to estimate these properties of low Global Warming Potential (GWP) working fluids. In particular, new correlations to calculate the studied properties of refrigerants and their blends, some of them specifically oriented to alternative working fluids, were developed and are presented.

3.1 Surface tension

The surfaces between different phases can be characterized by surface and interfacial tensions. On a molecular level, an explanation of this phenomenon is that, at the interface, there is an unequal distribution of forces acting upon the molecules compared to the forces in the bulks of the phases [166]. In particular, for a liquid-vapor interface, the surface molecules are mainly attracted toward the bulk of the liquid and less attracted toward the bulk of the vapor phase. And because of this, the surface layer is in tension and there is a tendency for the liquids to conform to the shape that corresponds to the minimum surface (i.e. spherical) compatible with the total mass, container restraints, and external forces [166]. A measure of this tension at the liquid-vapor interface is the surface tension (σ). In general, the surface tension (or surface energy) is defined as the work (W) necessary to isothermally increase the area of a surface (A) in the air by a unit amount ($\mathrm{d}W/\mathrm{d}A$) [166]. The SI unit of σ is ($\mathrm{N\,m^{-1}}$), usually expressed as ($\mathrm{mN\,m^{-1}}$). However, the units ($\mathrm{dyn\,cm^{-1}}$) and ($\mathrm{mJ\,m^{-2}}$) are sometimes used.

Liquid-vapor interfaces and σ are of relevance to diverse fields of science and engineering, such as absorption, distillation, and colloid science [166]. Besides, this thermophysical property is important for correlating and predicting heat transfer during a phase change. In particular, this property plays a crucial role in the study of phase transition and many phenomena like boiling and condensation. For these reasons, the surface tension of refrigerants and their blends is of great importance for the refrigeration processes (e.g. design of condensers and evaporators, heat pumps, and organic Rankine cycles, etc.).

The surface tension of fluids at the liquid-vapor interface can be directly measured

by using different experimental methods. The optimal measurement method for the different fluids depends upon many aspects such as the nature of the liquid being measured, the stability of its surface when it is deformed and the temperature and pressure conditions of measurement.

However, several models have been developed for estimating σ of different fluids when a limited number of (or no) experimental data are available. In particular, some of these models (e.g. correlations based on CSP, models based on EoSs, etc.) are expressly oriented to describe σ of refrigerants of different generations and their blends, but none was specifically designed to predict the surface tension of low GWP refrigerants. Therefore, since few experimental data of their σ are available in literature [36], a model for the surface tension prediction of low GWP refrigerants and their binary systems from a limited number of known parameters can be of great attraction for the refrigeration industry.

For the aforementioned reasons, the surface tension data of low GWP refrigerants, both pure fluids and blends, were collected and analyzed with different correlations for the prediction of σ of refrigerants available in the literature. Some of these models will be described below.

In addition, a simple empirical scaled equation based on the CSP, recently proposed by our group of work for other organic and inorganic fluids [167–170], was tested for σ of low GWP refrigerants. In this equation, besides the critical properties, the radius of gyration, G_r, was considered as a parameter to calculate the surface tension. In particular, the first expression of this scaled equation proposed to predict the surface tension of alcohols has the following form:

$$\frac{\sigma}{\sigma_o} = A(1 - T_r)^B (1 + \phi^C)^D \tag{3.1}$$

where σ is the surface tension in $\mathrm{N\,m^{-1}}$, $\sigma_o = (kT_c)/G_r^2$ is a scaled factor in $\mathrm{N\,m^{-1}}$, T_c is the critical temperature in K, k is Boltzmann's constant in $\mathrm{J\,K^{-1}}$, G_r is the radius of gyration in m, $\phi = N_A\,\rho_c\,G_r^3$ is an adimensional term, N_A is Avogadro's number in $\mathrm{mol^{-1}}$, ρ_c is the critical molar density in $\mathrm{mol\,m^{-3}}$ and $A - D$ are regressed coefficients. Equation (3.1) was also regressed to calculate the surface tension of carboxylic acids [169]. Two additional correlations, rather similar to Equation (3.1), were provided to calculate the surface tension of ketones [168], considering the critical compressibility factor (Z_c) as additional parameter, and to calculate the surface tension of silanes [170], considering the acentric factor (ω) as additional parameter.

The pure refrigerants under analysis were divided into two subgroups according to their chemical structure, namely ethylene derivatives and propylene derivatives. The same scaled equation was also considered for binary systems of low GWP refrigerants and conventional refrigerants. The equation was re-fitted considering the σ data for the ethylene derivatives, the propylene derivatives, and their binary systems, separately. The obtained results are described below and were also presented elsewhere [81].

3.1.1 Overview of the existing models

In the last years, detailed studies regarding σ of refrigerants were proposed to find reliable correlations. It has to be noted that the raw surface tension data (experimental, smoothed, and predicted) of refrigerants of different generations were collected and used in these studies. Therefore, none of the proposed correlations is specifically oriented to low GWP refrigerants. Some of these studies will be briefly described below.

Di Nicola & Moglie [171] and Di Nicola et al. [72] proposed two equations based on the CSP for the prediction of the temperature dependent σ of pure refrigerants.

The first equation for σ ($\mathrm{mN\,m^{-1}}$) [171] is a general correlation with five independent parameters (P_c, T_c, ω, μ^*, and V_c) and seven regressed constants [171].Since almost all refrigerants have a non zero dipole moment, the equation includes the reduced dipole moment (μ^*) and has the following form:

$$\sigma = 0.813\, P_c^{0.565}\, T_c^{0.364}\, (1 - T_r)^{1.266}\, (4.259\,\omega - 0.645\,\mu^*)^{0.143} \tag{3.2}$$

where P_c is the critical pressure in bar, T_c is the critical temperature in K, $T_r = T/T_c$ is the reduced temperature, ω is the acentric factor, $\mu^* = (N_A^2\,\mu^2)/(R\,T_c\,v_c) = (4300\,\mu^2)/(T_c\,V_c)$ is the reduced dipole moment, N_A is Avogadro's number in $\mathrm{mol^{-1}}$, R is the universal gas constant in $\mathrm{J\,mol^{-1}\,K^{-1}}$, μ is the dipole moment in D, and v_c is the critical volume in $\mathrm{cm^3\,mol^{-1}}$. This equation showed a significant improvement in the prediction of σ for the studied refrigerants, particularly in the low temperature range.

The second equation [72] is a general relation for σ ($\mathrm{mNm^{-1}}$), containing only three independent parameters (P_c (bar), T_c (K), and ω) and five constants [72]:

$$\sigma = 0.658 P_c^{0.618}\, T_c^{0.34} (1 + \omega)^{0.77} (1 - T_r)^{1.262} \tag{3.3}$$

The constants were obtained with a fitting procedure based on the ($\mu + \lambda$) - Evolution Strategy optimization algorithm [172] to minimize the deviation between the predicted data and the experimental values. This simple and extremely compact equation improved the prediction ability for the σ of refrigerants when compared with existing CSP based correlations.

Cachadiña et al. [71] proposed specific correlations for σ of 86 pure refrigerants. These specific correlations contain from two to six adjustable coefficients for each fluid to fit the raw data, appropriately selected from databases, books, and journal papers. Accurate results (Average Absolute Relative Deviations (AARDs) of σ below 2.7%) were obtained for the temperature range covered by surface tension data.

More recently, the same authors [173, 174] presented two correlating models based on the CSP for the prediction of the σ of pure refrigerants. The first equation [173] includes temperature and surface tension at the triple point as parameters and was developed from an updated version of the surface tension dataset reported in [71]. This relation is expressed as:

$$\sigma = \frac{\sigma_{tp}}{(\sigma_{tp})_R}\left[0.13045\left[1 - \frac{T^{**}}{(T_c^*)_R}\right]^{1.3239} - 0.029209\left[1 - \frac{T^{**}}{(T_c^*)_R}\right]^{1.6504}\right] \tag{3.4}$$

where $(\sigma_{tp})_R$=0.059 750 $\mathrm{N\,m^{-1}}$ and $(T_c^*)_R = (T_c)_R/[(T_c)_R - (T_{tp})_R]$=1.531276 are respectively the surface tension of the refrigerant R142b at the triple point and the reduced critical temperature of R142b (R142b was selected as reference fluid for the CSP), σ_{tp} is the surface tension at the triple point in $\mathrm{Nm^{-1}}$, $T^{**} = 1.531276 + (T - T_c)/(T_c - T_{tp})$ is the defined reduced temperature and T_{tp} is the temperature at the triple point in K. It is possible to calculate the surface tension of those refrigerants for which the properties at the triple point are not known by substituting $(T_{min}, \sigma(T_{min}))$ for (T_{tp}, σ_{tp}) where T_{min} is the minimum temperature at which a value of the surface tension $\sigma(T_{min})$ is available in the database. This equation is applicable over the entire vapor-liquid temperature range for which surface tension is defined and represents the surface tension data for 83 refrigerants from the triple point to the critical one with AARDs of σ below 10% for almost all fluids. As indicated by the authors, the main drawback of the model is that it needs at least one experimental σ value.

The second equation is a general corresponding states correlation model, considering T and σ values at the normal boiling point as parameters [174]. This equation was also developed from an updated version of the database created by [71] and give AARDs of σ below 9.5% for all the 80 fluids considered. However, as mentioned by the authors, the main shortcoming of this model is that it can only be used if the experimental or estimated value for the surface tension at the boiling point is known.

In additions, different Artificial Neural Networks (ANNs) were developed to estimate σ of pure refrigerants [74, 175]. Nabipour & Keshavarz [175] proposed a feed-forward back-propagation network with 4 input variables (T, T_c, P_c and ω), 1 hidden layer with 19 neurons and the output layer with 1 neuron. Since they showed to have the optimum performance, tan-sigmoid and purelin transfer functions were used in the hidden and output layers. The proposed architecture was trained, tested and validated on the basis of 793 reliable experimental σ values for 24 pure refrigerants by employing different training algorithms. The obtained results showed that this ANN could correlate and predict the surface tension of the studied refrigerants. However, these results were compared to different well-known correlations available in the literature which demonstrated better performances than the proposed ANN.

Mulero et al. [74] proposed an ANN for the estimation and prediction of σ of refrigerants along the liquid-vapor interphase. The architecture of the ANN that provided the best results had 4 input variables (T_r, T_c, P_c and ω), 2 hidden layers with 10 neurons each and the output layer with 1 neuron. The ANN was developed on a total amount of 2879 data for 76 refrigerants. More accurate results were provided by this ANN respect to different correlations available in literature.

On the other hand, only a limited number of surface tension estimation models were published in the open literature for blends of refrigerants.

Combining the linear gradient theory with the Heyen EoS [176], Khosharay et al. [177] developed a method to estimate the surface tension values of pure refrigerants, and binary, ternary, and quaternary refrigerant blends. More recently, the same authors [178] proposed a new model, combining the Laaksonen and Kulmala equation with the phase equilibrium between the bulk liquid and the surface phases, specifically oriented to predict the surface tension, the surface composition, and the surface mole density of the binary refrigerant system. The results of this model (the AARDs of σ is approximately 4.35%) show that the predicted surface tension agrees well with the experimental data for the studied refrigerant blends.

Di Nicola & Pierantozzi [179] developed a simple equation to predict the surface tension of binary systems of refrigerants, based on the CSP. The experimental data of 13 refrigerant binary systems were collected for the development of this correlation. The proposed equation is rather similar to Equation (3.3) and has the following expression:

$$\sigma = 6.098\,10^{-8}\omega_m^{0.203}(3.285\,10^6 + P_{cm}^{3.449})T_{cm}(1 - T_r)^{1.258} \tag{3.5}$$

where ω_m is the mixture acentric factor, P_{cm} is the mixture critical pressure in MPa, and T_{cm} is the mixture critical temperature in K. These three mixture parameters were simply approximated by the mole fraction average of the pure component properties. The results (the AARDs of σ is equal to 5.51%) show that Equation (3.5) is a reliable correlation specifically oriented to predict the surface tension of refrigerant binary systems.

3.1.2 Data analysis

To provide a reliable database for the experimental surface tensions of halogenated alkene refrigerants and blends containing these low GWP refrigerants and conventional refrigerants, a careful literature survey was performed. As first step, we collected the experimental data for halogenated alkene refrigerants and their binary systems available from journal papers, DIPPR database [51], and the DETHERM database [50, 53]. In particular, the two databases were accessed in January 2017. Moreover, additional experimental data were selected from recent journal papers and added in the database.

Then a fluid by fluid analysis and selection of the collected data were performed. In particular, among the experimental surface tension data reported in the DIPPR database, only the ones that are considered to be acceptable by the DIPPR database itself were selected. Applying this criterion, a total of 131 experimental points, subdivided in 8 refrigerants derived from ethylene, and a total of 152 experimental values, subdivided in 6 propylene derivative refrigerants, were selected. Finally, 147 available experimental data for 5 binary systems of halogenated alkene refrigerants and conventional ones were obtained from the sources mentioned above.

Tables 3.1 - 3.2 and Table 3.3 summarize the temperature and the surface tension data for the halogenated alkene refrigerants and the refrigerant blends, respectively, and include the references to the sources and the number of experimental points per dataset. In addition, the reported mole fraction ranges of the blends are provided in Table 3.3.

From Tables 3.1 and 3.2, it is possible to note that the experimental surface tension measurements for pure refrigerants were performed over wide surface tension (from 0.05 to 36.72 $\mathrm{mN\,m^{-1}}$) and temperature (from 116.00 to 443.15 K) ranges. In the same fashion, Table 3.3 shows that the measurements for refrigerant binary systems, in spite of the limited number of binary systems measured, were performed over wide surface tension (from 0.37 to 12.01 $\mathrm{mN\,m^{-1}}$) and temperature (from 266.89 to 369.15 K) ranges.

The collected experimental data were generally measured through two measurement techniques: the capillary rise method and surface light scattering.

The capillary rise method is based on the capillary action that occurs when the forces of accession to the walls of the container are of greater magnitude than cohesion between molecules of the liquid. The height at which the capillary action drags the liquid in a circular pipe depends on the surface tension of the fluid, but also the density and capillary radius. This phenomenon provides a simple and accurate technique for the measurement of the surface tension of fluids and is studied both in differential and singular capillary rise methods. In the differential capillary rise method, σ can be determined from the capillary radii, the differential capillary-rise-height of the liquid in capillary tubes and the orthobaric densities by using specific correlations [181]. Usually, the uncertainty of these methods is of the order of 0.05 - 0.1 $\mathrm{mN\,m^{-1}}$.

The surface light scattering consisting of the dynamic light scattering application to fluid surfaces. This method allows determining, under conditions of balance, various thermophysical properties of fluids, including surface tension, without any direct contact. The method is based on the analysis of light diffusion caused by microscopic fluctuations on the fluid surface. The uncertainty of the surface tension data provided by this method is of the order of 0.2 ($\mathrm{mN\,m^{-1}}$).

For the ethylene derivatives, all the data are coming from DIPPR and DETHERM databases, excluding few data coming from private communications [180]. Almost

Table 3.1: Surface tension experimental data for the refrigerants derived from ethylene.

Refrigerant	Chemical formula	Source	Number of data	T range, K	σ range, mN m^{-1}
R1150	C_2H_4	[51]	11	137.00-116.00	25.76-21.76
		[50, 53]	29	273.15-116.00	25.95-0.75
R1141	C_2H_3F	[51]	1	288.15-288.15	5.00-5.00
		[50, 53]	11	293.15-143.15	30.79-3.99
R1140	C_2H_3Cl	[51]	12	373.15-213.15	29.50-5.40
		[50, 53]	12	373.15-223.15	26.48-6.14
R1132a	$C_2F_2H_2$	[50, 53]	11	273.15-173.15	23.38-3.85
R1123	C_2F_3H	[180]	16	303.55-266.95	7.41-2.40
R1130	$C_2H_2C_2$	[51]	2	298.15-293.15	28.3-27.65
R1113	C_2ClF_3	[51]	1	293.15-293.15	12.00-12.00
R1120	C_2HC_3	[51]	8	303.15-288.15	29.73-27.76
		[50, 53]	17	443.15-243.15	36.72-10.57

Table 3.2: Surface tension experimental data for the refrigerants derived from propylene.

Refrigerant	Chemical formula	Source	Number of data	T range, K	σ range, mN m^{-1}
R1270	C_3H_6	[51]	1	226.15-226.15	16.70-16.70
		[50, 53]	31	363.65-153.15	27.40-0.05
R1243zf	$C_3F_3H_3$	[181]	11	352.22-273.50	10.63-1.78
R1234yf	$C_3F_4H_2$	[121]	29	338.38-273.21	9.30-1.82
		[182]	9	363.05-293.15	6.82-0.15
R1234ze(E)	$C_3F_4H_2$	[180]	9	341.60-273.31	11.87-3.23
		[182]	9	373.14-295.23	8.88-0.54
		[51]	4	313.15-253.15	14.66-6.16
		[183]	23	333.13-273.19	12.27-4.60
R1234ze(Z)	$C_3F_4H_2$	[181]	13	350.03-273.22	16.26-6.66
R1233zd(E)	$C_3ClF_3H_2$	[132]	3	323.15-273.15	16.48-9.01
		[181]	10	349.98-279.26	17.02-8.05

Table 3.3: Surface tension experimental data for the refrigerant binary systems of propene derivative refrigerants with traditional refrigerants.

Binary systems	Source	Number of data	T range, K	σ range mN m^{-1}	x_1 range
R134a(1) + R1234yf(2)	[184]	24	363.19-293.15	8.25-0.37	0.807-0.319
R134a(1) + R1234ze(E)(2)	[184]	9	369.15-293.10	8.89-0.53	0.445-0.445
R32(1) + R1123(2)	[180]	14	306.53-266.89	10.20-3.84	0.709-0.709
R32(1) + R1234yf(2)	[185]	18	343.18-293.15	7.04-0.59	0.794-0.519
R32(1) + R1234ze(E)(2)	[180]	35	324.72-272.91	12.01-3.74	0.695-0.508
	[185]	21	348.19-293.14	8.46-0.83	0.750-0.298
	[183]	26	322.87-273.21	11.10-3.96	0.687-0.687

all the data for propylene derivatives were individually collected from journal papers. These data are generally more recent and very reliable, being their uncertainties lower than 0.2 mN m^{-1} or 1.5% in most cases. The same consideration is also valid for blends, whose data are very recent and measured through the aforementioned techniques. The corresponding uncertainties are lower than 0.015 mN m^{-1} and than 0.2 mN m^{-1}.

Almost all the fluid physical parameters employed in this work were collected from the DIPPR database [51] and are reported in Table 2.1. However, the physical parameters for three fluids (R1123, R1233zd(E), and R1234ze(Z)) are unavailable in the DIPPR database. As shown in Table 2.1, these properties were selected from recent journal papers available in literature. It is worthwhile pointing out that the G_r for the three above-mentioned fluids was not available. As already demonstrated in the past [170], a correlation between radius of gyration and critical density exists, thus the three missing radii of gyration were calculated with the following regressed correlation:

$$G_r = -38.6119 + 3.41918 \exp(2.4083 + \frac{555.666}{\rho_c} - \frac{643.081}{\rho_c^2}) \tag{3.6}$$

where G_r is the radius of gyration in Å and ρ_c is the critical molar density in mol m^{-3}.

3.1.3 Proposed scaled equation

On the basis of the equations for σ developed by our group of work [167–170], the following form was found to be the best for the low GWP refrigerants:

$$\frac{\sigma}{\sigma_o} = A(1 - T_r)^B (1 + \phi^C)^D \omega^E \tag{3.7}$$

where $A - E$ are regressed coefficients. The optimized coefficients were obtained with the Random Search method [186]. To minimize or maximize the objective functions of the optimization problems, the Random Search method selects a population of points from a feasible region using an appropriate sampling strategy, performs simulations at the chosen points and successively uses the results to update the sampling strategy before proceeding to the next iteration.

To improve the accuracy of the surface tension data obtained by Equation (3.7) for the two subfamilies of refrigerants, the coefficients were regressed minimizing the AARD of σ for the ethylene derivative refrigerants and propylene derivative refrigerants separately. The AARD of σ was calculated as follows:

$$AARD(\sigma)\% = \frac{100}{N} \sum_{i=1}^{N} \frac{\mid \sigma_{exp,i} - \sigma_{calc,i} \mid}{\sigma_{exp,i}} \tag{3.8}$$

where N is the number of experimental data. The coefficients regressed for the two subgroups are reported in Table 3.4.

Starting from Equation (3.7), the following equation for the binary systems of halogenated alkene refrigerants with conventional refrigerants is proposed:

$$\frac{\sigma}{\sigma_{om}} = A(1 - T_{rm})^B (1 + \phi_m^C)^D \omega_m^E \tag{3.9}$$

where $\sigma_{om} = (kT_{cm})/G_{rm}^2$ is a mixture scaled factor in N m^{-1}, T_{rm} is the mixture reduced temperature, G_{rm} is the mixture radius of gyration in m, $\phi_m = N_A \rho_{cm} G_{rm}^3$ is a mixture adimensional term, ρ_{cm} is the mixture critical density in mol m^{-3}, and ω_m is the mixture acentric factor. The independent parameters T_{cm}, G_{rm}, ρ_{cm}, and ω_m were

Table 3.4: Regressed coefficients adopted for Equation (3.7)

Refrigerant	A	B	C	D	E
Ethylene derivative	16.008	1.177	-0.448	-2.188	-0.134
Propylene derivative	1.207	1.256	1.943	43.831	0.426
Binary blends	20.466	1.327	-0.962	-0.827	0.686

simply approximated by the mole fraction averages of the pure component properties $T_{c,i}$, $G_{r,i}$, $\rho_{c,i}$, and ω_i. As witnessed in [179], this simple method gave similar results in terms of deviations as the more complex empirical literature methods for the mixtures properties definition. The coefficients $A - E$ were also regressed with the Random Search method and are reported in Table 3.4.,

As explained in Subsection 3.1.2, Table 2.1 reports all the fluid physical parameters used in Equations (3.7) and (3.9) for the regression of the coefficients.

3.1.4 Results and discussion

The prediction capability of Equations (3.2) - (3.4) and Equation (3.7) for pure refrigerants and Equations (3.5) and (3.9) for refrigerant binary systems was analyzed for the subgroups of selected ethylene derivatives, selected propylene derivatives and selected binary systems of low GWP refrigerants and conventional refrigerants.

The input parameters and the number of coefficients included in the studied equations were summarized in Table 3.5. Moreover, this table shows the number of refrigerants and the experimental halogenated alkene refrigerants (both pure and binary systems) considered in the development of the equations.

Table 3.5: Summary of the input parameters and the number of the coefficients included in the equations under analysis and refrigerants considered in the development of these equations.

Equation	Input parameters	Number of coefficients	Number of refrigerants under analysis	Experimental halogenated alkene refrigerants considered
(3.2)	P_c, T_c, ω, μ^*, and V_c	7	32	R1234yf
(3.3)	P_c, T_c, and ω	5	33	R1234yf
(3.4)	T_c, T_t, and σ_t	4+2[a]	83	R1141 R1140 R1132a R1113 R1120 R1243zf R1234yf R1234ze(E)
(3.5)	P_{cm}, T_{cm}, and ω_m	5	13	-
(3.7)	T_c, ρ_c, G_r, and ω	5	14	R1150 R1141 R1140 R1132a R1123 R1130 R1113 R1120 R1270 R1243zf R1234yf R1234ze(E) R1234ze(Z) R1233zd(E)
(3.9)	T_{cm}, ρ_{cm}, G_{rm}, and ω_m	5	5	R134a + R1234yf R134a + R1234ze(E) R32 + R1123 R32 + R1234yf R32 + R1234ze(E)

[a] The numbers represent the regressed coefficients and the fixed input parameters, respectively

Table 3.6: Deviations between the experimental surface tension of the ethylene derivative refrigerants and the ones predicted by Equations (3.2), (3.3), (3.4), and (3.7).

Refrigerant	N. of data	AARD(σ) % Equation (3.2)	AARD(σ) % Equation (3.3)	AARD(σ) % Equation (3.4)	AARD(σ) % Equation (3.7)
R1150	40	2.67	4.84	2.32	2.21
R1141	12	14.29	8.10	3.12	8.84
R1140	24	11.37	3.88	2.61	1.83
R1132a	11	28.93	24.12	2.01	15.62
R1123	16	2.42	5.76	3.31	3.49
R1130	2	7.87	6.31	0.25	17.78
R1113	1	26.82	25.97	0.001	26.52
R1120	25	1.21	1.58	2.33	2.54
Average	-	7.49	6.25	2.49	4.51

The results for the ethylene derivative refrigerants in increasing order of molecular mass are reported in Table 3.6, where the equations under analysis were tested on 131 points. As a general comment, it is evident that Equation (3.4) performs very well (AARD(σ) = 2.49%) and is the best equation for predicting the surface tension of almost all the fluids. Particularly good results were achieved for fluids having a very limited number of points, such as R1130 and R1113. This behavior was expected, as it is due to the nature of the method itself. The predictions of Equations (3.2) and (3.3) in the original forms are adequate (AARD(σ)= 7.49% and AARD(σ) = 6.25%, respectively) considering also that the two equations are very simple and their coefficients were mostly obtained by fitting data of conventional refrigerants. Equation (3.7) generally shows low deviations for all the ethylene derivatives, excluding R1130, R1113, and R1132a. The average AARD(σ) is 4.51%. The results for Equation (3.7) are also illustrated in Figure 3.1 and Figure 3.2. It is worth noting that the AARDs of σ for this equation for the ethylene derivative fluids assume very different values. Probably, this behavior could be due to the fact that almost all the experimental data were collected from the DIPPR and DETHERM databases, where old (but acceptable) sources are considered.

Although the surface tension data of R1123 were not considered in the development of Equations (3.2) and (3.4), these models seem to produce lower deviations than that of Equation (3.7) (Figure 3.3). However, Equation (3.4) is only slightly better than the new proposed equation, while Equation (3.2) gives, anyway, the highest global AARD of σ among all correlations. As a general comment, it is worth noting that the models considered in the present work were built with different refrigerant sets (Table 3.5). Therefore, particular caution should be taken in making direct comparisons between the considered equations. Evidently, in a case such as that of R1123, Equations (3.2) and (3.4), which can predict new refrigerants with low deviations, have an appreciable value.

The results for the propylene derivatives, again in increasing order of molecular mass, are reported in Table 3.7, where the equations were tested on 151 points. Probably the most promising alternative refrigerants belong to this group. The best results were obtained for Equation (3.7), with an average AARD(σ) equal to 3.04%. The surface tensions of the most important refrigerants (R1234yf and R1234ze(E)) are predicted with AARD(σ) = 4.81% and AAD = 2.23%, respectively. Good results were also obtained for Equations (3.2), (3.3), and (3.4): deviations were found to be between 4-5%. The results for Equation (3.7) are also depicted in Figure 3.4 and Figure 3.5.

Finally, 147 data points for 5 blends of low GWP refrigerants and conventional refrigerants were analyzed with Equations (3.5) and (3.9). The corresponding results

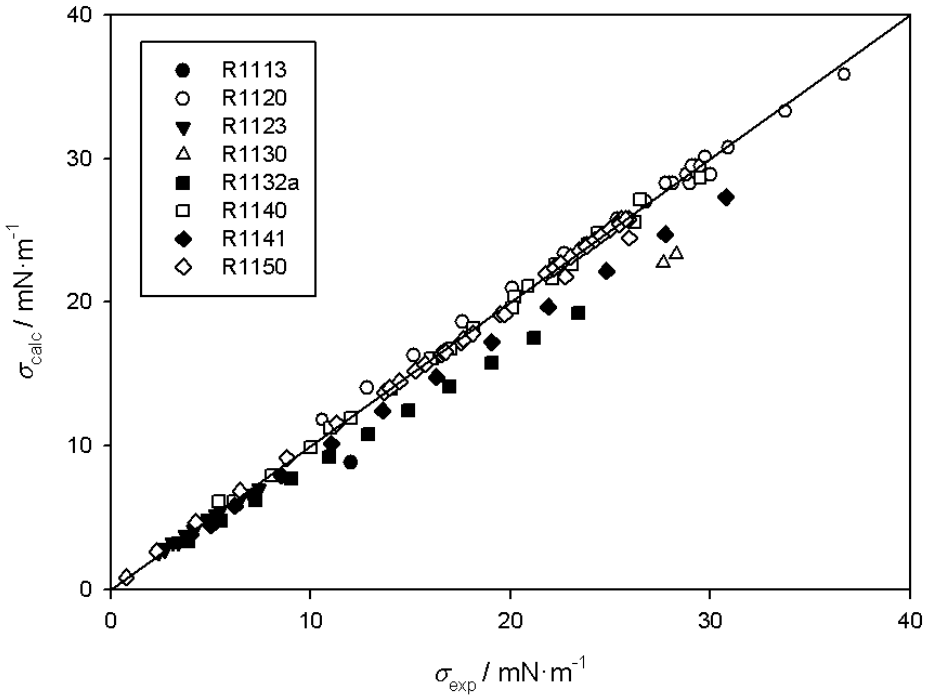

Figure 3.1: Calculated surface tension (Equation (3.7)) versus experimental surface tension of the ethylene derivative refrigerants.

Table 3.7: Deviations between the experimental surface tension of the propylene derivative refrigerants and the ones predicted by Equations (3.2), (3.3), (3.4), and (3.7).

Refrigerant	N. of data	AARD(σ) % Equation (3.2)	AARD(σ) % Equation (3.3)	AARD(σ) % Equation (3.4)	AARD(σ) % Equation (3.7)
R1270	32	3.31	2.69	6.17	1.59
R1243zf	11	1.43	2.61	1.38	2.70
R1234yf	38	4.77	7.12	5.71	4.81
R1234ze(E)	45	4.74	3.42	2.72	2.23
R1234ze(Z)	13	7.93	3.41	1.24	1.23
R1233zd(E)	13	5.43	5.01	5.46	6.33
Average	-	4.54	4.27	4.21	3.04

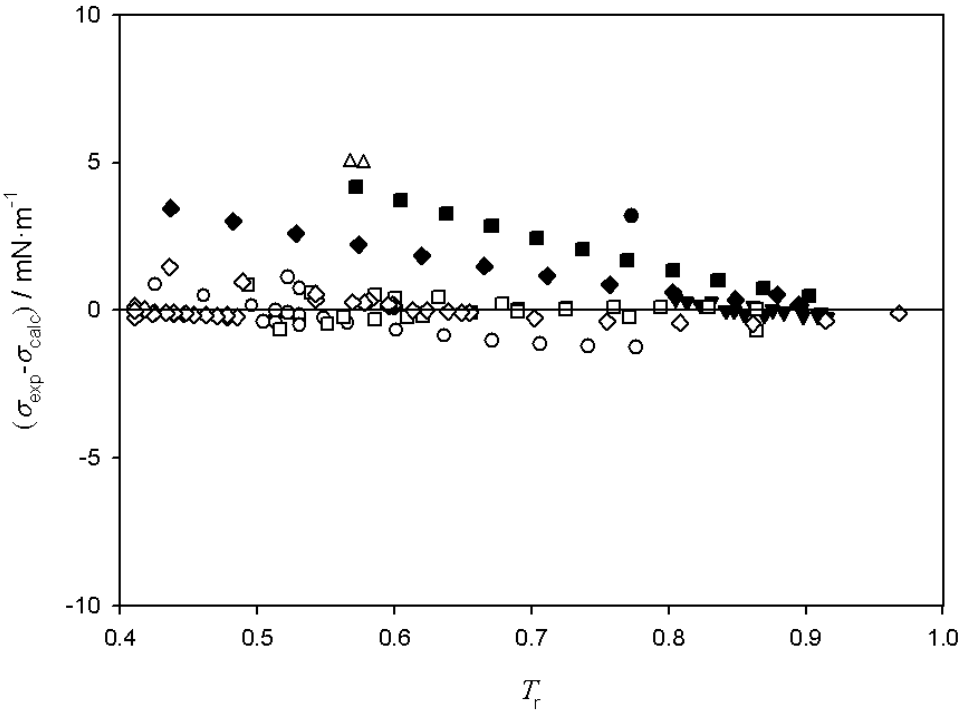

Figure 3.2: Residuals of surface tension data of ethylene derivative refrigerants versus reduced temperature. Notation as in Figure 3.1.

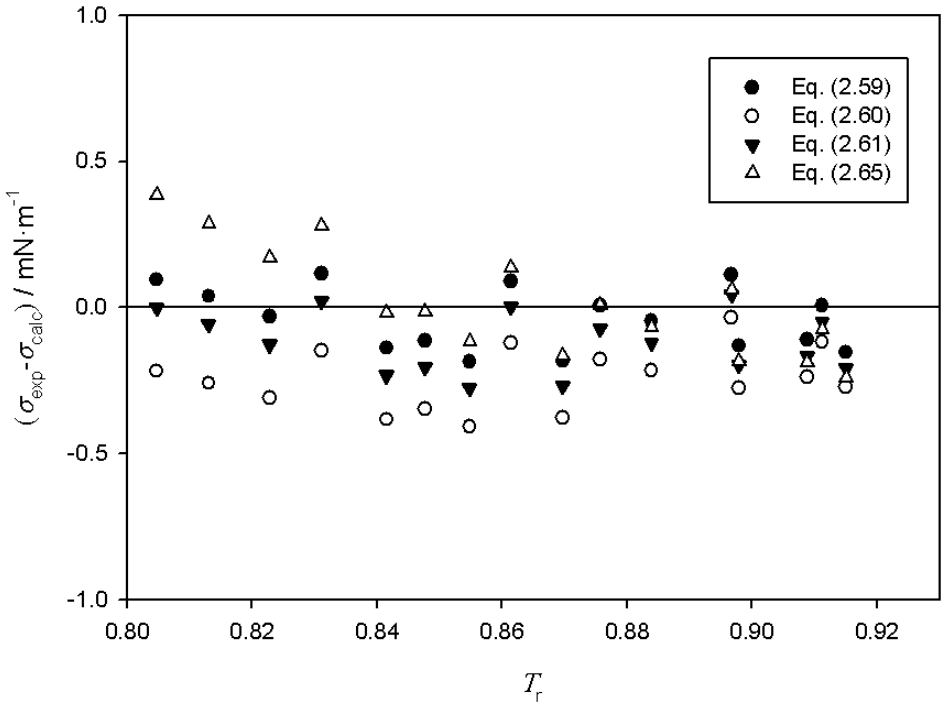

Figure 3.3: Residuals of surface tension data of R1123 for the studied equations versus reduced temperature.

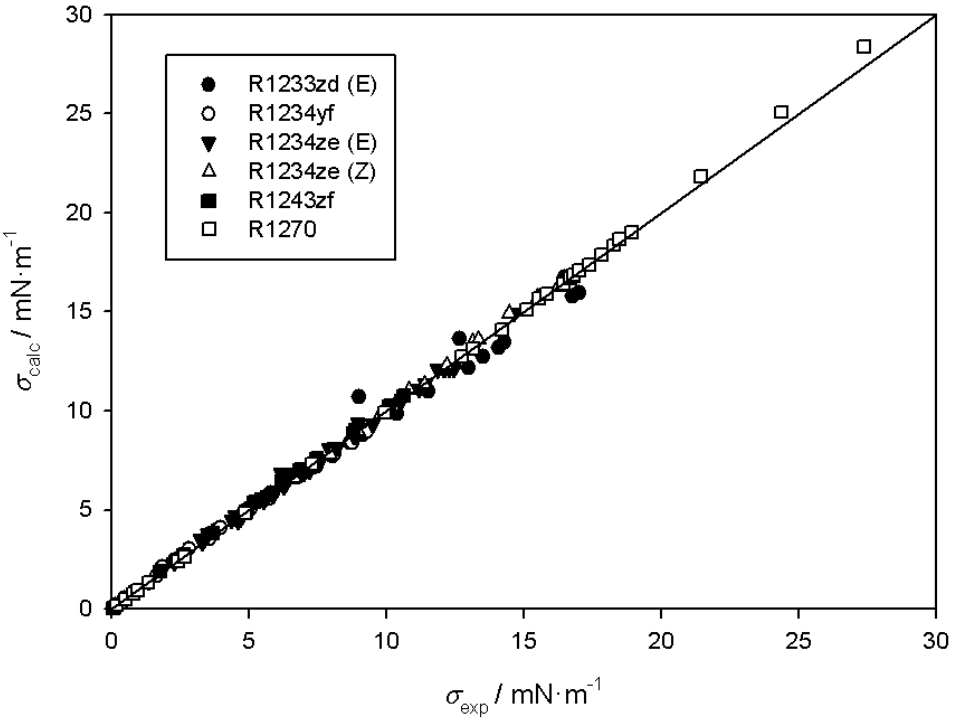

Figure 3.4: Calculated surface tension (Equation (3.7)) versus experimental surface tension of the propylene derivative refrigerants.

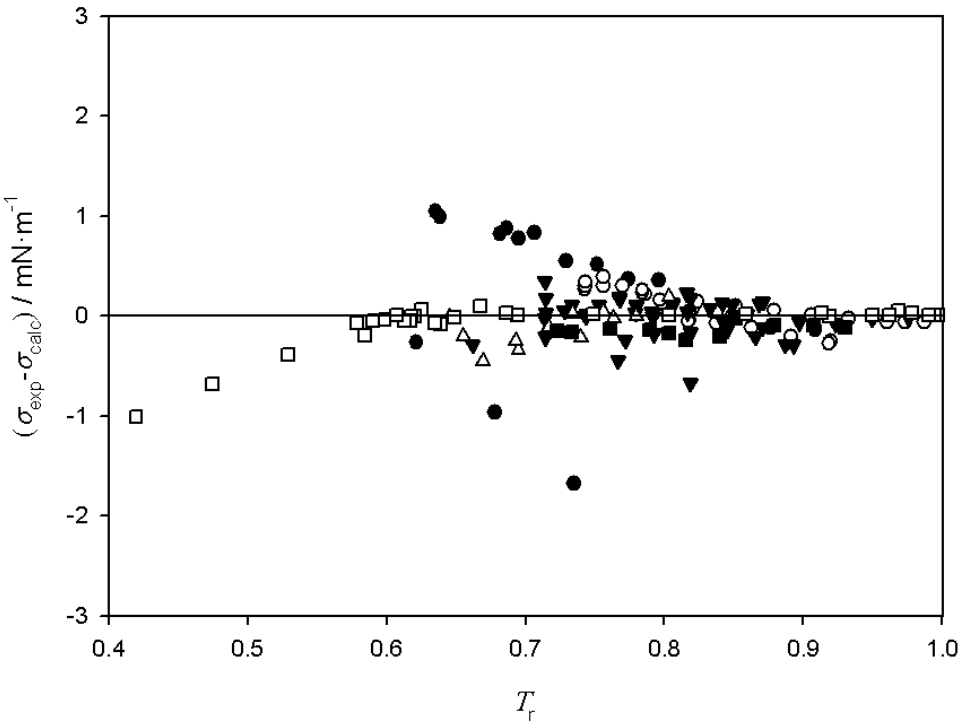

Figure 3.5: Residuals of surface tension data of propylene derivative refrigerants versus reduced temperature. Notation as in Figure 3.4.

Table 3.8: Deviations between the experimental surface tension of the refrigerant blends and the ones predicted by Equations (3.5) and (3.9).

Mixture	N. of data	AARD(σ) % Equation (3.5)	AARD(σ) % Equation (3.9)
R134a(1) + R1234yf(2)	24	10.19	2.19
R134a(1) + R1234ze(E)(2)	9	6.70	2.55
R32(1) + R1123(2)	14	14.81	2.03
R32(1) + R1234yf(2)	18	9.19	9.42
R32(1) + R1234ze(E)(2)	82	13.78	3.09
Average	-	12.30	3.58

are reported in Table 3.8 and further information for Equation (3.9) is provided in Figure 3.6 and Figure 3.7. The improvements of Equation (3.9) with respect to Equation (3.5) are evident (AARD(σ) = 3.58% and AARD(σ) = 12.30%, respectively). However, since none of the binary systems studied in the present work was considered to develop Equation (3.5) (Table 3.5), all the results obtained with this equation should be considered predictive for the studied blends. The achieved results are of the same level of the ones obtained by Khosharay et al. [177] (AAD = 4.35%) which were obtained for blends of HFCs and with an entirely different approach. The best and the poorest results for Equation (3.9) are visible in Figure 3.8 and Figure 3.9, that show a comparison between experimental and calculated data of R32 + R1123 (AARD(σ = 2.03%) and R32 + R1234yf (AARD(σ = 9.42%), respectively. However, from Figure 3.9, it clear that most of the experimental surface tension data are very small in value, thus their percentage deviations are high.

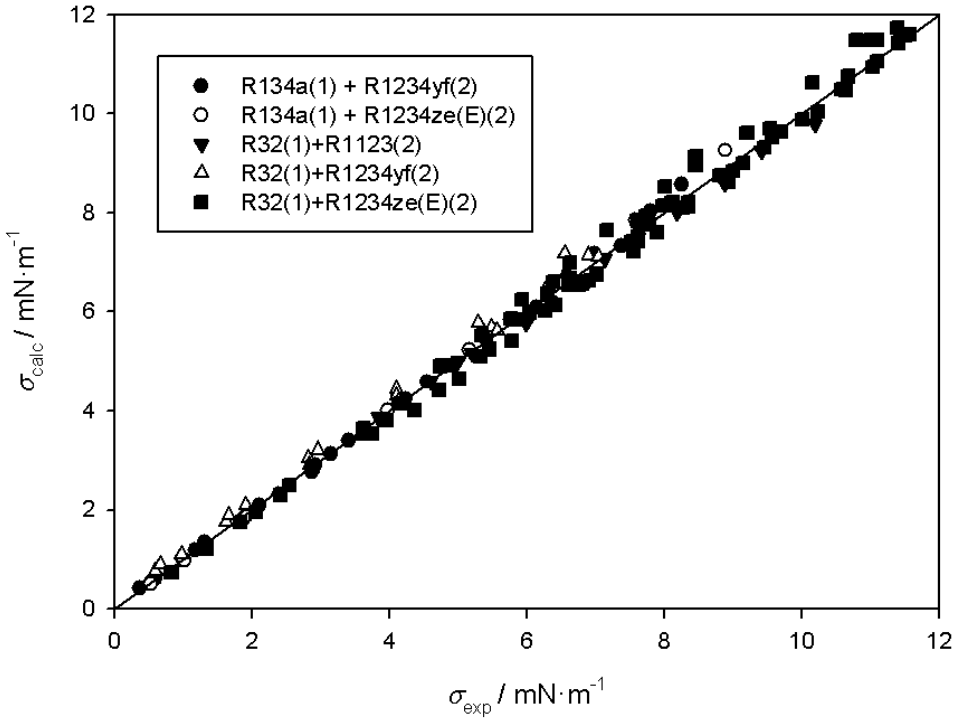

Figure 3.6: Calculated surface tension (Equation (3.9)) versus experimental surface tension of binary systems.

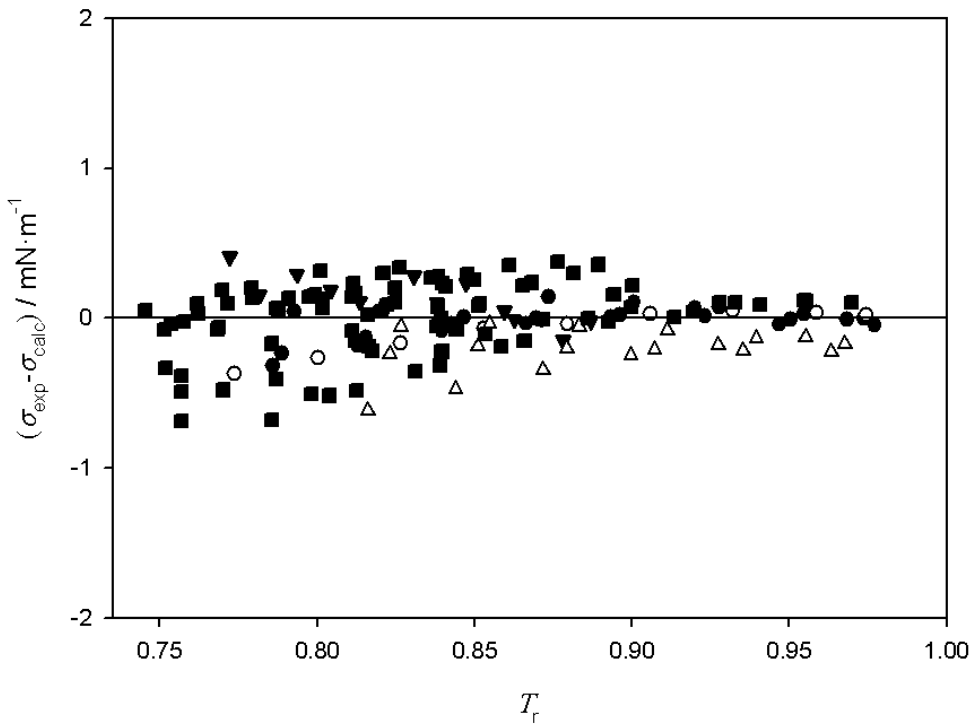

Figure 3.7: Residuals of surface tension data of binary systems versus reduced temperature. Notation as in Figure 3.6.

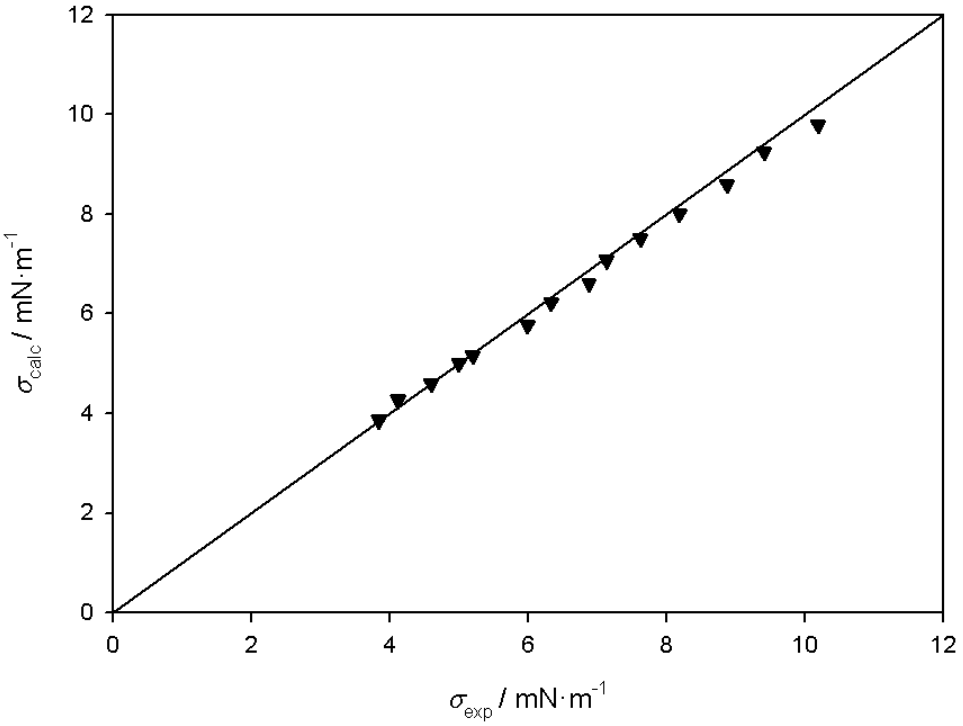

Figure 3.8: Calculated surface tension (Equation (3.9)) versus experimental surface tension of R32 + R1123.

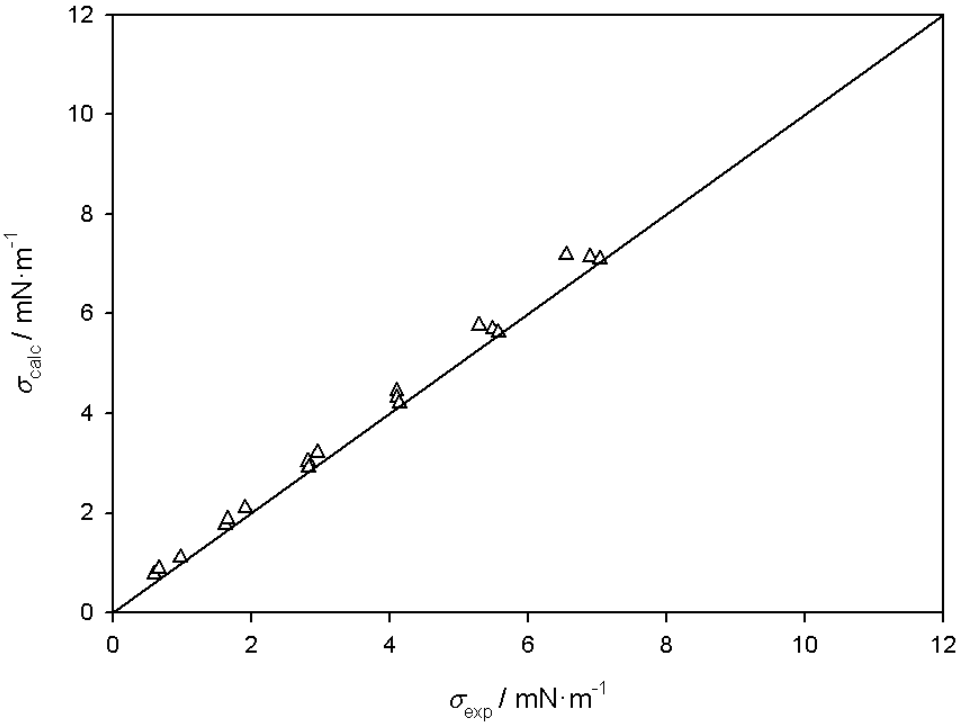

Figure 3.9: Calculated surface tension (Equation (3.9)) versus experimental surface tension of R32 + R1234yf.

3.2 Thermal conductivity

On the basis of the Fourier's law of heat conduction, the thermal conductivity (λ) can be defined as a measure of the ability of a material or substance to transfer heat through conduction. For this reason, thermal conductivity knowledge is essential for heat transfer processes, especially for refrigerating operations. Therefore, in addition to its experimental determination, estimation of λ for several substances, especially in the liquid and gas phases, has been the subject of many studies. The SI unit of λ is $\mathrm{W\,m^{-1}\,K^{-1}}$. For several simple organic liquids, their thermal conductivities (λ_L) are between 10 and 100 times larger than those of the same substance in the gaseous state (λ_V) at low pressure and same temperature [52].

Equations to predict the thermal conductivity of gasses are historically based on the kinetic theory of gases [187, 188]. A good compilation of the main historical equations is given in a past book [189]. Recently, a gene expression programming mathematical strategy was utilized for gases at atmospheric pressure [190]. As predicted by the kinetic theory of gasses and confirmed by experimental data, λ of low-pressure gasses increases with increasing temperature [52]. Instead, at high pressure, increasing temperature results in a smaller thermal conductivity. Besides, λ_V increases with pressure, but the effect is relatively small at low and moderate pressures [52]. Near the critical point, λ is quite sensitive to both temperature and pressure and shows an unusual behavior.

During the last century, several theories that provide equations to predict the thermal conductivity of liquids have appeared. These theories include equations based on specific material properties such as density and/or heat capacity [191, 192] and temperature, and theoretical calculations which consider intermolecular distances [193]. As for the gasses, the two properties that mostly influence λ_L are temperature and pressure. In particular, λ_L of most liquids decreases with increasing temperature, but water and some aqueous solutions are exceptions. Its variation for liquids is usually linear with the variation of temperature under the normal boiling point or near it [52]. Instead, at moderate pressure (up to values of 5-6 MPa), even if it increases with pressure, the effect of pressure on λ_L is usually neglected, except near the critical point that represents a singularity where the behavior of the liquid is like that of a dense gas [52]. Some of the theories for λ_L prediction are briefly described below.

Bridgman in 1923 proposed an equation for the calculation of λ_L starting from simple physical concepts [193]. A "cubic-like" distribution for molecules of liquids was assumed. Moreover, the author assumed that the difference in energy between adjacent molecules is transferred along a row of molecules in the direction of the temperature gradient with the velocity of sound. The Bridgman equation for thermal conductivity of liquid has the following form:

$$\lambda_\mathrm{L} = \frac{2\,\alpha\,W_\mathrm{L}}{\delta^2} \tag{3.10}$$

where α is a constant, W_L is the speed of sound in liquid in $\mathrm{m\,s^{-1}}$ and δ is the average distance between the centers of molecules in m. δ is the key parameter of the equation and is defined as:

$$\delta = \left(\frac{m}{\rho_\mathrm{L}}\right)^{0.33} \tag{3.11}$$

where m is the absolute weight of one molecule of the liquids and ρ_L is the liquid density.

Equation (3.10) gives approximately correct values of λ_L at atmospheric pressure (differences ranging from -13% to +29%). Instead, probably due to excessive equation simplifications, it provides inaccurate values for liquids under pressure.

Kardos in 1934 presented a theoretical equation for the estimation of λ_L based on the Debye theory for heat conduction in nonmetallic solids [194]. This theory establishes a certain apparent analogy between the heat conduction mechanism in solid insulators and gases. Kardos modified Equation (3.10) to avoid specifying the amount of molecular energy. Besides, the author assumed that the temperature drops in the liquid changes exponentially and that the energy drop occurs in the intermolecular spaces. Then it was assumed that the molecules in the liquid layer are oriented end to end on long chains in a two-dimensional pattern and that the heat is transferred along a row of molecules with the velocity of sound, as in Equation (3.10). The chains or layers repeat themselves. The author considered the distance l between the surfaces of adjacent molecules, instead of the distance of their centers δ. The Kardos scaled equation is:

$$\lambda_L = \rho_L \, C_{pL} \, W_L \, l \tag{3.12}$$

where ρ_L is the critical density in $\mathrm{kg\,m^{-3}}$, C_{pL} is the heat capacity of liquids at constant pressure in $\mathrm{kJ\,K^{-1}}$ and l is expressed in m. Deviations of the Kardos equation from the experimental data were checked by Vargaftik [195] for 11 liquids. These deviations were found to be about 40 % when l was assumed to be constant for all liquids, and from (6 to 18) % when individual values of l for each liquid were used. The same kind of deviations was confirmed also by Sakiadis & Coates [196, 197].

Although the Kardos equation has a strong theoretical basis and it was considered as a starting point to many other studies, the proposed formulas led often to very poor results or contained parameters difficult to manage and do not appear useful for engineering purposes [196]. It is worthwhile pointing out that theories have not been successful in formulating useful and accurate equations to estimate λ_L [52]. For this reason, empirical or semi-empirical estimation models are usually employed to evaluate λ_L for engineering applications at specific temperature and pressure conditions.

An empirically modified version of the Kardos equation for λ_L specifically oriented to refrigerants is presented in this thesis. This formula was correlated and was found to be valid both for the liquid and the vapor thermal conductivity estimation along saturation for different refrigerants, namely R12, R22, R23, R32, R123, R124, R125, R134a, R143a, R152a, R245fa, R1234yf, R1234ze(E), R717, R744, R50, R170, R290, R600, R600a, R1150 and R1270 (information about these fluids are reported in Table 2.1). In the proposed equation, the thermal conductivity is a function of two constant parameters, namely the critical density and the radius of gyration, substituting the liquid molar volume and the distance of adjacent molecules, respectively. Consequently, the resulting equation is much simpler, still being a scaled equation. In the proposed equations, an adimensional factor was regressed to minimize the deviations. To evaluate the goodness of the proposed correlation, the deviations between the selected data and the values calculated from these equations and different correlations specifically oriented to refrigerants available in literature were calculated and compared. These results have been also presented elsewhere [198]. Moreover, the results provided by the presented correlation were compared with the REFPROP 10.0 [65] predictions, which are calculated from fluid-specific correlations, a modification of the extended CSP model, or the friction theory model.

It is important to note that the thermal conductivity data of refrigerants of different generations were collected and used in the development of the proposed equation. Therefore, this equation is not specifically oriented to low GWP refrigerants.

3.2.1 Overview of the existing models

Some of the most well-known and widespread models available in the literature that can be used for the evaluation of λ of refrigerants are briefly described below. It is worth to point out that the selected models are based on a different approach, making use of certain fixed parameters to evaluate λ.

Recently, Khosharay et al. [199] carried out a literature survey of the available data of λ for 31 refrigerants both in liquid and vapor phases. Based on the similarity between the PvT and $T\lambda P$ diagrams for fluids, a thermal conductivity model based on Heyen EoS [176] was developed for pure refrigerants and their blends. In this model, a genetic algorithm was used to determine the adjustable parameters of the model.

The Sato-Riedel equation [200] is a rather simple equation to estimate the thermal conductivity of liquids that requires knowledge of a limited number of properties and is defined as:

$$\lambda_{\mathrm{L}} = \frac{1.11}{M^{0.5}} \frac{3 + 20\,(1 - T_{\mathrm{r}})^{0.66}}{3 + 20\,(1 - T_{\mathrm{b}})^{0.66}} \tag{3.13}$$

where M is the molecular mass, T_{r} is the reduced temperature and T_{b} is the reduced temperature at the boiling point.

The Sheffy & Johnson equation [201] is also a very simple equation for λ_{L} which has the following form:

$$\lambda_{\mathrm{L}} = 1.951 \frac{1 - 0.00126\,(1 - T_{\mathrm{m}})}{T_{\mathrm{m}}^{0.216}\, M^{0.3}} \tag{3.14}$$

where T_{m} is the melting temperature. In general, Equation (3.14) provides sufficiently accurate values for λ_{L} when the reduced temperature is less than 0.7.

The Latini equation is probably the most commonly known and widespread equation for λ_{L} of organic liquids [202] and is generally recommended [52]. This equation was proposed for several chemical families of compounds including olefins, saturated hydrocarbons, cycloparaffins, aromatics, alcohols, ketones, carboxylic acids, refrigerants and esters, but its main drawback is that it is inaccurate for reduced temperatures above 0.65. In particular, the most recent equation for λ_{L} of refrigerants has the following expression:

$$\lambda_{\mathrm{L}} = A \left[\sqrt{5} \frac{(\Phi - T_{\mathrm{r}})^2}{\Phi + T_{\mathrm{r}}} \right]^a \tag{3.15}$$

where Φ is the golden ratio whose value is linked with the Fibonacci's sequence, a is a parameter specif for each series of refrigerants and A is the value of the thermal conductivity of the specific fluid at the reduced temperature corresponding to the mantissa of the golden ratio. However, the main limit of A is the need for an experimental λ_{L} value of the studied fluids. To overcome this limit, the following expression for A was proposed [202]:

$$A = A' \frac{T_{\mathrm{b}}^{\alpha}}{M^{\beta}\, T_{\mathrm{c}}^{\gamma}} \tag{3.16}$$

where A', α, β and γ are regressed parameters for each series of refrigerants.

A recent equation that overcomes prediction limitations near the critical point was proposed by Gharagheizi et al. [203], who adopted a GEP [204] mathematical strategy:

$$\lambda_{\mathrm{L}} = 1 \cdot 10^{-4} \left[10\,\omega + 2\,P_{\mathrm{c}} - 2\,T + 4 + 1.908 \left(T_{\mathrm{b}} + \frac{1.009\,B^2}{M^2} \right) + \frac{3.9287\,M^4}{B^4} + \frac{A}{B^8} \right] \tag{3.17}$$

where

$$A = 3.8588\,M^8\,(1.0045\,B + 6.5152\,M - 8.9756) \tag{3.18}$$

and

$$B = 16.0407\,M + 2\,T_{\mathrm{b}} - 27.9074 \tag{3.19}$$

This equation was also used for λ_{L} estimation of amines, silanes/siloxanes, inorganic compounds, sulfides/thiophenes, mercaptanes, epoxides, peroxides, nitriles, elements, and aldehydes. On the other hand, the main drawback of this equation is that it was based on an empirical approach, with a huge number of coefficients being correlated.

In a recent paper proposed by Di Nicola et al. [69], a simple empirical correlation to represent λ_{L} of refrigerants was presented and has the following expression:

$$\frac{\lambda_{\mathrm{L}}}{\lambda_0} = a\,T_{\mathrm{r}} + b\,P_{\mathrm{c}} + c\,\omega + \left(\frac{e}{M} \right)^d + f\,\mu \tag{3.20}$$

where ω is the acentric factor, P_{c} is the critical pressure, μ is the dipole moment and a, b, c, d, e, f and λ_0 are the coefficients of the correlation specific for each series of refrigerants. In fact, the refrigerants were divided into four subgroups according to the different chemical halogen forming the compounds, and analyzed separately.

3.2.2 Proposed equation

Initially, the values of thermal conductivity, critical density, speed of sound and heat capacity at constant pressure for different refrigerants were collected from the 2013 ASHRAE handbook [205]. During the data collection, a fluid-by-fluid analysis was performed. The available data were smoothed from the triple point temperature up to the critical point both for the liquid and the vapor phases along saturation. Moreover, as explained in the original book, different EoSs were used to obtain the values of the critical density, heat capacity and speed of sound.

The values of the radius of gyration (G_{r}) for the studied refrigerants were collected from the DIPPR database [51] and are reported in Table 2.1. From the general definition, G_{r} can be calculated as the root mean square distance of the objects' parts from either a given axis or its center of gravity. This physical property can be defined as the radial distance from a given axis at which the mass of a body could be concentrated without altering the rotational inertia of the body about that axis. For a planar distribution of mass rotating about the same axis in the plane of the mass, G_{r} can be considered as the equivalent distance of the mass from the axis of rotation. G_{r} plays an important role in chemistry. It is usually a better estimate of the chain dimensions than the root-mean-squared end-to-end distance. The end-to-end distance is difficult to measure, while this property can be measured by a light scattering technique. Furthermore, excluding carbon dioxide, the radius of gyration is well related to molar mass, as witnessed by Figure 3.10, where G_{r} is showed as a function of M.

It is worthwhile pointing out that a great number of selected G_{r} values were obtained from Stuper et al. [206] where the radii of gyration of the compounds were derived from a molecular mechanics algorithm based on the strain function minimization. This algorithm simulates the actual structural shape of a molecule by an iterative

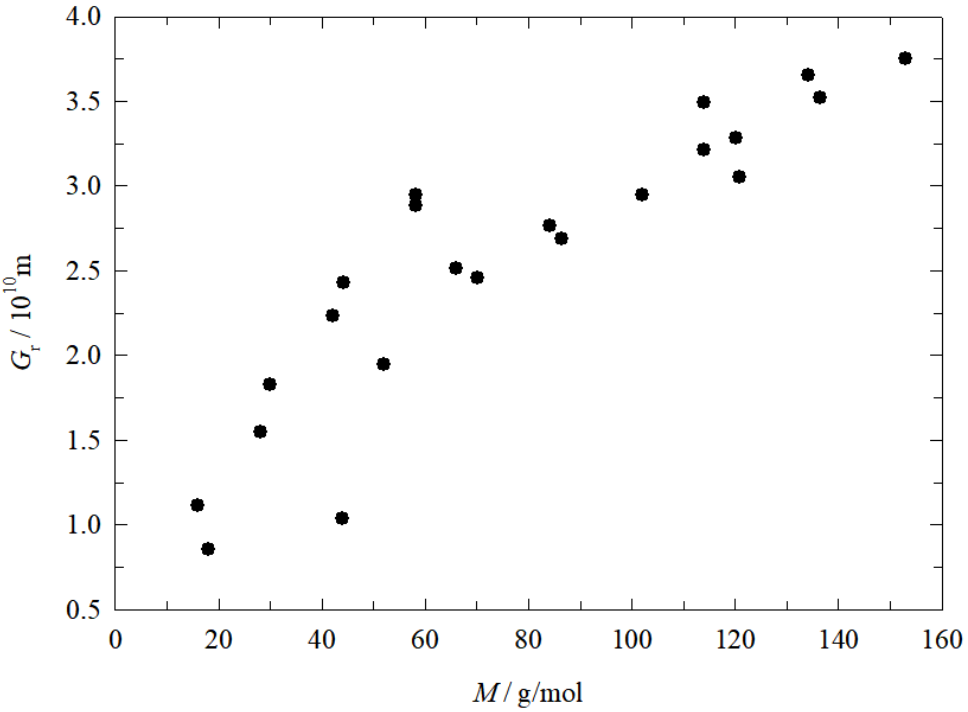

Figure 3.10: Radius of gyration as a function of the molar mass.

minimization of the potential energy functions, which define the simple harmonic and elastic forces that hold together the particles of a molecule. In the original book, it is pointed out that when the results of the molecular modeling program are compared with reliable experimental data and other molecular modeling routines, acceptable deviations were obtained. As indicated in the DIPPR database [51], the uncertainty of G_r calculated from the Stuper et al. [206] algorithm is less than 3 %.

Starting from these considerations, the following modified Kardos equation for λ_L was proposed:

$$\lambda_L = \epsilon_L \, \rho_c \, C_{pL} \, W_L \, G_r \tag{3.21}$$

where ϵ_L is an adimensional factor regressed fluid by fluid for each liquid refrigerant at reduced temperatures up to 0.90. To optimize this factor, the Levenberg-Marquardt curve-fitting method [207] was adopted. This method is a combination of two minimization methods: the gradient descent method and the Gauss-Newton method. The Root Mean Square Deviation of the thermal conductivity (RMSD(λ)) was minimized and is defined as:

$$RMSD(\lambda) = \sqrt{\frac{\sum_{i=1}^{N} \left(\lambda_{exp,i} - \lambda_{calc,i}\right)^2}{N}} \tag{3.22}$$

1 where N is the number of experimental data.

It is well known that the liquid state differs from the gas state in that the individual molecules are affected considerably by the presence of their neighboring molecules and that Kardos model considered the molecules to be aligned and perpendicular to the direction of the heat flow. However, a similar modified Kardos equation for the vapor thermal conductivity (λ_V) is proposed:

$$\lambda_V = \epsilon_V \, \rho_c \, C_{pV} \, W_V \, G_r \tag{3.23}$$

where C_{pV} is the heat capacity of vapor at constant pressure, W_V the speed of sound in the vapor phase and ϵ_V is an adimensional factor regressed fluid by fluid for the vapor refrigerant, optimized again by the Levenberg-Marquardt curve-fitting method by minimizing RMSD(λ) at reduced temperatures up to 0.90.

The coefficients for liquids and vapors are reported in Table 3.9, together with the deviations between the experimental and the calculated λ for each fluid. In particular, the Average Absolute Relative Deviation of the thermal conductivity (AARD(λ)) reported in Table 3.9 for each fluid was calculated according to:

$$AARD(\lambda)\% = \frac{100}{N} \sum_{i=1}^{N} \frac{\mid \lambda_{exp,i} - \lambda_{calc,i} \mid}{\lambda_{exp,i}} \tag{3.24}$$

3.2.3 Results and discussion

From the results of Table 3.9, it is possible to state that, even if G_r replaces the intermolecular distance for chain compounds in the proposed equations, the Kardos assumption is still valid for the liquid refrigerants: the molecules can be considered to be aligned, like rods in a bundle, perpendicular to the direction of the heat flow. This arrangement is a reliable approximation for long-chain molecules. For shorter molecules, the disorder increases and the molecular arrangement changes. This is probably the reason why fluids with lower radii of gyration (i.e. R50, R717, R170, R744, R23 and R1150), corresponding to smaller molecular masses, generally showed higher

Table 3.9: Adopted parameters and deviations for Equations (3.21) and (3.23).

Refrigerant	ϵ_L	AARD(λ_L) %	RMSD(λ_L) ($W\,m^{-1}\,K^{-1}$)	ϵ_V	AARD(λ_V) %	RMSD(λ_V) ($W\,m^{-1}\,K^{-1}$)
R12	0.77641	0.8	0.0008	0.62636	8.1	0.0008
R22	0.86914	0.4	0.0007	0.56705	6.4	0.0006
R23	1.06893	7.6	0.0147	0.54491	2.6	0.0003
R32	1.43009	1.9	0.0051	0.5591	6.2	0.0014
R123	0.52532	3.5	0.003	0.54673	14.1	0.0014
R124	0.5839	2.3	0.0019	0.60065	10.7	0.0013
R125	0.6503	1.7	0.0015	0.58118	9.3	0.001
R134a	0.73318	1.9	0.002	0.59879	13.7	0.0013
R143a	0.86548	1.5	0.0017	0.65242	9.7	0.0011
R152a	0.91102	1.5	0.0017	0.6777	-	0.002
R245fa	0.53365	3.9	0.0039	0.57561	5.1	0.0009
R1234yf	0.6907	3.6	0.003	0.6354	8.2	0.0011
R1234ze (E)	0.70283	4.1	0.0038	0.67749	8	0.0012
R717	4.13607	7.3	0.0435	1.06528	7.7	0.0024
R744	3.07933	4.1	0.0063	1.81605	2.5	0.0004
R50	2.02643	9.8	0.0149	1.15924	7.3	0.0011
R170	1.37046	7.3	0.0115	0.81834	19.7	0.0018
R290	0.92499	2.6	0.0039	0.77607	13.5	0.0016
R600	0.7443	2.3	0.0028	0.71549	12.8	0.0021
R600a	0.69095	2.3	0.0026	0.71694	12.8	0.0019
R1150	1.7536	5.2	0.0094	0.90406	3.1	0.0004
R1270	1.15227	2.8	0.0047	0.83963	13.6	0.0018
Average	1.2	3.6	0.0065	0.8	9.3	0.0013

AARD(λ_L), as witnessed also by Figure 3.11, where AARD(λ_L) for each refrigerant are reported as a function of G_r. However, in general, deviations for liquids are very low (average AARD(λ_L) = 3.6 %).

For the liquid refrigerants, the model generally works for reduced temperatures up to 0.90. In some cases, the model overestimates λ_L approaching the critical point, as shown in Figure 3.12 for R22. In particular, the model describes very well the trend of λ_L for the methane derivatives, ethane derivatives, R290, R600 and R600a, as showed in Figure 3.13, where the experimental values from DIPPR [51], smoothed values from ASHRAE [205] and calculated λ_L values are reported for R134a as example. For R744, R717, R50, R170, R1150, R1234yf and R1234ze(E), the model slightly underestimates λ_L at lower reduced temperatures and overestimates λ_L at higher reduced temperatures.

Instead, as expected, due to the increasing of the molecular disorder, deviations for vapor refrigerants are higher (average AARD(λ_V) = 9.8 %). In this case, deviations are rather scattered and do not seem to be depending on G_r. Figure 3.14 shows the AARD(λ_V) values as function of G_r. However, even if the equation was not originally developed for vapors, it was found to be surprisingly accurate for many refrigerants in the vapor phase, with the deviations being well below 10 % for the main part of them. An example of behavior of λ_V is reported in Figure 3.15, where the experimental values from DIPPR [51], smoothed values from ASHRAE [205] and calculated λ_V values are reported for R290. However, the proposed equation was not working for R152a, with the deviations being higher than 100 %.

In addition, Figures 3.16 and 3.17 show the adimensional factors ϵ_L and ϵ_V versus G_r for each refrigerant. From these figures, a strong dependence of the adimensional factors on G_r is evident, especially for the liquid refrigerants.

The chemical reason for this behavior is probably related to the general different shapes of the molecules of some refrigerants, such as R717, R744, R50 and R1150. These fluids have molecules with a general compact shape and show a ϵ_L coefficient very far from unity (from 4.1 to 1.7 as shown in Table 3.9). On the other hand, the other

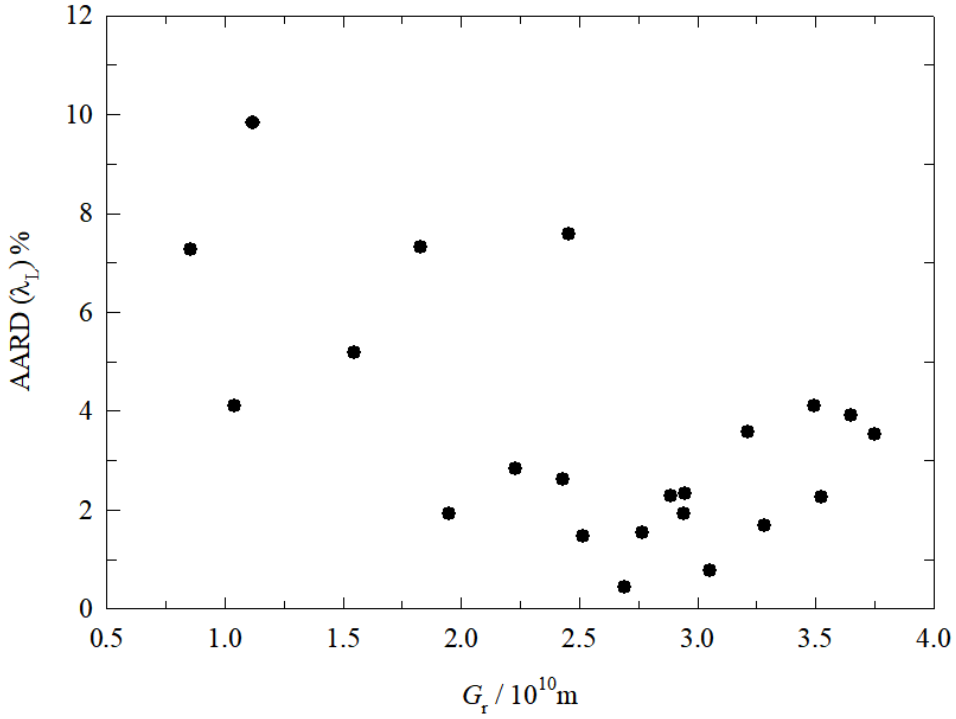

Figure 3.11: Deviations for each liquid refrigerant as a function of radius of gyration.

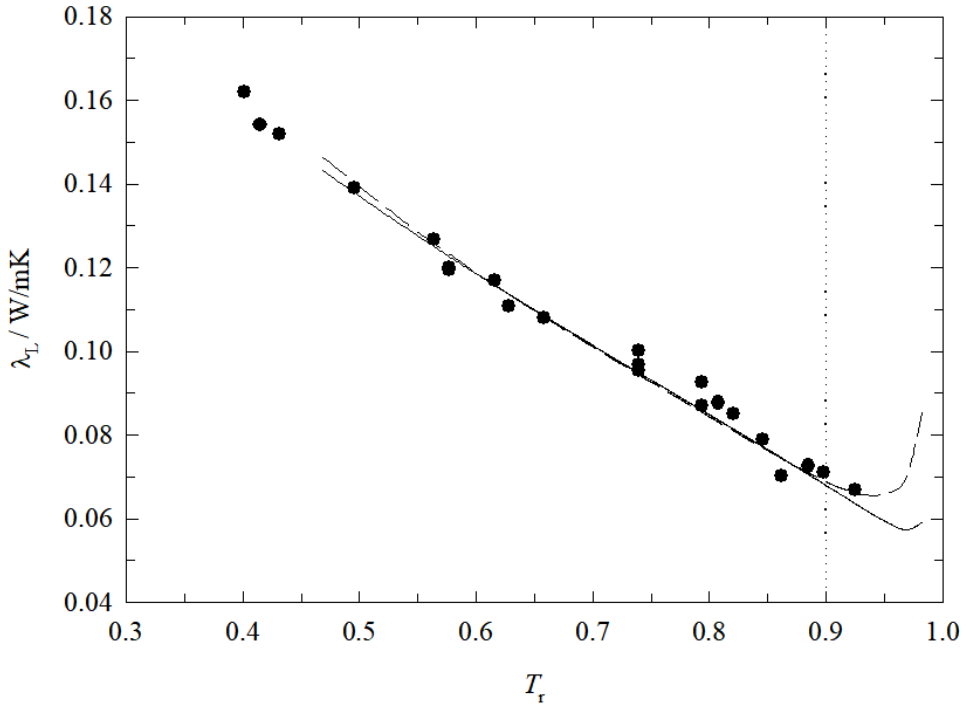

Figure 3.12: Experimental values from DIPPR (black points), smoothed values from ASHRAE (solid line) and calculated liquid thermal conductivities (dashed line) for R22.

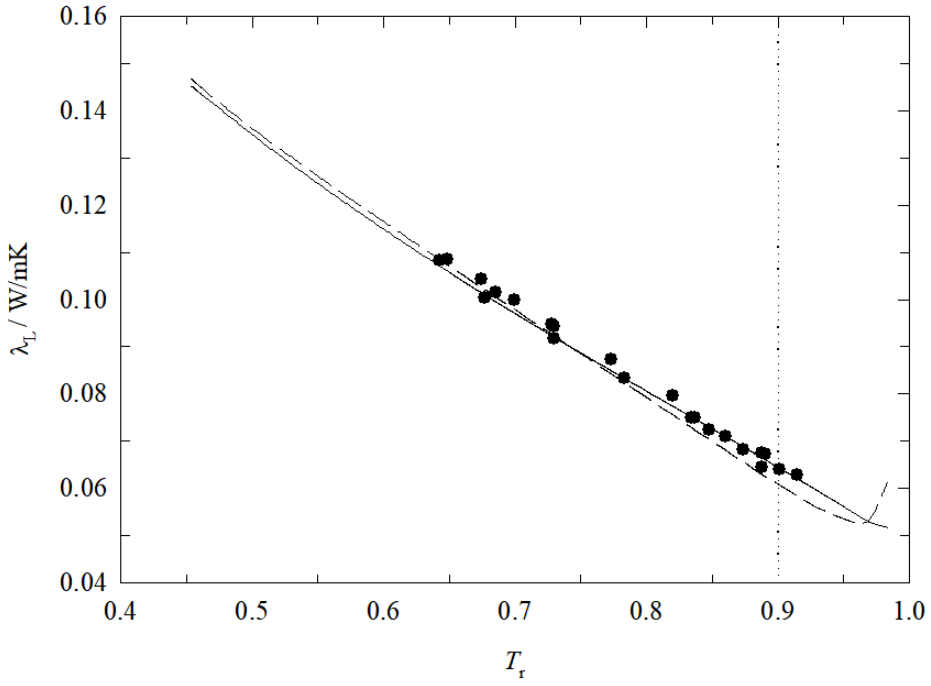

Figure 3.13: Experimental values from DIPPR (black points), smoothed values from ASHRAE (solid line) and calculated liquid thermal conductivities (dashed line) for R134a.

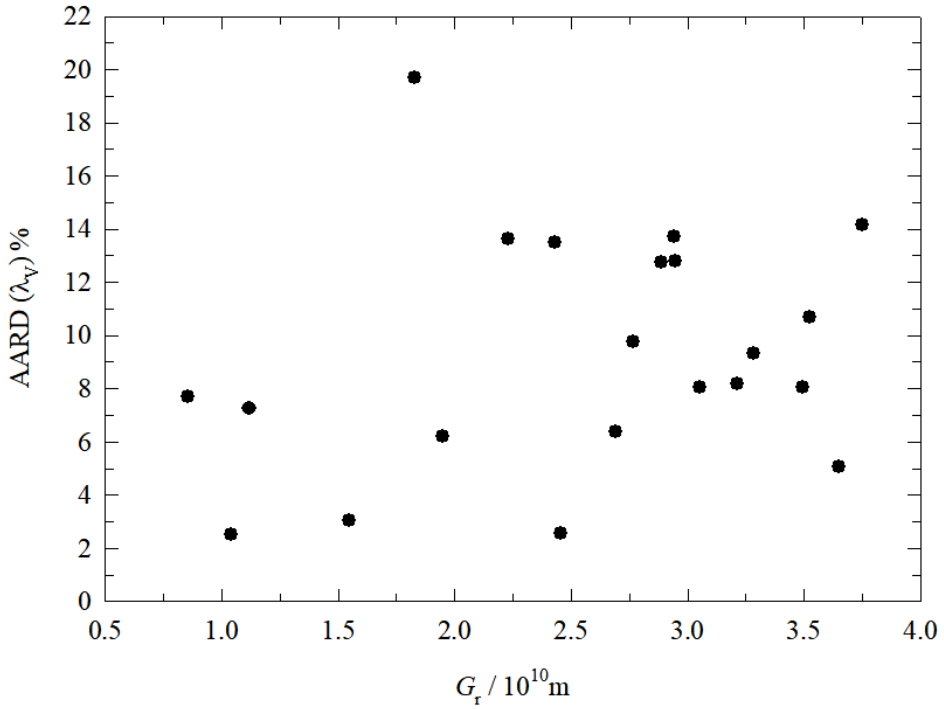

Figure 3.14: AARD(λ_V) for each refrigerant as a function of radius of gyration.

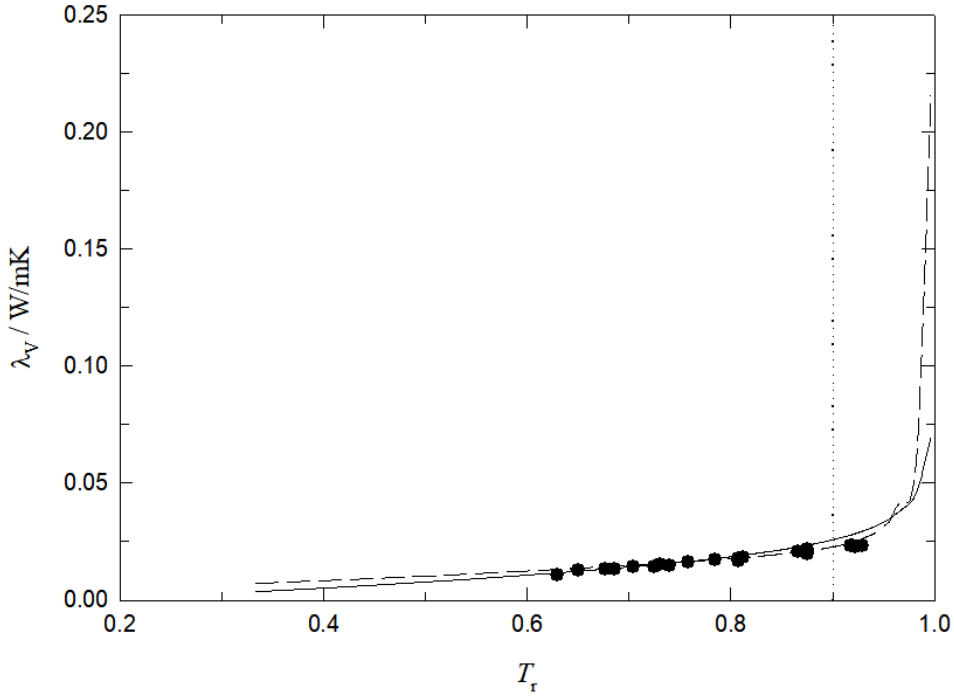

Figure 3.15: Experimental values from DIPPR (black points), smoothed values from ASHRAE (solid line) and calculated vapor thermal conductivities (dashed line) for propane (R290).

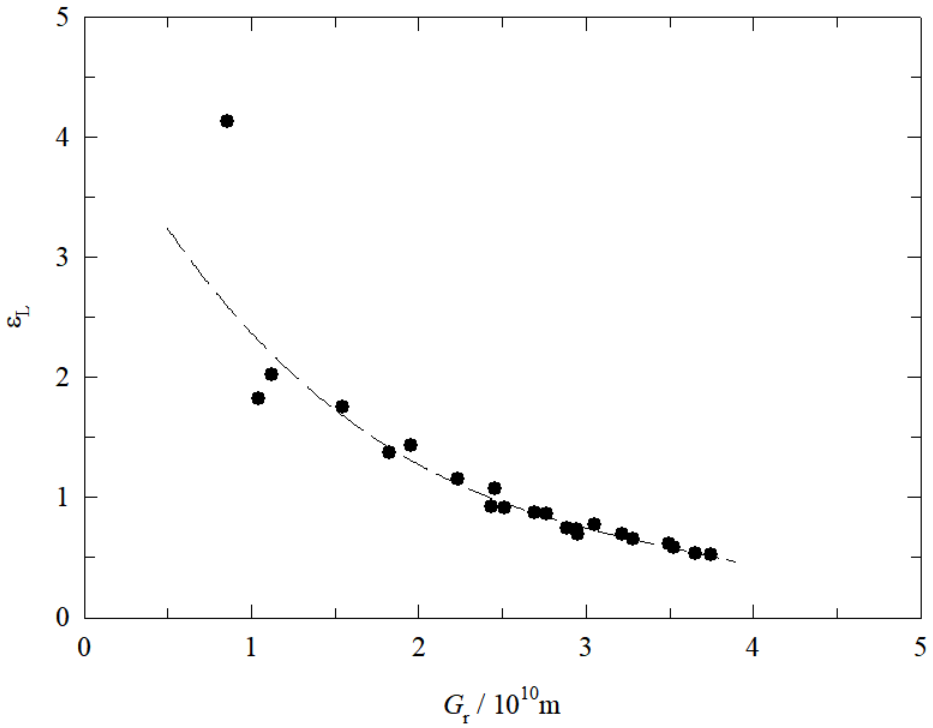

Figure 3.16: Adimensional factor ϵ_L versus the radius of gyration. The dashed line represents the polynomial regression.

selected refrigerants have a linear or a branched molecular shape and their coefficient ϵ_L is generally very close to unity (from 0.5 to 1.3 as shown in Table 3.9). It has to be considered that, since the refrigerant category is very heterogeneous, these fluids are very different in terms of chemical structure. The different shapes of the molecules of refrigerants together with the polarity are strongly influencing the thermophysical properties, especially λ. G_r is well related to the shape of the molecules and this is probably the reason way ϵ_L was found to be so sensitive to G_r, as visible in Figure 3.16.

For the liquid refrigerants, the following polynomial regressing equation for ϵ_L as function of G_r was obtained:

$$\epsilon_L = -0.2941\, G_r^3 + 2.44\, G_r^2 - 6.9302\, G_r + 7.5856 \tag{3.25}$$

To simplify Equation (3.25), G_r was considered in angstrom (Å) units. Since the adimensional factorϵ_L can be described with Equation (3.25) without significant loss of accuracy, Equation (3.21) could be extended to other organic liquids for which G_r is known. From Figure 3.17, the dependence of ϵ_V on G_r is still evident. However, the regression brought a significant increase of deviations for Equation (3.23) during λ_V prediction, and in this case the polynomial regression was not considered.

To compare the goodness of the aforementioned literature models [69, 194, 199–203], REFPROP 10.0 [65], and the proposed equation for λ_L, the deviations between the calculated and experimental data were calculated and their AARD(λ_L) are reported in Table 3.10.

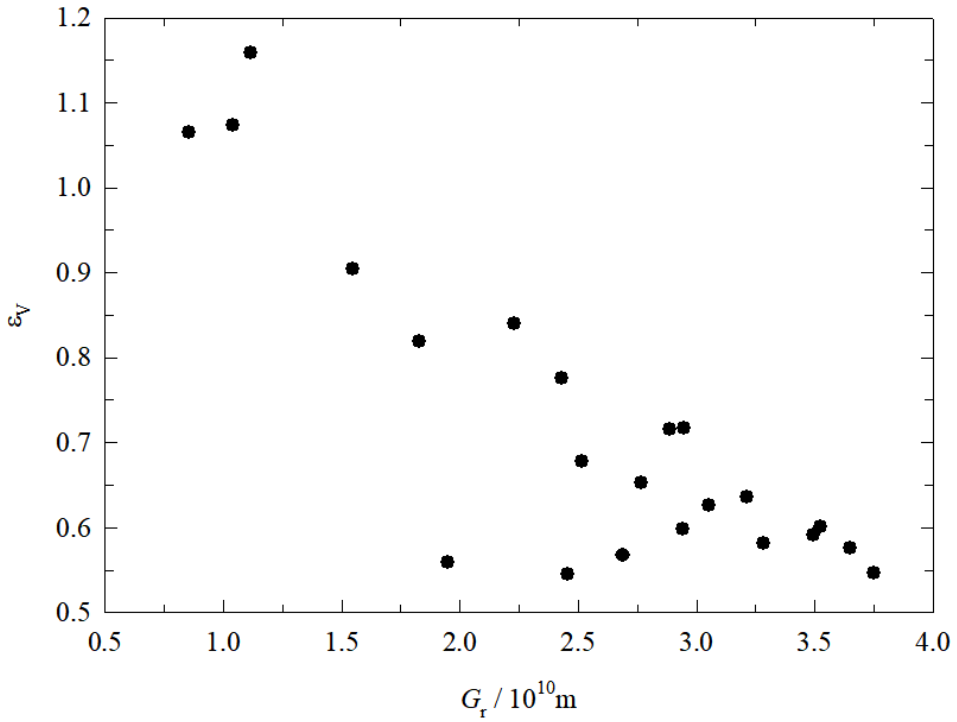

Figure 3.17: Adimensional factor ϵ_V versus the radius of gyration.

Table 3.10: Deviations between smoothed values from ASHRAE and calculated liquid thermal conductivities.

Refrigerant	Number of points	AARD(λ_L) % Equation (3.12)	AARD(λ_L) % Equation (3.13)	AARD(λ_L) % Equation (3.14)	AARD(λ_L) % Equation (3.15)	AARD(λ_L) % Equation (3.17)	AARD(λ_L) % Equation (3.20)	AARD(λ_L) % Equation (3.21)	AARD(λ_L) % REFPROP 10.0
R12	59	22.4	15.6	83.5	8.3	7.9	3.3	0.8	0.1
R22	61	19.9	3.7	56.4	4.4	10.4	3.8	0.4	0.2
R23	48	23.6	4.9	51.7	5	22.7	7.7	7.6	0.02
R32	53	29	19	17.2	1.8	26.2	13.1	1.9	0.02
R123	63	10.3	16.3	61.9	4.1	8.4	3.5	3.5	0.2
R124	60	12.2	15.3	82.9	1.1	8.1	3.3	2.3	0.1
R125	53	14	9.6	76.9	10	8.9	1.8	1.7	0.03
R134a	56	14.2	4.2	56.3	7.5	9.8	3.4	1.9	0.03
R143a	53	20.7	15.9	75.1	2.7	7.9	2.2	1.5	1.3
R152a	63	16.1	9.7	50.4	1.2	8.5	6.6	1.5	0.1
R245fa	60	11.2	3.4	57	17.6	5.6	1.3	3.9	0.2
R1234yf	49	17.8	30.6	87.1	-	15.5	5.8	3.6	5.4
R1234ze(E)	53	15.3	19.8	63.9	-	11.2	1.5	4.1	4.82
R717	59	38.8	57.1	54.2	-	30.5	48.7	7.3	6.9
R744	37	9.9	15	39.1	-	14.4	12	4.1	1.4
R50	24	19.4	50.4	114.2	4.7	22	32.9	9.8	0.2
R170	61	22	21.3	60.8	19.2	19.5	16.9	7.3	0.1
R290	59	15.6	27.2	68	33.5	20.6	17.3	2.6	0.02
R600	58	9	22.9	47.3	-	14.2	9.7	2.3	0.03
R600a	55	7.9	37.4	88.7	-	22.7	18.9	2.3	0.02
R1150	56	29.4	11.7	50.2	-	16.4	12.3	5.2	4.8
R1270	63	25.9	13.1	48.4	-	8.2	4.2	2.8	6.6
Average	-	18.5	18.4	62.1	9	14.2	9.9	3.6	1.5

As a starting comparison for λ_L prediction, the original Kardos equation [194] where the original constant value was assigned to l, was considered. From the analysis of the results reported in Table 3.10, the higher prediction capability of the proposed model is evident (overall AARD(λ_L) = 18.5 % and AARD(λ_L) = 3.6 % for Equations (3.12) and (3.21), respectively).

As shown in Table 3.10, all the studied literature correlations provided similar results apart from the Sheffy & Johnson equation [201] that, probably because of its simplicity, showed rather high deviations. Instead, good quality of prediction was shown by Latini et al. [202] and Di Nicola et al. [69] equations.

Moreover, the results provided by Equation (3.21) were compared with the ones obtained by Khosharay et al. [199]. Higher deviations were obtained for the model proposed by Khosharay et al. [199] for the liquids (overall AARD(λ) = 6.6 %) when results are compared with the results obtained with the proposed equation, while slightly lower deviations (overall AARD(λ) = 7.8 %) for the vapors were obtained, confirming the validity of the proposed model. However, it has to be pointed out that the datasets under analysis in the two studies are rather different.

Finally, a comparison between the results given by Equation (3.21) and by REFPROP 10.0 [65] was performed. As shown in Table 3.10, REFPROP 10.0 usually ensured lower deviations for λ_L of the selected refrigerants than the proposed correlation. This outcome was expected since REFPROP 10.0 uses accurate models developed for each fluid. A similar outcome was also obtained for the λ_V predicted from REFPROP 10.0 (overall AARD(λ) = 1.6 %).

It is important to point out that, as mentioned above, the presented equations for λ_L and λ_V are not specifically oriented to low GWP refrigerants. However, since few values of critical density, speed of sound and heat capacity at constant pressure for these alternative working fluids are available in literature, these equations can be used for a very limited number of low GWP refrigerants, such as R1234yf and R1234ze(E) (already considered in the development of the equation). Therefore, it could be important to study the prediction capability of the simpler literature models for this type of refrigerants and, if necessary for obtaining more accurate λ descriptions, to develop a new correlation specifically oriented to these fluids.

Chapter 4

Experimental measurements of thermodynamic properties

This chapter presents the experimental values of the Pressure - Specific Volume - Temperature - Composition ($PvTz$) properties of nine binary systems containing six different low GWP refrigerants measured both in the two-phase and superheated vapor regions through an isochoric apparatus. Furthermore, the triple point temperature of a low GWP refrigerant and the Solid-Liquid Equilibrium (SLE) of a binary system containing this fluid measured with an experimental apparatus specifically built for this purpose are reported. The measured data were compared with the values calculated with different models. A discussion about the obtained results is presented. Besides, the measured properties of the studied refrigerants and binary systems were compared with the experimental data available in literature and the results are reported.

4.1 *PvTz* measurements of binary systems

As mentioned in the previous chapters, the experimental data of the thermodynamic properties of blends containing low GWP refrigerants are fundamental for evaluating their potential performance in different HVAC&R applications and developing accurate models for their description. For these reasons, the $PvTz$ measurements of nine binary systems of synthetic low GWP refrigerants and conventional or natural refrigerants were carried out by using an isochoric apparatus.

In particular, the vapor-phase $PvTz$ properties for binary systems containing isobutane (R600a) and six fluorinated propene isomers were measured along different isochores for different compositions, usually in the temperature range from (303 to 383) K. The studied fluorinated propene isomers are:

- 2,3,3,3-tetrafluoroprop-1-ene (R1234yf);
- trans-1,3,3,3-tetrafluoroprop-1-ene (R1234ze(E));
- *cis*-1,3,3,3-tetrafluoroprop-1-ene (R1234ze(Z));
- *trans*-1-chloro-3,3,3-trifluoroprop-1-ene (R1233zd(E));
- *cis*-1,2,3,3,3-pentafluoroprop-1-ene (R1225ye(Z));
- 3,3,3-trifluoropropene (R1243zf).

The values of the direct environmental impact and physical properties of these refrigerants are reported in Table 2.1. Since it is becoming increasingly necessary to blend working fluids to achieve the right combination of environmental characteristics, thermophysical properties, and safety characteristics, the knowledge base of blends containing hydrocarbons and fluorinated propene isomers can be useful to evaluate their potential use in different applications. In particular, blends of hydrocarbons and unsaturated halocarbons can offer potential benefits over the single-component refrigerants alone. For example, these blends could potentially allow for the tailoring of thermodynamic and transport properties, flammability, and toxicity in ways that could allow for the blends to be used in a particular application even though the single-component options may not be appropriate or adequate for the application. Moreover, for many applications, these blends could potentially lower cost, increase lubricant solubility, and improve heat exchanger performance when compared to the single-component halogenated propene isomer working fluid options. An additional motive for undertaking these measurements is simply to expand the scientific knowledge of low-GWP blends consisting of a variety of working fluids.

Moreover, the $PvTz$ properties for different compositions of binary systems containing difluoromethane (R32) and three HFOs (R1234yf, R1234ze(E),
and R1234ze(Z)) were measured both in two-phase and superheated vapor regions along different isochores for different compositions at temperatures from (263 to 373) K. To overcome the potential limitations of different low GWP synthetic refrigerants and to improve their thermodynamic performances, blends of these alternative refrigerants, especially fluorinated propene isomers, and other more traditional refrigerants possessing better thermophysical properties, and higher, but still sufficiently low, GWP values are investigated. In particular, because of its high performance, relatively low GWP and excellent thermodynamic properties among all HFCs, R32 is considered as one of the most suitable components for low GWP refrigerant blends.

After presenting an overview of the thermophysical properties for the studied binary systems available in the literature, information about the studied samples, the experimental setup, and the measurement procedure is given. Then, the measured data for the studied binary systems are reported. Finally, the results obtained by correlating these experimental data with some models presented in Chapter 2 are presented and discussed. Moreover, the experimental values were compared with the experimentally-determined data available in the open literature.

Part of the reported $PvTz$ measurements for the nine binary systems have been already presented elsewhere [208–211].

4.1.1 Overview of measured thermophysical properties

Table 4.1 summarizes the publicly available literature of experimentally-determined data for different thermophysical properties of the measured binary systems (R1234yf + R600a, R1234ze(E) + R600a, R600a + R1233zd(E), R600a + R1234ze(Z), R1225ye(Z) + R600a, R1243zf + R600a, R32 + R1234yf, R32 + R1234ze(E), and R32 + R1234ze(Z)). It is important to point out that, although the search of the publicly available literature provided in this section is not exhaustive, a wide-ranging analysis was conducted. In particular, Table 4.1 shows the references reported in the review work of experimentally-determined thermophysical properties for low GWP working fluids and their blends proposed by Bobbo et al. [36]. Moreover, some of the most recent works available in the open literature that present experimental values of different thermophysical properties for the studied binary systems are reported in this table.

Table 4.1: Available experimental data for the binary systems measured with the isochoric apparatus.[a]

		Base component	
2nd component	Property	R600a	R32
R1234yf	VLE	[150]	[159]
			[153]
	$PvTz$	[212]	[213]
			[214]
			[215]
			[216]
	σ		[185]
			[217]
	μ		[185]
			[218]
			[219]
			[220]
	CP		[213]
R1234ze(E)	VLE	[152]	[159]
			[163]
			[221]
			[222]
	$PvTz$	[223]	[224]
			[225]
			[226]
	σ		[185]
			[180]
			[183]
			[217]
	μ		[185]
	λ		[227]
	CP		[228]
	c_p		[225]
	c_v		[229]
R1234ze(Z)	VLE	[164]	

[a] The following thermophysical property nomenclature is used in the table: Vapor-Liquid Equilibrium (VLE), Pressure - Specific volume - Temperature - Composition ($PvTz$), surface tension (σ), dynamic viscosity (μ), thermal conductivity (λ), isobaric specific heat capacity (c_p), isochoric specific heat capacity (c_v), and Critical Point (CP).

From Table 4.1, it is possible to note that no experimental have been found for R600a + R1233zd(E), R1225ye(Z) + R600a, R1243zf + R600a, and R32 + R1234ze(Z) binary systems in the open literature. Only a limited number of thermophysical properties for R1234yf + R600a, R1234ze(E) + R600a, and R600a + R1234ze(Z) binary systems were measured and reported in the open literature. In particular, Hu et al. [150] measured the VLE of R1234yf + R600a in the temperature range from (283 to 323) K founding an azeotropic behavior at R1234yf mole fraction of approximately 0.88. Zhang et al. [212] measured the gaseous densities of R1234yf + R600a binary systems at temperatures from (270.105 to 300.214) K by using a compact single-sinker densimeter based on the Archimedes' buoyancy principle. Dong et al. [152] characterized the VLE behavior of R1234ze(E) + R600a binary systems over the temperature range from (258 to 288) K, funding an azeotropic behavior. The vapor-phase $PvTz$ properties of R1234ze(E) + R600a binary systems were measured by Cao et al. [223] at temperatures from (280.15 to 330.15) K through the Burnett isothermal expansion method. The VLE behavior of R1234ze(Z) + R600a binary systems was characterized by Zhang et al. [164] at temperatures from (303 to 353) K.

Instead, different works reporting experimentally determined data for thermodynamic and transport properties of R32 + R1234yf and R32 + R1234ze(E) binary systems has been reported in the open literature. In particular, Kamiaka et al. [153] and Hu et al. [159] characterized the VLE behavior of R32 + R1234yf binary systems in the temperature ranges from (273 to 333) K and (283 to 323) K, respectively. The saturated liquid and vapor densities of R1234yf + R32 binary systems in the critical region and the vapor-liquid coexistence curves were measured for three different compositions by Akasaka [213]. Kayukawa [214] measured the liquid densities of R32 + R1234yf binary systems over the temperature range from (283 to 373) K by using a vibrating-tube measurement technique. Moreover, Cai et al. [215] and Yang et al. [216] measured vapor-phase $PvTz$ data for this binary pair over the temperature ranges from (280 to 348) K and (298 to 383) K, respectively, through a single sinker magnetic suspension densimeter and a Burnett apparatus. The VLE behavior of R32 + R1234ze(E) binary pair was measured by Hu et al. [159, 163], Koyama et al. [221] and Kou et al. [222] in the temperature ranges of (283.15 to 323.15) K, (243 to 313) K and (283.15 to 323.14) K, respectively. Jia et al. [224] measured the compressed liquid density for five compositions of R32 + R1234ze(E) binary systems at temperatures from (283 to 363) K and at pressures up to 100 MPa by using a vibrating-tube densimeter. Tanaka et al. [225] measured the liquid density and isobaric specific heat capacity of this binary pair in the temperature range from (310 to 350) K and the pressure range from (1.4 to 5.0) MPa with a metal-bellows calorimeter. The $PvTz$ measurements for R1234ze(E) + R32 binary systems at only two different mass fractions were measured by Kobayashi et. al. [226].

4.1.2 Measured Samples

Table 4.2 presents the characteristics of the following samples:

- isobutane (R600a, $CH(CH_3)_3$, CAS number 75-28-5);
- difluoromethane (R32, CH_2F_2, CAS number 75-10-5);
- 2,3,3,3-tetrafluoroprop-1-ene (R1234yf, $CF_3CF{=}CH_2$, CAS number 754-12-1);
- *trans*-1,3,3,3-tetrafluoroprop-1-ene (R1234ze(E), $CF_3CH = CHF$, CAS number 29118-24-9);

- *trans*-1-chloro-3,3,3-trifluoroprop-1-ene (R1233zd(E), $CF_3CH{=}CHCl$, CAS number 102687-65-0);
- *cis*-1,3,3,3-tetrafluoroprop-1-ene, (R1234ze(Z), $CF_3CH{=}CHF$, CAS number 29118-25-0);
- *cis*-1,2,3,3,3-pentafluoroprop-1-ene (R1225ye(Z), $CF_3CF{=}CHF$, CAS number 5528-43-8);
- 3,3,3-trifluoropropene (R1243zf, $CF_3CH{=}CH_2$, CAS number 677-21-4).

The purity of the samples, with the exception of the R600a sample, was measured by Gas Chromatography (GC) using a thermal conductivity detector. To remove non-condensable gases, almost all the measured samples were subjected to several cycles of freezing, evacuation, thawing, and ultrasonic stirring.

4.1.3 Experimental apparatus

The experimental apparatus used for the $PvTz$ measurements of the studied refrigerant binary systems is shown in Figure 4.1. Since details of this apparatus have been previously reported [230, 231], only the main information is reported below.

The core of the experimental apparatus consisted of a constant-volume spherical cell (1) made of AISI 304 stainless steel and two temperature baths (7) filled with different silicone oils (Baysilone M10 and Baysilone M100, Bayer): one of which operated at temperatures from (210 to 290) K while the other operated at temperatures from (290 to 390) K. An auxiliary thermostat (14) is used to reach below-ambient temperatures. The isochoric cell (1) containing the refrigerant sample is connected to a differential diaphragm pressure transducer (Ruska 7000) (4) connected to an electronic null indicator (5). The transducer and sphere were placed vertically, and a magnetic pump (3) for mixing the sample was connected to the sphere. A second spherical cell (2) was also connected and used for volume calibration. Because of the complex volume of the constant-volume spherical cell (1), its total volume (including the piping, the pressure transducer cavity, and magnetic pump volumes) was calibrated according to the classic Burnett calibration procedure, using helium as the reference fluid [231]. The volume of the measurement cell (V_{iso}) was found to be 273.5 cm^3 at room temperature. As described elsewhere [230], a correction for the thermal expansion and pressure distortion of the measurement cell was considered. The spherical cells and pressure transducer are immersed in one of the two thermostatic baths (7). The temperature of the thermostatic baths is controlled by a PID device (9,15) and measured with a calibrated 25 Ω platinum resistance thermometer (Hart Scientific 5680) (8).

4.1.4 Experimental procedure

Since details regarding this procedure are reported elsewhere [230, 231], a summary of the experimental procedure is provided here. A gravimetric method was used to prepare the different compositions of the studied binary system samples. For each pure refrigerant, two vacuumed titanium bottles were used as the charging bottle and recovery bottle. The required amount of refrigerant was charged into the charging bottle and weighed using a Gibertini E42S-B analytical balance (uncertainty of ±0.3 mg), while the vacuumed recovery bottle was also weighed. After connecting both bottles to the connection tubing (6), the measurement cell (1) and tubing were evacuated. Part of the mass of refrigerant contained in the charging bottle was charged into the isochoric

Table 4.2: R600a, R32, R1234yf, R1234ze(E), R1233zd(E), R1234ze(Z), R1225ye(Z), and R1243zf Sample Descriptions.

Chemical Name	Source	Initial Mole Fraction Purity	Purification Method	Final Mole Fraction Purity	Analysis Method
R600a[a]	Matheson Gas Products	0.999	none		
R32[b]	Ausimont SpA	0.9957	several cycles of freezing, evacuation, melting, and ultrasonic agitation	0.9998	GC
R1234yf[c]	Arkema, France	0.9995	several cycles of freezing, evacuation, melting, and ultrasonic agitation	0.9997	GC
R1234ze(E)[d]	Honeywell	0.995	several cycles of freezing, evacuation, melting, and ultrasonic agitation	0.999	GC
R1233zd(E)[e]	Central Glass, Ltd.	>0.995	several cycles of freezing, evacuation, melting, and ultrasonic agitation	>0.995	GC
R1234ze(Z)[f]	Central Glass, Ltd.	>0.99	several cycles of freezing, evacuation, melting, and ultrasonic agitation	>0.99	GC
R1225ye(Z)[g]	Mexichem Fluor S.A. de C.V.	>0.97	several cycles of freezing, evacuation, melting, and ultrasonic agitation	>0.98	GC
R1243zf[h]	Mexichem Fluor S.A. de C.V.	0.995	several cycles of freezing, evacuation, melting, and ultrasonic agitation	0.9975	GC

[a] isobutane [b] difluoromethane [c] 2,3,3,3-tetrafluoroprop-1-ene [d] *trans*-1,3,3,3-tetrafluoroprop-1-ene
[e] *trans*-1-chloro-3,3,3-trifluoroprop-1-ene [f] *cis*-1,3,3,3-tetrafluoroprop-1-ene
[g] *cis*-1,2,3,3,3-pentafluoroprop-1-ene [h] 3,3,3-trifluoropropene

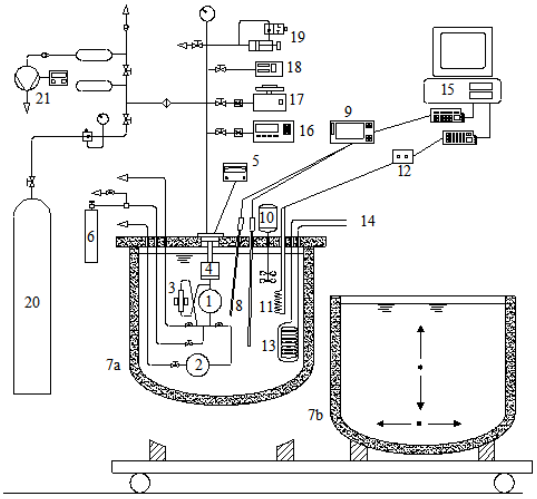

1	Constant volume spherical cell	12	Power system
2	Auxiliary cell	13	Cooling coil
3	Magnetic pump	14	Connections to auxiliary thermostatic bath
4	Differential pressure transducer		
5	Electronic null indicator	15	Acquisition system
6	Charging system	16	Bourdon gage
7	Thermostatic baths	17	Dead weight gage
8	Platinum thermo-resistances	18	Vibrating cylinder pressure gage
9	Thermometric bridge	19	Precision pressure controller
10	Stirrer	20	Nitrogen reservoir
11	Heater	21	Vacuum pump system

Figure 4.1: Schematic view of the experimental setup.

cell. Once the refrigerant was charged and the isochoric cell was isolated, the amount of refrigerant remained in the connection tubing was recovered into the recovery bottle. Then, these two bottles were weighted again. The masses of the two bottles before and after the charging process were used to determine both the refrigerant amount removed from the charging bottle and the refrigerant collected in the recovery bottle. The difference between these values provided the mass of refrigerant charged into the isochoric cell. To perform the measurements, the thermostatic bath (7) was allowed to reach stable conditions. Once the temperature set-point of the thermostatic bath was achieved, but before making measurements, a circulating pump (3) within the isochoric cell was activated for fifteen minutes to mix the sample. Afterward, the sample was allowed to stabilize for an hour before the values of pressure and temperature were recorded. After recording the measured values, the set-point of the thermostatic bath was changed to the next set temperature. The measurement procedure was then repeated.

4.1.5 Experimental uncertainties

Details about the calculation of the temperature, volume, and pressure uncertainties are reported elsewhere [230, 231]. The expanded uncertainty at the 95 % confidence level (coverage factor of 2) for the temperature was found to be 0.03 K. This uncertainty for the temperature measurement is due to the thermometer and the bath instability and was estimated based on the propagation of uncertainty. The uncertainty in the pressure measurements is due to the uncertainty of the transducer and null indicator system and the pressure gauges. Moreover, this uncertainty includes a contribution to fluctuations in the thermostatic bath temperature. The expanded uncertainty at the 95 % confidence level for pressure was found to be 1 kPa. Based on the calibration procedure to estimate V_{iso}, the expanded uncertainty of the volume at the 95 % confidence level was found to be 0.3 cm^3.

Considering the charging procedure described above, the combined uncertainty of the mass was calculated according to the propagation of uncertainty as:

$$u(m) = \sqrt{4\, m(u_{\mathrm{b}})^2} \tag{4.1}$$

where $u(m)$ is the combined uncertainty of the charged mass in mg and $u(m_{\mathrm{b}})$ is the uncertainty of the analytical balance in mg. From Equation (4.1), the expanded uncertainty in mass at the 95 % confidence level was determined to be 1.2 mg.

The uncertainty in the specific volume is a function of the uncertainties in the volume estimation and the mass measurement. The expanded uncertainty in the specific volume for the measured binary systems was calculated for each isochore from the following equation

$$U(v)^2 = v^2 \left[\left(\frac{U(V_{\mathrm{iso}})}{V_{\mathrm{iso}}} \right)^2 + \left(\frac{U(m^*)\, v}{V_{\mathrm{iso}}} \right)^2 \right] \tag{4.2}$$

where the $U(v)$ is the expanded specific volume uncertainty in $\mathrm{m}^3\,\mathrm{kg}^{-1}$, $U(V)$ is the expanded volume uncertainty in m^3, v is the sample specific volume in $\mathrm{m}^3\,\mathrm{kg}^{-1}$, V_{iso} is the total volume of the isochoric cell, tubing, and pressure transducer cavity and $U(m^*)$ is twice the expanded uncertainty in mass in kg. From Equation (4.2), the following ranges for the expanded specific volume uncertainties at 95 % level of confidence were found for the studied binary systems:

- (0.000097 to 0.000266) $m^3\,kg^{-1}$ for R1234yf + R600a;
- (0.000104 to 0.000138) $m^3\,kg^{-1}$ for R1234ze(E) + R600a;
- (0.000057 to 0.000276) $m^3\,kg^{-1}$ for R600a + R1233zd(E);
- (0.000091 to 0.000225) $m^3\,kg^{-1}$ for R600a + R1234ze(Z);
- (0.000068 to 0.000165) $m^3\,kg^{-1}$ for R1225ye(Z) + R600a;
- (0.000119 to 0.002562) $m^3\,kg^{-1}$ for R1243zf + R600a;
- (0.000034 to 0.000753) $m^3\,kg^{-1}$ for R32 + R1234yf;
- (0.000015 to 0.000186) $m^3\,kg^{-1}$ for R32 + R1234ze(E);
- (0.000015 to 0.000091) $m^3\,kg^{-1}$ for R32 + R1234ze(Z).

The uncertainty in the mole fraction is a function of the mass of the sample charged into the isochoric sphere, of the specific volume of the binary system sample, and of the mole fraction itself. The expanded uncertainties in the mole fraction were determined as:

$$U(z_i)^2 = \left(\frac{v\,U(m)}{V_{\text{iso}}}\right)^2 \left[\left(1+\frac{1}{\alpha}\right)^2 + (1+\alpha)^2\right] \tag{4.3}$$

$$\alpha = \frac{\left(\frac{M_i}{M_{j\neq i}} z_i\right)}{(1-z_i)} \tag{4.4}$$

where $U(z_i)$ is the expanded mole fraction uncertainty of the i-th component, M_i is the molar mass of the i-th component, $M_{j\neq i}$ is the molar mass of the other component, and z_i is the overall mole fraction of the i-th component. From Equation (4.3), the following ranges for the expanded mole fraction uncertainties at 95 % level of confidence were found for the studied binary systems:

- (0.0011 to 0.0023) for z_2 of R1234yf (1) + R600a (2) binary systems;
- (0.0009 to 0.0018) for z_2 of R1234ze(E) (1) + R600a (2) binary systems;
- (0.0005 to 0.0096) for z_1 of R600a (1) + R1233zd(E) (2) binary systems;
- (0.0007 to 0.0078) for z_1 of R600a (1) + R1234ze(Z) (2) binary systems;
- (0.0007 to 0.0024) for z_2 of R1225ye(Z) (1) + R600a (2) binary systems;
- (0.0018 to 0.0108) for z_2 of R1243zf (1) + R600a (2) binary systems;
- (0.0004 to 0.0046) for z_1 of R32 (1) + R1234yf (2) binary systems;
- (0.0004 to 0.0044) for z_1 of R32 (1) + R1234ze(E) (2) binary systems;
- (0.0005 to 0.0016) for z_1 of R32 (1) + R1234ze(Z) (2) binary systems.

4.1.6 Experimental data

The following experimental data for the studied refrigerant binary systems were measured through the isochoric apparatus:

- 96 vapor-phase $PvTz$ data points for R1234yf + R600a binary systems along six isochores of (0.079806, 0.094104, 0.094392, 0.128013, 0.166637, 0.170142) $m^3\,kg^{-1}$ for temperatures from (303 to 383) K for six R600a mole fractions (0.2340, 0.4005, 0.4723, 0.6061, 0.7720, 0.8504);

- 102 vapor-phase $PvTz$ data points for R1234ze(E) + R600a binary systems along six isochores of (0.084552, 0.085765, 0.089171, 0.089681, 0.100595, 0.106374) $m^3\,kg^{-1}$ for temperatures from (303 to 383) K for six R600a mole fractions (0.2899, 0.4275, 0.5156, 0.6124, 0.6851, 0.7551);

- 84 vapor-phase $PvTz$ data points for R600a + R1233zd(E) binary systems along six isochores of (0.049946, 0.053587, 0.092697, 0.126329, 0.143141, 0.174350) $m^3\,kg^{-1}$ for temperatures from (303 to 383) K for six R600a mole fractions (0.1245, 0.4527, 0.5638, 0.6438, 0.7460, 0.8647);

- 97 vapor-phase $PvTz$ data points for R600a + R1234ze(Z) binary systems along six isochores of (0.075853, 0.090738, 0.127222, 0.128793, 0.151676, 0.152283) $m^3\,kg^{-1}$ for temperatures from (303 to 383) K for six R600a mole fractions (0.1176, 0.2220, 0.4271, 0.5095, 0.6585, 0.7250);

- 97 vapor-phase $PvTz$ data points for R1225ye(Z) + R600a binary systems along six isochores of (0.058601, 0.063330, 0.071820, 0.090234, 0.107550, and 0.121791) $m^3\,kg^{-1}$ for temperatures from (303 to 383) K for six R600a mole fractions (0.1747, 0.3453, 0.4768, 0.5041, 0.7969, 0.9160)

- 66 vapor-phase $PvTz$ data points for R1243zf + R600a binary systems along four isochores of (0.094396, 0.161341, 0.230619, and 0.614524) $m^3\,kg^{-1}$ for temperatures from (303 to 383) K for four R600a mole fractions (0.2254, 0.2821, 0.4342, 0.8982).

- 217 two-phase and vapor-phase $PvTz$ data points for R32 + R1234yf binary systems along eleven isochores (0.029794, 0.029936, 0.030724, 0.032113, 0.061323, 0.063915, 0.102150, 0.111536, 0.116592, 0.144796, 0.280627) $m^3\,kg^{-1}$ for temperatures from (263 to 383) K for eleven R32 mole fractions (0.1214, 0.1330, 0.1792, 0.2712, 0.3432, 0.5229, 0.6231, 0.6489, 0.7020, 0.8122, 0.9460).

- 182 two-phase and vapor-phase $PvTz$ data points for R32 + R1234ze(E) binary systems along ten isochores (0.013173, 0.039422, 0.043115, 0.046522, 0.062966, 0.068225, 0.068959, 0.110447, 0.115156, 0.121732) $m^3\,kg^{-1}$ for temperatures from (263 to 373) K for ten R32 mole fractions (0.1677, 0.2360, 0.2551, 0.4634, 0.5374, 0.6715, 0.7383, 0.7544, 0.9532, 0.9533)

- 150 two-phase and vapor-phase $PvTz$ data points for R32 + R1234ze(Z) binary systems along seven isochores (0.013352, 0.016365, 0.023746, 0.026769, 0.035001, 0.070089, 0.071713) $m^3\,kg^{-1}$ for temperatures from (263 to 373) K for seven R32 mole fractions (0.0871, 0.2980, 0.3620, 0.5232, 0.7138, 0.8025, 0.8973).

Table 4.3: Bulk mole fractions (z), temperature ranges (ΔT), pressure ranges (ΔP), numbers of charged moles n, and amounts of charged masses m for R1234yf (1) + R600a (2) binary systems.

Series	z_2	ΔT K	ΔP kPa	n mol	m_1 g	m_2 g
1	0.2340	303.15 - 383.15	246.7 - 317.4	0.0289	2.521	0.393
2	0.4005	303.15 - 383.15	269.3 - 347.4	0.0317	2.167	0.738
3	0.4723	303.15 - 383.15	163.5 - 208.5	0.0184	1.107	0.505
4	0.6061	303.15 - 383.15	180.2 - 230.6	0.0205	0.922	0.723
5	0.7720	303.15 - 358.15	260.6 - 312.6	0.0302	0.785	1.356
6	0.8504	308.15 - 383.15	426.8 - 552.4	0.0517	0.882	2.554

Table 4.4: Bulk mole fractions (z), temperature ranges (ΔT), pressure ranges (ΔP), numbers of charged moles n, and amounts of charged masses m for R1234ze(E) (1) + R600a (2) binary systems.

Series	z_2	ΔT K	ΔP kPa	n mol	m_1 g	m_2 g
1	0.2899	303.15 - 383.15	267.9 - 346.2	0.0313	2.531	0.527
2	0.4275	303.15 - 383.15	305.5 - 396.3	0.0350	2.349	0.894
3	0.5156	303.15 - 383.15	259.6 - 335.1	0.0303	1.671	0.907
4	0.6124	303.15 - 383.15	321.0 - 417.6	0.0385	1.703	1.372
5	0.6851	303.15 - 383.15	304.9 - 395.9	0.0360	1.293	1.433
6	0.7551	303.15 - 383.15	367.4 - 481.6	0.0445	1.243	1.954

Tables 4.3, 4.4, 4.5, 4.6, 4.7, 4.8, 4.9, 4.10, and 4.11 present the temperature ranges, the pressure ranges, the compositions of the studied binary systems, the number of moles charged, and the masses charged for the measured isochores of the binary systems.

The T, P behaviors of the several isochores for the measured binary systems are shown in Figures 4.2, 4.3, 4.4, 4.5, 4.6, 4.7, 4.8, 4.9, and 4.10. From Figures 4.8 and 4.9, it is possible to note that different isochores of R32 + R1234yf binary systems with R32 mole fractions equal to (0.1214, 0.2712, 0.3432, 0.6231, 0.7020, 0.9460) and six isochores of R32 + R1234ze(E) with R32 mole fractions equal to (0.2360, 0.4634, 0.5374, 0.6715, 0.7544, 0.9533) were measured only in the superheated vapor region. After analyzing the slope of the T, P sequences of the additional series of R32 + R1234yf and R32 + R1234ze(E) binary systems, the experimental $PvTz$ properties were attributed either to the two-phase and superheated vapor regions. As shown in Figure 4.10, almost all the isochores of R32 + R1234ze(Z) binary pair were measured both in the two-phase and superheated vapor regions. The experimental $PvTz$ properties of these binary systems were attributed either to the two-phase and superheated vapor regions on the basis of the slope of the T, P sequences.

All the experimental data of the studied binary pairs measured both in the two-phase and in the superheated vapor regions are reported in Appendix B

Table 4.5: Bulk mole fractions (z), temperature ranges (ΔT), pressure ranges (ΔP), numbers of charged moles n, and amounts of charged masses m for R600a (1) + R1233zd(E) (2) binary systems.

Series	z_1	ΔT K	ΔP kPa	n mol	m_1 g	m_2 g
1	0.1245	303.15 - 383.15	113.3 - 146.5	0.0129	0.094	1.479
2	0.4527	313.15 - 383.15	197.4 - 246.4	0.0222	0.584	1.587
3	0.5638	303.15 - 383.15	186.5 - 241.7	0.0214	0.700	1.216
4	0.6438	338.15 - 383.15	576.1 - 675.0	0.0655	2.450	3.044
5	0.7460	318.15 - 383.15	340.9 - 423.2	0.0387	1.677	1.282
6	0.8647	333.15 - 383.15	648.1 - 776.5	0.0754	3.789	1.331

Table 4.6: Bulk mole fractions (z), temperature ranges (ΔT), pressure ranges (ΔP), numbers of charged moles n, and amounts of charged masses m for R600a (1) + R1234ze(Z) (2) binary systems.

Series	z_1	ΔT K	ΔP kPa	n mol	m_1 g	m_2 g
1	0.1176	303.15 - 383.15	145.9 - 188.1	0.0168	0.115	1.686
2	0.2220	303.15 - 383.15	155.7 - 200.5	0.0178	0.230	1.578
3	0.4271	303.15 - 383.15	206.5 - 267.4	0.0239	0.594	1.562
4	0.5095	303.15 - 383.15	213.5 - 275.5	0.0249	0.737	1.392
5	0.6585	313.15 - 383.15	398.1 - 505.8	0.0468	1.792	1.824
6	0.7250	318.15 - 383.15	362.3 - 448.3	0.0411	1.733	1.290

Table 4.7: Bulk mole fractions (z), temperature ranges (ΔT), pressure ranges (ΔP), numbers of charged moles n, and amounts of charged masses m for R1225ye(Z) (1) + R600a (2) binary systems.

Series	z_2	ΔT K	ΔP kPa	n mol	m_1 g	m_2 g
1	0.1747	308.15 - 383.15	316.0 - 403.1	0.0364	3.961	0.369
2	0.3453	308.15 - 383.15	309.8 - 394.6	0.0358	3.099	0.719
3	0.4768	308.15 - 383.15	410.6 - 529.0	0.0483	3.340	1.340
4	0.5041	303.15 - 383.15	207.0 - 265.6	0.0238	1.555	0.696
5	0.7969	308.15 - 383.15	303.6 - 387.0	0.0349	0.935	1.615
6	0.9160	308.15 - 383.15	394.7 - 509.9	0.0472	0.524	2.515

Table 4.8: Bulk mole fractions (z), temperature ranges (ΔT), pressure ranges (ΔP), numbers of charged moles n, and amounts of charged masses m for R1243zf (1) + R600a (2) binary systems.

Series	z_2	ΔT K	ΔP kPa	n mol	m_1 g	m_2 g
1	0.2254	308.15 - 383.15	289.5 - 367.5	0.0332	2.470	0.435
2	0.2821	303.15 - 383.15	47.6 - 60.5	0.0052	0.361	0.086
3	0.4342	308.15 - 383.15	192.7 - 240.1	0.0214	1.161	0.539
4	0.8982	303.15 - 383.15	169.8 - 217.1	0.0192	0.188	1.000

Table 4.9: Bulk mole fractions (z), temperature ranges (ΔT), pressure ranges (ΔP), numbers of charged moles n, and amounts of charged masses m for R32 (1) + R1234yf (2) binary systems.

Series	z_1	ΔT K	ΔP kPa	n mol	m_1 g	m_2 g
1	0.1214	303.15 - 383.15	357.6 - 465.7	0.0420	0.265	4.206
2	0.1330	263.15 - 373.15	248.8 - 438.6	0.0405	0.28	4.005
3	0.1792	263.15 - 373.15	285.0 - 915.2	0.0889	0.829	8.321
4	0.2712	303.15 - 383.15	174.9 - 223.2	0.0195	0.275	1.619
5	0.3432	303.15 - 383.15	234.0 - 300.1	0.0265	0.473	1.985
6	0.5229	263.15 - 373.15	426.1 - 1131.5	0.1092	2.971	5.944
7	0.6231	303.15 - 383.15	117.3 - 149.0	0.0130	0.420	0.557
8	0.6489	263.15 - 373.15	480.9 - 1283.0	0.1246	4.205	4.988
9	0.7020	303.15 - 383.15	294.7 - 378.1	0.0334	1.218	1.134
10	0.8122	263.15 - 373.15	537.4 - 1385.8	0.1340	5.661	2.868
11	0.9460	303.15 - 383.15	422.8 - 545.6	0.0485	2.386	0.299

Table 4.10: Bulk mole fractions (z), temperature ranges (ΔT), pressure ranges (ΔP), numbers of charged moles n, and amounts of charged masses m for R32 (1) + R1234ze(E) (2) binary systems.

Series	z_1	ΔT K	ΔP kPa	n mol	m_1 g	m_2 g
1	0.1677	263.15 - 373.15	190.9 - 604.5	0.0568	0.496	5.392
2	0.2360	303.15 - 373.15	200.6 - 250.6	0.0227	0.278	1.974
3	0.2551	263.15 - 373.15	256.7 - 1933.5	0.2117	2.810	17.982
4	0.4634	303.15 - 373.15	400.5 - 506.1	0.0466	1.124	2.852
5	0.5374	303.15 - 373.15	271.4 - 339.4	0.0308	0.860	1.622
6	0.6715	303.15 - 373.15	291.4 - 364.3	0.0329	1.149	1.232
7	0.7383	263.15 - 373.15	432.1 - 1070.6	0.1018	3.910	3.038
8	0.7544	303.15 - 373.15	512.1 - 648.1	0.0597	2.345	1.673
10	0.9532	263.15 - 373.15	552.2 - 1213.9	0.1157	5.735	0.618
11	0.9533	303.15 - 373.15	669.1 - 852.3	0.0793	3.932	0.422

Table 4.11: Bulk mole fractions (z), temperature ranges (ΔT), pressure ranges (ΔP), numbers of charged moles n, and amounts of charged masses m for R32 (1) + R1234ze(Z) (2) binary systems.

Series	z_1	ΔT K	ΔP kPa	n mol	m_1 g	m_2 g
1	0.0871	263.15 - 353.15	79.5 - 976.6	0.1887	0.855	19.649
2	0.2980	263.15 - 353.15	170.4 - 1270.8	0.1751	2.714	14.016
3	0.3620	263.15 - 373.15	123.8 - 443.2	0.0417	0.785	3.034
4	0.5232	268.15 - 373.15	276.8 - 981.0	0.0959	2.610	5.214
5	0.7128	263.15 - 373.15	264.9 - 600.6	0.0560	2.075	1.833
6	0.8015	268.15 - 373.15	498.2 - 1752.9	0.1793	7.477	4.059
7	0.8973	268.15 - 373.15	579.9 - 1747.3	0.1753	8.181	2.052

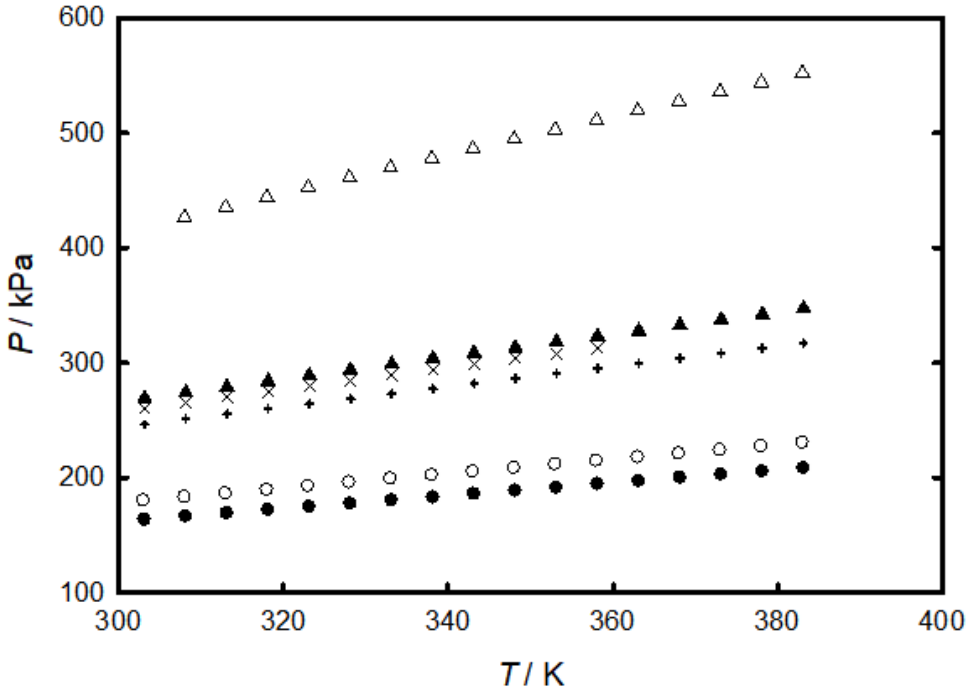

Figure 4.2: Pressure (P), specific volume (v), temperature (T), and bulk mole fraction (z) data (Table B.4) for R1234yf (1) + R600a (2) binary systems measured in the superheated vapor region; +, $z_2 = 0.2340$ and $v = 0.094104$ m^3 kg^{-1}; ▲, $z_2 = 0.4005$ and $v = 0.094392$ m^3 kg^{-1}; ●, $z_2 = 0.4723$ and $v = 0.170142$ m^3 kg^{-1}; ○, $z_2 = 0.6061$ and $v = 0.166637$ m^3 kg^{-1}; ×, $z_2 = 0.7720$ and $v = 0.128013$ m^3 kg^{-1}; △, $z_2 = 0.8504$ and $v = 0.079806$ m^3 kg^{-1}.

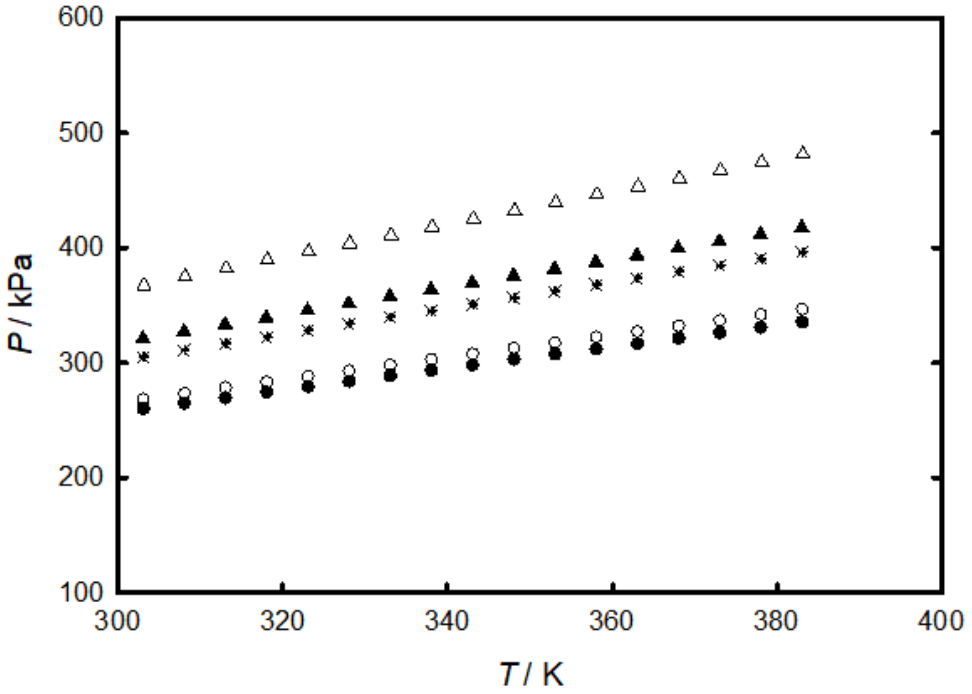

Figure 4.3: Pressure (P), specific volume (v), temperature (T), and bulk mole fraction (z) data (Table B.5) for R1234ze(E) (1) + R600a (2) binary systems measured in the superheated vapor region; ○, z_2 = 0.2899 and v = 0.089681 $m^3\,kg^{-1}$; +, z_2 = 0.4275 and v = 0.084552 $m^3\,kg^{-1}$; ●, z_2 = 0.5156 and v = 0.106374 $m^3\,kg^{-1}$; ▲, z_2 = 0.6124 and v = 0.089171 $m^3\,kg^{-1}$; ×, z_2 = 0.6851 and v = 0.100595 $m^3\,kg^{-1}$; △, z_2 = 0.7551 and v = 0.085765 $m^3\,kg^{-1}$.

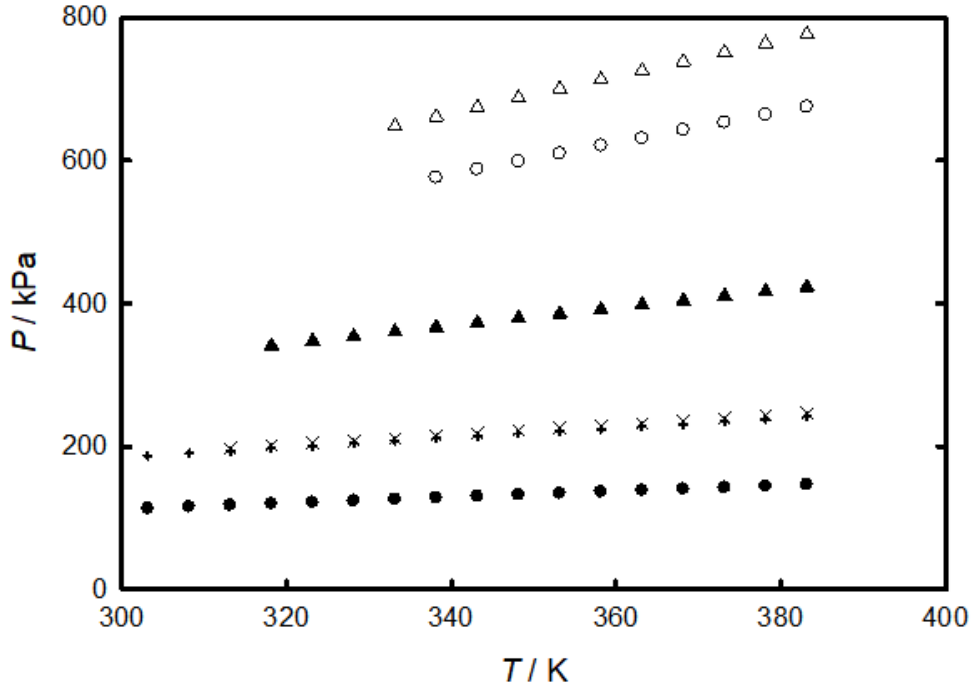

Figure 4.4: Pressure (P), specific volume (v), temperature (T), and bulk mole fraction (z) data (Table B.6) for R600a (1) + R1233zd(E) (2) binary systems measured in the superheated vapor region; ●, $z_1 = 0.1245$ and $v = 0.174350$ m^3 kg^{-1}; ×, $z_1 = 0.4527$ and $v = 0.126329$ m^3 kg^{-1}; +, $z_1 = 0.5638$ and $v = 0.143141$ m^3 kg^{-1}; ○, $z_1 = 0.6438$ and $v = 0.049946$ m^3 kg^{-1}; ▲, $z_1 = 0.7460$ and $v = 0.092697$ m^3 kg^{-1}; △, $z_1 = 0.8647$ and $v = 0.053587$ m^3 kg^{-1}.

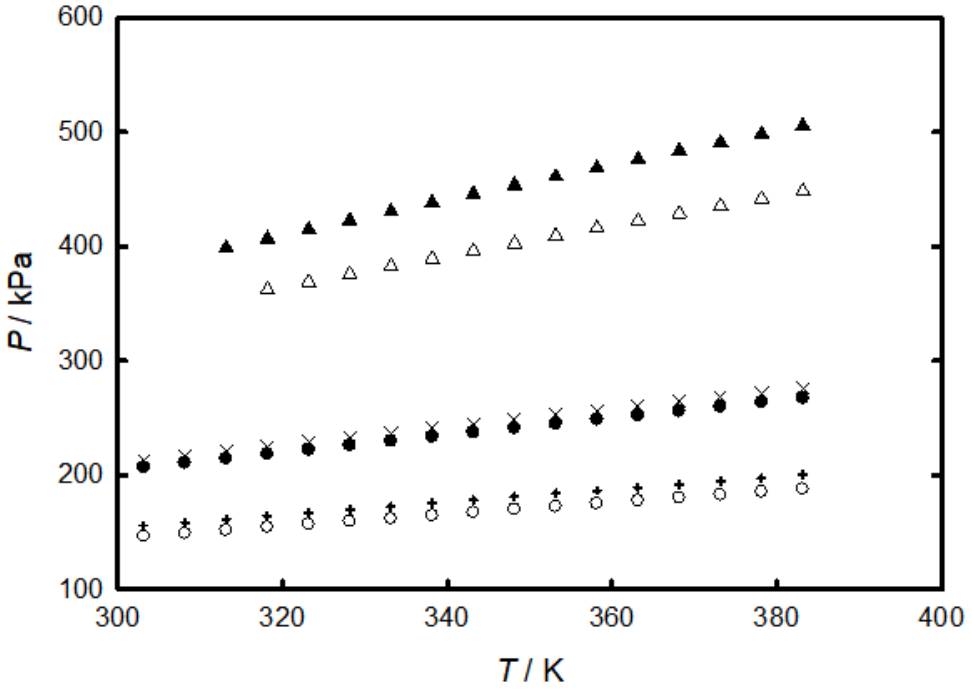

Figure 4.5: Pressure (P), specific volume (v), temperature (T), and bulk mole fraction (z) data (Table B.7) for R600a (1) + R1234ze(Z) (2) binary systems measured in the superheated vapor region; ○, $z_1 = 0.1176$ and $v = 0.152283$ m^3 kg^{-1}; +, $z_1 = 0.2220$ and $v = 0.151676$ m^3 kg^{-1}; ●, $z_1 = 0.4271$ and $v = 0.127222$ m^3 kg^{-1}; ×, $z_1 = 0.5095$ and $v = 0.127222$ m^3 kg^{-1}; ▲, $z_1 = 0.6585$ and $v = 0.075853$ m^3 kg^{-1}; △, $z_1 = 0.7250$ and $v = 0.090738$ m^3 kg^{-1}.

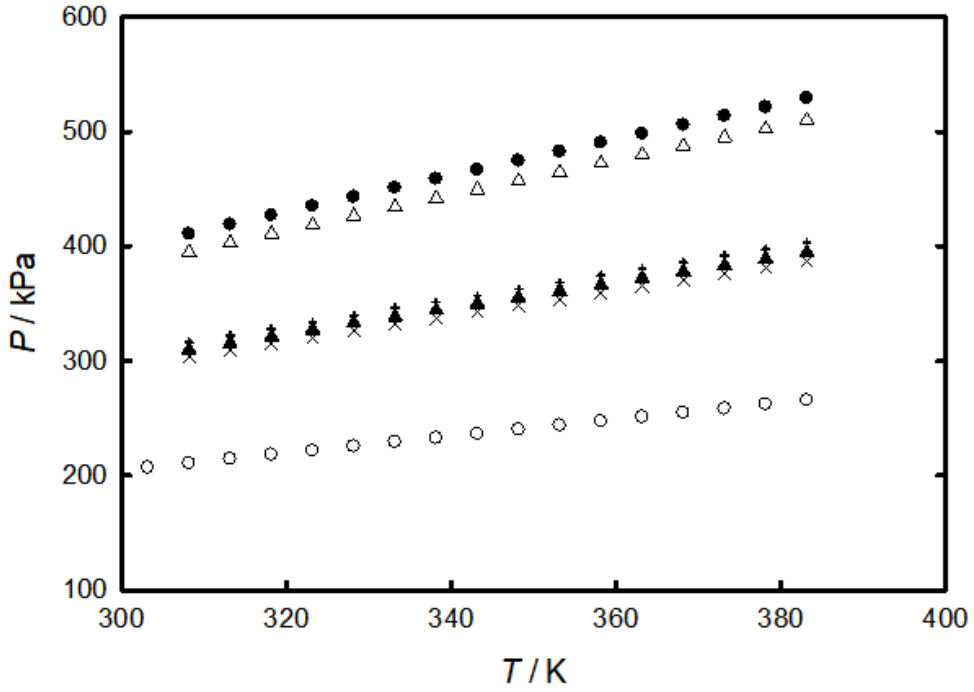

Figure 4.6: Pressure (P), specific volume (v), temperature (T), and bulk mole fraction (z) data (Table B.8) for R1225ye(Z) (1) + R600a (2) binary systems measured in the superheated vapor region; +, $z_2 = 0.1747$ and $v = 0.063330$ m^3 kg^{-1}; ▲, $z_2 = 0.3453$ and $v = 0.071820$ m^3 kg^{-1}; ●, $z_2 = 0.4768$ and $v = 0.058601$ m^3 kg^{-1}; ○, $z_2 = 0.5041$ and $v = 0.121791$ m^3 kg^{-1}; ×, $z_2 = 0.7969$ and $v = 0.107550$ m^3 kg^{-1}; △, $z_2 = 0.9160$ and $v = 0.090234$ m^3 kg^{-1}.

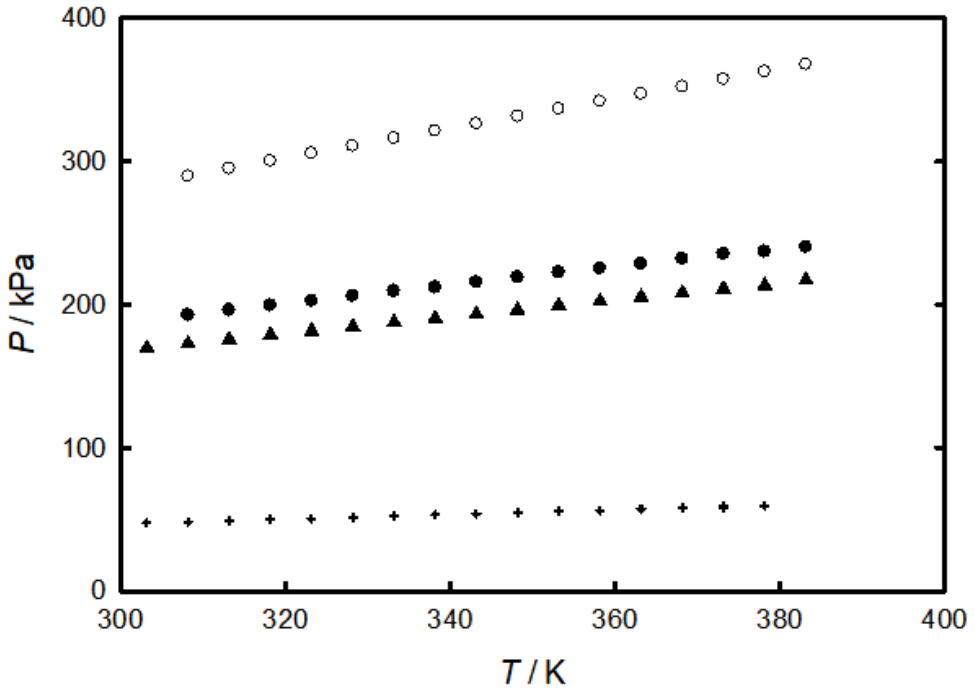

Figure 4.7: Pressure (P), specific volume (v), temperature (T), and bulk mole fraction (z) data (Table B.9) for R1243zf (1) + R600a (2) binary systems measured in the superheated vapor region; ○, $z_2 = 0.2254$ and $v = 0.094396$ m^3 kg^{-1}; +, $z_2 = 0.2821$ and $v = 0.614524$ m^3 kg^{-1}; ●, $z_2 = 0.4342$ and $v = 0.161341$ m^3 kg^{-1}; ▲, $z_2 = 0.8982$ and $v = 0.230619$ m^3 kg^{-1}.

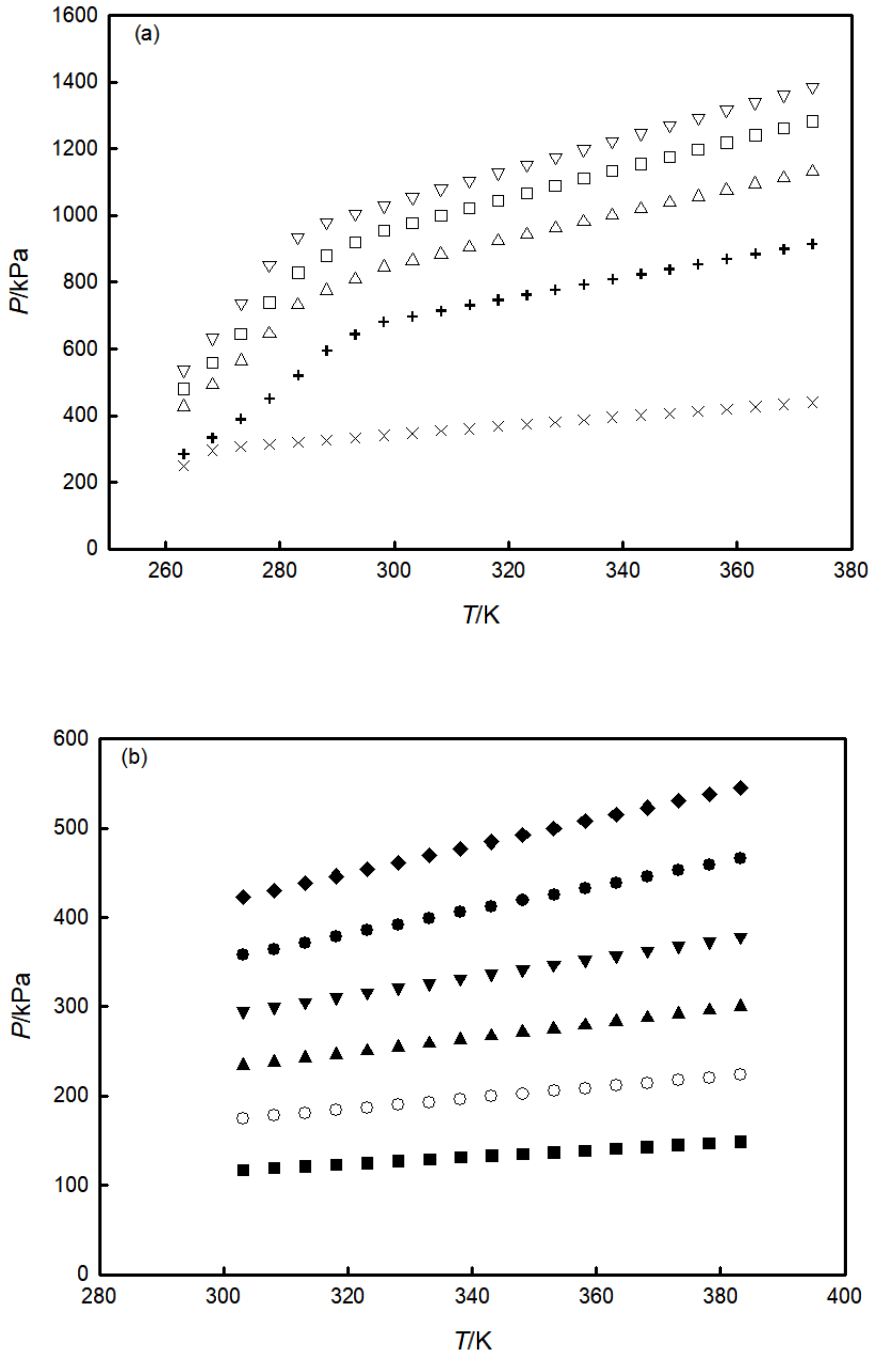

Figure 4.8: Pressure (P), specific volume (v), temperature (T), and bulk mole fraction (z) data (Tables B.1 and B.10) for five isochores of R32 (1) + R1234yf (2) binary systems measured both in the two-phase and superheated vapor regions (a) and six isochores measured in the superheated vapor region (b); ●, $z_1 = 0.1214$ and $v = 0.061323$ m^3 kg^{-1}; ×, $z_1 = 0.1330$ and $v = 0.063915$ m^3 kg^{-1}; +, $z_1 = 0.1792$ and $v = 0.029936$ m^3 kg^{-1}; ○, $z_1 = 0.2712$ and $v = 0.144796$ m^3 kg^{-1}; ▲, $z_1 = 0.3432$ and $v = 0.111536$ m^3 kg^{-1}; △, $z_1 = 0.5229$ and $v = 0.030724$ m^3 kg^{-1}; ■, $z_1 = 0.6231$ and $v = 0.280627$ m^3 kg^{-1}; □, $z_1 = 0.6489$ and $v = 0.029794$ m^3 kg^{-1}; ▼, $z_1 = 0.7020$ and $v = 0.116592$ m^3 kg^{-1}; ▽, $z_1 = 0.8122$ and $v = 0.032113$ m^3 kg^{-1}; ◆, $z_1 = 0.9460$ and $v = 0.102150$ m^3 kg^{-1}.

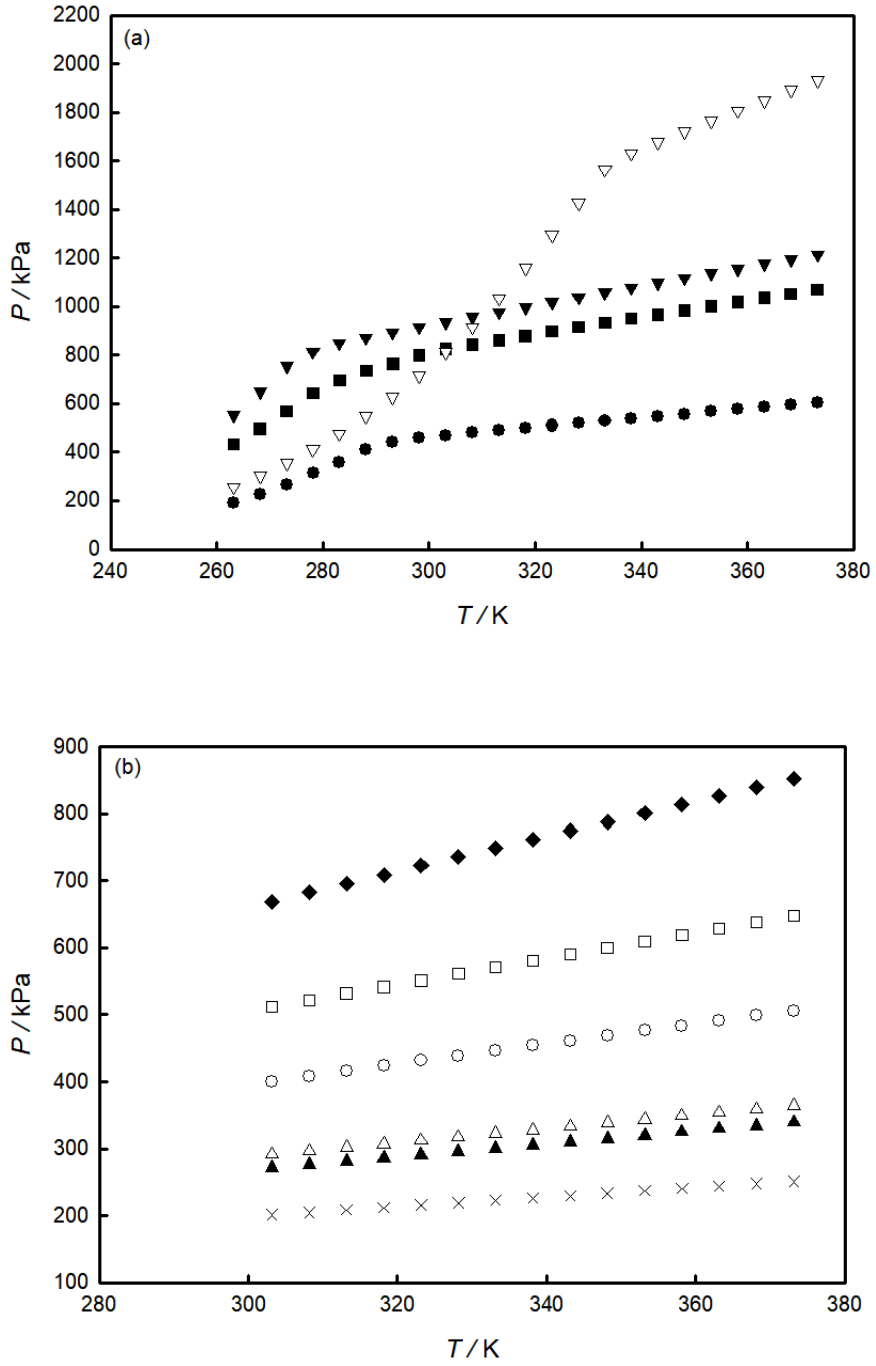

Figure 4.9: Pressure (P), specific volume (v), temperature (T), and bulk mole fraction (z) data (Tables B.2 and B.11) for five isochores of R32 (1) + R1234ze(E) (2) binary systems measured both in the two-phase and superheated vapor regions (a) and six isochores measured in the superheated vapor region (b); ●, $z_1 = 0.1677$ and $v = 0.046522$ m^3 kg^{-1}; ×, $z_1 = 0.2360$ and $v = 0.121732$ m^3 kg^{-1}; ▽, $z_1 = 0.2551$ and $v = 0.013173$ m^3 kg^{-1}; ○, $z_1 = 0.4634$ and $v = 0.068959$ m^3 kg^{-1}; ▲, $z_1 = 0.5374$ and $v = 0.110447$ m^3 kg^{-1}; △, $z_1 = 0.6715$ and $v = 0.115156$ m^3 kg^{-1}; ■, $z_1 = 0.7383$ and $v = 0.039422$ m^3 kg^{-1}; □, $z_1 = 0.7544$ and $v = 0.068225$ m^3 kg^{-1}; ▼, $z_1 = 0.9532$ and $v = 0.043115$ m^3 kg^{-1}; ◆, $z_1 = 0.9533$ and $v = 0.062966$ m^3 kg^{-1}.

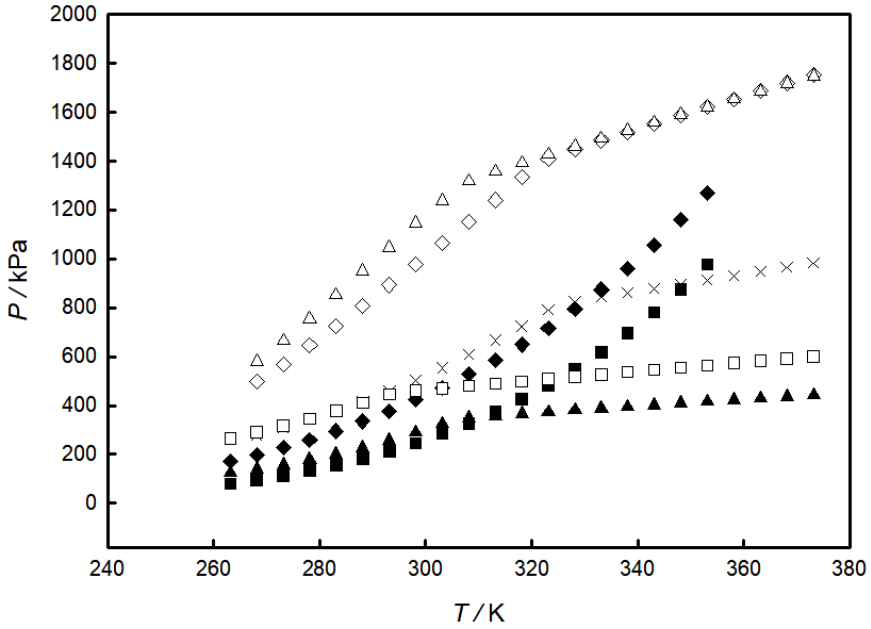

Figure 4.10: Pressure (P), specific volume (v), temperature (T), and bulk mole fraction (z) data (Table B.3 and B.12) for R32 (1) + R1234ze(Z) (2) binary systems measured both in the two-phase and superheated vapor regions; ■, $z_1 = 0.0871$ and $v = 0.013352$ m^3 kg^{-1}; ◆, $z_1 = 0.2980$ and $v = 0.016365$ m^3 kg^{-1}; ▲, $z_1 = 0.3620$ and $v = 0.071713$ m^3 kg^{-1}; ×, $z_1 = 0.5232$ and $v = 0.035001$ m^3 kg^{-1}; □, $z_1 = 0.7128$ and $v = 0.070089$ m^3 kg^{-1}; ◇, $z_1 = 0.8015$ and $v = 0.023746$ m^3 kg^{-1}; △, $z_1 = 0.8973$ and $v = 0.026769$ m^3 kg^{-1}.

Table 4.12: Coefficients of the Carnahan - Starling - De Santis EoS for R32, R1234yf, R1234ze(E), and R1234ze(Z).

Coef.	R32	R1234yf	R1234ze(E)	R1234ze(Z)
a_0	$1.66227 \cdot 10^{3}$	$3.93994 \cdot 10^{3}$	$4.16116 \cdot 10^{3}$	$4.30402 \cdot 10^{3}$
a_1	$-2.19752 \cdot 10^{-3}$	$-2.67820 \cdot 10^{-3}$	$-2.51800 \cdot 10^{-3}$	$-1.66809 \cdot 10^{-3}$
a_2	$-1.88903 \cdot 10^{-6}$	$-1.54750 \cdot 10^{-6}$	$-1.92770 \cdot 10^{-6}$	$-2.20567 \cdot 10^{-6}$
b_0	$7.79879 \cdot 10^{-2}$	$1.71700 \cdot 10^{-1}$	$1.63000 \cdot 10^{-1}$	$1.64124 \cdot 10^{-1}$
b_1	$-7.52381 \cdot 10^{-5}$	$-2.14670 \cdot 10^{-4}$	$-1.53150 \cdot 10^{-4}$	$-1.30312 \cdot 10^{-4}$
b_2	$-5.30107 \cdot 10^{-8}$	$-5.07060 \cdot 10^{-8}$	$-1.49710 \cdot 10^{-7}$	$-1.10866 \cdot 10^{-7}$

4.1.7 Vapor-liquid equilibrium derivation

The Vapor-Liquid Equilibrium (VLE) of R32 + R1234yf, R32 + R1234ze(E), and R32 + R1234ze(Z) binary systems was derived from the two-phase isochoric data points by using the flash method with three Equations of State (EoSs). Details regarding the flash method are reported in Subsection 2.4.2 of Chapter 2. The EoSs used in this method for the VLE assessment are the Carnahan - Starling - De Santis (CSD) EoS [110], the Peng Robinson (PR) EoS [103], and a two-parameter cubic EoS proposed by Stryjek [105, 106]. The expressions of these EoSs are reported in Subsection 2.2.1 of Chapter 2. In particular, the CES proposed by Stryjek is called CES(A) in Table 2.2 of Subsection 2.2.1. Table 4.12 reports the CSD coefficients for R32, R1234yf, R1234ze(E), and R1234ze(Z) used in this work. The EoSs were extended to the studied binary systems through the van der Waals one-fluid mixing rules with a single binary interaction parameter ($k_{ij} = k_{ji}$), described in Subsection 2.2.2 of Chapter 2. Almost all the physical properties of the pure refrigerants used in the EoSs were collected from Lemmon et al. [64, 65].

The average values of k_{ij} for the flash method with CSD EoS, PR EoS, and CES(A) and the Average Absolute Relative Deviation of the pressure (AARD (ΔP) %) obtained for the three binary pairs are reported in Table 4.13. The average absolute relative deviation of the pressure is defined as:

$$\text{AARD}\,(\Delta P)\,\% = \frac{100}{N}\sum_{i=1}^{N}\left|\frac{P_{i,\text{exp}} - P_{i,\text{calc}}}{P_{i,\text{exp}}}\right| \tag{4.5}$$

where N is the number of the experimental data, P_{exp} is the experimental pressure and P_{calc} is the calculated pressure.

The VLE properties (pressures and compositions of liquid and vapor phases) of the studied binary pairs derived from the flash method with the three EoSs are reported in Tables 4.14, 4.15, and 4.16. Figures 4.11, 4.12, and 4.13 show the relative deviations between the experimental pressures and the values calculated with the selected EoSs for R32 + R1234yf, R32 + R1234ze(E), and R32 + R1234ze(Z) binary systems, respectively.

For R32 + R1234yf binary systems, it is possible to state from Tables 4.13 and 4.14 and Figure 4.11 that the three EoSs provided similar and accurate results, since the pressure deviations never exceeded 1.5 % for all of the series. However, CES(A) provided the most accurate results for this binary pair. Also for R32 + R1234ze(E) binary systems, Tables 4.13 and 4.15 and Figure 4.12 show that the studied EoSs provided similar and accurate descriptions, since the pressure deviations exceeded 1 % for few data of the series. In particular, it is possible to note that the PR EoS and CES(A) provided slightly lower pressure deviations for these binary systems. Instead,

Table 4.13: Binary interaction parameter (k_{ij}) for the flash method with CSD EoS, PR EoS, and CES(A) and Average Absolute Relative Deviation of the pressure (AARD (ΔP) %) obtained for R32 + R1234yf, R32 + R1234ze(E), and R32 + R1234ze(Z) binary systems.

	CSD EoS		PR EoS		CES(A)		REFPROP 10.0
Binary system	k_{ij}	AARD (ΔP) %	k_{ij}	AARD (ΔP) %	k_{ij}	AARD (ΔP) %	AARD (ΔP) %
R32 + R1234yf	0.01528	0.53	0.03860	0.42	0.03769	0.39	1.34
R32 + R1234ze(E)	0.00040	0.63	0.02047	0.46	0.01838	0.45	2.16
R32 + R1234ze(Z)	-0.02243	1.25	0.00281	1.04	-0.00037	1.08	7.12

as shown in Tables 4.13 and 4.16 and Figure 4.13, slightly higher deviations between the experimental pressures for R32 + R1234ze(Z) binary pair and the values calculated from the three EoSs were obtained. However, it is possible to note that all the models provided similar results. The reasons behind these higher deviations could be that a high number of data points in wide ranges of temperature and pressures were analyzed for this binary pair. In this case, to perform a more detailed study of the EoS capability to describe these properties, temperature and/or composition-dependent k_{ij} for the used mixing rules could be regressed and studied.

Furthermore, the experimental pressures of the three binary pairs were compared with the REFPROP 10.0 [65] predictions and the obtained AARD (ΔP)) are reported in Table 4.13. As explained in Subsection 2.2.1 of Chapter 2, REFPROP 10.0 property estimation is based on EoSs explicit in reduced Helmholtz energy. As shown in Table 4.13 and Figures 4.11 and 4.12, even if the results are slightly less accurate than those of the EoSs, the REFPROP 10.0 predictions for R32 + R1234yf and R32 + R1234ze(E) binary systems generally agree with experimental data, since the pressure deviations exceeded 3 % only for few points. Therefore, the software can provide a sufficiently accurate description of the two binary pairs in the two-phase region. Instead, as evident in Table 4.13 and Figure 4.13, very high deviations between the experimental pressures of R32 + R1234ze(Z) binary systems and REFPROP 10.0 predictions were obtained. Therefore, it can be stated that the software cannot provide an accurate description of this pair of refrigerants in the studied pressure, temperature, and specific volume conditions. A possible reason for this software limitation could be that mixing models with parameters unsuitable for this binary pair are adopted.

Table 4.14: Pressures (P_{calc}), mole fractions of the liquid phase (x_1), and mole fractions of the vapor phase (y_1) obtained from the flash method with the studied EoSs in the two-phase region for the experimental temperatures (T) and bulk mole fraction (z_1) of the R32 (1) + R1234yf (2) binary systems.

	CSD EoS			PR EoS			CES(A)		
T K	P_{calc} kPa	x_1	y_1	P_{calc} kPa	x_1	y_1	P_{calc} kPa	x_1	y_1
$z_1 = 0.1330$									
263.15	250.8	0.0491	0.1496	250.3	0.0480	0.1504	251.0	0.0482	0.1504
268.15	296.4	0.0454	0.1346	295.8	0.0442	0.1353	296.4	0.0444	0.1353
$z_1 = 0.1792$									
263.15	282.5	0.1050	0.2803	282.7	0.1036	0.2826	283.5	0.1041	0.2828
268.15	331.8	0.0995	0.2607	331.9	0.0979	0.2628	332.7	0.0984	0.2631
273.15	387.4	0.0942	0.2420	387.5	0.0924	0.2438	388.2	0.0929	0.2443
278.15	450.1	0.0892	0.2242	449.8	0.0872	0.2257	450.5	0.0877	0.2262
283.15	520.4	0.0844	0.2074	519.7	0.0822	0.2085	520.2	0.0827	0.2092
288.15	599.0	0.0798	0.1915	597.6	0.0776	0.1924	598.0	0.0780	0.1930
$z_1 = 0.5229$									
263.15	422.8	0.3905	0.6437	423.0	0.3908	0.6436	423.9	0.3920	0.6438
268.15	489.4	0.3734	0.6216	490.3	0.3728	0.6216	491.2	0.3741	0.6221
273.15	562.5	0.3559	0.5978	563.9	0.3542	0.5979	564.8	0.3557	0.5986
278.15	642.2	0.3382	0.5728	644.0	0.3355	0.5726	645.0	0.3371	0.5735
283.15	729.2	0.3207	0.5467	731.1	0.3169	0.5461	732.1	0.3186	0.5472
$z_1 = 0.6489$									
263.15	480.9	0.5414	0.7466	479.5	0.5435	0.7453	480.4	0.5446	0.7455
268.15	559.0	0.5233	0.7303	558.6	0.5248	0.7293	559.5	0.5262	0.7297
273.15	644.4	0.5035	0.7118	645.1	0.5042	0.7109	645.9	0.5058	0.7115
278.15	737.0	0.4823	0.6910	738.6	0.4819	0.6900	739.5	0.4838	0.6909
283.15	836.8	0.4601	0.6681	839.2	0.4584	0.6667	840.2	0.4605	0.6678
$z_1 = 0.8122$									
263.15	543.4	0.7571	0.8567	540.2	0.7587	0.8559	540.9	0.7593	0.8560
268.15	638.1	0.7443	0.8491	635.5	0.7462	0.8482	636.1	0.7470	0.8485
273.15	742.9	0.7285	0.8395	741.4	0.7307	0.8386	741.8	0.7318	0.8389
278.15	857.7	0.7093	0.8273	857.4	0.7116	0.8263	857.8	0.7131	0.8269

Table 4.15: Pressures (P_{calc}), mole fractions of the liquid phase (x_1), and mole fractions of the vapor phase (y_1) obtained from the flash method with the studied EoSs in the two-phase region for the experimental temperatures (T) and bulk mole fraction (z_1) of the R32 (1) + R1234ze(E) (2) binary systems.

	CSD EoS			PR EoS			CES(A)		
T K	P_{calc} kPa	x_1	y_1	P_{calc} kPa	x_1	y_1	P_{calc} kPa	x_1	y_1
$z_1 = 0.1677$									
263.15	190.6	0.0811	0.2783	190.6	0.0811	0.2790	191.0	0.0820	0.2783
268.15	225.8	0.0757	0.2540	225.8	0.0755	0.2549	226.1	0.0764	0.2546
273.15	266.1	0.0707	0.2314	266.0	0.0703	0.2324	266.3	0.0712	0.2323
278.15	312.0	0.0660	0.2106	311.8	0.0655	0.2115	312.1	0.0663	0.2116
$z_1 = 0.2551$									
263.15	255.6	0.2073	0.5225	255.1	0.2074	0.5226	254.9	0.2087	0.5213
268.15	301.1	0.2019	0.5022	300.9	0.2019	0.5029	300.7	0.2033	0.5020
273.15	352.5	0.1963	0.4817	352.4	0.1961	0.4830	352.1	0.1976	0.4824
278.15	410.0	0.1906	0.4612	410.1	0.1902	0.4628	409.8	0.1919	0.4626
283.15	474.2	0.1849	0.4406	474.5	0.1843	0.4425	474.2	0.1860	0.4427
288.15	545.5	0.1792	0.4202	546.1	0.1783	0.4221	545.7	0.1801	0.4227
293.15	624.5	0.1734	0.4001	625.2	0.1724	0.4019	624.8	0.1743	0.4027
298.15	711.7	0.1678	0.3802	712.6	0.1665	0.3818	712.2	0.1685	0.3829
303.15	807.6	0.1622	0.3606	808.8	0.1608	0.3619	808.3	0.1627	0.3633
308.15	912.9	0.1567	0.3416	914.4	0.1552	0.3424	913.8	0.1572	0.3440
313.15	1028.1	0.1514	0.3231	1030.0	0.1497	0.3234	1029.3	0.1517	0.3251
318.15	1153.8	0.1463	0.3051	1156.3	0.1445	0.3048	1155.6	0.1465	0.3067
323.15	1290.7	0.1414	0.2878	1294.0	0.1395	0.2868	1293.2	0.1415	0.2888
$z_1 = 0.7383$									
263.15	435.9	0.6013	0.8396	432.7	0.6038	0.8395	432.2	0.6054	0.8400
268.15	503.7	0.5767	0.8216	500.8	0.5790	0.8216	500.3	0.5810	0.8223
273.15	576.3	0.5499	0.8008	573.9	0.5518	0.8008	573.3	0.5543	0.8018
278.15	653.4	0.5216	0.7772	651.5	0.5228	0.7771	650.9	0.5258	0.7783
$z_1 = 0.9532$									
263.15	556.4	0.9243	0.9684	554.2	0.9230	0.9691	554.5	0.9228	0.9694
268.15	655.9	0.9159	0.9643	653.7	0.9141	0.9648	653.6	0.9140	0.9651
273.15	766.3	0.9041	0.9588	763.9	0.9018	0.9588	763.4	0.9018	0.9592

Table 4.16: Pressures (P_{calc}), mole fractions of the liquid phase (x_1), and mole fractions of the vapor phase (y_1) obtained from the flash method with the studied EoSs in the two-phase region for the experimental temperatures (T) and bulk mole fraction (z_1) of the R32 (1) + R1234ze(Z) (2) binary systems.

	CSD EoS			PR EoS			CES(A)		
T	P_{calc}	x_1	y_1	P_{calc}	x_1	y_1	P_{calc}	x_1	y_1
K	kPa			kPa			kPa		
$z_1 = 0.0871$									
263.15	78.9	0.0676	0.4529	78.4	0.0675	0.4687	78.5	0.0668	0.4735
268.15	94.3	0.0655	0.4287	93.9	0.0654	0.4423	93.9	0.0646	0.4465
273.15	112.0	0.0633	0.4046	111.6	0.0632	0.4164	111.7	0.0624	0.4199
278.15	132.2	0.0612	0.3809	132.0	0.0610	0.3910	132.0	0.0602	0.3939
283.15	155.3	0.0590	0.3577	155.2	0.0589	0.3664	155.2	0.0580	0.3687
288.15	181.4	0.0568	0.3351	181.6	0.0567	0.3426	181.5	0.0559	0.3443
293.15	211.1	0.0547	0.3132	211.4	0.0546	0.3197	211.3	0.0537	0.3209
298.15	244.6	0.0526	0.2922	245.0	0.0526	0.2978	244.9	0.0517	0.2985
303.15	282.3	0.0506	0.2721	282.8	0.0506	0.2769	282.6	0.0497	0.2773
308.15	324.6	0.0486	0.2529	325.0	0.0487	0.2572	324.9	0.0478	0.2571
313.15	372.0	0.0468	0.2347	372.2	0.0468	0.2385	372.1	0.0459	0.2382
318.15	424.9	0.0450	0.2175	424.8	0.0451	0.2209	424.7	0.0442	0.2204
323.15	483.8	0.0432	0.2014	483.1	0.0434	0.2045	483.0	0.0425	0.2037
328.15	549.3	0.0416	0.1863	547.6	0.0418	0.1891	547.6	0.0409	0.1882
333.15	621.9	0.0400	0.1721	618.8	0.0403	0.1747	618.9	0.0394	0.1737
338.15	702.1	0.0386	0.1590	697.2	0.0388	0.1614	697.4	0.0380	0.1602
343.15	790.7	0.0372	0.1467	783.2	0.0375	0.1489	783.6	0.0367	0.1477
348.15	888.1	0.0359	0.1353	877.5	0.0362	0.1374	878.1	0.0354	0.1362
353.15	995.2	0.0346	0.1248	980.5	0.0350	0.1267	981.3	0.0343	0.1254
$z_1 = 0.2980$									
263.15	163.2	0.2360	0.7752	165.0	0.2353	0.7853	166.0	0.2334	0.7877
268.15	189.5	0.2285	0.7560	191.7	0.2278	0.7652	192.7	0.2257	0.7674
273.15	218.5	0.2208	0.7355	221.1	0.2200	0.7439	222.0	0.2178	0.7458
278.15	250.4	0.2130	0.7138	253.3	0.2122	0.7214	254.2	0.2098	0.7230
283.15	285.4	0.2051	0.6909	288.6	0.2043	0.6977	289.4	0.2018	0.6989
288.15	323.6	0.1972	0.6669	327.1	0.1964	0.6730	327.8	0.1938	0.6738
293.15	365.2	0.1894	0.6420	369.0	0.1887	0.6474	369.6	0.1860	0.6478
298.15	410.6	0.1818	0.6163	414.6	0.1811	0.6211	415.0	0.1783	0.6211
303.15	460.1	0.1743	0.5901	464.2	0.1737	0.5943	464.5	0.1709	0.5939
308.15	514.1	0.1671	0.5634	518.2	0.1666	0.5671	518.3	0.1638	0.5664
313.15	572.8	0.1601	0.5366	576.8	0.1597	0.5398	576.7	0.1569	0.5387
318.15	636.9	0.1535	0.5097	640.5	0.1532	0.5126	640.3	0.1504	0.5112
323.15	706.8	0.1471	0.4830	709.7	0.1469	0.4856	709.3	0.1442	0.4839
328.15	782.9	0.1411	0.4567	784.8	0.1410	0.4590	784.3	0.1383	0.4570
333.15	865.8	0.1354	0.4309	866.4	0.1355	0.4329	865.8	0.1328	0.4308

Continues to the following page

Continues from the previous page

	CSD EoS			PR EoS			CES(A)		
T K	P_{calc} kPa	x_1	y_1	P_{calc} kPa	x_1	y_1	P_{calc} kPa	x_1	y_1
338.15	956.2	0.1300	0.4057	954.8	0.1302	0.4075	954.1	0.1277	0.4052
343.15	1054.6	0.1250	0.3813	1050.7	0.1253	0.3829	1049.9	0.1228	0.3804
348.15	1161.6	0.1202	0.3577	1154.5	0.1207	0.3591	1153.7	0.1183	0.3566
353.15	1278.0	0.1158	0.3350	1266.9	0.1164	0.3363	1266.0	0.1141	0.3336
$z_1 = 0.3620$									
263.15	125.5	0.1612	0.6842	125.0	0.1582	0.6933	125.1	0.1557	0.6952
268.15	142.1	0.1480	0.6475	141.6	0.1451	0.6553	141.6	0.1426	0.6569
273.15	160.6	0.1358	0.6095	160.0	0.1331	0.6160	159.9	0.1307	0.6173
278.15	181.2	0.1246	0.5709	180.6	0.1221	0.5762	180.4	0.1199	0.5771
283.15	204.2	0.1145	0.5323	203.7	0.1122	0.5364	203.4	0.1101	0.5370
288.15	230.0	0.1054	0.4941	229.5	0.1033	0.4972	229.3	0.1013	0.4975
293.15	259.1	0.0972	0.4569	258.6	0.0953	0.4591	258.3	0.0934	0.4592
298.15	291.7	0.0898	0.4210	291.2	0.0881	0.4226	290.9	0.0863	0.4224
303.15	328.3	0.0831	0.3869	327.8	0.0816	0.3879	327.5	0.0800	0.3875
$z_1 = 0.5232$									
268.15	263.0	0.3511	0.8478	265.5	0.3479	0.8524	266.5	0.3446	0.8531
273.15	296.2	0.3323	0.8278	298.8	0.3290	0.8320	299.6	0.3254	0.8324
278.15	331.3	0.3137	0.8058	334.0	0.3103	0.8093	334.7	0.3065	0.8096
283.15	368.5	0.2956	0.7817	371.2	0.2921	0.7847	371.8	0.2883	0.7847
288.15	408.0	0.2782	0.7558	410.8	0.2747	0.7581	411.2	0.2708	0.7579
293.15	450.2	0.2615	0.7282	453.0	0.2582	0.7300	453.2	0.2542	0.7295
298.15	495.5	0.2458	0.6992	498.1	0.2426	0.7004	498.1	0.2387	0.6997
303.15	544.2	0.2311	0.6691	546.7	0.2280	0.6698	546.5	0.2242	0.6688
308.15	596.8	0.2173	0.6382	599.0	0.2145	0.6385	598.7	0.2108	0.6372
313.15	653.9	0.2046	0.6068	655.7	0.2020	0.6067	655.3	0.1984	0.6052
318.15	716.0	0.1928	0.5753	717.1	0.1905	0.5748	716.6	0.1870	0.5731
$z_1 = 0.7128$									
263.15	263.2	0.4299	0.8916	264.4	0.4238	0.8944	264.8	0.4197	0.8945
268.15	290.8	0.3964	0.8705	291.8	0.3901	0.8730	292.1	0.3856	0.8729
273.15	319.1	0.3646	0.8466	319.9	0.3582	0.8486	320.1	0.3535	0.8484
278.15	348.5	0.3349	0.8200	349.2	0.3286	0.8215	349.2	0.3239	0.8211
283.15	379.7	0.3076	0.7910	380.2	0.3015	0.7919	380.0	0.2969	0.7913
288.15	412.9	0.2828	0.7598	413.3	0.2770	0.7601	413.0	0.2725	0.7594
293.15	448.7	0.2603	0.7270	449.0	0.2549	0.7267	448.6	0.2505	0.7258
$z_1 = 0.8015$									
268.15	493.7	0.7133	0.9611	498.1	0.7130	0.9615	499.0	0.7113	0.9612
273.15	567.0	0.6967	0.9551	572.2	0.6962	0.9554	573.3	0.6941	0.9550
278.15	644.6	0.6780	0.9480	650.8	0.6771	0.9481	652.0	0.6744	0.9475
283.15	725.8	0.6572	0.9395	732.7	0.6558	0.9393	733.9	0.6526	0.9386
288.15	809.6	0.6344	0.9293	817.2	0.6325	0.9288	818.2	0.6287	0.9280

Continues to the following page

Continues from the previous page

	CSD EoS			PR EoS			CES(A)		
T K	P_{calc} kPa	x_1	y_1	P_{calc} kPa	x_1	y_1	P_{calc} kPa	x_1	y_1
293.15	895.4	0.6102	0.9174	903.3	0.6077	0.9165	903.9	0.6032	0.9155
298.15	982.8	0.5849	0.9037	990.7	0.5818	0.9023	990.8	0.5768	0.9010
303.15	1071.5	0.5592	0.8881	1079.1	0.5555	0.8862	1078.6	0.5500	0.8846
308.15	1161.9	0.5334	0.8705	1168.8	0.5292	0.8680	1167.6	0.5235	0.8662
313.15	1254.3	0.5081	0.8512	1260.2	0.5036	0.8480	1258.2	0.4976	0.8460
318.15	1349.3	0.4836	0.8301	1353.9	0.4789	0.8263	1351.2	0.4727	0.8239
$z_1 = 0.8973$									
268.15	575.6	0.8342	0.9802	578.6	0.8344	0.9800	578.9	0.8335	0.9797
273.15	664.8	0.8193	0.9765	668.6	0.8194	0.9762	669.1	0.8182	0.9758
278.15	759.3	0.8012	0.9718	764.1	0.8010	0.9713	764.8	0.7992	0.9708
283.15	857.5	0.7793	0.9658	863.1	0.7786	0.9650	863.8	0.7762	0.9644
288.15	957.2	0.7536	0.9580	963.4	0.7522	0.9570	963.8	0.7491	0.9561
293.15	1056.6	0.7246	0.9483	1063.0	0.7222	0.9468	1063.0	0.7183	0.9457
298.15	1154.6	0.6929	0.9365	1160.6	0.6895	0.9344	1159.9	0.6848	0.9331
303.15	1250.8	0.6598	0.9224	1256.0	0.6553	0.9196	1254.4	0.6498	0.9180

The VLE behaviors of R32 + R1234yf (k_{ij} = 0.03769), R32 + R1234ze(E) (k_{ij} = 0.01838), and R32 + R1234ze(Z) (k_{ij} = -0.00037) binary systems estimated with CES(A) at different temperatures are showed in Figures 4.14, 4.15, and 4.16. Moreover, the experimental VLE data for R32 + R1234yf and R32 + R1234ze(E) binary pairs available in the open literature [153, 159, 163, 222] at the studied temperatures are shown in Figures 4.14 and 4.15. It is possible to note that the VLE of both binary systems obtained from CES(A) agree with the experimental data. Instead, since no experimental VLE data are available in literature, it was not possible to compare the estimated description of the VLE of R32 + R1234ze(Z) binary pair with the experimental VLE behavior. It is worthwhile pointing out that also the other studied EoSs with k_{ij} calculated from the flash method result in reliable descriptions of VLE of the studied binary systems.

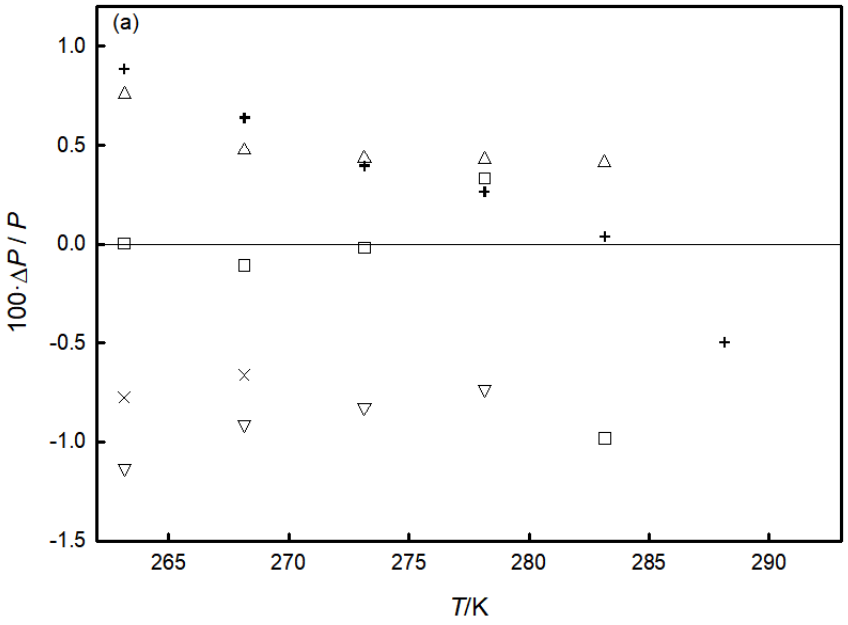
(a)
1.0
0.5
0.0
-0.5
-1.0
-1.5
100·ΔP / P
265
270
275
280
285
290
T/K

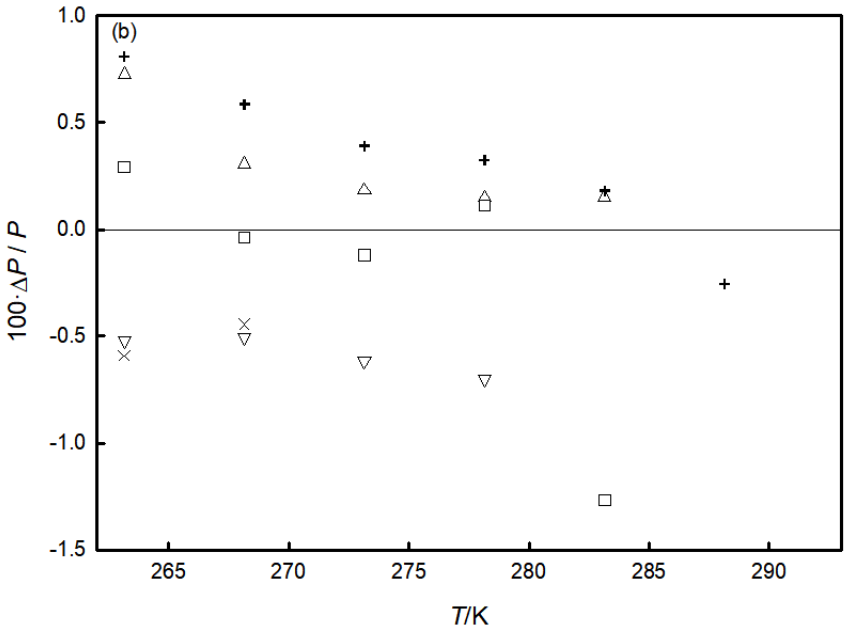
(b)
1.0
0.5
0.0
-0.5
-1.0
-1.5
100·ΔP / P
265
270
275
280
285
290
T/K

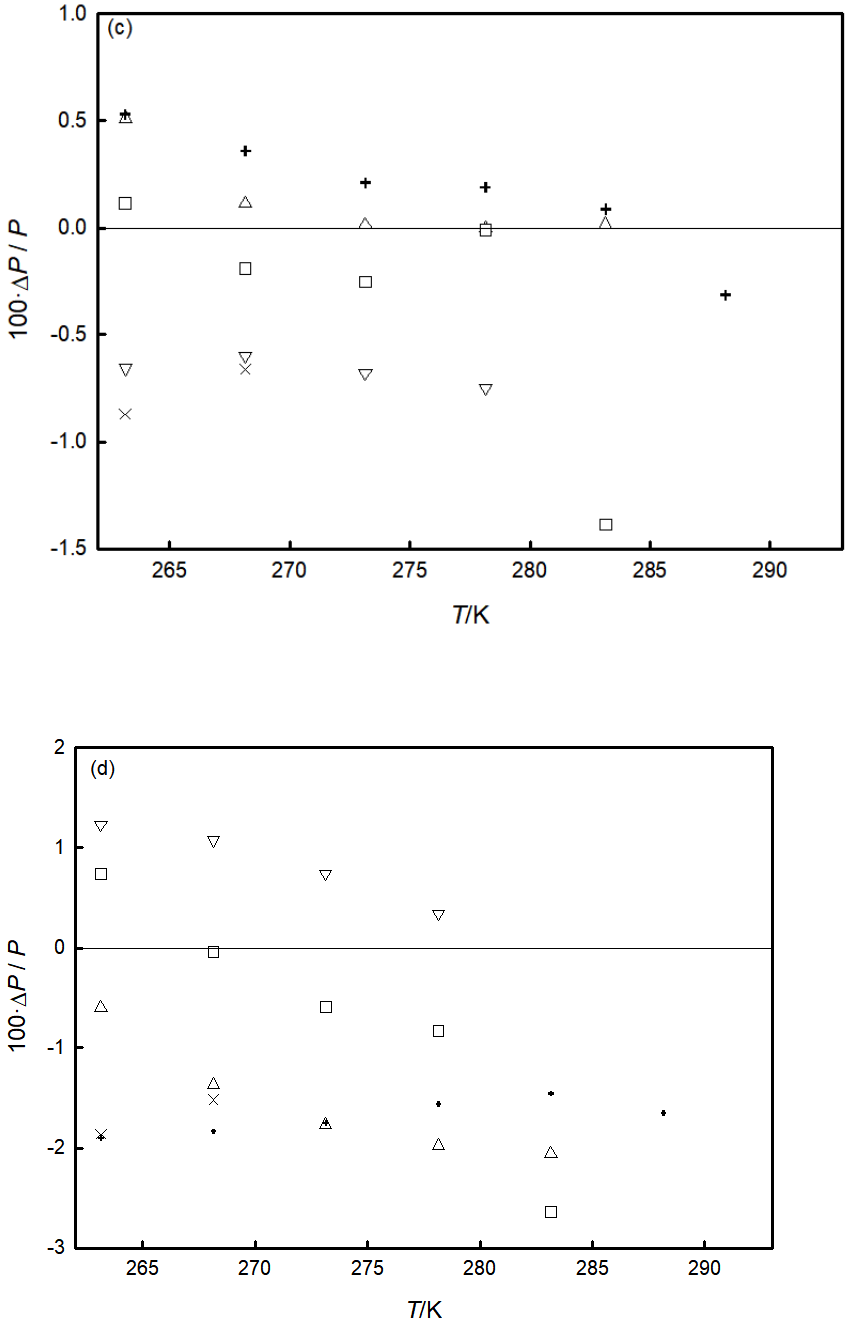

Figure 4.11: Deviations between experimental pressures for the R32 (1) + R1234yf (2) binary systems of Table B.1 (P_{exp}) and values calculated (P_{calc}) from the flash method with the Carnahan - Starling - De Santis EoS (a), Peng Robinson EoS (b), CES(A) (c), and from REFPROP 10.0 (d); ×, $z_1 = 0.1330$ and $v = 0.063915$ m^3 kg^{-1}; +, $z_1 = 0.1792$ and $v = 0.029936$ m^3 kg^{-1}; △, $z_1 = 0.5229$ and $v = 0.030724$ m^3 kg^{-1}; □, $z_1 = 0.6489$ and $v = 0.029794$ m^3 kg^{-1}; ▽, $z_1 = 0.8122$ and $v = 0.032113$ m^3 kg^{-1}.

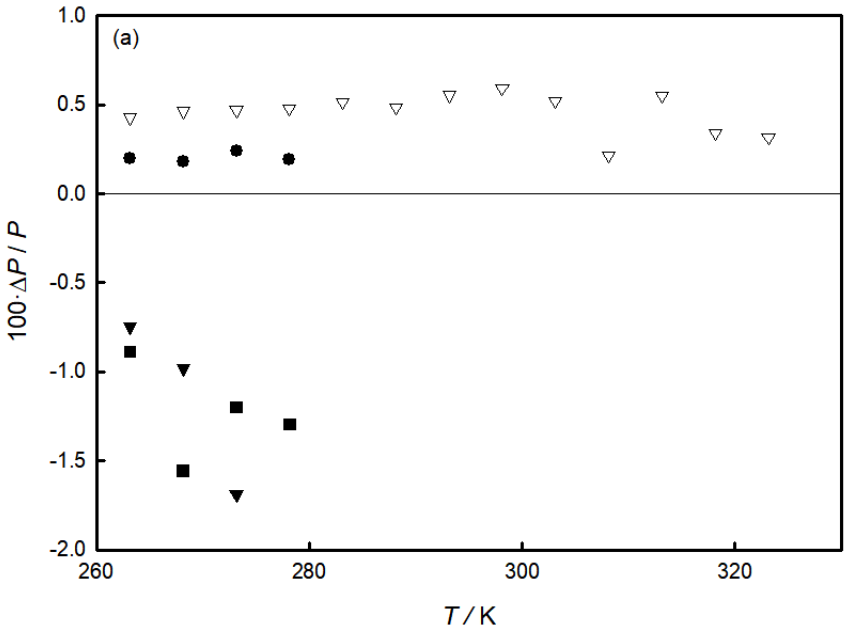
(a)
1.0
0.5
0.0
-0.5
-1.0
-1.5
-2.0
100·ΔP / P
260
280
300
320
T / K

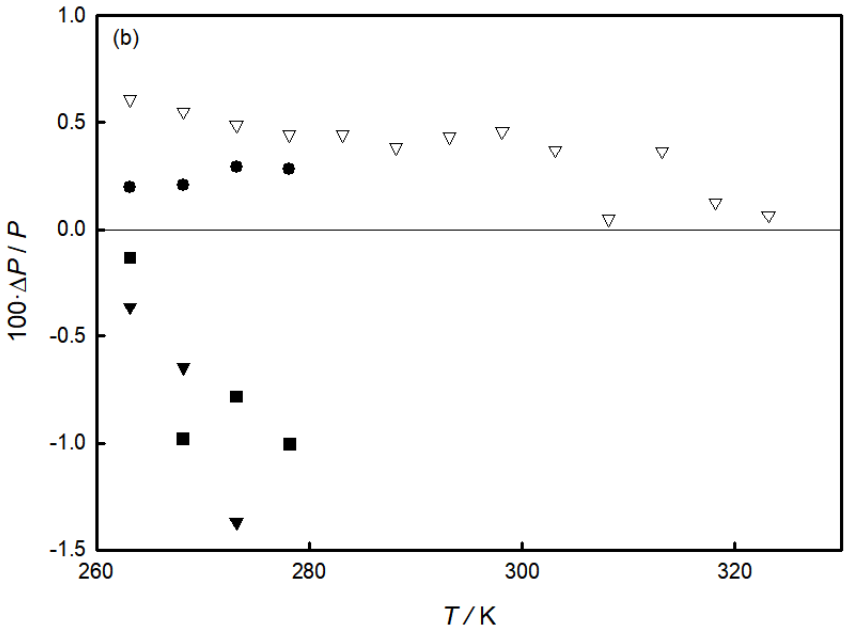
(b)
1.0
0.5
0.0
-0.5
-1.0
-1.5
100·ΔP / P
260
280
300
320
T / K

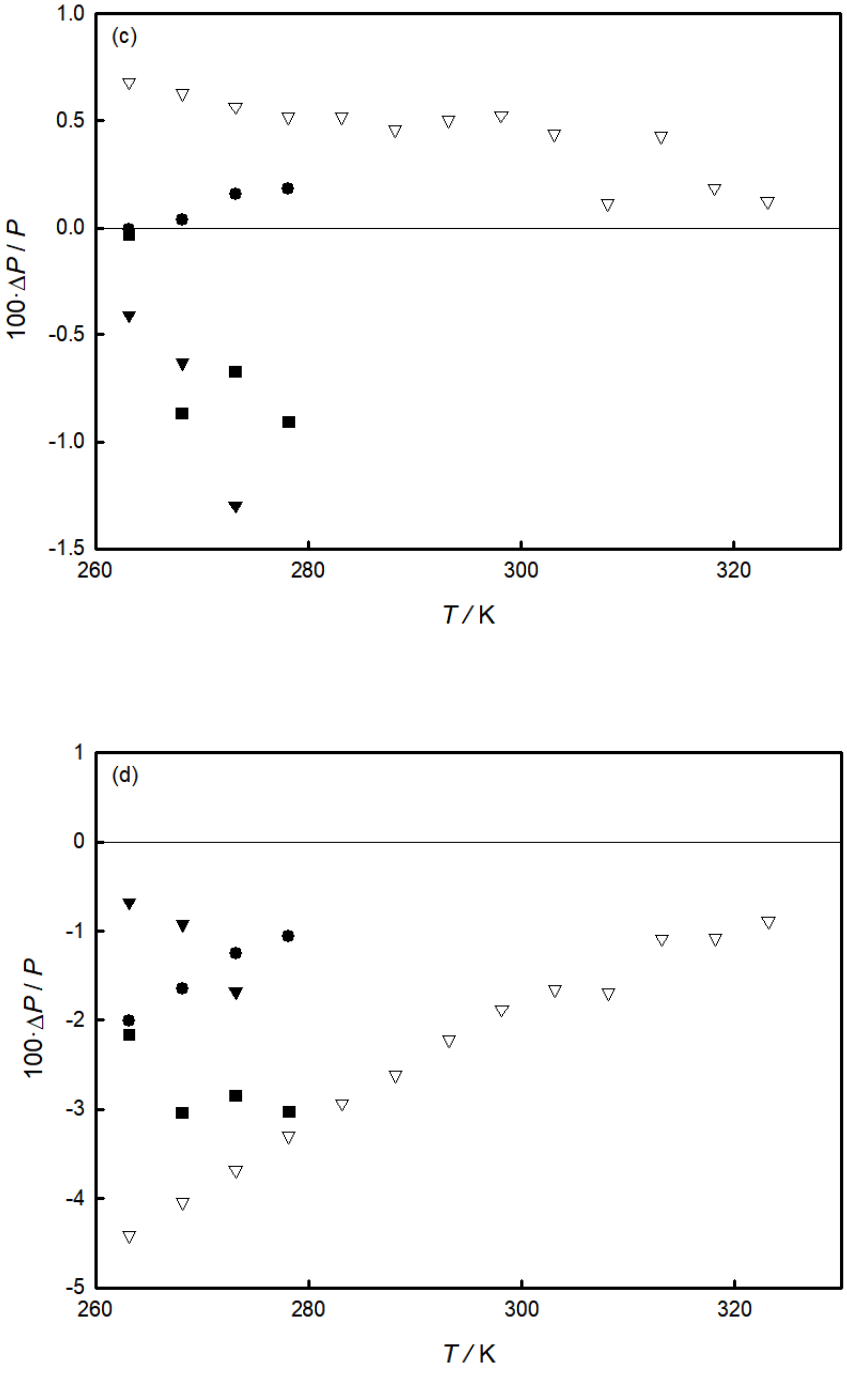

Figure 4.12: Deviations between experimental pressures for the R32 (1) + R1234ze(E) (2) binary systems of Table B.2 (P_{exp}) and values calculated (P_{calc}) from the flash method with the Carnahan - Starling - De Santis EoS (a), Peng Robinson EoS (b), CES(A) (c), and from REFPROP 10.0 (d); ●, $z_1 = 0.1677$ and $v = 0.046522$ m^3 kg^{-1}; ▽, $z_1 = 0.2551$ and $v = 0.013173$ m^3 kg^{-1}; ■, $z_1 = 0.7383$ and $v = 0.039422$ m^3 kg^{-1}; ▼, $z_1 = 0.9532$ and $v = 0.043115$ m^3 kg^{-1}.

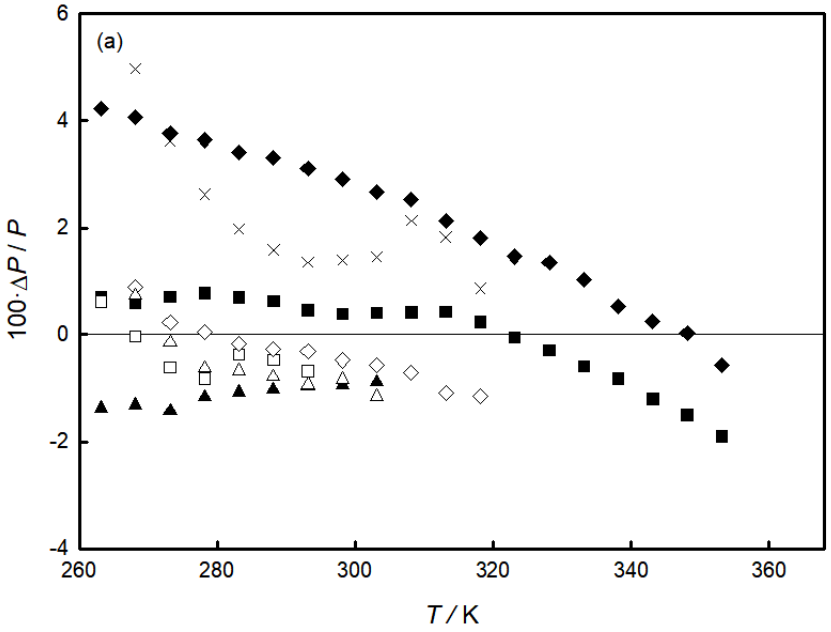
(a)
100·ΔP / P
T / K
6
4
2
0
-2
-4
260
280
300
320
340
360

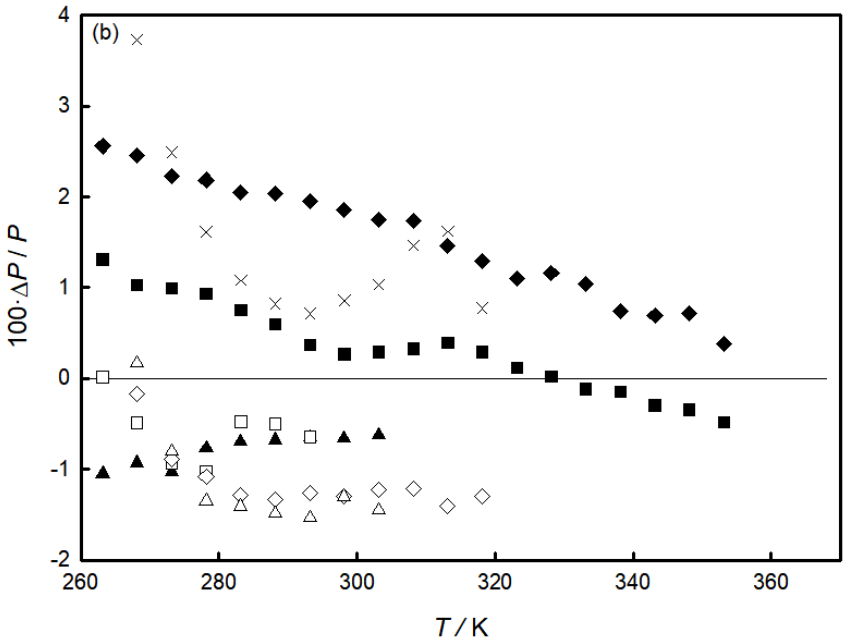
(b)
100·ΔP / P
T / K
4
3
2
1
0
-1
-2
260
280
300
320
340
360

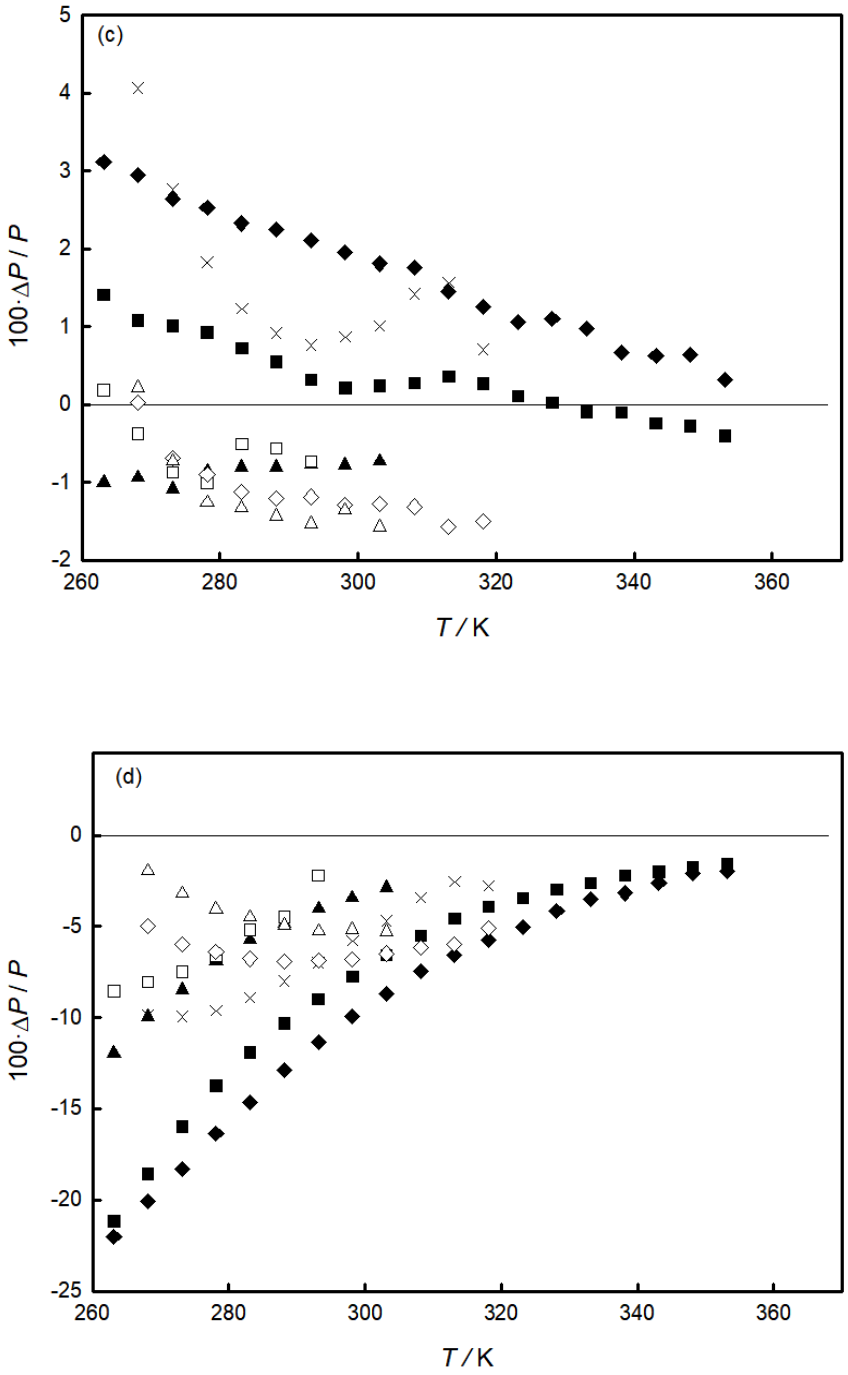

Figure 4.13: Deviations between experimental pressures for the R32 (1) + R1234ze(Z) (2) binary systems of Table B.3 (P_{exp}) and values calculated (P_{calc}) from the flash method with the Carnahan - Starling - De Santis EoS (a), Peng Robinson EoS (b), CES(A) (c), and from REFPROP 10.0 (d); ■, $z_1 = 0.0871$ and $v = 0.013352$ m^3 kg^{-1}; ◆, $z_1 = 0.2980$ and $v = 0.016365$ m^3 kg^{-1}; ▲, $z_1 = 0.3620$ and $v = 0.071713$ m^3 kg^{-1}; ×, $z_1 = 0.5232$ and $v = 0.035001$ m^3 kg^{-1}; □, $z_1 = 0.7128$ and $v = 0.070089$ m^3 kg^{-1}; ◇, $z_1 = 0.8015$ and $v = 0.023746$ m^3 kg^{-1}; △, $z_1 = 0.8973$ and $v = 0.026769$ m^3 kg^{-1}.

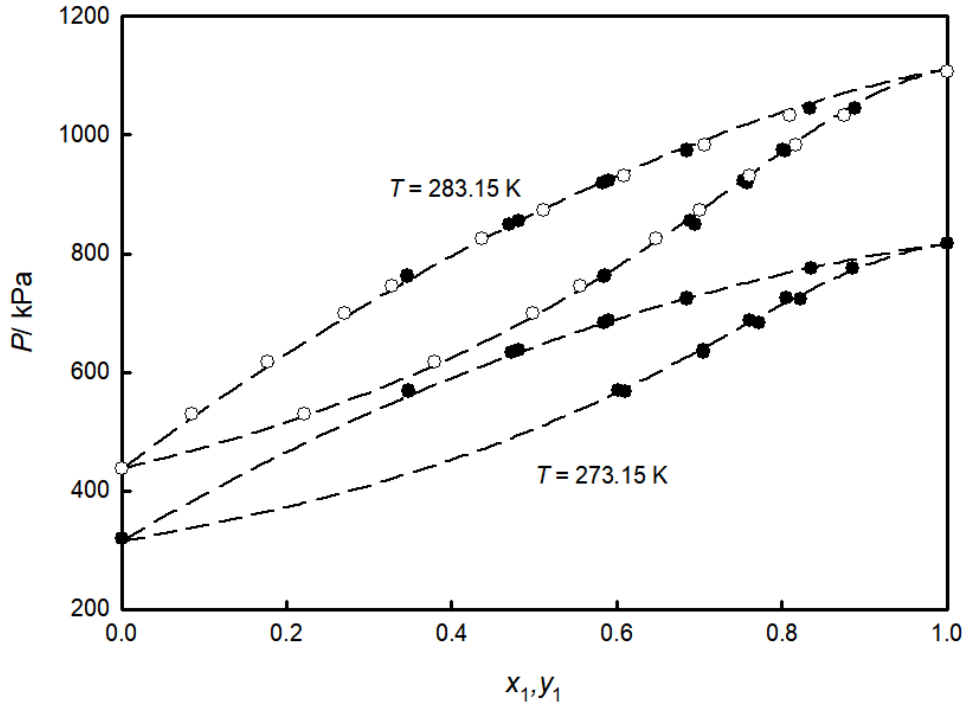

Figure 4.14: VLE representation for the R32 (1) + R1234yf (2) binary pair using CES(A) (dashed lines) at two temperatures: $T = 273.15$ K and $T = 283.15$ K. Black circles (●) and white circles (○) are the experimental data reported in Kamiaka et al. [153] and Hu et al. [159], respectively.

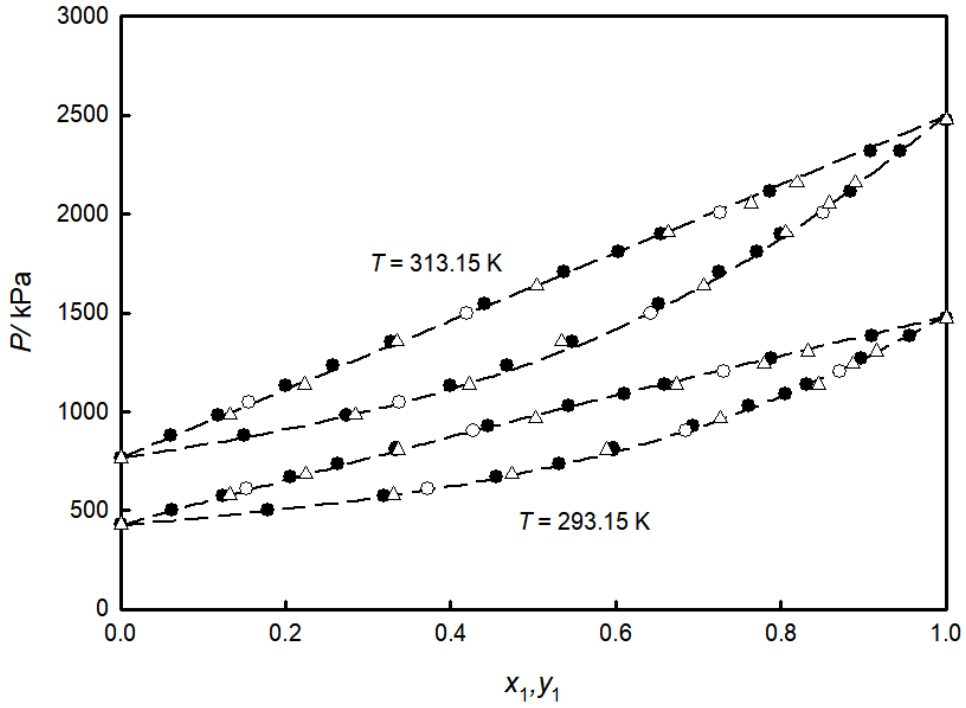

Figure 4.15: VLE representation for the R32 (1) + R1234ze(E) (2) binary pair using CES(A) (dashed lines) at two temperatures: $T = 293.15$ K and $T = 313.15$ K. Black circles (●) and white circles (○), and white triangles (△) are experimental data reported in Hu et al. [163], Hu et al. [159], and Kou et al. [222], respectively.

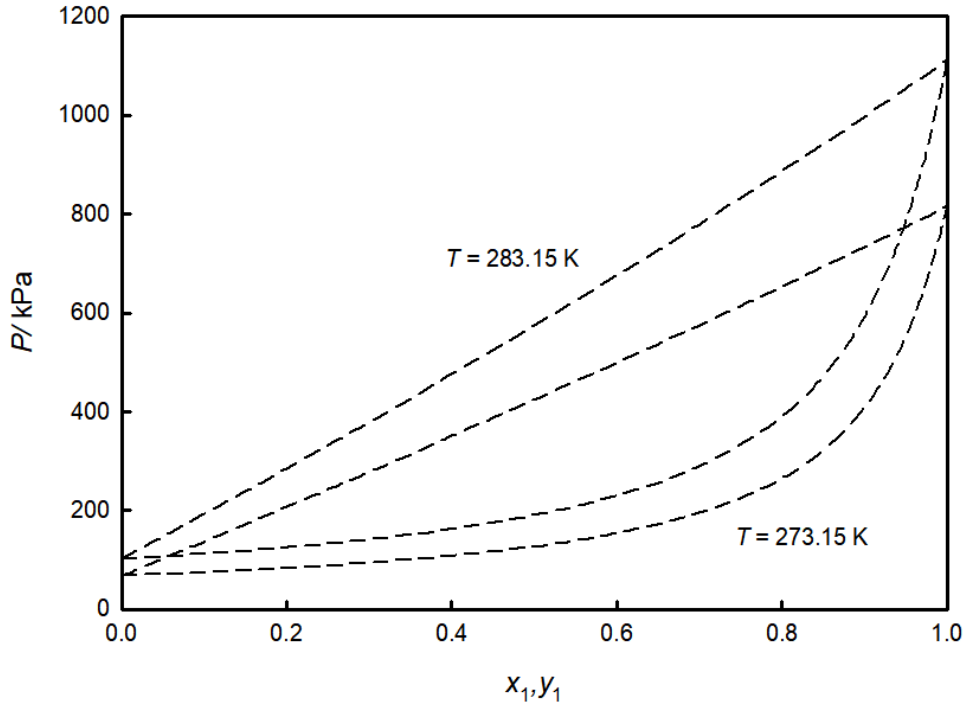

Figure 4.16: VLE representation for the R32 (1) + R1234ze(Z) (2) binary pair using CES(A) (dashed lines) at two temperatures: $T = 273.15$ K and $T = 283.15$ K.

Table 4.17: Average Absolute Relative Deviation of the pressure (AARD (ΔP) %) obtained for vapor-phase $PvTz$ data of the measured binary systems and their binary interaction parameter (k_{ij}) for PR EoS.

Binary system	PR EoS AARD (ΔP) %	k_{ij}	Virial EoS AARD (ΔP) %	REFPROP 10.0 AARD (ΔP) %
R1234yf + R600a	0.60	-0.3161	0.04	1.27
R1234ze(E) + R600a	0.25	-0.2215	0.02	1.31
R600a + R1233zd(E)	0.58	-0.1865	0.09	1.09
R600a + R1234ze(Z)	0.60	-0.1841	0.06	0.35
R1225ye(Z) + R600a	0.46	0.0039	0.03	0.76 [a]
R1243zf + R600a	0.37	0.1232	0.07	0.37
R32 + R1234yf	0.30	0.0077	0.18	0.25
R32 + R1234ze(E)	0.31	-0.0210	0.16	0.14
R32 + R1234ze(Z)	0.49	-0.11090	0.10	0.77

[a] Obtained from REFPROP 9.1.

4.1.8 Vapor-phase *PvTz* calculation

The experimental vapor-phase $PvTz$ data for the studied binary pairs were correlated with the PR EoS [103] and a truncated virial EoS. The PR EoS was coupled with the van der Waals one-fluid mixing rules with a single k_{ij} calculated by minimizing the AARD (ΔP) % of the selected data sets. Instead, the empirical mixing rules described in Subsection 2.2.2 of Chapter 2 were used to extend the virial EoS to the measured binary systems. Moreover, the experimental data were compared with the REFPROP 10.0 [65] predictions. Since it was not possible to use this version of the software for the property estimation of R1225ye(Z) + R600a, the measured data of this binary pair were compared with the REFPROP 9.1 [64] predictions. Having showed much higher pressure deviations, the experimental data for R32 + R1234yf, R32 + R1234ze(E), and R32 + R1234ze(Z) binary systems in the proximity of the two-phase region (denoted in Tables B.10, B.11, and B.12 with a "b") were neglected in the calculations. Table 4.17 presents the AARD (ΔP) % for the selected models for the different binary systems, together with the k_{ij} obtained for the van der Waals one-fluid mixing rules used in the PR EoS. Instead, the coefficients of the mixing rules coupled with the virial EoS, which were determined by minimizing the AARD (ΔP) % for the studied binary pairs, are reported in Table 4.18.

The deviations between the experimental pressures of the binary pairs measured in the superheated vapor region and the values calculated from the selected models are shown from Figure 4.17 to Figure 4.25.

From these figures and Table 4.17, it can be stated that the truncated virial EoS provided the most accurate $PvTz$ description of all the studied binary systems in the superheated vapor region among the selected models. This outcome was expected since the mixing rules used for extending this EoS to the measured binary systems present several coefficients regressed on the experimental data. Moreover, accurate vapor-phase $PvTz$ values for all the binary pairs were given by the PR Eos, ensuring deviations within ±2 % for all the series, except for few points.

Although REFPROP 10.0 generally provided accurate predictions in agreement with the experimental data, slightly higher deviations between the measured pressures and the REFPROP 10.0 values were obtained for R1234yf + R600a, R1234ze(E) + R600a, and R600a + R1233zd(E) binary systems. As shown in Figures 4.17c and 4.19c for R1234yf + R600a and R600a + R1233zd(E) binary systems, only the deviations for some series are higher than ±2 %. This result can be due to the model inaccuracy, but also to possible inaccuracies during the experimental measurements. Instead, Figure 4.18c

Table 4.18: Coefficients for B [Eq. (2.30)] and for C [Eq. (2.31)] for the measured binary systems.

Binary system	B_1	B_2	B_3	B_4	B_5	C_1	C_2	C_3	C_4	C_5
R1234yf + R600a	-0.81425	-490.49	8.1658	-11.116	9.3180	-2.5532	-1429.7	-82.357	112.44	-17.479
R1234ze(E) + R600a	1.2044	142.11	-9.9051	14.035	-12.407	-16.436	-5865.6	99.518	-133.96	154.43
R600a + R1233zd(E)	-3.7808	-1786.1	0.16910	-5.5388	30.348	9.1326	3570.5	-141.45	234.06	-156.41
R600a + R1234ze(Z)	0.51083	-269.91	-7.3826	7.5947	-4.9763	-22.690	-7295.9	95.182	-108.62	186.82
R1225ye(Z) + R600a	0.78614	-12.372	-8.0381	12.419	-9.3286	-13.354	-4840.1	63.906	-97.185	125.41
R1243zf + R600a	-1.2596	-1221.3	541.76	-690.12	160.47	-6.9015	2717.5	-6091.1	7812.3	-1600.7
R32 + R1234yf	-3.3975	-1459.6	-0.2065	0.3929	23.668	5.1850	1985.1	0.2528	-0.2850	-35.945
R32 + R1234ze(E)	-6.2182	-2364.0	-0.2214	0.4647	42.749	14.724	5116.0	0.3192	-0.4754	-100.72
R32 + R1234ze(Z)	-1.7750	-923.871	-98.6313	100.3795	-8.3694	-3.6723	1371.08	3.6659	-70.491	-29.8528

shows that the deviations for R1234ze(E) + R600a binary pair are systematically lower than -0.5 %. This outcome is more likely due to the inaccuracy of the REFPROP 10.0 mixing models used to extend the EoSs for the pure refrigerants to the studied binary systems. In general, the obtained deviations between the experimental data and REFPROP 10.0 predictions for these three binary pairs are still adequate for many engineering calculations.

Finally, the measured data for R1234yf + R600a, R1234ze(E) + R600a, and R32 + R1234yf binary systems were compared with the vapor-phase $PvTz$ values available in literature. In particular, the measurements reported in this work with the data presented by Zhang et al. [212] for R1234yf + R600a binary pair, the data measured by Cao et al. [223] for R1234ze(E) + R600a binary pair, and the values reported by Cai et al. [215] and Yang et al. [216] for R32 + R1234yf binary pair were correlated separately with the PR EoS coupled with the van der Waals one-fluid mixing rules with a single k_{ij}. Values of k_{ij} equal to -0.0599 and -0.0974 were obtained for R1234yf + R600a and R1234ze(E) + R600a binary systems, respectively, providing an AARD $(\Delta P) = 0.50$ % for the former refrigerant pair and an AARD $(\Delta P) = 0.38$ % for the latter refrigerant pair. The agreement between the selected data of the two pairs is evident for the PR EoS also in Figures 4.26 and 4.27 where almost all the deviations are within ±1.5 %. For R32 + R1234yf, k_{ij} was obtained equal to 0.0583, yielding an AARD $(\Delta P) = 0.53$ %. As also shown in Figure 4.28, the agreement between all datasets is evident for this model, having deviations well within ±2 %, excluding a few points of Yang et al. [216].

Since the $PvTz$ measurements for the R32 + R1234ze(E) binary systems presented by Kobayashi et. al. [226] are not accessible, they were not compared with the presented experimental data.

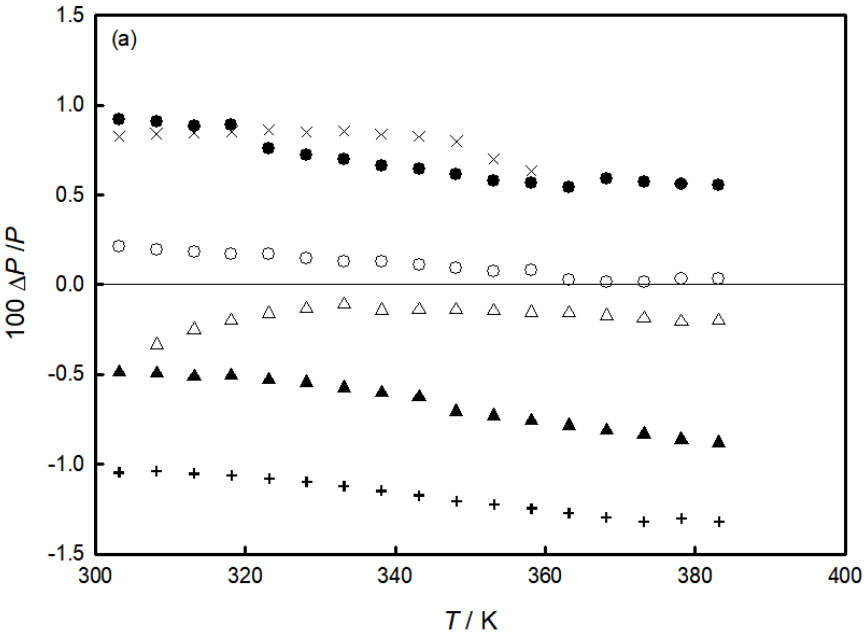
(a)
1.5
1.0
0.5
0.0
-0.5
-1.0
-1.5
100 ΔP /P
300
320
340
360
380
400
T / K

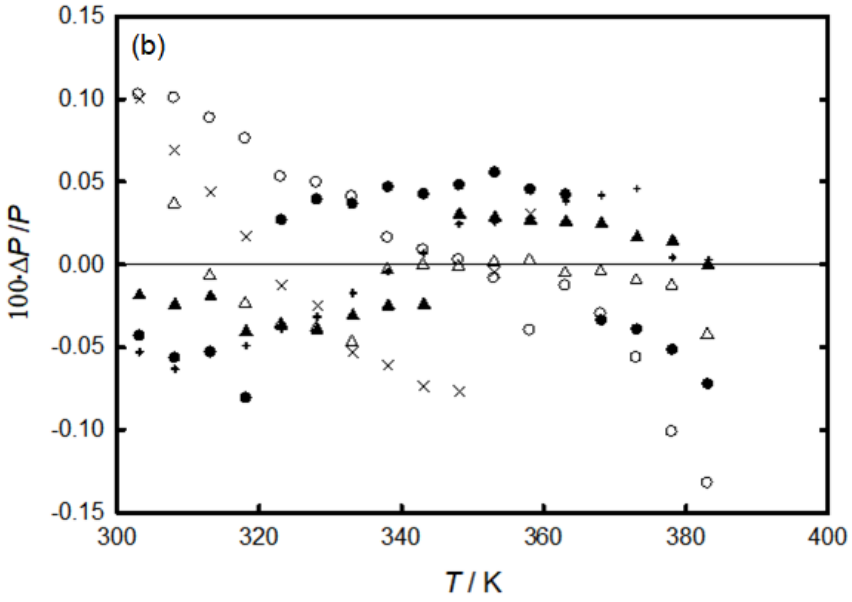
(b)
0.15
0.10
0.05
0.00
-0.05
-0.10
-0.15
100·ΔP /P
300
320
340
360
380
400
T / K

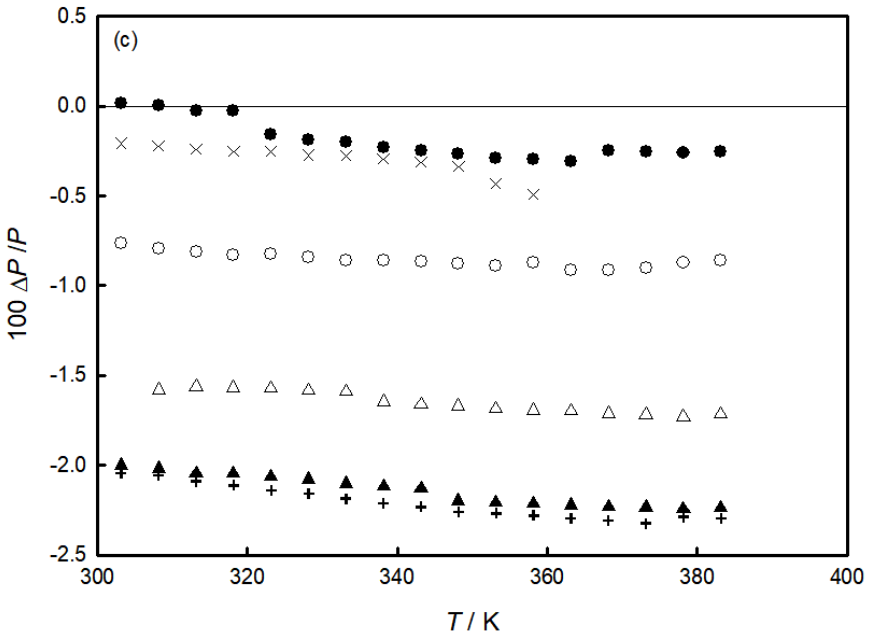

Figure 4.17: Deviations ($\Delta P/P = (P_{\text{exp}} - P_{\text{calc}})/P_{\text{exp}}$) between vapor-phase experimental pressures for the R1234yf (1) + R600a (2) binary systems of Table B.4 (P_{exp}) and values calculated (P_{calc}) with the Peng Robinson EoS (a), the virial EoS (b), and from REFPROP 10.0 (c); +, $z_2 = 0.2340$ and $v = 0.094104$ m^3 kg^{-1}; ▲, $z_2 = 0.4005$ and $v = 0.094392$ m^3 kg^{-1}; ●, $z_2 = 0.4723$ and $v = 0.170142$ m^3 kg^{-1}; ○, $z_2 = 0.6061$ and $v = 0.166637$ m^3 kg^{-1}; ×, $z_2 = 0.7720$ and $v = 0.128013$ m^3 kg^{-1}; △, $z_2 = 0.8504$ and $v = 0.079806$ m^3 kg^{-1}.

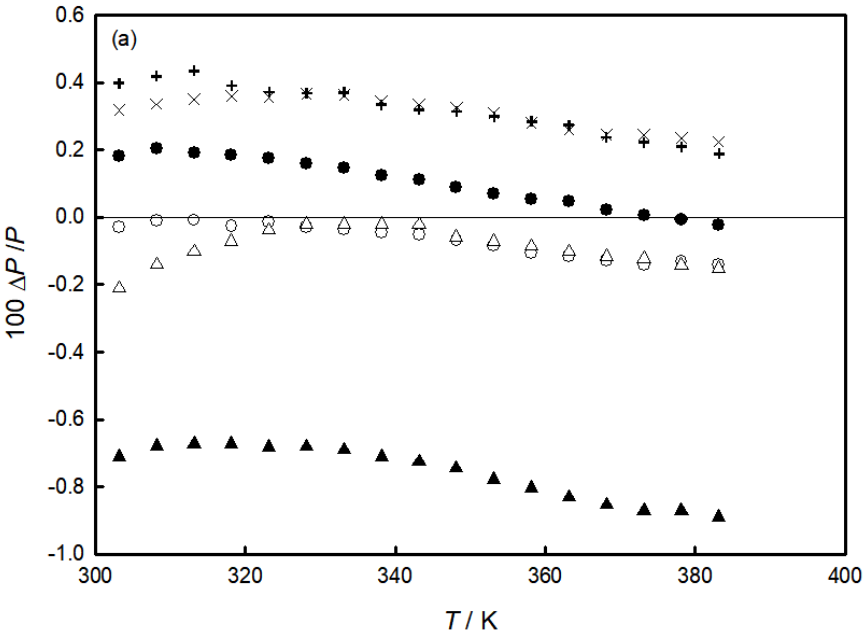
(a)
100 ΔP /P
T / K
0.6
0.4
0.2
0.0
-0.2
-0.4
-0.6
-0.8
-1.0
300
320
340
360
380
400

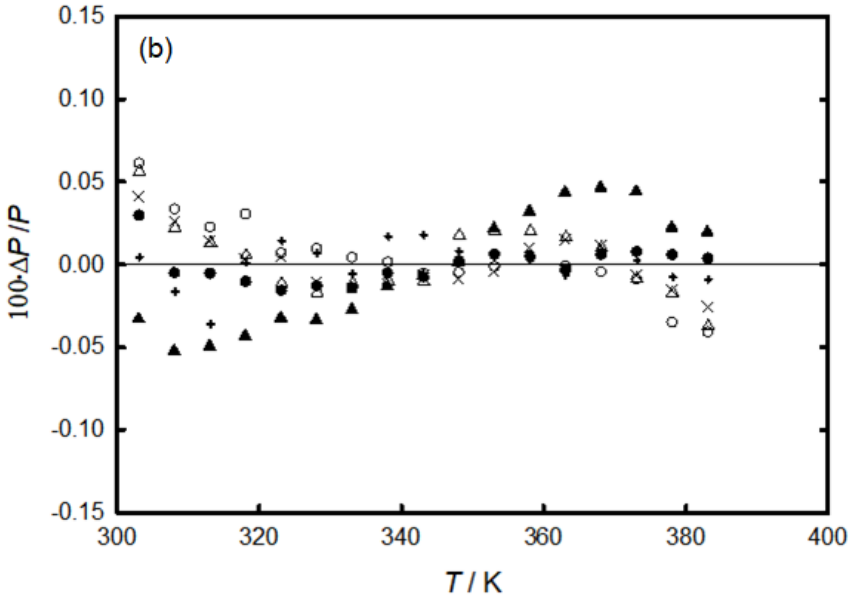
(b)
100·ΔP /P
T / K
0.15
0.10
0.05
0.00
-0.05
-0.10
-0.15
300
320
340
360
380
400

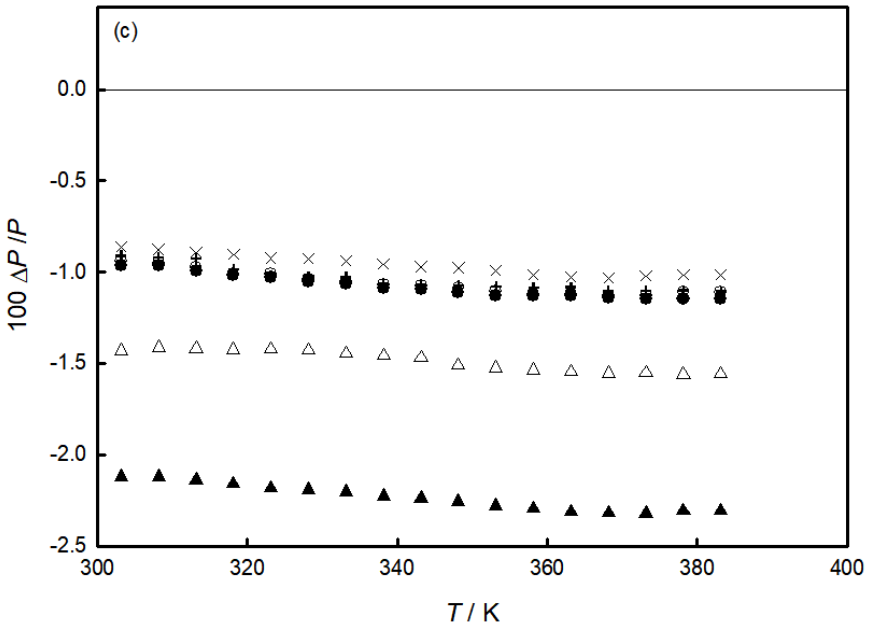

Figure 4.18: Deviations ($\Delta P/P = (P_{exp} - P_{calc})/P_{exp}$) between vapor-phase experimental pressures for the R1234ze(E) (1) + R600a (2) binary systems of Table B.5 (P_{exp}) and values calculated (P_{calc}) with the Peng Robinson EoS (a), the virial EoS (b), and from REFPROP 10.0 (c); ○, $z_2 = 0.2899$ and $v = 0.089681$ $m^3\,kg^{-1}$; +, $z_2 = 0.4275$ and $v = 0.084552$ $m^3\,kg^{-1}$; ●, $z_2 = 0.5156$ and $v = 0.106374$ $m^3\,kg^{-1}$; ▲, $z_2 = 0.6124$ and $v = 0.089171$ $m^3\,kg^{-1}$; ×, $z_2 = 0.6851$ and $v = 0.100595$ $m^3\,kg^{-1}$; △, $z_2 = 0.7551$ and $v = 0.085765$ $m^3\,kg^{-1}$.

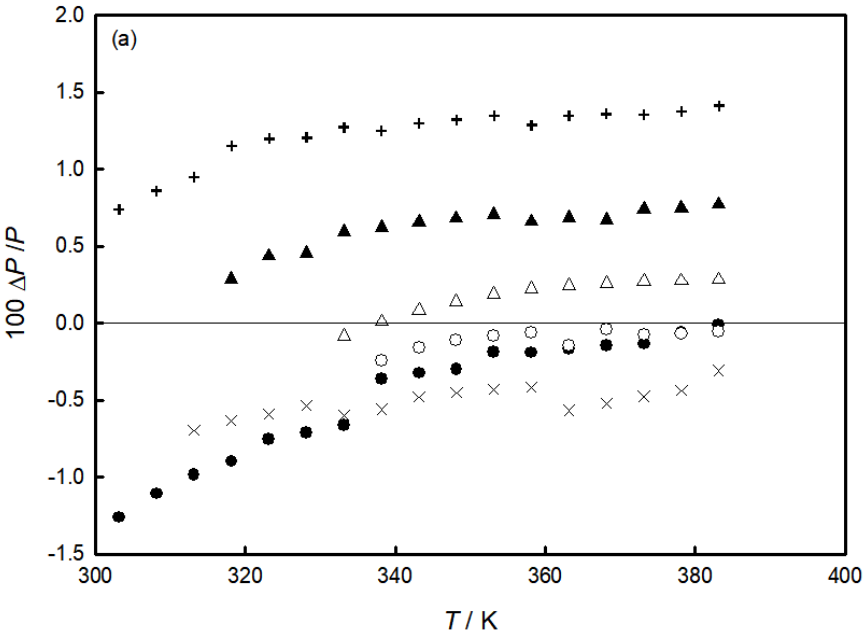
(a)
100 ΔP /P
T / K
2.0
1.5
1.0
0.5
0.0
-0.5
-1.0
-1.5
300
320
340
360
380
400

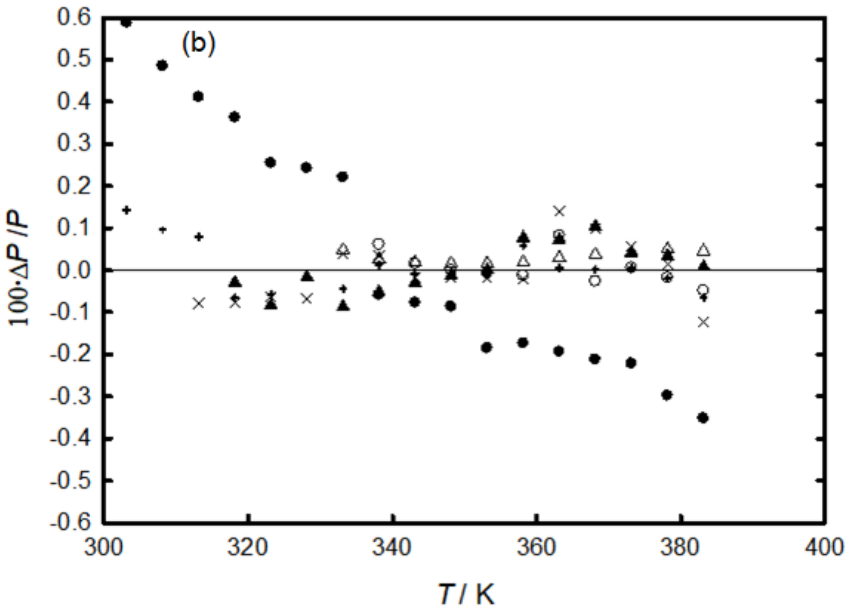
(b)
100·ΔP /P
T / K
0.6
0.5
0.4
0.3
0.2
0.1
0.0
-0.1
-0.2
-0.3
-0.4
-0.5
-0.6
300
320
340
360
380
400

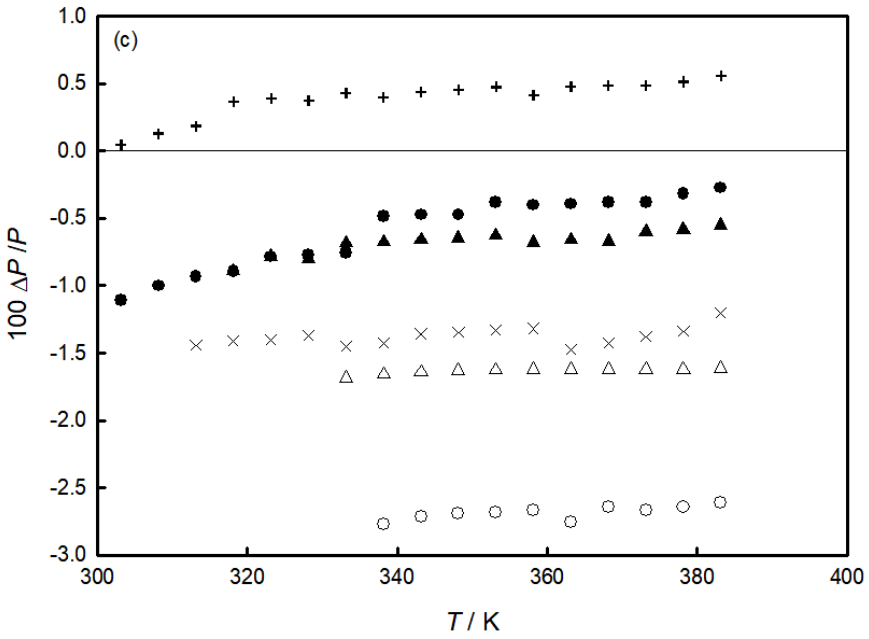

Figure 4.19: Deviations ($\Delta P/P = (P_{exp} - P_{calc})/P_{exp}$) between vapor-phase experimental pressures for the R600a (1) + R1233zd(E) (2) binary systems of Table B.6 (P_{exp}) and values calculated (P_{calc}) with the Peng Robinson EoS (a), the virial EoS (b), and from REFPROP 10.0 (c); ●, $z_1 = 0.1245$ and $v = 0.174350$ $m^3\,kg^{-1}$; ×, $z_1 = 0.4527$ and $v = 0.126329$ $m^3\,kg^{-1}$; +, $z_1 = 0.5638$ and $v = 0.143141$ $m^3\,kg^{-1}$; ○, $z_1 = 0.6438$ and $v = 0.049946$ $m^3\,kg^{-1}$; ▲, $z_1 = 0.7460$ and $v = 0.092697$ $m^3\,kg^{-1}$; △, $z_1 = 0.8647$ and $v = 0.053587$ $m^3\,kg^{-1}$.

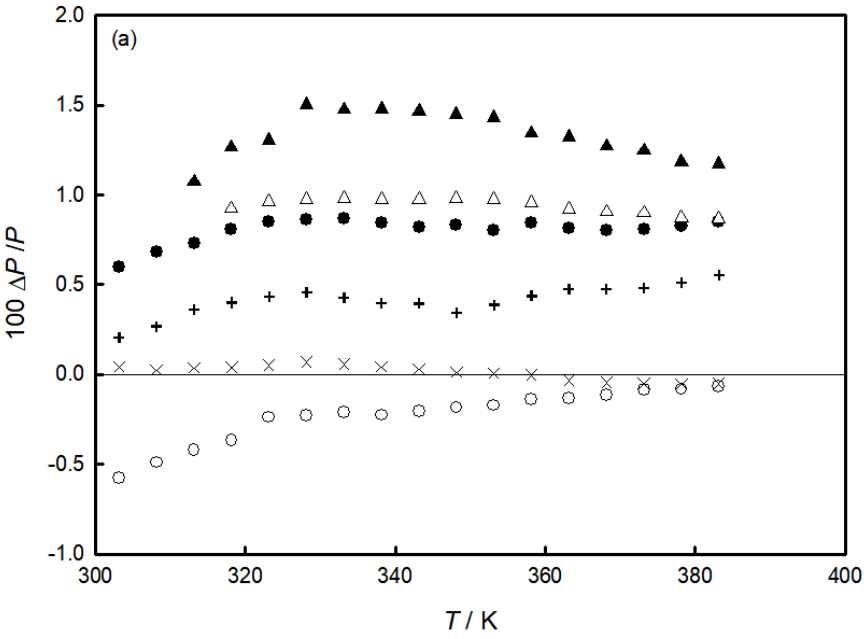
(a)
100 ΔP /P
T / K
2.0
1.5
1.0
0.5
0.0
-0.5
-1.0
300
320
340
360
380
400

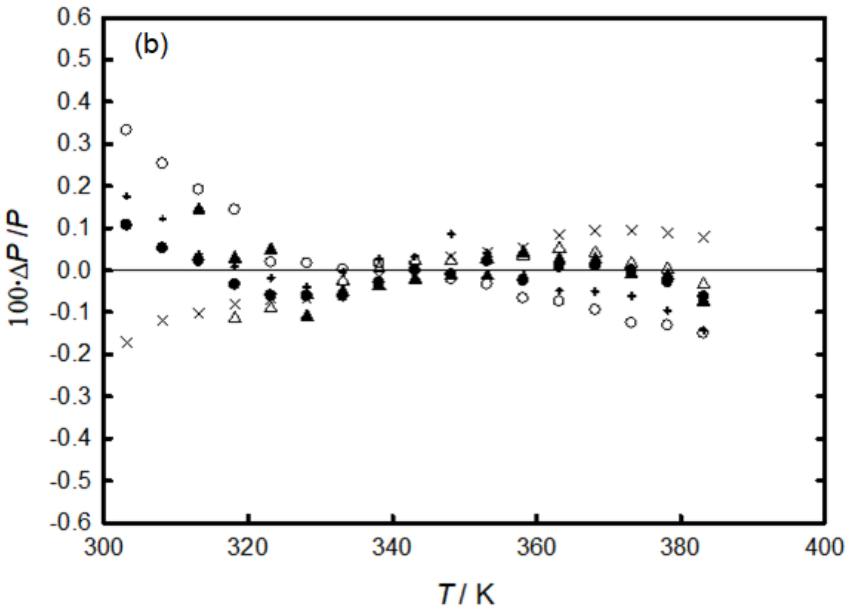
(b)
100·ΔP /P
T / K
0.6
0.5
0.4
0.3
0.2
0.1
0.0
-0.1
-0.2
-0.3
-0.4
-0.5
-0.6
300
320
340
360
380
400

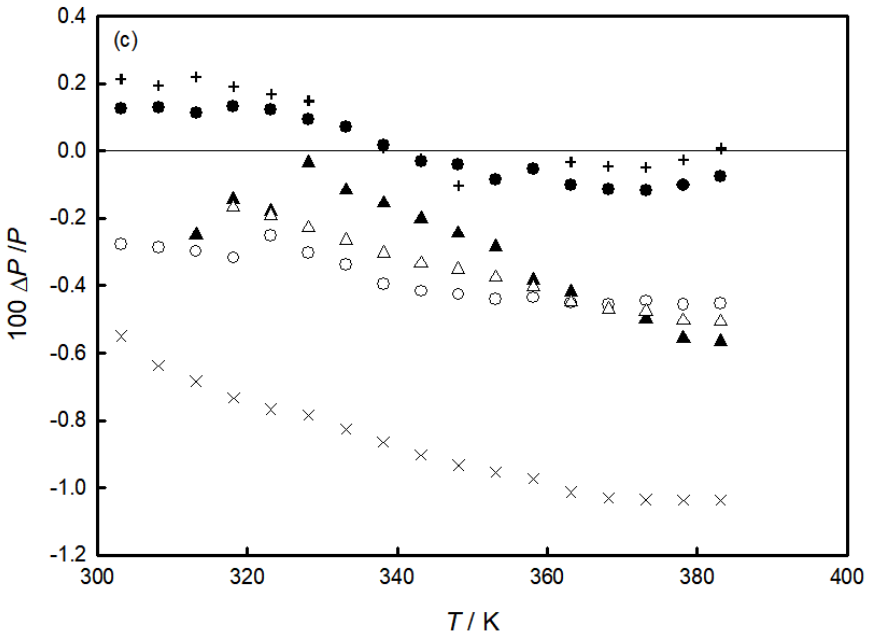

Figure 4.20: Deviations ($\Delta P/P = (P_{exp} - P_{calc})/P_{exp}$) between vapor-phase experimental pressures for the R600a (1) + R1234ze(Z) (2) binary systems of Table B.7 (P_{exp}) and values calculated (P_{calc}) with the Peng Robinson EoS (a), the virial EoS (b), and from REFPROP 10.0 (c); ○, $z_1 = 0.1176$ and $v = 0.152283$ $m^3\,kg^{-1}$; +, $z_1 = 0.2220$ and $v = 0.151676$ $m^3\,kg^{-1}$; ●, $z_1 = 0.4271$ and $v = 0.127222$ $m^3\,kg^{-1}$; ×, $z_1 = 0.5095$ and $v = 0.127222$ $m^3\,kg^{-1}$; ▲, $z_1 = 0.6585$ and $v = 0.075853$ $m^3\,kg^{-1}$; △, $z_1 = 0.7250$ and $v = 0.090738$ $m^3\,kg^{-1}$.

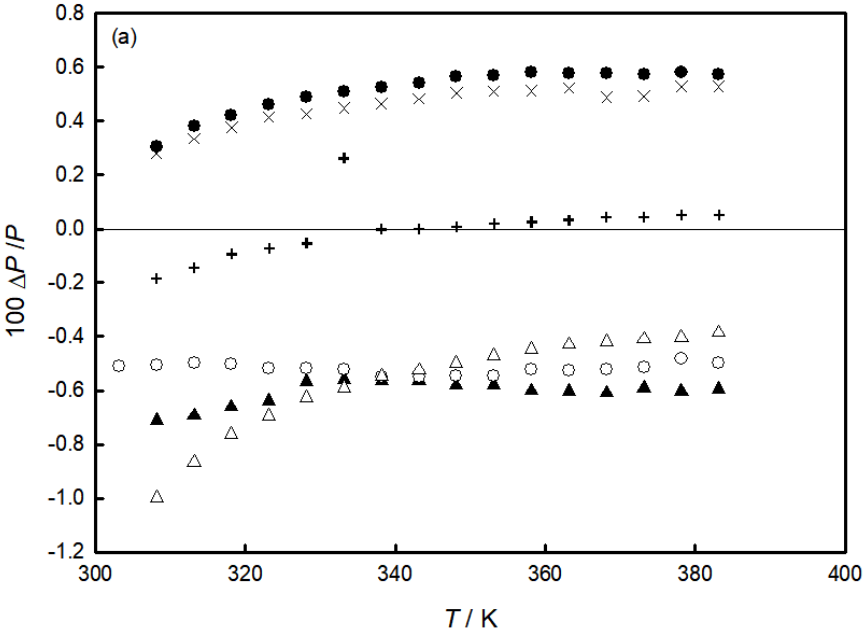
(a)
100 ΔP/P
T / K
0.8
0.6
0.4
0.2
0.0
-0.2
-0.4
-0.6
-0.8
-1.0
-1.2
300
320
340
360
380
400

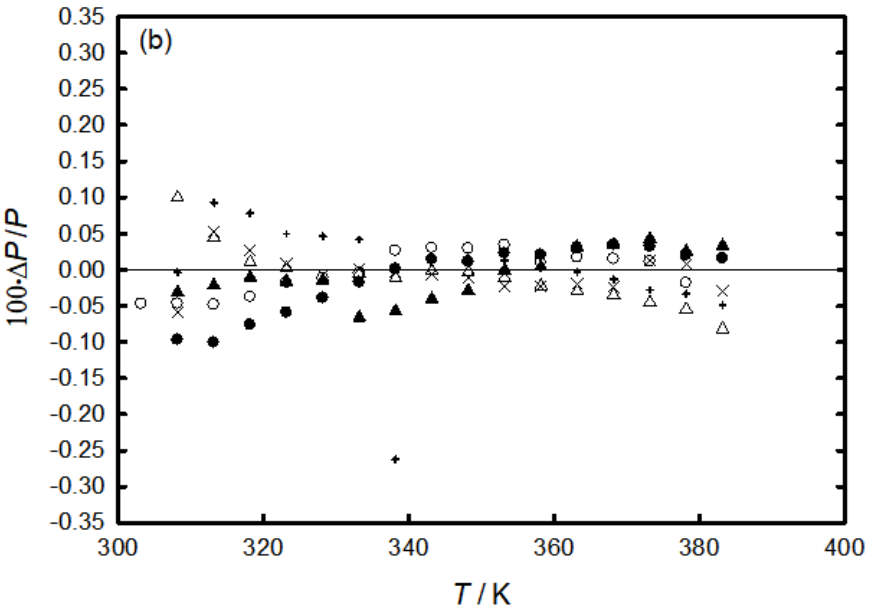
(b)
100·ΔP/P
T / K
0.35
0.30
0.25
0.20
0.15
0.10
0.05
0.00
-0.05
-0.10
-0.15
-0.20
-0.25
-0.30
-0.35
300
320
340
360
380
400

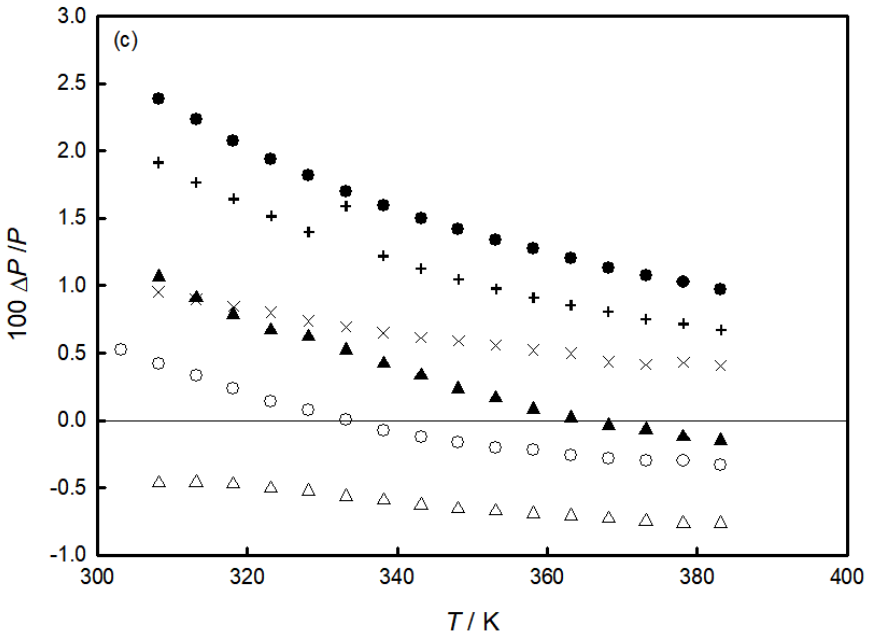

Figure 4.21: Deviations ($\Delta P/P = (P_{exp} - P_{calc})/P_{exp}$) between vapor-phase experimental pressures for the R1225ye(Z) (1) + R600a (2) binary systems of Table B.8 (P_{exp}) and values calculated (P_{calc}) with the Peng Robinson EoS (a), the virial EoS (b), and from REFPROP 9.1 (c); +, $z_2 = 0.1747$ and $v = 0.063330$ $m^3\,kg^{-1}$; ▲, $z_2 = 0.3453$ and $v = 0.071820$ $m^3\,kg^{-1}$; ●, $z_2 = 0.4768$ and $v = 0.058601$ $m^3\,kg^{-1}$; ○, $z_2 = 0.5041$ and $v = 0.121791$ $m^3\,kg^{-1}$; ×, $z_2 = 0.7969$ and $v = 0.107550$ $m^3\,kg^{-1}$; △, $z_2 = 0.9160$ and $v = 0.090234$ $m^3\,kg^{-1}$.

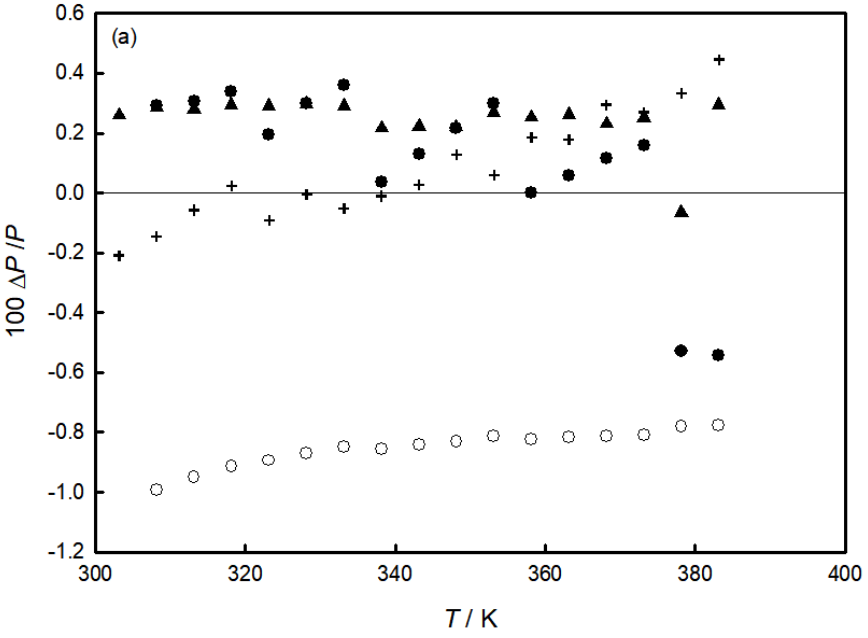
(a)
0.6
0.4
0.2
0.0
-0.2
-0.4
-0.6
-0.8
-1.0
-1.2
100 ΔP/P
300
320
340
360
380
400
T / K

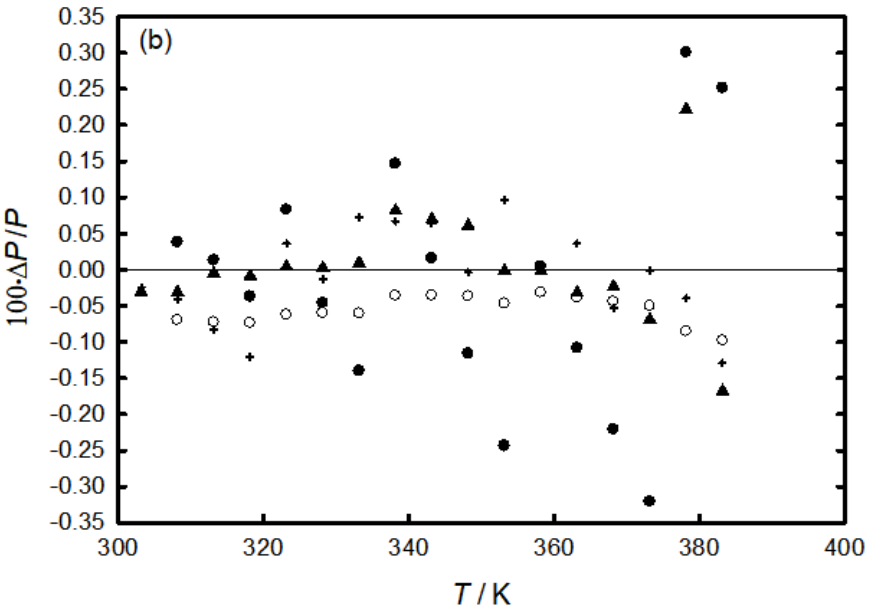
(b)
0.35
0.30
0.25
0.20
0.15
0.10
0.05
0.00
-0.05
-0.10
-0.15
-0.20
-0.25
-0.30
-0.35
100·ΔP/P
300
320
340
360
380
400
T / K

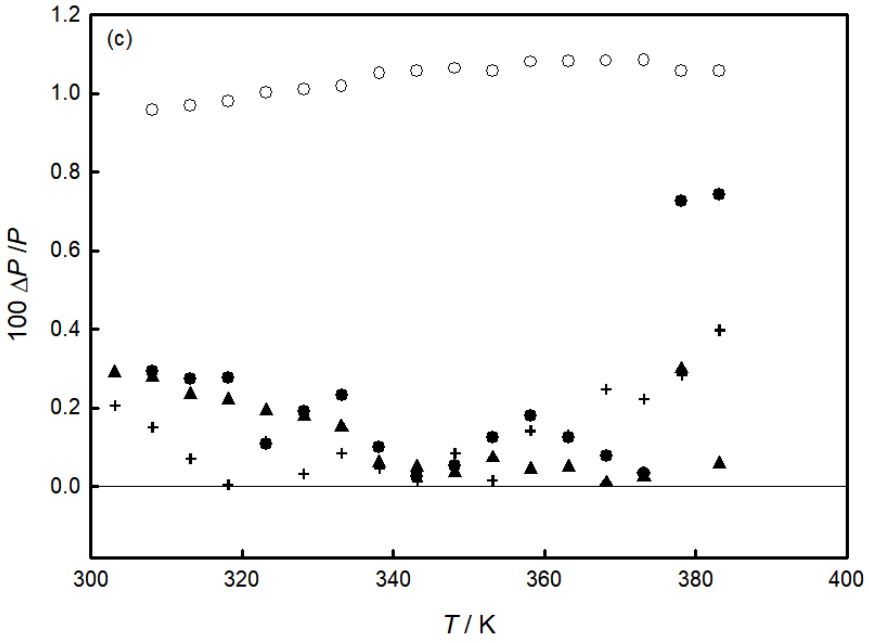

Figure 4.22: Deviations ($\Delta P/P = (P_{exp} - P_{calc})/P_{exp}$) between vapor-phase experimental pressures for the R1243zf (1) + R600a (2) binary systems of Table B.9 (P_{exp}) and values calculated (P_{calc}) with the Peng Robinson EoS (a), the virial EoS (b), and from REFPROP 10.0 (c); ○, $z_2 = 0.2254$ and $v = 0.094396$ m^3 kg^{-1}; +, $z_2 = 0.2821$ and $v = 0.614524$ m^3 kg^{-1}; ●, $z_2 = 0.4342$ and $v = 0.161341$ m^3 kg^{-1}; ▲, $z_2 = 0.8982$ and $v = 0.230619$ m^3 kg^{-1}.

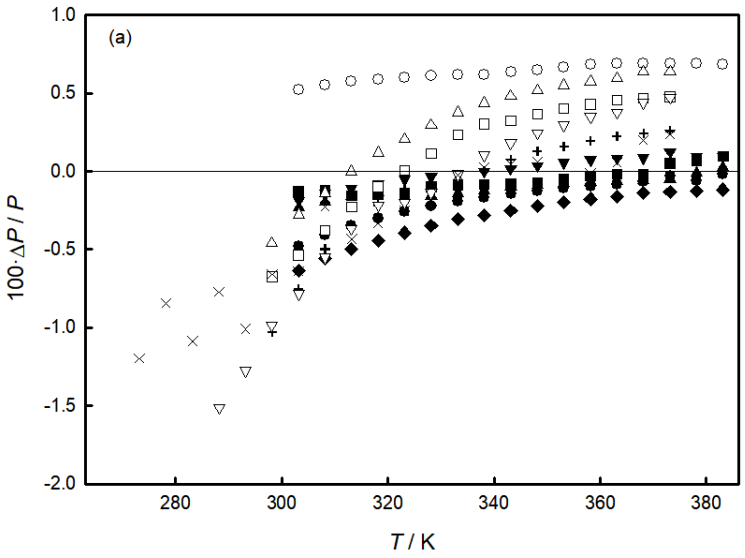
(a)
1.0
0.5
0.0
-0.5
-1.0
-1.5
-2.0
100·ΔP / P
280
300
320
340
360
380
T / K

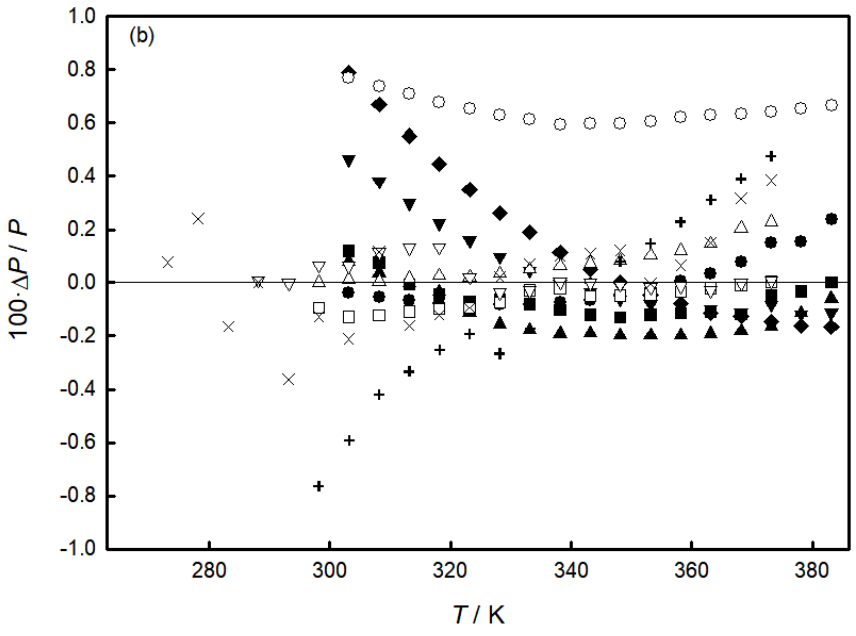
(b)
1.0
0.8
0.6
0.4
0.2
0.0
-0.2
-0.4
-0.6
-0.8
-1.0
100·ΔP / P
280
300
320
340
360
380
T / K

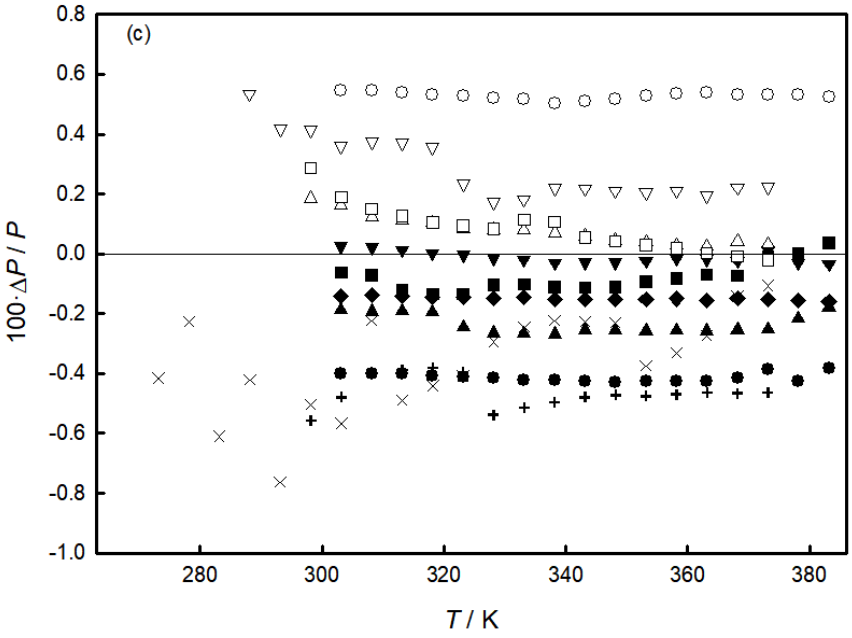

Figure 4.23: Deviations ($\Delta P/P = (P_{\text{exp}} - P_{\text{calc}})/P_{\text{exp}}$) between vapor-phase experimental pressures for the R32 (1) + R1234yf (2) binary systems of Table B.10 (P_{exp}) and values calculated (P_{calc}) with the Peng Robinson EoS (a), the virial EoS (b), and from REFPROP 10.0 (c); ●, $z_1 = 0.1214$ and $v = 0.061323$ m^3 kg^{-1}; ×, $z_1 = 0.1330$ and $v = 0.063915$ m^3 kg^{-1}; +, $z_1 = 0.1792$ and $v = 0.029936$ m^3 kg^{-1}; ○, $z_1 = 0.2712$ and $v = 0.144796$ m^3 kg^{-1}; ▲, $z_1 = 0.3432$ and $v = 0.111536$ m^3 kg^{-1}; △, $z_1 = 0.5229$ and $v = 0.030724$ m^3 kg^{-1}; ■, $z_1 = 0.6231$ and $v = 0.280627$ m^3 kg^{-1}; □, $z_1 = 0.6489$ and $v = 0.029794$ m^3 kg^{-1}; ▼, $z_1 = 0.7020$ and $v = 0.116592$ m^3 kg^{-1}; ▽, $z_1 = 0.8122$ and $v = 0.032113$ m^3 kg^{-1}; ◆, $z_1 = 0.9460$ and $v = 0.102150$ m^3 kg^{-1}.

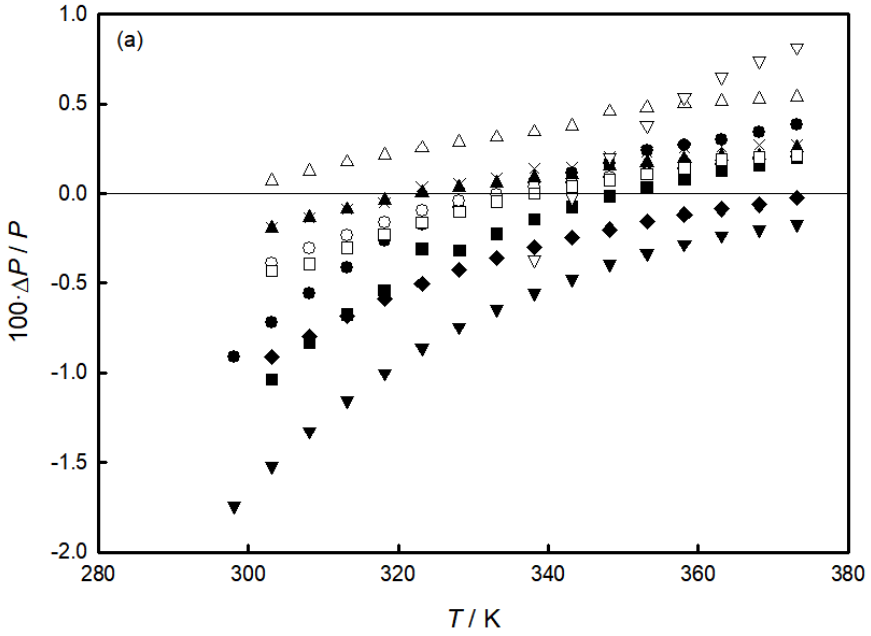
(a)
100·ΔP / P
T / K
1.0
0.5
0.0
-0.5
-1.0
-1.5
-2.0
280
300
320
340
360
380

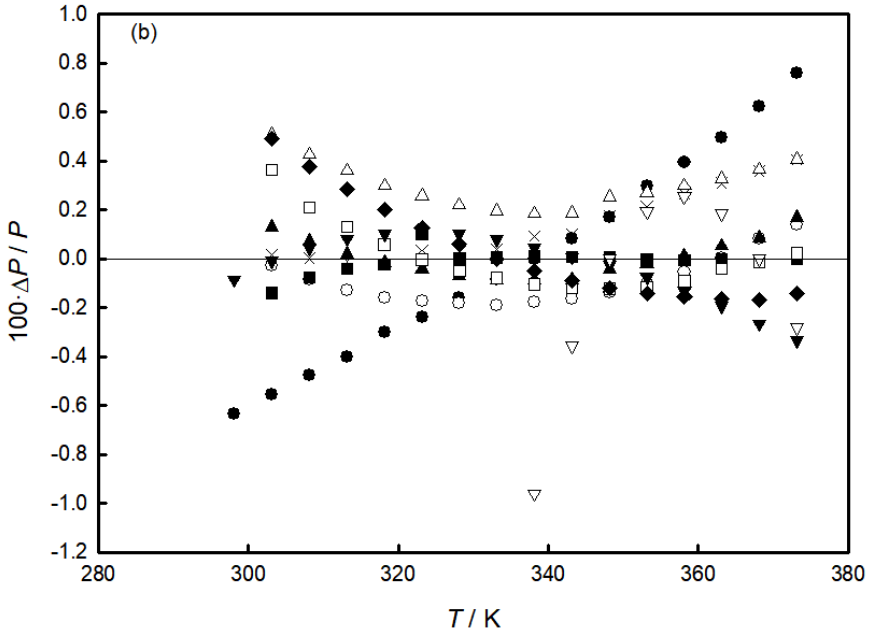
(b)
100·ΔP / P
T / K
1.0
0.8
0.6
0.4
0.2
0.0
-0.2
-0.4
-0.6
-0.8
-1.0
-1.2
280
300
320
340
360
380

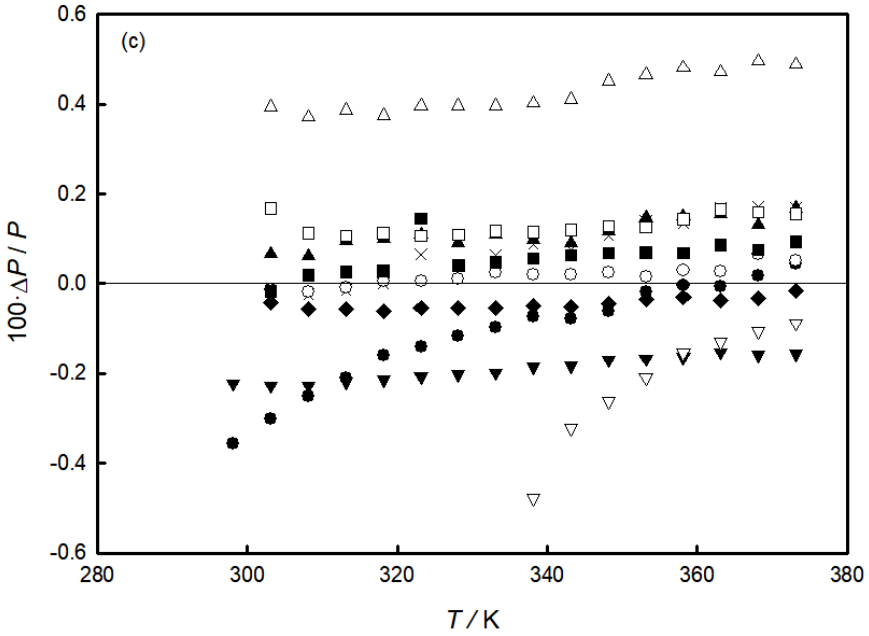

Figure 4.24: Deviations ($\Delta P/P = (P_{exp} - P_{calc})/P_{exp}$) between vapor-phase experimental pressures for the R32 (1) + R1234ze(E) (2) binary systems of Table B.11 (P_{exp}) and values calculated (P_{calc}) with the Peng Robinson EoS (a), the virial EoS (b), and from REFPROP 10.0 (c); ●, $z_1 = 0.1677$ and $v = 0.046522$ m^3 kg^{-1}; ×, $z_1 = 0.2360$ and $v = 0.121732$ m^3 kg^{-1}; ▽, $z_1 = 0.2551$ and $v = 0.013173$ m^3 kg^{-1}; ○, $z_1 = 0.4634$ and $v = 0.068959$ m^3 kg^{-1}; ▲, $z_1 = 0.5374$ and $v = 0.110447$ m^3 kg^{-1}; △, $z_1 = 0.6715$ and $v = 0.115156$ m^3 kg^{-1}; ■, $z_1 = 0.7383$ and $v = 0.039422$ m^3 kg^{-1}; □, $z_1 = 0.7544$ and $v = 0.068225$ m^3 kg^{-1}; ▼, $z_1 = 0.9532$ and $v = 0.043115$ m^3 kg^{-1}; ◆, $z_1 = 0.9533$ and $v = 0.062966$ m^3 kg^{-1}.

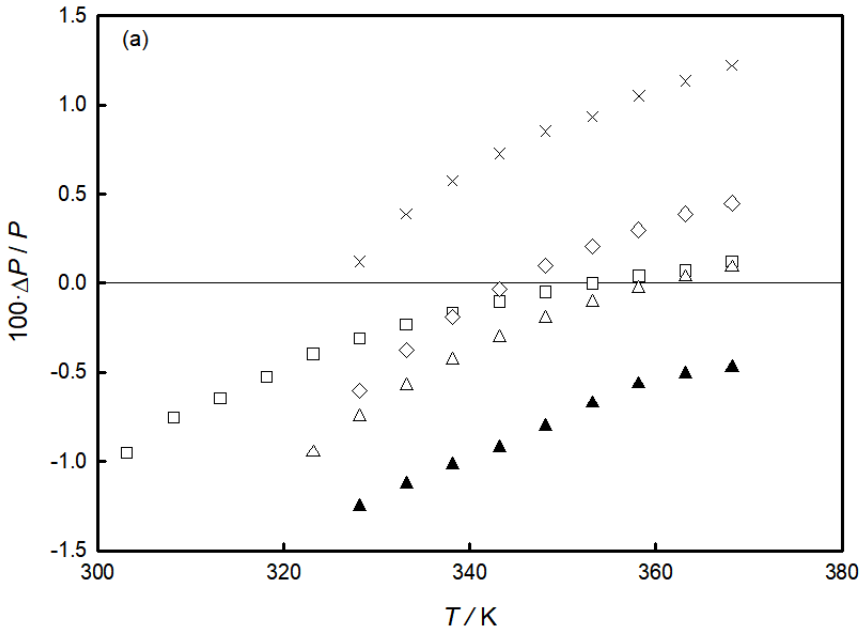
(a)
1.5
1.0
0.5
0.0
-0.5
-1.0
-1.5
100·ΔP / P
300
320
340
360
380
T / K

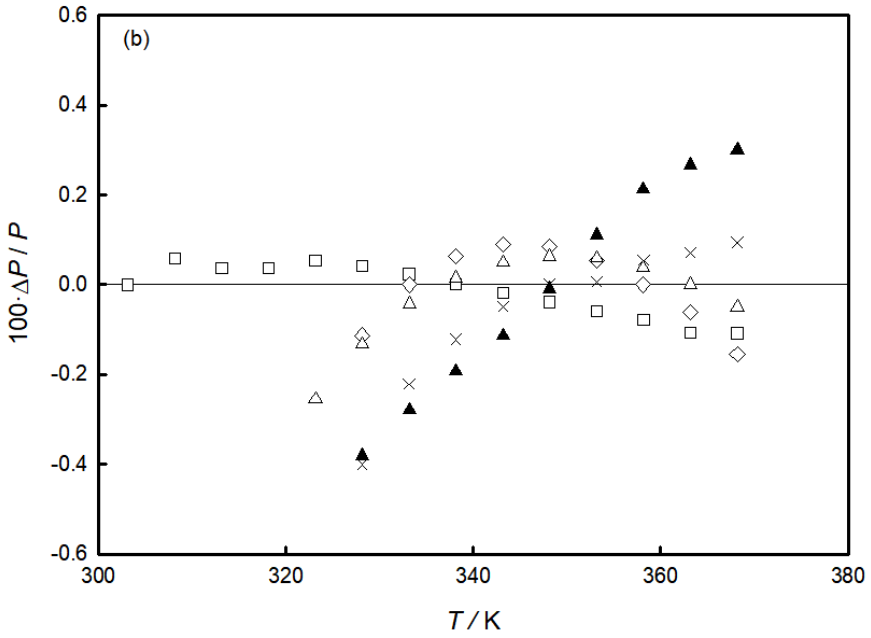
(b)
0.6
0.4
0.2
0.0
-0.2
-0.4
-0.6
100·ΔP / P
300
320
340
360
380
T / K

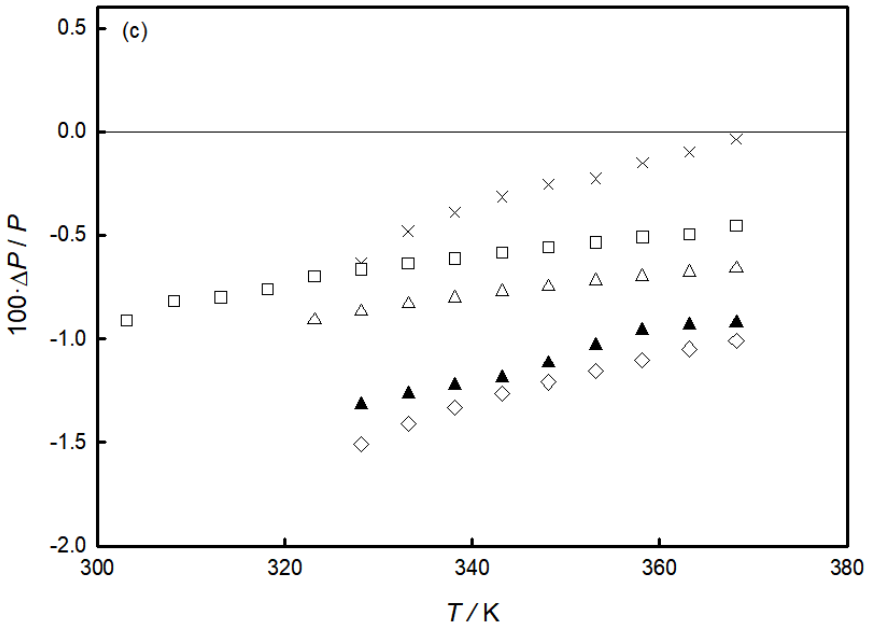

Figure 4.25: Deviations ($\Delta P/P = (P_{exp} - P_{calc})/P_{exp}$) between vapor-phase experimental pressures for the R32 (1) + R1234ze(Z) (2) binary systems of Table B.12 (P_{exp}) and values calculated (P_{calc}) with the Peng Robinson EoS (a), the virial EoS (b), and from REFPROP 10.0 (c); ▲, $z_1 = 0.3620$ and $v = 0.071713$ m^3 kg^{-1}; ×, $z_1 = 0.5232$ and $v = 0.035001$ m^3 kg^{-1}; □, $z_1 = 0.7128$ and $v = 0.070089$ m^3 kg^{-1}; ◇, $z_1 = 0.8015$ and $v = 0.023746$ m^3 kg^{-1}; △, $z_1 = 0.8973$ and $v = 0.026769$ m^3 kg^{-1}.

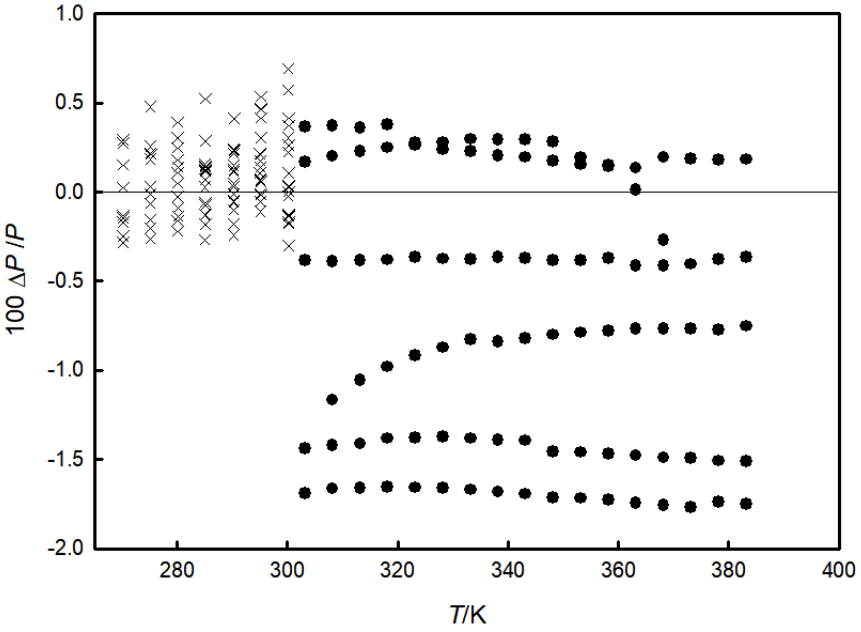

Figure 4.26: Deviations between the vapor-phase pressures (P_{exp}) for R1234yf (1) + R600a (2) binary systems of this work and the open literature and the values calculated (P_{calc}) with the Peng-Robinson EoS coupled with a van der Waals one-fluid linear mixing model with a mean interaction parameter of -0.0599; ●, this work; ×, Zhang et al. [212].

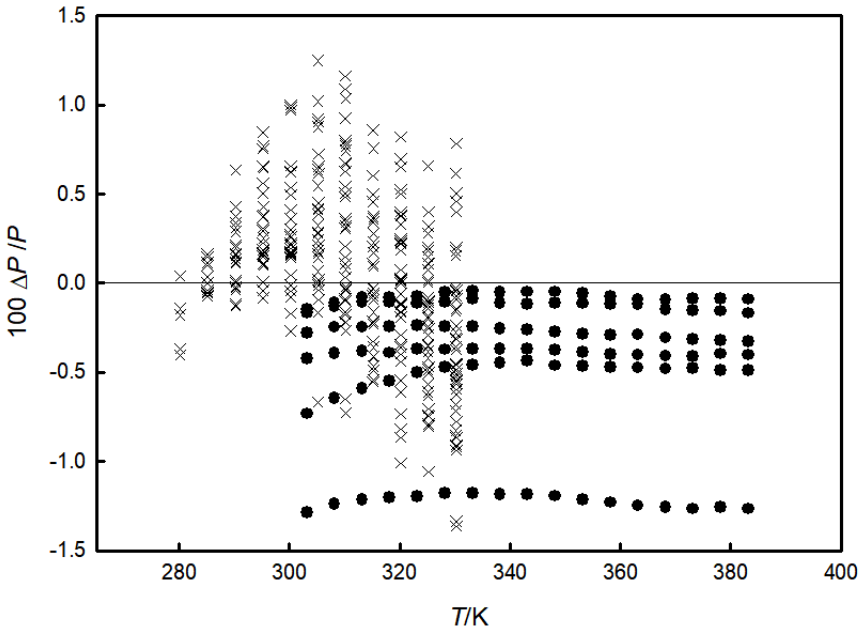

Figure 4.27: Deviations between the vapor-phase pressures (P_{exp}) for R1234ze(E) (1) + R600a (2) binary systems of this work and the open literature and the values calculated (P_{calc}) with the Peng-Robinson EoS coupled with a van der Waals one-fluid linear mixing model with a mean interaction parameter of -0.0974; ●, this work; ×, Cao et al. [223].

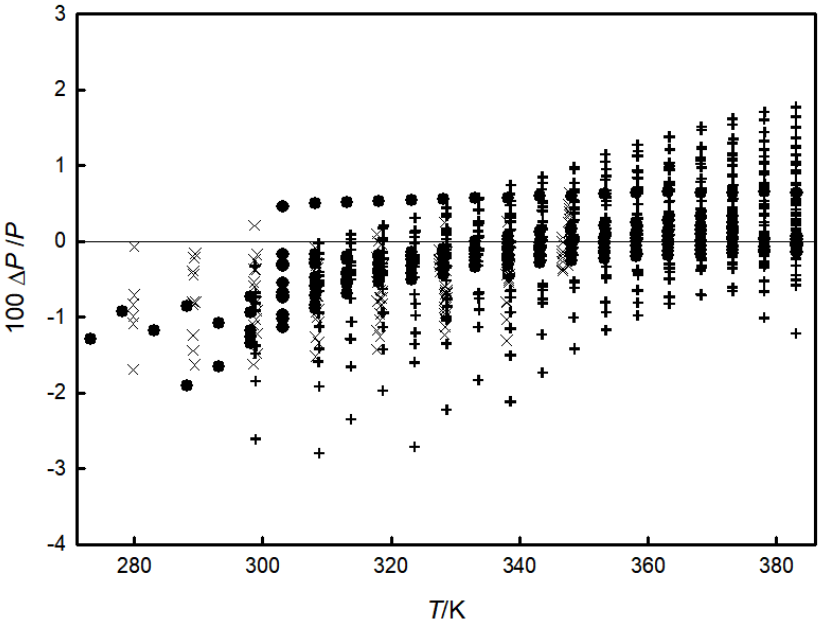

Figure 4.28: Deviations between the vapor-phase pressures (P_{exp}) for R32 (1) + R1234yf (2) pairs of this work and the open literature and the values calculated (P_{calc}) with the Peng-Robinson EoS coupled with a van der Waals one-fluid linear mixing model with a mean interaction parameter of 0.0583; ●, this work; ×, Cai et al. [215]; +, Yang et al. [216].

4.2 Triple points and solid-liquid equilibrium measurements

Triple point data and Solid-Liquid Equilibrium (SLE) data of refrigerants and their blends are fundamental in the refrigerating industry, in particular for very low-temperature applications (i.e., cascade refrigerating units). In fact, these properties define the lowest temperature limit at which these working fluids can be used in a fluid state. In more general terms, the SLE of multicomponent systems of fluids provides useful information for the chemical and petrochemical industries, such as for pipelines design and in the transport of liquid gases in which the formation of solids could lead to safety problems. Moreover, the SLE data generally plays an important role for the comprehensive thermodynamic description of the studied systems. Specifically, these properties are necessary to give the theoretical behavior of the activity coefficients for the studied systems at low temperatures and to develop more accurate models (e.g., equations of state) for the thermodynamic description of the multicomponent systems.

Some of the most well-known and widely used experimental techniques for the triple point temperature measurements of refrigerants are the calorimetry technique [232] and the cooling curve method [233, 234]. The calorimetry technique allows performing accurate static heat capacity measurements of fluids in wide temperature and pressure ranges that can be used to evaluate their triple point temperatures [235]. Instead, the cooling curve method is based on a dynamic technique of measurement that allows measuring the triple point temperature without the visual observation of phase behavior. It is important to note that the accuracy and the reproducibility of this method can be lower than that of other techniques. However, the cooling curve method can be also used to measure the freezing temperatures of refrigerant blends down to very low temperatures. It is also possible to measure the melting temperatures of refrigerant blends with the experimental setups based on this method.

It is worthwhile pointing out that properties for low GWP refrigerants and their blends at low temperatures, such as triple points and SLE, are very scarce in the literature. Recently, experimental data of these properties for some low GWP working fluids were given in studies previously presented by our group of research [236, 237].

The SLE for the R32 + R1234ze(E) binary system measured down to temperatures of 132 K is presented in this thesis. These measurements were performed with an apparatus based on the cooling curve method built to reach temperatures down to about 100 K. The predicted values for the SLE of this binary pair provided by the Schröder equation [143] were compared with the experimental data. Besides, to test the validity of the experimental setup, the triple point temperatures of the components of the binary system and four well-known refrigerants (namely R125, R152a, R143a, and R41) were measured. These experimental data have already been presented elsewhere [238].

4.2.1 Measured samples

Table 4.19 reports information for the following measured samples:

- fluoromethane (R41, CH_3F, CAS number 593-53-3);
- difluoromethane (R32, CH_2F_2, CAS number 75-10-5);
- 1,1-difluoroethane (R152a, $C_2H_4F_2$, CAS number 75-37-6);

Table 4.19: Descriptions of the measured samples.

Chemical Name	Source	Final Mole Fraction Purity	Analysis Method
R41[a]	Lancaster Inc	0.999	GC
R32[b]	Ausimont SpA	0.9998	GC
R152a[c]	Union Carbide	0.9994	GC
R143a[d]	Ausimont SpA	0.999	GC
R1234ze(E)[e]	Honeywell	0.999	GC
R125[f]	Ausimont SpA	0.9996	GC

[a] fluoromethane [b] difluoromethane [c] 1,1-difluoroethane
[d] 1,1,1-trifluoroethane [e] *trans*-1,3,3,3-tetrafluoroprop-1-ene
[f] pentafluoroethane

- 1,1,1-trifluoroethane (R143a, $C_2H_3F_3$, CAS number 420-46-2);
- *trans*-1,3,3,3-tetrafluoroprop-1-ene (R1234ze(E), $CF_3CH = CHF$, CAS number 29118-24-9);
- pentafluoroethane (R125, C_2HF_5, CAS number 354-33-6).

The purity of the samples was measured by GC using a thermal conductivity detector. To remove non-condensable gases from samples, they were subjected to several cycles of freezing, evacuation, thawing, and ultrasonic stirring.

4.2.2 Experimental apparatus and procedure

The apparatus used for the triple point and SLE measurements is based on the cooling curve method. As previously mentioned, this method allows measuring the freezing and melting points with no visual observation of the phase behavior. Figure 4.29 shows the experimental setup. Since details regarding the experimental setup and the testing procedure were given elsewhere [141, 142, 237], only a summary description of the apparatus and procedure is reported below.

The apparatus includes a measuring cell (1) consisting of a stainless-steel cylinder with a volume of approximately 47 cm^3. The body of the cylinder is surrounded by a cover with three holes, which is welded to the cell. To charge the sample in the cell, a stainless-steel tube (4 mm diameter) was inserted through and welded to one of the holes. The remaining two holes, instead, house two T-type thermocouples (2), protected with a 316 stainless steel sheath (1.2 mm diameter). These thermocouples measure the temperature at the center and the boundary of the cell. Before starting the new series of measurements, the calibration of the thermocouples was performed by comparison with a 25 Ω platinum resistance thermometer (model: 5680, SN1083, Hart Scientific) having an uncertainty of 0.0016 K. An absolute pressure transducer (HBM, Mod. P8A) (6) was installed in the charging tube. While the pressures were acquired as described elsewhere [141], a Pico Technology TC-08 thermocouple data logger was used for recording the signals of the T-type thermocouples. Since the recorded vapor pressure values were very low at the studied temperatures, even lower than the declared precision of the instrument, these data were not reported.

To avoid any premature stratification of the components of the studied systems and to ensure homogeneity during the samples liquefaction and crystallization, a stirrer (3) was placed inside the cell. The stirrer is turned by a magnet (4) connected to the shaft of an electric engine (5). The measuring cell is surrounded by a copper coil that exchanges heat with the cell through its contact surface and a working fluid (air or

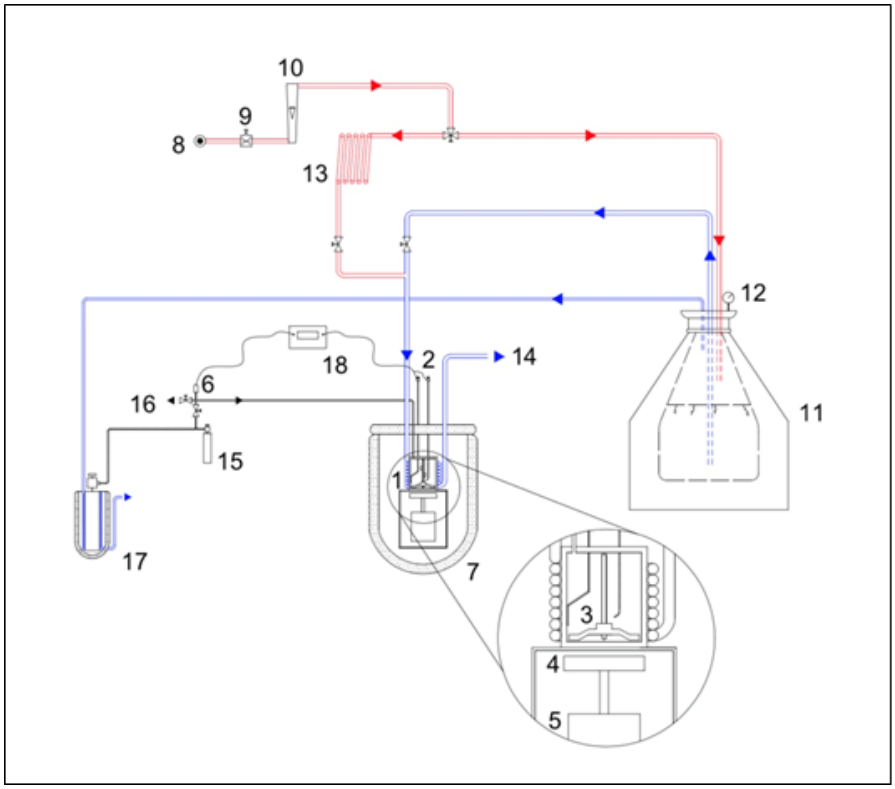

Figure 4.29: Schematic view of the solid-liquid equilibrium apparatus. Notation: 1. measuring cell; 2. Type T thermocouples; 3. stirrer; 4. magnet; 5. electric engine; 6. pressure transducer; 7. Dewar flask; 8. dry air supplier; 9. mass flow controller; 10. rotameter; 11. liquid nitrogen Dewar tank; 12. liquid nitrogen Dewar manometer; 13. external heating coil; 14. nitrogen outlet; 15. charging bottle; 16. vacuum pump system; 17. recovering bottle; 18. acquisition system.

liquid nitrogen). The cell and the copper coil are placed inside a Dewar flask (7). To assure thermal insulation, the whole system is covered with neoprene foam.

The apparatus has two separate circuits: a compressed air circuit and a liquid nitrogen circuit. One end of the compressed air circuit is connected to the dry air supplier (8). A mass flow control (9) was installed downstream of the dry air supplier to adjust the airflow rate, while a rotameter (10) measures the airflow rate. On the other end, the compressed air circuit is connected both to the thermally insulated liquid nitrogen Dewar tank (11) and to an external heating coil (13) that is connected to the copper coil surrounding the measuring cell. The airflow direction is established by opening and closing two valves: one valve installed upstream the liquid nitrogen tank and one valve installed upstream the heating coil. One end of the liquid nitrogen circuit is connected to the liquid nitrogen Dewar tank through a hose including a faucet, while its other end is directly connected to the copper coil.

The two circuits allowed to perform measurements in the cooling and heating operating modes. During the cooling mode, the compressed air passes through several dehumidifier filters and is then delivered to the liquid nitrogen Dewar tank. Since the dry compressed air creates a positive pressure in the tank (controlled by a manometer (12)), the liquid nitrogen begins to flow through a polyvinyl chloride hose. When a steady state is reached, the refrigerant fluid flows through a silicone-made circuit capillary, then moves through the copper coil surrounding the cell and finally flows out from the nitrogen outlet (14). Flowing in the circuit, the liquid nitrogen cools all the circuit surfaces down to temperatures of 100 K and exchanges heat with the measuring cell by evaporation. In this configuration, the valve upstream of the liquid nitrogen tank is open and the valve upstream of the heating coil is closed. During the heating mode, instead, the dry compressed air circuit is directly connected to the heating exchanger and the air, acting as a carrier fluid, flows in the copper coil warming the measuring cell. Therefore, in this case, the valve upstream the liquid nitrogen tank remains closed. The external copper coil can be heated by the operator to accelerate the process.

The charging of the apparatus is the first step carried out during experimental tests and is performed as follows. Firstly, a titanium bottle (15) is charged with the sample. A gravimetrical method is used to identify the charged masses and to determine the composition of the studied sample. In particular, the titanium bottle is weighted on an analytical balance (uncertainty of ± 0.3 mg) during each step of the charging process. Then, the bottle containing the sample, either a pure refrigerant or a system, is connected to the apparatus and a vacuum pump (16) (Vacuumbrand RZ2). The sample is charged inside the measuring system by opening the bottle valve after that a vacuum is created in the apparatus itself. To charge all the fluid contained in the bottle and to insert the whole mass in the cell, the charging bottle remains open and connected to the apparatus during the entire measurement. In this way, only a negligible amount of mass remains in the charging tube and the bottle as the pressure in the cell drops below the atmospheric value.

Once the valve of the charging bottle is open, the cooling phase begins and a cooling curve is drawn in real-time. During the sample solidification, the heat removed by cooling is compensated by the latent heat of the phase change, resulting in a slope modification of the temperature trend in correspondence to the freezing point. After the sample is brought in the solid state, the cooling mode is arrested and the measuring cell is heated through compressed dry air. During the heating period, the sample melting point is identified on the time-temperature curve. When binary systems are tested, the collected freezing and melting temperatures can be plotted versus the composition

to obtain a phase diagram. In particular, the values of freezing and melting points are numerically determined by selecting the first recorded points that showed significant reductions of the cooling/heating rate among the points recorded in proximity of the changes of the slope of the temperature trend.

When the measurement run is over, both the cell and the charging tube are emptied by recovering the sample in another bottle (17), cooled by liquid nitrogen.

4.2.3 Experimental uncertainties

As already explained in Di Nicola et al. [141], the uncertainties of the reported properties were calculated using the law of propagation of uncertainty. In particular, the combined uncertainty of the sample mass charged in the titanium bottle, $u(m)$, was calculated from the following expression:

$$u(m) = \sqrt{n\, m(u_{\mathrm{b}})^2} \tag{4.6}$$

where $u(m_{\mathrm{b}})$ is the uncertainty of the analytical balance (equal to ±0.3 mg) and n is the number of times that the charging bottle is weighted. For a pure refrigerant, n is equal to 2 since the titanium bottle is weighted twice: when it is empty and when it is charged. Instead, n is equal to 4 for the binary systems because, to estimate the masses of the two components, the bottle is weighted four times. Therefore, $u(m)$ are equal to ±0.4 mg and ±0.6 for a pure refrigerant and a binary system, respectively.

The combined uncertainty in mole fraction estimations depends on the mass of binary system charged into the apparatus and on the mole fraction itself. The mole fraction uncertainties for the studied compositions were calculated as follows:

$$u(z_1)^2 = \left(\frac{u(m)}{m}\right)^2 \left[\left(1 + \frac{1}{\alpha}\right)^2 + (1+\alpha)^2\right] \tag{4.7}$$

$$\alpha = \frac{\left(\frac{M_1}{M_2} z_1\right)}{(1 - z_1)} \tag{4.8}$$

where $u(z_1)$ is the combined mole fraction uncertainty of R32, M_1 is the molar mass of R32, M_2 is the molar mass of R1234ze(E), and z_1 is the mole fraction of R32. From this equation, the combined mole fraction uncertainties for the studied compositions of R32 (1) + R1234ze(E) (2) ranged from (±0.0001 to ±0.001).

The uncertainty of the measured temperatures was estimated from the uncertainty of the reference instrument (25 Ω platinum resistance thermometer) of ±0.0016 K, the interpolated standard deviation of ±0.4 K which was established from the data obtained by the calibration procedure, and the accuracy of the Pico Technology TC-08 thermocouple data logger of ±0.8 K at low temperatures. Using the law of propagation of uncertainty, the combined uncertainty for the thermocouples was determined to be ±0.9 K; however, a more conservative value of ±1 K was finally used.

4.2.4 Triple point temperatures

The triple point temperatures (T_{tp}) of the components of the studied binary systems were measured along with different runs. To not interfere with the solidification of the sample [236], the tests were carried out switching off the stirrer at about 40 - 50 K before reaching the temperature at which the T_{tp} is expected. Since the difference

Table 4.20: Triple point temperatures of different pure refrigerants.[a]

Fluid	T_{lit1} K	Ref. of T_{lit1}	T_{lit2} K	T_{tp}^{c} K	T_{tp}^{h} K	T_{tp}^{m} K
R41	129.8	[239]	129.8	129.7	129.6	129.6
R32	136.3	[240]	136	136.3	136.3	136.3
R152a	154.3	[241]	154.3	154.7	155	154.8
R143a	161.3	[241]	161.5	161.3	161.7	161.5
R1234ze(E)	168.6	[64]	169.1	167.5	168.2	167.9
R125	172.5	[240]	172.67	171.7	172.2	171.9

[a] The combined uncertainty of the temperature $u(T)$ is ±1 K

between the temperature measurements achieved in the middle of the cell and along its boundary was found to be very low and always well within the experimental uncertainty, only the values recorded with the thermocouple placed in the center of the cell are reported in this thesis.

To check the functional efficiency and the reliability of the experimental setup, the measurements of T_{tp} for four well-known refrigerants (R41, R152a, R143a, and R125) were performed. Four runs were performed for each pure fluid. Since during the tests none of the studied refrigerants showed a metastable phase (supercooling effect), the reproducibility of the results was considered not dependent on the cooling rate. However, the cooling rate was always monitored during the runs and kept as low as possible (approximately 0.03 $K\,s^{-1}$). Table 4.20 presents the average experimental values of the triple points for the seven pure refrigerants obtained in the cooling mode (T_{tp}^{c}) (freezing point temperatures), in the heating mode (T_{tp}^{h}) (melting point temperatures) and their mean values (T_{tp}^{m}). These results were compared with the experimental data available in literature (T_{lit1}) and the mean values (T_{lit2}) of the data proposed by our research group [237]. In particular, the values of T_{lit2} reported in Table 4.20 are mean values of the data obtained with a platinum resistance thermometer and thermocouples reported in the original paper.

The values of Table 4.20 prove that the results obtained in the cooling mode and the heating mode are mutually consistent. However, the triple point temperatures obtained in the heating mode were generally found to be slightly higher than those obtained in the cooling mode, as also appeared in the work by Skau [242] where it is stated that this phenomenon occurs when crystallization does not take place very rapidly. Moreover, the author pointed out that, since the values of the cooling curves were more dependent on the cooling rate and the purity of the samples, the results from the heating curves were more reproducible and generally more accurate than those from the cooling curves. However, considering that the real triple point temperatures would lie between the heating curve and cooling curve values [242] and that the differences between the heating curve and cooling curve values are always lower than the uncertainty of the measured temperatures, the triple point temperatures presented in this work are taken as the mean of the values obtained in the two measurement modes.

Going into details, R32 (a run is shown in Figure 4.30), R41, R152a showed differences between the two modes always lower than 0.3 K, while R1234ze(E), R125 and R143a showed slightly higher deviations, however always lower than the declared experimental uncertainty of ±1 K.

As shown in Table 4.20, the measured values for the selected refrigerants generally show a consistency with the literature values, both the ones measured through a static calorimetric method [239–241] and the ones previously measured through a dynamic and no-visual method [237].

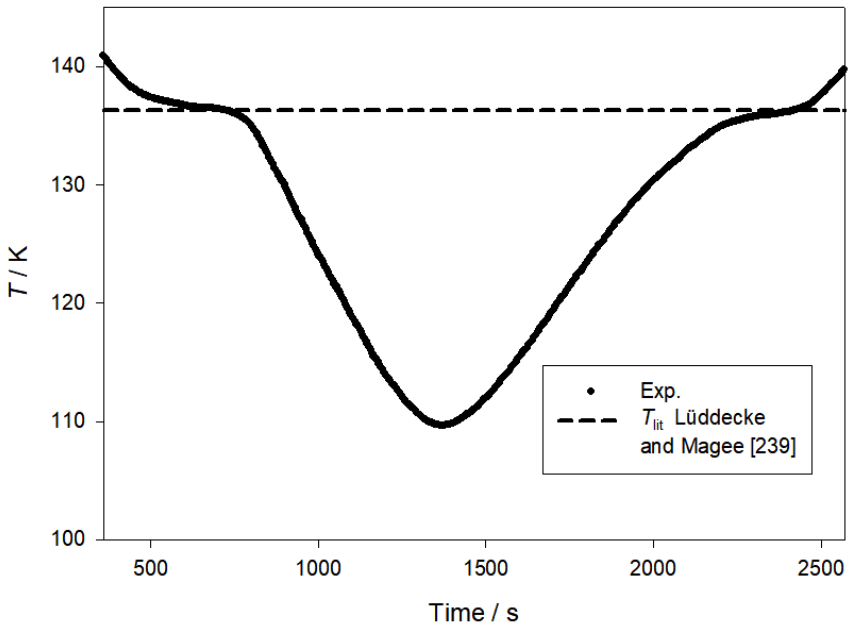

Figure 4.30: An example of measurement for R32.

In particular, the average results achieved for R32, R152a, R143a, and R41 are in very good agreement with data coming from different sources [239–241], while higher differences were found for R1234ze(E) and R125, however always well within the experimental uncertainty. About R1234ze(E), it has to be considered that for this fluid the only literature source available, excluding results reported in Di Nicola et al. [237], was collected from REFPROP [64] and it is not declared if it is an experimental or a calculated value. In fact, from the present measurements, the freezing point temperature of R1234ze(E) seems to appear at a value slightly lower than T_{lit1} (1.1 K in the cooling mode and 0.4 K in the heating mode).

Finally, it can be stated that the results achieved for the pure fluids were found to be reliable since deviations with literature always well within the experimental uncertainties.

4.2.5 SLE measurements for R32 + R1234ze(E)

Several tests on different compositions of R32 + R1234ze(E) were performed, obtaining a sufficient number of temperature values to accurately describe the points where the solid crystals begin to form (*liquidus*) and the points where the system is completely solid (*solidus*) as a function of the composition. As for the pure fluids, the tests were again carried out by switching off the stirrer at a temperature higher than that of phase transition.

It was generally possible to detect clear changes of slope in the temperature trend at the temperatures that represent the *liquidus* and the *solidus* of the system. This aspect is shown in Figure 4.31, where an example of the temperature data acquisitions

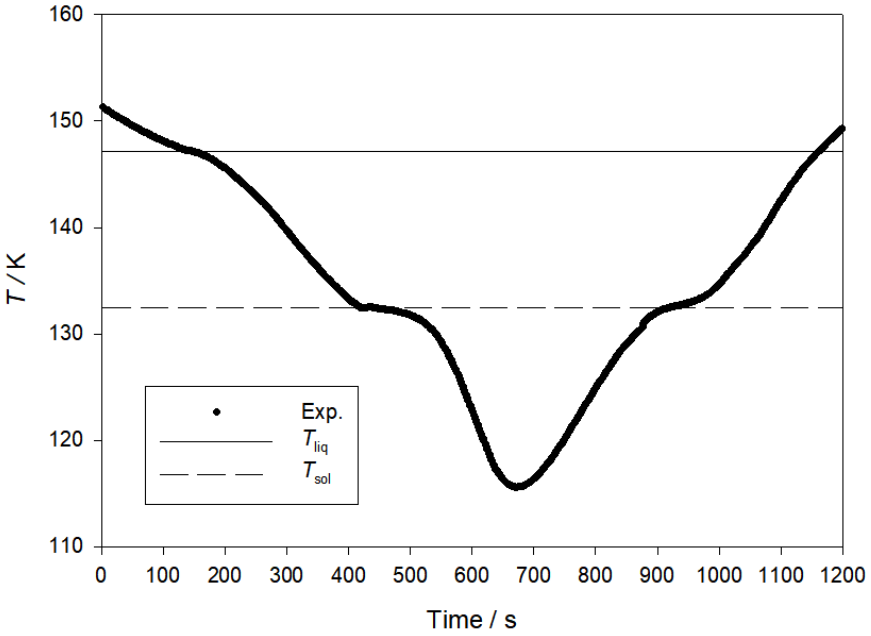

Figure 4.31: An example of measurement for R32 (1) + R1234ze(E) (2) binary system at $z_1 = 0.576$.

as function of the time for R32 + R1234ze(E) is reported. This figure witnesses that it was not always possible to record the solid-liquid transition. In fact, Figure 4.31 does not show a clear change of slope in the temperature trend in the heating mode which represents the melting point. A significant reduction in the heating rate was not detected in this case. This aspect is probably due to a small amount of sample charged.

The temperatures of *liquidus* (T^{c}_{liq}) and *solidus* (T^{c}_{sol}) of R32 + R1234ze(E) measured in the cooling mode for different compositions are reported in Table 4.21. Table 4.22 presents the temperatures of *liquidus* (T^{h}_{liq}) and *solidus* (T^{h}_{sol}) of the binary pair obtained in the heating mode for different compositions. As stated above, the tables confirm that it was not always possible to observe the changes of slope in the temperature trend in the cooling mode or in the heating mode. Figure 4.32 shows the *liquidus* and *solidus* temperatures measured in the two modes as function of the compositions. From these experimental data, it was possible to detect the eutectic point which was estimated at approximately $T = 132.00 \pm 1$ K in the range of mole fractions of R32, z_1, from (0.814 ± 0.001 to 0.819 ± 0.001). In particular, the proposed value of temperature for the eutectic point is in good agreement with the solidus temperatures measured at different compositions, showing deviations well within the experimental uncertainty.

Table 4.21: T - z data for R32 (1) + R1234ze(E) (2) measured in the cooling mode (freezing points).[a]

z_1	T^{c}_{liq} K	T^{c}_{sol} K
0	167.5	-
0.055	165.3	-
0.123	164.6	-
0.181	162.2	-
0.262	160.9	-
0.357	156.5	-
0.456	151	-
0.468	150.2	-
0.576	147.1	132.4
0.692	140.1	132.6
0.697	139.9	132.2
0.758	135.8	132
0.807	132.2	-
0.814	132.3	-
0.819	131.9	-
0.873	133.3	132.2
0.926	133.5	-
0.97	134.8	-
1	136.3	-

[a] The combined uncertainties are: $u(T) = \pm 1$ K and $u(z_1) = \pm 0.001$

Table 4.22: T - z data for R32 (1) + R1234ze(E) (2) measured in the heating mode (melting points).[a]

z_1	T^{h}_{liq} K	T^{h}_{sol} K
0	168.2	-
0.055	165.6	-
0.123	164.7	132
0.181	-	132.6
0.262	160.1	132.8
0.357	-	132.7
0.456	-	131.4
0.468	151.5	-
0.576	-	132.5
0.624	143.3	-
0.692	141.1	132.8
0.697	139.9	132.7
0.758	135.8	132.5
0.807	132.6	-
0.814	132.2	-
0.819	132.1	-
0.873	133.1	-
0.926	133.3	132.4
0.97	-	132.6
1	136.2	-

[a] The combined uncertainties are: $u(T) = \pm 1$ K and $u(z_1) = \pm 0.001$

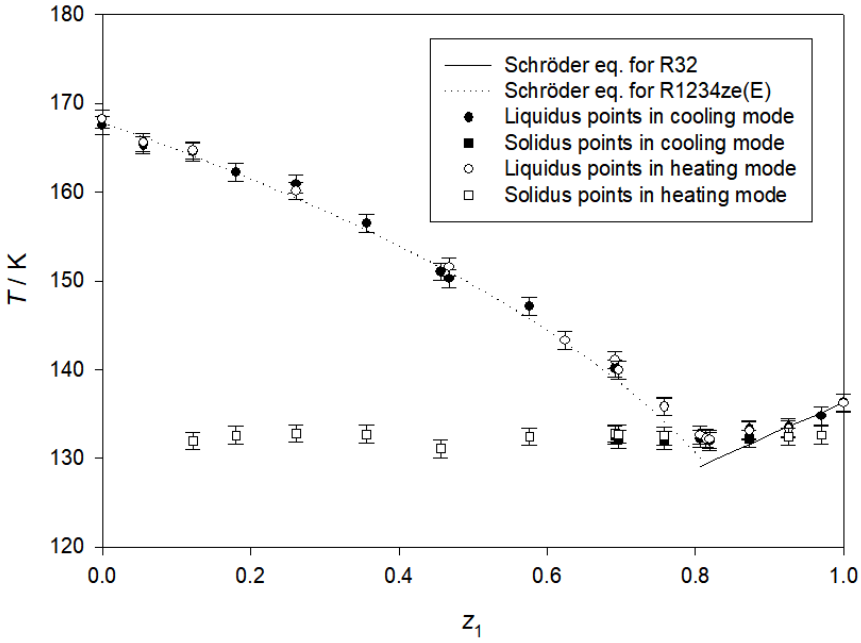

Figure 4.32: SLE for the R32 (1) + R1234ze(E) (2) binary pair.

4.2.6 Discussion of the binary system results

As explained in Subsection 2.4 of Chapter 2, the behavior of the *liquidus* of an organic system with an eutectic and a solid phase formed by pure system components is usually well described by the Schröder equation [143] defined as Equation (2.47).

At first, it can be assumed that the solubility of the solid solute is independent of the solvent. This implies that the activity coefficient of the solute (γ^*) can be set equal to 1. The enthalpies of fusion at the melting point (Δh_{fus}) used for the studied binary pair are equal to 4356 J mol^{-1} [240] and 7890 J mol^{-1} [51] for R32 and R1234ze(E), respectively. It is worthwhile pointing out that Δh_{fus} of R1234ze(E) was not measured, but it was predicted using the method proposed by Chickos et al. [243] and has an uncertainty of 25 % of its value. Instead, the value for R32 is more accurate, since it has been experimentally determined.

The *liquidus* behavior calculated according to the Schröder equation is shown in Figure 4.32. It is possible to note an agreement (generally within 2 - 3 K) between the equation predictions and the experimental results at almost all compositions. Higher deviations (about 4 - 5 K) with respect to the Schröder equation were obtained near the eutectic point ($0.758 < z_1 < 0.873$), confirmed also by a shift in the eutectic concentration. This higher discrepancy between the experimental data and the prediction of the simplified model may be due to the high uncertainty of the predicted Δh_{fus} for R1234ze(E) and to the assumption that $\gamma^* = 1$.

Chapter 5

Conclusions

The purpose of the work presented in this thesis was to theoretically and experimentally investigate the thermophysical properties of low Global Warming Potential (GWP) refrigerants and their blends.

About the theoretical part, the prediction capability of some of the main models for different properties was analyzed for the alternative working fluids. In particular, their vapor pressure and Vapor-Liquid Equilibrium (VLE) were calculated with four two-parameters Cubic Equations of State (CESs), including the original Redlich-Kwong-Soave (RKS) EoS and Peng-Robinson (PR) EoS, a modified PR EOS proposed by Stryjek and a CES proposed by Stryjek. The calculated properties were compared with the experimental data for the studied pure refrigerants and binary systems collected from the literature. In general, the results were generally accurate and confirm the representation ability of the CESs, in spite of their simplicity. For the vapor pressure, even if all the studied models were good, the CES proposed by Stryjek provided the lowest deviations between the experimental and calculated data. About the VLE, all the models provide satisfactory and similar results both when the standard one-binary-parameter mixing rules independent on temperature and the same mixing rules dependent on temperature were used.

Then, the experimental surface tension data of low GWP refrigerants, both pure fluids and blends, were collected and compared with the values calculated from equations available in literature. The studied literature equations were expressly oriented to refrigerants of different generations, but none was specifically designed to predict the surface tension of alternative refrigerants. These equations, mainly oriented to HFCs, showed a good prediction capability for these fluids. Moreover, a simple empirical scaled equation, recently proposed for other organic and inorganic fluids, was considered and tested for those alternative working fluids. The same scaled equation was also considered for binary systems containing low GWP refrigerants and conventional refrigerants. The equation was re-fitted considering the surface tension data for the ethylene derivatives, the propylene derivatives, and the blends, separately. It confirmed its accuracy for the studied working fluids, giving low deviations between the experimental and calculated values.

Successively, an empirical Kardos equation specifically oriented to estimate the thermal conductivities of saturated liquid refrigerants and saturated vapor refrigerants was presented. This scaled equation is very simple and predicted the thermal conductivity with very low deviations for the selected refrigerants, especially for liquids. It is worthwhile pointing out that this equation was not specifically designed to predict

the surface tension of alternative refrigerants. A future step will be the study of the prediction capability of the proposed equation and additional literature models for low GWP refrigerants. Moreover, a new correlation specifically oriented to these fluids could be developed for obtaining more accurate descriptions of the thermal conductivity.

About the experimental study, the following measurements were performed for different compositions using an isochoric apparatus:

- 96 vapor-phase $PvTz$ data for R1234yf + R600a binary pair;
- 102 vapor-phase $PvTz$ data for R1234ze(E) + R600a binary pair;
- 84 vapor-phase $PvTz$ data for R600a + R1233zd(E) binary pair;
- 97 vapor-phase $PvTz$ data for R600a + R1234ze(Z) binary pair;
- 97 vapor-phase $PvTz$ data for R1225ye(Z) + R600a binary pair;
- 66 vapor-phase $PvTz$ data for R1243zf + R600a binary pair;
- 217 two-phase and vapor-phase $PvTz$ data for R32 + R1234yf binary pair;
- 182 two-phase and vapor-phase $PvTz$ data for R32 + R1234ze(E) binary pair;
- 150 two-phase and vapor-phase $PvTz$ data for R32 + R1234ze(Z) binary pair.

The VLE behaviors of R32 + R1234yf, R32 + R1234ze(E), and R32 + R1234ze(Z) binary pairs were derived from the data measured in the two-phase region through the flash method with the Carnahan-Starling-De Santis EoS, the Peng-Robinson EoS and a two-parameter CES proposed by Stryjek. Accurate results were obtained for all the EoSs. A good agreement between the behavior of the calculated VLE and the VLE experimental data collected from the literature was found. The properties of the different binary systems measured in the superheated vapor region were compared with the values estimated from the Peng-Robinson EoS, a truncated virial EoS, and REFPROP 10.0. In general, low deviations between the experimental and calculated values were found, showing good accuracy of these models in the vapor-phase $PvTz$ description.

The Solid-Liquid Equilibrium (SLE) for R32 + R1234ze(E) binary pair, together with the *liquidus* and the *solidus*, were measured down to temperatures of about 132.00 K, using an apparatus that operates both in the cooling and in heating mode. The results obtained from these two configurations were found to be mutually consistent. The deviations between the experimental data and the predictions from the Schröder equation were generally within 2–3 K, confirming that the assumptions made for the model are appropriate. To test the accuracy of the apparatus, the triple point of the two binary system components and four additional well-known refrigerants were measured. The measured triple point temperatures showed consistency with the data available in the literature.

In the next future, the thermophysical properties of additional low GWP refrigerants and their blends for specific applications will be therotically and experimentally investigated. In particular, the $PvTz$ and SLE properties of blends containing R1132a that could be potentially suitable low GWP alternatives for very low temperature applications will be measured with the experimental apparatuses described in this thesis.

Appendix A

Fugacity coefficients calculated from equations of state

The fugacity coefficients (ϕ) of a pure fluid both for vapor and liquid phases calculated from a general two-parameter Cubic Equation of State (CES) have the following expressions:

$$\ln\phi = Z - 1 - \ln\left(Z - B\right) + \frac{A \ln\left[\frac{2\,Z+(u-\Delta)\,B}{2\,Z+(u+\Delta)\,B}\right]}{\Delta\,B} \tag{A.1}$$

$$\ln\phi = Z - 1 - \ln\left(Z - B\right) - \frac{2\,A}{\left(2\,Z + u\,B\right)} \tag{A.2}$$

Equations (A.1) and (A.2) are valid for $\Delta = \left(u^2 - 4w\right)^{0.5} > 0$ and $\Delta = 0$, respectively. In these equations, $Z = P\,v_{\mathrm{m}}\,R^{-1}\,T^{-1}$ is the compressibility factor, $A = a\,P\,R^{-2}\,T^{-2}$ and $B = b\,P\,R^{-1}\,T^{-1}$ are parameters of CESs, a is the attraction parameter of CESs, b is the repulsive parameter of CESs, called covolume, u and w are two constants that define a specific two-parameter CES, R is the universal gas constant, P is the pressure, v_{m} is the molar volume and T is the temperature.

The fugacity coefficients (ϕ) of a component i in a homogeneous blend both for vapor and liquid phases calculated from a general two-parameter CES by using the van der Waals one-fluid mixing rules have following expressions:

$$\begin{aligned}\ln\phi_i = \frac{b_i}{b}\left(Z - 1\right) - \ln\left(Z - B\right)\\ + \frac{A}{\Delta\,B}\left(\frac{2\sum_{j=1}^{n}\bar{z}_j\,a_{ij}}{a} - \frac{b_i}{b}\right)\ln\left[\frac{2\,Z + (u+\Delta)\,B}{2\,Z + (u-\Delta)\,B}\right]\end{aligned} \tag{A.3}$$

$$\ln\phi_i = \frac{b_i}{b}\left(Z - 1\right) - \ln\left(Z - B\right) - \frac{2\,A}{\left(2\,Z + u\,B\right)}\left(\frac{2\sum_{j=1}^{n}\bar{z}_j\,a_{ij}}{a} - \frac{b_i}{b}\right) \tag{A.4}$$

Equations (A.3) and (A.4) are valid for $\Delta > 0$ and $\Delta = 0$, respectively. In the equations, $\bar{z}_{\mathrm{j}}$ represents both the mole fractions of the liquid phase (x_{j}) and vapor phase (y_{j}) for the j-th component of the blend.

The fugacity coefficients (ϕ) of a component i in a homogeneous blend both for vapor and liquid phases calculated from the Carnahan-Starling-De Santis (CSD) EoS [110] by using the van der Waals one-fluid mixing rules have following expressions:

$$\begin{aligned}\ln \phi_i = \frac{4\,\eta - 3\,\eta^2}{(1-\eta)^2} + \frac{b_i\left(4\,\eta - 2\,\eta^2\right)}{b\,(1-\eta)^3} + \frac{2}{R\,T\,b}\sum_{j=1}^{n} \bar{z}_j\, a_{ji} \ln \frac{v_\mathrm{m}}{v_\mathrm{m}+b} \\ + \frac{b_i\, a}{R\,T\,b^2} \ln \frac{v_\mathrm{m}+b}{v_\mathrm{m}} - \frac{b_i\, a}{R\,T\left(b\,v_\mathrm{m}+b^2\right)} - \ln Z\end{aligned} \tag{A.5}$$

where $\eta = b\,(4 v_\mathrm{m})^{-1}$

Appendix B

Experimental isochoric *PvTz* data of binary systems

The experimental $PvTz$ data for R32 + R1234yf, R32 + R1234ze(E), and R32 + R1234ze(Z) measured in the two-phase region through the isochoric apparatus described in Section 4.1 of Chapter 4 are reported in Tables B.1, B.2, and B.3, respectively. Instead, Tables B.4, B.5, B.6, B.7, B.8, B.9, B.10, B.11, and B.12 present the vapor-phase experimental data for R1234yf + R600a, R1234ze(E) + R600a, R600a + R1233zd(E), R600a + R1234ze(Z), R1225ye(Z) + R600a, R1243zf + R600a, R32 + R1234yf, R32 + R1234ze(E), and R32 + R1234ze(Z) binary pairs, respectively.

Table B.1: Experimental values of pressure (P), specific volume (v), temperature (T), and bulk mole fraction (z) in the two-phase region for R32 (1) + R1234yf (2) binary systems.[a]

T	P	v	T	P	v
K	kPa	$m^3\,kg^{-1}$	K	kPa	$m^3\,kg^{-1}$
$z_1 = 0.1330$			$z_1 = 0.6489$		
263.15	248.8	0.064	263.15	480.9	0.03
268.15	294.5	0.064	268.15	558.4	0.03
			273.15	644.3	0.03
			278.15	739.4	0.03
			283.15	828.7	0.03
$z_1 = 0.1792$			$z_1 = 0.8122$		
263.15	285	0.03	263.15	537.4	0.032
268.15	333.9	0.03	268.15	632.3	0.032
273.15	389	0.03	273.15	736.8	0.032
278.15	451.3	0.03	278.15	851.5	0.032
283.15	520.6	0.03			
288.15	596.1	0.03			
$z_1 = 0.5229$					
263.15	426.1	0.031			
268.15	491.8	0.031			
273.15	564.9	0.031			
278.15	645	0.031			
283.15	732.2	0.031			

[a] Expanded uncertainties are $U(T) = 0.03$ K and $U(P) = 1$ kPa, $U(v) = (0.000034$ to $0.000753)$ $m^3\,kg^{-1}$, and $U(z) = (0.0004$ to $0.0046)$ at the 95 % confidence level.

Table B.2: Experimental values of pressure (P), specific volume (v), temperature (T), and bulk mole fraction (z) in the two-phase region for R32 (1) + R1234ze(E) (2) binary systems.[a]

T / K	P / kPa	v / $m^3\,kg^{-1}$	T / K	P / kPa	v / $m^3\,kg^{-1}$
$z_1 = 0.1677$			$z_1 = 0.7383$		
263.15	190.9	0.046409	263.15	432.1	0.039327
268.15	226.2	0.04642	268.15	496	0.039336
273.15	266.8	0.04643	273.15	569.4	0.039344
278.15	312.6	0.04644	278.15	645.1	0.039353
283.15[b]	360.0[b]	0.046450[b]	283.15[b]	696.3[b]	0.039362[b]
288.15[b]	410.8[b]	0.046460[b]			
$z_1 = 0.2551$			$z_1 = 0.9532$		
263.15	256.7	0.013142	263.15	552.2	0.043011
268.15	302.5	0.013144	268.15	649.5	0.04302
273.15	354.1	0.013147	273.15	753.6	0.04303
278.15	412	0.01315			
283.15	476.6	0.013153			
288.15	548.2	0.013156			
293.15	628	0.013159			
298.15	715.9	0.013162			
303.15	811.8	0.013165			
308.15	914.8	0.013168			
313.15	1033.8	0.01317			
318.15	1157.7	0.013173			
323.15	1294.9	0.013176			
328.15[b]	1426.2[b]	0.013179[b]			

[a] Expanded uncertainties are $U(T) = 0.03$ K and $U(P) = 1$ kPa, $U(v) = (0.000015$ to $0.000186)$ $m^3\,kg^{-1}$, and $U(z) = (0.0004$ to $0.0044)$ at the 95 % confidence level.

[b] Not considered in the regression.

Table B.3: Experimental values of pressure (P), specific volume (v), temperature (T), and bulk mole fraction (z) in the two-phase region for R32 (1) + R1234ze(Z) (2) binary systems.[a]

T / K	P / kPa	v / $m^3\,kg^{-1}$	T / K	P / kPa	v / $m^3\,kg^{-1}$
$z_1 = 0.0871$			$z_1 = 0.7128$		
263.15	79.5	0.013326	263.15	264.9	0.069920
268.15	94.9	0.013329	268.15	290.7	0.069935
273.15	112.8	0.013332	273.15	317.1	0.069951
278.15	133.2	0.013335	278.15	345.7	0.069966
283.15	156.4	0.013338	283.15	378.2	0.069981
288.15	182.6	0.013341	288.15	410.9	0.069997
293.15	212.1	0.013344	293.15	445.7	0.070012
298.15	245.5	0.013346			
303.15	283.5	0.013349			
308.15	326.0	0.013352			
313.15	373.6	0.013355			
318.15	425.9	0.013358			
323.15	483.6	0.013361			
328.15	547.7	0.013364			
333.15	618.2	0.013367			
338.15	696.4	0.013370			
343.15	781.3	0.013373			
348.15	875.0	0.013376			
353.15	976.6	0.013379			
$z_1 = 0.2980$			$z_1 = 0.8015$		
263.15	170.4	0.016332	268.15	498.2	0.023692
268.15	197.5	0.016336	273.15	568.3	0.023697
273.15	227.1	0.016340	278.15	645.0	0.023702
278.15	259.9	0.016343	283.15	724.6	0.023707
283.15	295.5	0.016347	288.15	807.4	0.023712
288.15	334.6	0.016350	293.15	892.7	0.023718
293.15	376.9	0.016354	298.15	978.1	0.023723
298.15	422.9	0.016357	303.15	1065.5	0.023728
303.15	472.8	0.016361	308.15	1153.6	0.023733
308.15	527.4	0.016365	313.15	1240.7	0.023739
313.15	585.3	0.016368	318.15	1333.9	0.023744
318.15	648.6	0.016372			
323.15	717.2	0.016375			
328.15	793.6	0.016379			
333.15	874.9	0.016383			
338.15	961.2	0.016386			
343.15	1057.3	0.016390			
348.15	1162.0	0.016393			
353.15	1270.8	0.016397			
$z_1 = 0.3620$			$z_1 = 0.8973$		
263.15	123.8	0.071540	268.15	579.9	0.026708

Continues to the following page

Continues from the previous page

T / K	P / kPa	v / $m^3\,kg^{-1}$	T / K	P / kPa	v / $m^3\,kg^{-1}$
268.15	140.3	0.071556	273.15	663.8	0.026714
273.15	158.3	0.071571	278.15	754.6	0.026719
278.15	179.1	0.071587	283.15	851.7	0.026725
283.15	202.0	0.071603	288.15	949.7	0.026731
288.15	227.7	0.071619	293.15	1046.9	0.026737
293.15	256.6	0.071634	298.15	1145.0	0.026743
298.15	289.0	0.071650	303.15	1236.5	0.026749
303.15	325.5	0.071666			
$z_1 = 0.5232$					
268.15	276.8	0.034920			
273.15	307.3	0.034936			
278.15	340.2	0.034936			
283.15	375.8	0.034943			
288.15	414.6	0.034951			
293.15	456.4	0.034959			
298.15	502.4	0.034966			
303.15	552.2	0.034974			
308.15	607.6	0.034982			
313.15	666.1	0.034989			
318.15	722.2	0.034997			

[a] Expanded uncertainties are $U(T) = 0.03$ K and $U(P) = 1$ kPa, $U(v) = (0.000015$ to $0.000091)$ $m^3\,kg^{-1}$, and $U(z) = (0.0005$ to $0.0016)$ at the 95 % confidence level.

Table B.4: Experimental values of pressure (P), specific volume (v), temperature (T), and bulk mole fraction (z) in the vapor-phase region for R1234yf (1) + R600a (2) binary systems.[a]

T	P	v	T	P	v
K	kPa	$m^3\,kg^{-1}$	K	kPa	$m^3\,kg^{-1}$
$z_2 = 0.2340$			$z_2 = 0.6061$		
303.15	246.7	0.093939	303.15	180.2	0.166345
308.15	251.2	0.093960	308.15	183.3	0.166381
313.15	255.6	0.093981	313.15	186.5	0.166418
318.15	260.1	0.094001	318.15	189.7	0.166454
323.15	264.6	0.094022	323.15	192.9	0.166491
328.15	269.0	0.094042	328.15	196.0	0.166527
333.15	273.4	0.094063	333.15	199.2	0.166564
338.15	277.8	0.094084	338.15	202.3	0.166600
343.15	282.2	0.094104	343.15	205.5	0.166637
348.15	286.6	0.094125	348.15	208.6	0.166673
353.15	291.0	0.094145	353.15	211.8	0.166710
358.15	295.4	0.094166	358.15	214.9	0.166746
363.15	299.8	0.094187	363.15	218.0	0.166783
368.15	304.1	0.094207	368.15	221.1	0.166819
373.15	308.5	0.094228	373.15	224.3	0.166856
378.15	313.0	0.094248	378.15	227.5	0.166892
383.15	317.4	0.094269	383.15	230.6	0.166929
$z_2 = 0.4005$			$z_2 = 0.7720$		
303.15	269.3	0.094227	303.15	260.6	0.127859
308.15	274.3	0.094248	308.15	265.4	0.127887
313.15	279.2	0.094268	313.15	270.2	0.127915
318.15	284.2	0.094289	318.15	275.1	0.127943
323.15	289.2	0.094310	323.15	279.9	0.127971
328.15	294.1	0.094330	328.15	284.6	0.127999
333.15	299.0	0.094351	333.15	289.4	0.128027
338.15	303.9	0.094372	338.15	294.2	0.128055
343.15	308.8	0.094392	343.15	298.9	0.128083
348.15	313.5	0.094413	348.15	303.6	0.128111
353.15	318.3	0.094434	353.15	308.1	0.128139
358.15	323.2	0.094455	358.15	312.6	0.128167
363.15	328.1	0.094475			
368.15	332.9	0.094496			
373.15	337.7	0.094517			
378.15	342.6	0.094537			
383.15	347.4	0.094558			
$z_2 = 0.4723$			$z_2 = 0.8504$		
303.15	163.5	0.169844	308.15	426.8	0.079675
308.15	166.4	0.169881	313.15	435.6	0.079693
313.15	169.2	0.169918	318.15	444.2	0.079710
318.15	172.1	0.169956	323.15	452.8	0.079728
323.15	174.7	0.169993	328.15	461.2	0.079745

Continues to the following page

Continues from the previous page

T / K	P / kPa	v / $m^3\,kg^{-1}$	T / K	P / kPa	v / $m^3\,kg^{-1}$
328.15	177.5	0.170030	333.15	469.7	0.079763
333.15	180.3	0.170067	338.15	477.9	0.079780
338.15	183.1	0.170105	343.15	486.3	0.079798
343.15	185.9	0.170142	348.15	494.6	0.079815
348.15	188.7	0.170179	353.15	502.9	0.079833
353.15	191.5	0.170216	358.15	511.2	0.079850
358.15	194.3	0.170254	363.15	519.5	0.079868
363.15	197.1	0.170291	368.15	527.7	0.079885
368.15	200.1	0.170328	373.15	535.9	0.079903
373.15	202.9	0.170366	378.15	544.1	0.079920
378.15	205.7	0.170403	383.15	552.4	0.079937
383.15	208.5	0.170440			

[a] Expanded uncertainties are $U(T) = 0.03$ K and $U(P) = 1$ kPa, $U(v) = (0.000097$ to $0.000266)$ $m^3\,kg^{-1}$, and $U(z) = (0.0011$ to $0.0023)$ at the 95 % confidence level.

Table B.5: Experimental values of pressure (P), specific volume (v), temperature (T), and bulk mole fraction (z) in the vapor-phase region for R1234ze(E) (1) + R600a (2) binary systems.[a]

T	P	v	T	P	v
K	kPa	$m^3\,kg^{-1}$	K	kPa	$m^3\,kg^{-1}$
$z_2 = 0.2899$			$z_2 = 0.6124$		
303.15	267.9	0.089524	303.15	321.0	0.089015
308.15	273.0	0.089544	308.15	327.2	0.089034
313.15	277.9	0.089564	313.15	333.4	0.089054
318.15	282.8	0.089583	318.15	339.5	0.089073
323.15	287.8	0.089603	323.15	345.6	0.089093
328.15	292.7	0.089622	328.15	351.7	0.089112
333.15	297.6	0.089642	333.15	357.8	0.089132
338.15	302.5	0.089662	338.15	363.8	0.089151
343.15	307.4	0.089681	343.15	369.8	0.089171
348.15	312.2	0.089701	348.15	375.8	0.089191
353.15	317.1	0.089721	353.15	381.8	0.089210
358.15	321.9	0.08974	358.15	387.8	0.089230
363.15	326.8	0.08976	363.15	393.7	0.089249
368.15	331.6	0.08978	368.15	399.7	0.089269
373.15	336.5	0.089799	373.15	405.6	0.089288
378.15	341.4	0.089819	378.15	411.7	0.089308
383.15	346.2	0.089838	383.15	417.6	0.089327
$z_2 = 0.4275$			$z_2 = 0.6851$		
303.15	305.5	0.084403	303.15	304.9	0.100418
308.15	311.3	0.084422	308.15	310.7	0.100440
313.15	317.1	0.084440	313.15	316.5	0.100462
318.15	322.8	0.084459	318.15	322.2	0.100484
323.15	328.5	0.084478	323.15	328.0	0.100506
328.15	334.2	0.084496	328.15	333.7	0.100529
333.15	339.9	0.084515	333.15	339.5	0.100551
338.15	345.6	0.084533	338.15	345.1	0.100573
343.15	351.2	0.084552	343.15	350.8	0.100595
348.15	356.9	0.084570	348.15	356.5	0.100617
353.15	362.6	0.084589	353.15	362.1	0.100639
358.15	368.2	0.084607	358.15	367.7	0.100661
363.15	373.9	0.084626	363.15	373.3	0.100683
368.15	379.5	0.084644	368.15	379.0	0.100705
373.15	385.1	0.084663	373.15	384.7	0.100727
378.15	390.7	0.084681	378.15	390.3	0.100749
383.15	396.3	0.084700	383.15	395.9	0.100771
$z_2 = 0.5156$			$z_2 = 0.7551$		
303.15	259.6	0.106188	303.15	367.4	0.085615
308.15	264.5	0.106211	308.15	374.9	0.085634
313.15	269.2	0.106234	313.15	382.2	0.085653
318.15	274.0	0.106258	318.15	389.5	0.085672
323.15	278.8	0.106281	323.15	396.8	0.085690

Continues to the following page

Continues from the previous page

T K	P kPa	v $m^3\,kg^{-1}$	T K	P kPa	v $m^3\,kg^{-1}$
328.15	283.5	0.106304	328.15	404.0	0.085709
333.15	288.2	0.106328	333.15	411.2	0.085728
338.15	292.9	0.106351	338.15	418.3	0.085747
343.15	297.6	0.106374	343.15	425.4	0.085765
348.15	302.3	0.106397	348.15	432.4	0.085784
353.15	307.0	0.106421	353.15	439.4	0.085803
358.15	311.7	0.106444	358.15	446.5	0.085822
363.15	316.4	0.106467	363.15	453.5	0.085841
368.15	321.1	0.106491	368.15	460.5	0.085859
373.15	325.7	0.106514	373.15	467.6	0.085878
378.15	330.4	0.106537	378.15	474.5	0.085897
383.15	335.1	0.106561	383.15	481.6	0.085916

[a] Expanded uncertainties are $U(T) = 0.03$ K and $U(P) = 1$ kPa, $U(v) = (0.000104$ to $0.000138)$ $m^3\,kg^{-1}$, and $U(z) = (0.0009$ to $0.0018)$ at the 95 % confidence level.

Table B.6: Experimental values of pressure (P), specific volume (v), temperature (T), and bulk mole fraction (z) in the vapor-phase region for R600a (1) + R1233zd(E) (2) binary systems.[a]

T / K	P / kPa	v / $m^3\,kg^{-1}$	T / K	P / kPa	v / $m^3\,kg^{-1}$
$z_1 = 0.1245$			$z_1 = 0.6438$		
303.15	113.3	0.174045	338.15	576.1	0.049897
308.15	115.4	0.174083	343.15	587.5	0.049908
313.15	117.5	0.174121	348.15	598.7	0.049919
318.15	119.6	0.174159	353.15	609.8	0.049930
323.15	121.8	0.174198	358.15	620.8	0.049941
328.15	123.8	0.174236	363.15	631.1	0.049952
333.15	125.8	0.174274	368.15	642.6	0.049963
338.15	128.2	0.174312	373.15	653.2	0.049974
343.15	130.2	0.174350	378.15	664.1	0.049985
348.15	132.2	0.174389	383.15	675.0	0.049996
353.15	134.4	0.174427			
358.15	136.3	0.174465			
363.15	138.3	0.174503			
368.15	140.4	0.174541			
373.15	142.3	0.174579			
378.15	144.4	0.174618			
383.15	146.5	0.174656			
$z_1 = 0.4527$			$z_1 = 0.7460$		
313.15	197.4	0.126136	318.15	340.9	0.092565
318.15	200.9	0.126163	323.15	347.6	0.092586
323.15	204.5	0.126191	328.15	353.9	0.092606
328.15	208.0	0.126219	333.15	360.6	0.092626
333.15	211.4	0.126246	338.15	366.9	0.092646
338.15	214.9	0.126274	343.15	373.2	0.092667
343.15	218.5	0.126302	348.15	379.5	0.092687
348.15	222.0	0.126329	353.15	385.8	0.092707
353.15	225.5	0.126357	358.15	391.8	0.092728
358.15	229.0	0.126385	363.15	398.1	0.092748
363.15	232.1	0.126412	368.15	404.2	0.092768
368.15	235.6	0.126440	373.15	410.7	0.092788
373.15	239.1	0.126468	378.15	416.9	0.092809
378.15	242.6	0.126495	383.15	423.2	0.092829
383.15	246.4	0.126523			
$z_1 = 0.5638$			$z_1 = 0.8647$		
303.15	186.5	0.142890	333.15	648.1	0.053528
308.15	190.1	0.142921	338.15	661.4	0.053540
313.15	193.7	0.142953	343.15	674.5	0.053552
318.15	197.5	0.142984	348.15	687.5	0.053563
323.15	200.9	0.143016	353.15	700.5	0.053575
328.15	204.3	0.143047	358.15	713.3	0.053587
333.15	207.8	0.143078	363.15	726.1	0.053599

Continues to the following page

Continues from the previous page

T K	P kPa	v $m^3\,kg^{-1}$	T K	P kPa	v $m^3\,kg^{-1}$
338.15	211.1	0.143110	368.15	738.7	0.053610
343.15	214.6	0.143141	373.15	751.4	0.053622
348.15	218.0	0.143172	378.15	763.9	0.053634
353.15	221.4	0.143204	383.15	776.5	0.053646
358.15	224.6	0.143235			
363.15	228.1	0.143266			
368.15	231.5	0.143298			
373.15	234.8	0.143329			
378.15	238.2	0.143360			
383.15	241.7	0.143392			

[a] Expanded uncertainties are $U(T) = 0.03$ K and $U(P) = 1$ kPa, $U(v) = (0.000057$ to $0.000276)$ $m^3\,kg^{-1}$, and $U(z) = (0.0005$ to $0.0096)$ at the 95 % confidence level.

Table B.7: Experimental values of pressure (P), specific volume (v), temperature (T), and bulk mole fraction (z) in the vapor-phase region for R600a (1) + R1234ze(Z) (2) binary systems.[a]

T	P	v	T	P	v
K	kPa	$m^3\,kg^{-1}$	K	kPa	$m^3\,kg^{-1}$
$z_1 = 0.1176$			$z_1 = 0.5095$		
303.15	145.9	0.152016	303.15	213.5	0.128568
308.15	148.7	0.152050	308.15	217.4	0.128596
313.15	151.4	0.152083	313.15	221.3	0.128624
318.15	154.0	0.152116	318.15	225.2	0.128652
323.15	156.8	0.152150	323.15	229.2	0.128680
328.15	159.4	0.152183	328.15	233.1	0.128709
333.15	162.0	0.152216	333.15	237.0	0.128737
338.15	164.6	0.152250	338.15	240.9	0.128765
343.15	167.2	0.152283	343.15	244.7	0.128793
348.15	169.8	0.152316	348.15	248.6	0.128821
353.15	172.5	0.152350	353.15	252.4	0.128850
358.15	175.1	0.152383	358.15	256.3	0.128878
363.15	177.7	0.152416	363.15	260.1	0.128906
368.15	180.3	0.152450	368.15	263.9	0.128934
373.15	182.9	0.152483	373.15	267.8	0.128962
378.15	185.5	0.152516	378.15	271.7	0.128991
383.15	188.1	0.152550	383.15	275.5	0.129019
$z_1 = 0.2220$			$z_1 = 0.6585$		
303.15	155.7	0.151411	313.15	398.1	0.075736
308.15	158.6	0.151444	318.15	406.6	0.075753
313.15	161.5	0.151477	323.15	414.5	0.075770
318.15	164.3	0.151510	328.15	423.1	0.075786
323.15	167.2	0.151544	333.15	430.7	0.075803
328.15	170.0	0.151577	338.15	438.4	0.075820
333.15	172.7	0.151610	343.15	446.0	0.075836
338.15	175.4	0.151643	348.15	453.6	0.075853
343.15	178.2	0.151676	353.15	461.2	0.075869
348.15	180.8	0.151710	358.15	468.5	0.075886
353.15	183.7	0.151743	363.15	476.0	0.075903
358.15	186.5	0.151776	368.15	483.4	0.075919
363.15	189.4	0.151809	373.15	490.9	0.075936
368.15	192.1	0.151843	378.15	498.2	0.075952
373.15	194.9	0.151876	383.15	505.8	0.075969
378.15	197.7	0.151909			
383.15	200.5	0.151942			
$z_1 = 0.4271$			$z_1 = 0.7250$		
303.15	206.5	0.126999	318.15	362.3	0.090609
308.15	210.5	0.127027	323.15	369.1	0.090628
313.15	214.4	0.127054	328.15	375.8	0.090648
318.15	218.3	0.127082	333.15	382.5	0.090668
323.15	222.2	0.127110	338.15	389.1	0.090688

Continues to the following page

Continues from the previous page

T K	P kPa	v $m^3\,kg^{-1}$	T K	P kPa	v $m^3\,kg^{-1}$
328.15	226.0	0.127138	343.15	395.8	0.090708
333.15	229.8	0.127166	348.15	402.5	0.090728
338.15	233.6	0.127194	353.15	409.1	0.090748
343.15	237.3	0.127222	358.15	415.6	0.090767
348.15	241.1	0.127249	363.15	422.1	0.090787
353.15	244.7	0.127277	368.15	428.6	0.090807
358.15	248.6	0.127305	373.15	435.2	0.090827
363.15	252.3	0.127333	378.15	441.7	0.090847
368.15	256.0	0.127361	383.15	448.3	0.090867
373.15	259.8	0.127389			
378.15	263.6	0.127417			
383.15	267.4	0.127445			

[a] Expanded uncertainties are $U(T) = 0.03$ K and $U(P) = 1$ kPa, $U(v) = (0.000091$ to $0.000225)$ $m^3\,kg^{-1}$, and $U(z) = (0.0007$ to $0.0078)$ at the 95 % confidence level.

Table B.8: Experimental values of pressure (P), specific volume (v), temperature (T), and bulk mole fraction (z) in the vapor-phase region for R1225ye(Z) (1) + R600a (2) binary systems.[a]

T	P	v	T	P	v
K	kPa	$m^3\,kg^{-1}$	K	kPa	$m^3\,kg^{-1}$
$z_2 = 0.1747$			$z_2 = 0.5041$		
308.15	316.0	0.063226	303.15	207.0	0.121578
313.15	321.9	0.063240	308.15	210.7	0.121605
318.15	327.8	0.063254	313.15	214.4	0.121631
323.15	333.7	0.063267	318.15	218.0	0.121658
328.15	339.5	0.063281	323.15	221.7	0.121685
333.15	346.4	0.063295	328.15	225.3	0.121711
338.15	351.2	0.063309	333.15	229.0	0.121738
343.15	357.0	0.063323	338.15	232.6	0.121765
348.15	362.8	0.063337	343.15	236.3	0.121791
353.15	368.6	0.063351	348.15	239.9	0.121818
358.15	374.3	0.063364	353.15	243.6	0.121845
363.15	380.1	0.063378	358.15	247.3	0.121871
368.15	385.9	0.063392	363.15	251.0	0.121898
373.15	391.6	0.063406	368.15	254.6	0.121925
378.15	397.3	0.063420	373.15	258.3	0.121951
383.15	403.1	0.063434	378.15	262.0	0.121978
			383.15	265.6	0.122005
$z_2 = 0.3453$			$z_2 = 0.7969$		
308.15	309.8	0.071702	308.15	303.6	0.107373
313.15	315.5	0.071718	313.15	309.3	0.107397
318.15	321.3	0.071734	318.15	315.0	0.107420
323.15	327.0	0.071749	323.15	320.6	0.107444
328.15	332.9	0.071765	328.15	326.2	0.107467
333.15	338.6	0.071781	333.15	331.8	0.107491
338.15	344.2	0.071797	338.15	337.4	0.107515
343.15	349.8	0.071812	343.15	342.9	0.107538
348.15	355.4	0.071828	348.15	348.5	0.107562
353.15	361.0	0.071844	353.15	354.1	0.107585
358.15	366.6	0.071859	358.15	359.6	0.107609
363.15	372.2	0.071875	363.15	365.1	0.107632
368.15	377.8	0.071891	368.15	370.4	0.107656
373.15	383.4	0.071907	373.15	375.9	0.107679
378.15	389.0	0.071922	378.15	381.6	0.107703
383.15	394.6	0.071938	383.15	387.0	0.107727
$z_2 = 0.4768$			$z_2 = 0.9160$		
308.15	410.6	0.058505	308.15	394.7	0.090086
313.15	418.8	0.058518	313.15	402.8	0.090106
318.15	426.9	0.058531	318.15	410.7	0.090126
323.15	434.9	0.058544	323.15	418.5	0.090145
328.15	442.8	0.058556	328.15	426.4	0.090165
333.15	450.8	0.058569	333.15	434.0	0.090185

Continues to the following page

Continues from the previous page

T K	P kPa	v $m^3\,kg^{-1}$	T K	P kPa	v $m^3\,kg^{-1}$
338.15	458.7	0.058582	338.15	441.7	0.090205
343.15	466.6	0.058595	343.15	449.4	0.090224
348.15	474.5	0.058608	348.15	457.0	0.090244
353.15	482.3	0.058621	353.15	464.6	0.090264
358.15	490.2	0.058633	358.15	472.2	0.090284
363.15	497.9	0.058646	363.15	479.8	0.090303
368.15	505.7	0.058659	368.15	487.3	0.090323
373.15	513.5	0.058672	373.15	494.9	0.090343
378.15	521.3	0.058685	378.15	502.4	0.090363
383.15	529.0	0.058698	383.15	509.9	0.090382

[a] Expanded uncertainties are $U(T) = 0.03$ K and $U(P) = 1$ kPa, $U(v) = (0.000068$ to $0.000165)$ $m^3\,kg^{-1}$, and $U(z) = (0.0007$ to $0.0024)$ at the 95 % confidence level.

Table B.9: Experimental values of pressure (P), specific volume (v), temperature (T), and bulk mole fraction (z) in the vapor-phase region for R1243zf(Z) (1) + R600a (2) binary systems.[a]

T	P	v	T	P	v
K	kPa	$m^3\,kg^{-1}$	K	kPa	$m^3\,kg^{-1}$
$z_2 = 0.2254$			$z_2 = 0.4342$		
308.15	289.5	0.094241	308.15	192.7	0.161076
313.15	294.8	0.094262	313.15	196.0	0.161111
318.15	300.1	0.094283	318.15	199.4	0.161146
323.15	305.3	0.094303	323.15	202.4	0.161182
328.15	310.5	0.094324	328.15	205.9	0.161217
333.15	315.8	0.094345	333.15	209.4	0.161252
338.15	320.9	0.094365	338.15	212.0	0.161288
343.15	326.1	0.094386	343.15	215.5	0.161323
348.15	331.3	0.094407	348.15	218.9	0.161358
353.15	336.5	0.094427	353.15	222.4	0.161394
358.15	341.6	0.094448	358.15	225.0	0.161429
363.15	346.8	0.094469	363.15	228.5	0.161464
368.15	351.9	0.094489	368.15	231.9	0.161500
373.15	357.1	0.094510	373.15	235.2	0.161535
378.15	362.3	0.094531	378.15	236.9	0.161570
383.15	367.5	0.094551	383.15	240.1	0.161606
$z_2 = 0.2821$			$z_2 = 0.8982$		
303.15	47.6	0.613448	303.15	169.8	0.230215
308.15	48.4	0.613582	308.15	172.8	0.230265
313.15	49.2	0.613717	313.15	175.8	0.230316
318.15	50.0	0.613851	318.15	178.7	0.230366
323.15	50.8	0.613986	323.15	181.7	0.230417
328.15	51.6	0.614121	328.15	184.7	0.230467
333.15	52.4	0.614255	333.15	187.6	0.230518
338.15	53.2	0.614390	338.15	190.4	0.230568
343.15	54.0	0.614524	343.15	193.4	0.230619
348.15	54.8	0.614659	348.15	196.3	0.230669
353.15	55.6	0.614794	353.15	199.4	0.230720
358.15	56.4	0.614928	358.15	202.3	0.230770
363.15	57.2	0.615063	363.15	205.3	0.230821
368.15	58.1	0.615197	368.15	208.1	0.230871
373.15	58.8	0.615332	373.15	211.1	0.230922
378.15	59.7	0.615466	378.15	213.4	0.230972
383.15	60.5	0.615601	383.15	217.1	0.231023

[a] Expanded uncertainties are $U(T) = 0.03$ K and $U(P) =$ 1 kPa, $U(v) =$ (0.000119 to 0.002562) $m^3\,kg^{-1}$, and $U(z) =$ (0.0018 to 0.0108) at the 95 % confidence level.

Table B.10: Experimental values of pressure (P), specific volume (v), temperature (T), and bulk mole fraction (z) in the vapor-phase region for R32 (1) + R1234yf (1) binary systems.[a]

T / K	P / kPa	v / $m^3\,kg^{-1}$	T / K	P / kPa	v / $m^3\,kg^{-1}$
$z_1 = 0.1214$			$z_1 = 0.6231$		
303.15	357.6	0.061216	303.15	117.3	0.280135
308.15	364.6	0.061229	308.15	119.3	0.280197
313.15	371.5	0.061243	313.15	121.2	0.280258
318.15	378.3	0.061256	318.15	123.2	0.280320
323.15	385.1	0.061270	323.15	125.1	0.280381
328.15	391.9	0.061283	328.15	127.1	0.280443
333.15	398.7	0.061296	333.15	129.1	0.280504
338.15	405.5	0.061310	338.15	131.1	0.280566
343.15	412.2	0.061323	343.15	133.1	0.280627
348.15	418.9	0.061337	348.15	135.0	0.280689
353.15	425.6	0.061350	353.15	137.0	0.280750
358.15	432.3	0.061364	358.15	139.0	0.280812
363.15	439.0	0.061377	363.15	141.0	0.280873
368.15	445.7	0.061390	368.15	142.9	0.280934
373.15	452.4	0.061404	373.15	145.0	0.280996
378.15	458.9	0.061417	378.15	147.0	0.281057
383.15	465.7	0.061431	383.15	149.0	0.281119
$z_1 = 0.1330$			$z_1 = 0.6489$		
273.15	305.3	0.063789	288.15[b]	880.5[b]	0.029755[b]
278.15	312.8	0.063803	293.15[b]	920.6[b]	0.029762[b]
283.15	318.5	0.063817	298.15	954.3	0.029768
288.15	325.9	0.063831	303.15	976.8	0.029775
293.15	331.5	0.063845	308.15	999.6	0.029781
298.15	339.1	0.063859	313.15	1022.3	0.029788
303.15	345.6	0.063873	318.15	1044.8	0.029794
308.15	353.5	0.063887	323.15	1067.1	0.029801
313.15	359.2	0.063901	328.15	1089.4	0.029808
318.15	365.9	0.063915	333.15	1111.9	0.029814
323.15	372.6	0.063929	338.15	1133.8	0.029821
328.15	379.6	0.063943	343.15	1155.1	0.029827
333.15	386.3	0.063957	348.15	1176.7	0.029834
338.15	392.9	0.063971	353.15	1198.2	0.029840
343.15	399.4	0.063985	358.15	1219.5	0.029847
348.15	405.9	0.063999	363.15	1240.8	0.029853
353.15	411.8	0.064013	368.15	1262.0	0.029860
358.15	418.4	0.064027	373.15	1283.0	0.029866
363.15	425.0	0.064041			
368.15	432.0	0.064055			
373.15	438.6	0.064069			
$z_1 = 0.1792$			$z_1 = 0.7020$		
293.15[b]	644.7[b]	0.029903[b]	303.15	294.7	0.116388

Continues to the following page

Continues from the previous page

T / K	P / kPa	v / $m^3\,kg^{-1}$	T / K	P / kPa	v / $m^3\,kg^{-1}$
298.15	681.6	0.029910	308.15	300.0	0.116413
303.15	698.5	0.029916	313.15	305.3	0.116439
308.15	715.2	0.029923	318.15	310.6	0.116464
313.15	731.3	0.029930	323.15	315.8	0.116490
318.15	747.3	0.029936	328.15	321.1	0.116515
323.15	763.0	0.029943	333.15	326.3	0.116541
328.15	777.7	0.029949	338.15	331.5	0.116566
333.15	793.3	0.029956	343.15	336.7	0.116592
338.15	808.9	0.029962	348.15	341.9	0.116617
343.15	824.4	0.029969	353.15	347.1	0.116643
348.15	839.7	0.029975	358.15	352.3	0.116668
353.15	854.9	0.029982	363.15	357.5	0.116694
358.15	870.1	0.029989	368.15	362.7	0.116720
363.15	885.2	0.029995	373.15	367.9	0.116745
368.15	900.2	0.030002	378.15	373.0	0.116771
373.15	915.2	0.030008	383.15	378.1	0.116796
$z_1 = 0.2712$			$z_1 = 0.8122$		
303.15	174.9	0.144543	283.15[b]	934.7[b]	0.032064[b]
308.15	177.9	0.144574	288.15	979.8	0.032071
313.15	181.0	0.144606	293.15	1004.8	0.032078
318.15	184.0	0.144638	298.15	1030.4	0.032085
323.15	187.1	0.144669	303.15	1055.1	0.032092
328.15	190.1	0.144701	308.15	1080.2	0.032099
333.15	193.1	0.144733	313.15	1104.9	0.032106
338.15	196.1	0.144765	318.15	1129.2	0.032113
343.15	199.2	0.144796	323.15	1152.1	0.032120
348.15	202.2	0.144828	328.15	1175.4	0.032127
353.15	205.2	0.144860	333.15	1199.4	0.032134
358.15	208.3	0.144891	338.15	1223.5	0.032141
363.15	211.3	0.144923	343.15	1247.0	0.032148
368.15	214.3	0.144955	348.15	1270.4	0.032155
373.15	217.3	0.144987	353.15	1293.6	0.032162
378.15	220.3	0.145018	358.15	1316.8	0.032169
383.15	223.2	0.145050	363.15	1339.6	0.032176
			368.15	1362.9	0.032183
			373.15	1385.8	0.032190
$z_1 = 0.3432$			$z_1 = 0.9460$		
303.15	234.0	0.111341	303.15	422.8	0.101971
308.15	238.2	0.111365	308.15	430.6	0.101993
313.15	242.4	0.111390	313.15	438.4	0.102016
318.15	246.5	0.111414	318.15	446.2	0.102038
323.15	250.6	0.111439	323.15	454.0	0.102060
328.15	254.7	0.111463	328.15	461.8	0.102083
333.15	258.8	0.111487	333.15	469.5	0.102105
338.15	263.0	0.111512	338.15	477.1	0.102127

Continues to the following page

Continues from the previous page

T / K	P / kPa	v / $m^3\,kg^{-1}$	T / K	P / kPa	v / $m^3\,kg^{-1}$
343.15	267.1	0.111536	343.15	484.8	0.102150
348.15	271.2	0.111561	348.15	492.5	0.102172
353.15	275.3	0.111585	353.15	500.1	0.102195
358.15	279.4	0.111610	358.15	507.7	0.102217
363.15	283.5	0.111634	363.15	515.3	0.102239
368.15	287.6	0.111658	368.15	522.9	0.102262
373.15	291.7	0.111683	373.15	530.5	0.102284
378.15	295.9	0.111707	378.15	538.0	0.102306
383.15	300.1	0.111732	383.15	545.6	0.102329
$z_1 = 0.5229$					
288.15[b]	774.9[b]	0.030683[b]			
293.15[b]	808.4[b]	0.030690[b]			
298.15	844.7	0.030697			
303.15	864.8	0.030703			
308.15	884.5	0.030710			
313.15	904.3	0.030717			
318.15	923.9	0.030724			
323.15	943.2	0.030730			
328.15	962.5	0.030737			
333.15	981.7	0.030744			
338.15	1000.8	0.030751			
343.15	1019.7	0.030757			
348.15	1038.5	0.030764			
353.15	1057.2	0.030771			
358.15	1075.8	0.030777			
363.15	1094.4	0.030784			
368.15	1113.2	0.030791			
373.15	1131.5	0.030798			

[a] Expanded uncertainties are $U(T) = 0.03$ K and $U(P) = 1$ kPa, $U(v) = (0.000034$ to $0.000753)$ $m^3\,kg^{-1}$, and $U(z) = (0.0004$ to $0.0046)$ at the 95 % confidence level. [b] Not considered in the regression.

Table B.11: Experimental values of pressure (P), specific volume (v), temperature (T), and bulk mole fraction (z) in the vapor-phase region for R32 (1) + R1234ze(E) (1) binary systems.[a]

T / K	P / kPa	v / $m^3\,kg^{-1}$	T / K	P / kPa	v / $m^3\,kg^{-1}$
$z_1 = 0.1677$			$z_1 = 6715$		
293.15[b]	440.3[b]	0.046471[b]	303.15	291.4	0.11498
298.15	460	0.046481	308.15	296.6	0.115005
303.15	470.1	0.046491	313.15	301.9	0.11503
308.15	480.1	0.046501	318.15	307.1	0.115055
313.15	490	0.046511	323.15	312.4	0.11508
318.15	499.9	0.046522	328.15	317.6	0.115106
323.15	509.6	0.046532	333.15	322.8	0.115131
328.15	519.3	0.046542	338.15	328	0.115156
333.15	528.9	0.046552	343.15	333.2	0.115181
338.15	538.5	0.046562	348.15	338.5	0.115207
343.15	547.9	0.046573	353.15	343.7	0.115232
348.15	557.4	0.046583	358.15	348.9	0.115257
353.15	567	0.046593	363.15	354	0.115282
358.15	576.4	0.046603	368.15	359.2	0.115307
363.15	585.7	0.046613	373.15	364.3	0.115333
368.15	595.1	0.046624			
373.15	604.5	0.046634			
$z_1 = 0.2360$			$z_1 = 0.7383$		
303.15	200.6	0.121545	288.15[b]	736.4[b]	0.039370[b]
308.15	204.2	0.121572	293.15[b]	764.5[b]	0.039379[b]
313.15	207.8	0.121599	298.15[b]	801.0[b]	0.039387[b]
318.15	211.4	0.121625	303.15	825.3	0.039396
323.15	215.1	0.121652	308.15	843.8	0.039405
328.15	218.6	0.121679	313.15	861.9	0.039413
333.15	222.2	0.121705	318.15	879.8	0.039422
338.15	225.8	0.121732	323.15	898.6	0.039431
343.15	229.3	0.121759	328.15	915.3	0.039439
348.15	232.9	0.121785	333.15	932.9	0.039448
353.15	236.5	0.121812	338.15	950.4	0.039457
358.15	240	0.121839	343.15	967.8	0.039465
363.15	243.6	0.121865	348.15	985.1	0.039474
368.15	247.1	0.121892	353.15	1002.3	0.039483
373.15	250.6	0.121919	358.15	1019.4	0.039491
			363.15	1036.6	0.0395
			368.15	1053.5	0.039508
			373.15	1070.6	0.039517
$z_1 = 0.2551$			$z_1 = 0.7544$		
333.15[b]	1565.5[b]	0.013182[b]	303.15	512.1	0.06812
338.15	1630.9	0.013185	308.15	521.8	0.068135
343.15	1677	0.013188	313.15	531.7	0.06815

Continues to the following page

Continues from the previous page

T / K	P / kPa	v / $m^3\,kg^{-1}$	T / K	P / kPa	v / $m^3\,kg^{-1}$
348.15	1721.2	0.013191	318.15	541.6	0.068165
353.15	1764.7	0.013194	323.15	551.4	0.06818
358.15	1807.8	0.013196	328.15	561.2	0.068195
363.15	1850.1	0.013199	333.15	571	0.06821
368.15	1892	0.013202	338.15	580.7	0.068225
373.15	1933.5	0.013205	343.15	590.4	0.06824
			348.15	600.1	0.068255
			353.15	609.7	0.06827
			358.15	619.4	0.068285
			363.15	629.1	0.068299
			368.15	638.6	0.068314
			373.15	648.1	0.068329
$z_1 = 0.4634$			$z_1 = 0.9532$		
303.15	400.5	0.068854	278.15[b]	813.8[b]	0.043039[b]
308.15	408.2	0.068869	283.15[b]	849.0[b]	0.043049[b]
313.15	415.9	0.068884	288.15[b]	871.8[b]	0.043058[b]
318.15	423.6	0.068899	293.15[b]	893.3[b]	0.043068[b]
323.15	431.2	0.068914	298.15	914.7	0.043077
328.15	438.8	0.068929	303.15	935.6	0.043087
333.15	446.4	0.068944	308.15	956.3	0.043096
338.15	453.9	0.068959	313.15	976.9	0.043105
343.15	461.4	0.068974	318.15	997.3	0.043115
348.15	468.9	0.068989	323.15	1017.6	0.043124
353.15	476.3	0.069005	328.15	1037.7	0.043134
358.15	483.8	0.069020	333.15	1057.7	0.043143
363.15	491.2	0.069035	338.15	1077.6	0.043153
368.15	498.8	0.069050	343.15	1097.3	0.043162
373.15	506.1	0.069065	348.15	1117.1	0.043172
			353.15	1136.6	0.043181
			358.15	1156.1	0.043191
			363.15	1175.5	0.043200
			368.15	1194.7	0.043209
			373.15	1213.9	0.043219
$z_1 = 0.5374$			$z_1 = 0.9533$		
303.15	271.4	0.110278	303.15	669.1	0.062869
308.15	276.3	0.110302	308.15	682.5	0.062883
313.15	281.3	0.110326	313.15	695.9	0.062897
318.15	286.2	0.110350	318.15	709.2	0.062911
323.15	291.1	0.110375	323.15	722.5	0.062924
328.15	295.9	0.110399	328.15	735.7	0.062938
333.15	300.8	0.110423	333.15	748.8	0.062952
338.15	305.6	0.110447	338.15	761.9	0.062966
343.15	310.4	0.110471	343.15	774.9	0.062980
348.15	315.3	0.110495	348.15	787.9	0.062993

Continues to the following page

Continues from the previous page

T K	P kPa	v $m^3\,kg^{-1}$	T K	P kPa	v $m^3\,kg^{-1}$
353.15	320.2	0.110520	353.15	800.9	0.063007
358.15	325.0	0.110544	358.15	813.8	0.063021
363.15	329.8	0.110568	363.15	826.6	0.063035
368.15	334.5	0.110592	368.15	839.4	0.063049
373.15	339.4	0.110616	373.15	852.3	0.063062

[a] Expanded uncertainties are $U(T) = 0.03$ K and $U(P) = 1$ kPa, $U(v) =$ (0.000015 to 0.000186) $m^3\,kg^{-1}$, and $U(z) =$ (0.0004 to 0.0044) at the 95 % confidence level. [b] Not considered in the regression.

Table B.12: Experimental values of pressure (P), specific volume (v), temperature (T), and bulk mole fraction (z) in the vapor-phase region for R32 (1) + R1234ze(Z) (1) binary systems.[a]

T / K	P / kPa	v / $m^3\,kg^{-1}$	T / K	P / kPa	v / $m^3\,kg^{-1}$
$z_1 = 0.3620$			$z_1 = 0.8015$		
308.15[b]	348.4[b]	0.071682[b]	323.15[b]	1411.0[b]	0.023749[b]
313.15[b]	358.7[b]	0.071697[b]	328.15	1450.1	0.023754
318.15[b]	366.4[b]	0.071713[b]	333.15	1485.3	0.023759
323.15[b]	373.6[b]	0.071729[b]	338.15	1519.9	0.023765
328.15	380.7	0.071744	343.15	1554.1	0.023770
333.15	387.8	0.071760	348.15	1587.9	0.023775
338.15	394.8	0.071776	353.15	1621.4	0.023780
343.15	401.7	0.071792	358.15	1654.6	0.023785
348.15	408.8	0.071807	363.15	1687.8	0.023791
353.15	415.9	0.071823	368.15	1720.5	0.023796
358.15	422.9	0.071839	373.15	1752.9	0.023801
363.15	429.8	0.071854			
368.15	436.5	0.071870			
373.15	443.2	0.071886			
$z_1 = 0.5232$			$z_1 = 0.8973$		
323.15[b]	791.3[b]	0.035005[b]	308.15[b]	1318.8[b]	0.026755[b]
328.15	823.9	0.035012	313.15[b]	1358.1[b]	0.026761[b]
333.15	842.5	0.035020	318.15[b]	1393.0[b]	0.026766[b]
338.15	860.4	0.035028	323.15	1427.2	0.026772
343.15	878.1	0.035035	328.15	1460.5	0.026778
348.15	895.6	0.035043	333.15	1493.5	0.026784
353.15	912.6	0.035051	338.15	1526.1	0.026790
358.15	930.1	0.035058	343.15	1558.4	0.026796
363.15	947.2	0.035066	348.15	1590.4	0.026802
368.15	964.3	0.035074	353.15	1622.2	0.026807
373.15	981.0	0.035081	358.15	1653.8	0.026813
			363.15	1685.1	0.026819
			368.15	1716.3	0.026825
			373.15	1747.3	0.026831
$z_1 = 0.7128$					
298.15[b]	460.5[b]	0.070027[b]			
303.15	470.5	0.070043			
308.15	480.3	0.070058			
313.15	489.8	0.070074			
318.15	499.3	0.070089			
323.15	508.8	0.070104			
328.15	518.2	0.070120			
333.15	527.5	0.070135			
338.15	536.8	0.070150			
343.15	546.0	0.070166			

Continues to the following page

Continues from the previous page

T K	P kPa	v $m^3\,kg^{-1}$	T K	P kPa	v $m^3\,kg^{-1}$
348.15	555.2	0.070181			
353.15	564.4	0.070196			
358.15	573.5	0.070212			
363.15	582.6	0.070227			
368.15	591.7	0.070243			
373.15	600.6	0.070258			

[a] Expanded uncertainties are $U(T) = 0.03$ K and $U(P) = 1$ kPa, $U(v) = (0.000015$ to $0.000091)$ $m^3\,kg^{-1}$, and $U(z) = (0.0005$ to $0.0016)$ at the 95 % confidence level.

[b] Not considered in the regression.

Appendix C

Nomenclature

C.1 Latin Symbols

A	Parameter of equations of state, term related to the equation of Gharagheizi et al., coefficient of the proposed surface tension equation, Latini equation's parameter
a	Parameter of the equations of state ($\mathrm{kJ\,m^3\,kmol^{-2}}$), Latini equation's parameter
a_1	Term related to the reduced dipole moment
a^*	Radiative forcing for unit of mass ($\mathrm{W\,m^{-2}\,kg^{-1}}$)
B	Parameter of equations of state, second virial coefficient ($\mathrm{cm^3\,mol^{-1}}$), coefficient of the proposed surface tension equation
B_c	Term related to the equation of Iglesias-Silva and Hall
b	Parameter of equations of state ($\mathrm{m^3\,kmol^{-1}}$)
b_0	Term related to the equation of Iglesias-Silva and Hall
b_1	Term related to the reduced dipole moment
C	Third virial coefficient ($\mathrm{cm^6\,mol^{-2}}$), coefficient of the proposed surface tension equation
C_p	Isobaric heat capacity ($\mathrm{J\,K^{-1}}$)
c_i	Coefficients of cubic equations of state, terms related to the equation of Virendra et al.
c^*	Concentration
D	Fourth virial coefficient ($\mathrm{cm^9\,mol^{-3}}$), coefficient of the proposed surface tension equation
E	Coefficient of the proposed surface tension equation

E^a	Energy consumption per year ($\mathrm{kWh\,a^{-1}}$)
Er	Error
F	Fraction of dissociated compound in the stratosphere
F_L	Overall mole fraction of the liquid phase
f	Fugacity (kPa)
f_i	Terms related to the Tsonopoulos' equation
G	Gibbs energy (J)
Gr	Radius of gyration (Å)
Δh_fus	Enthalpy of fusion at the melting point ($\mathrm{J\,mol^{-1}}$)
K	Distribution factor
k	Parameter of cubic equations of state, Boltzmann constant ($\mathrm{J\,K^{-1}}$)
k_{ij} k_{ji}	Binary interaction parameter
L	Annual system leakage rate (kg)
l	distance between the surfaces of adjacent molecules (m)
l_{ij} l_{ji}	Binary interaction parameter
M	Molar mass ($\mathrm{kg\,kmol^{-1}}$)
m	Mass (g)
m_b	Mass measured by the analytical balance (g)
N	Number of points
N^{**}	System lifetime (a)
N_A	Avogadro's number ($\mathrm{mol^{-1}}$)
n	Number of moles (mol), term related to the equation of Iglesias-Silva and Hall, number of times that the charging bottle is weighted
n^*	Number of years
n^{**}	System running time (a)
n_hal	Number of halogen atoms
P	Pressure (kPa)
P_A	Pressure attractive contribution (kPa)
P_R	Pressure repulsive contribution (kPa)
P_sat	Vapor pressure (kPa)
Q	Objective function of the flash method

R	Universal gas constant ($\mathrm{J\,K^{-1}\,mol^{-1}}$)
T	Temperature (K)
T_{lit}	Literature triple point temperature (K)
T_{m}	Temperature at the melting point (K)
t	Time (a)
t_{s}	Time for a molecule for transportation to the stratosphere region (a)
U	Expanded uncertainty
u	Uncertainty, constant of cubic equations of state
V_{iso}	Volume of the isochoric cell ($\mathrm{cm^3}$)
v	Specific volume ($\mathrm{m^3kg^{-1}}$)
v_{c}	Critical molar volume ($\mathrm{m^3kmol^{-1}}$)
v_{m}	Molar volume ($\mathrm{m^3kmol^{-1}}$)
W	Work (J), speed of sound ($\mathrm{m\,s^{-1}}$)
w	Constant of cubic equations of state
x	Liquid phase mole fraction
y	Vapor phase mole fraction
Z	Compressibility factor
z	Overall mole fraction

C.2 Greek Symbols

α	Function of cubic equations of state, parameter for the calculation of the mole fraction uncertainty, Bridgman equation's constant, Latini equation's parameter
α^*	Enhancement factor for the relative efficiency of ozone destruction
β	Latini equation's parameter
β^{**}	CO_2 emission factor ($\mathrm{g\,kWh^{-1}}$)
γ	Activity coefficient, Latini equation's parameter
Δ	Parameter of activity coefficient calculated from cubic equations of state
δ	Average distance between the centers of molecules (m)
η	Function of Carnahan-Starling-De Santis

ϵ	Residual value, dimensionless factor of the proposed thermal conductivity equation
λ	Thermal conductivity ($\mathrm{W\,m^{-1}\,K^{-1}}$)
μ	Dipole moment (D), chemical potential ($\mathrm{J\,mol^{-1}}$)
ρ	Density ($\mathrm{kg\,m^{-3}}$)
ρ_c	Critical molar density ($\mathrm{mol\,m^{-3}}$)
σ	Surface tension ($\mathrm{N\,m^{-1}}$)
τ	Total atmospheric lifetimes (a)
Φ	Golden ratio
ϕ	Fugacity coefficient ,volume fraction, surface tension dimensionless term
ω	Acentric factor
Ω_a	Constant of cubic equation of state
Ω_b	Constant of cubic equation of state

C.3 Subscripts/Superscripts

Boyle	Boyle
b	Normal boiling point
c	Critical, cooling
calc	Calculated
exp	Experimental
h	Heating
ig	Ideal gas
in	Initial
iter	Iteration
L	Liquid
liq	Liquidus
m	Molar, mean value, mixture
min	Minimum
r	Reduced
sat	Saturated

sol	Solidus
tp	Triple point
V	Vapor
X	Compound X
*	Solute

C.4 Acronyms

AAD	Average absolute deviation
AARD	Average absolute relative deviation (%)
ANN	Artificial neural network
ASHRAE	American Society of Heating, Refrigerating and Air-Conditioning Engineers
CES	Cubic equation of state
CFC	Chlorofluorocarbon
COP	Conference of Parties
CSP	Corresponding states principle
EoS	Equation of state
EU	European Union
GC	Group contribution, gas chromatography
GHG	Greenhouse gas
GWP	Global warming potential
HC	Hydrocarbon
HCFC	Hydrochlorofluorocarbon
HCFO	Hydrochlorofluoroolefin
HFC	Hydrofluorocarbon
HFO	Hydrofluoroolefin
HVAC&R	Heating, Ventilating, Air Conditioning & Refrigeration
LCCP	Life-cycle climate performance
LLE	Liquid-liquid equilibrium
MLP	Multi-layers perceptron

ODP	Ozone depletion potential
ODS	Ozone-depleting substance
PR	Peng Robinson
RKS	Redlich Kwong Soave
RMSD	Root mean square deviation
SLE	Solid-liquid equilibrium
TEWI	Total equivalent warming impact
UNEP	United Nations Environment Programme
UNFCCC	United Nations Framework Convention on Climate Change
VLE	Vapor-liquid equilibrium
WMO	World Meteorological Organization

Bibliography

[1] ASHRAE Standard. "Standard 34-2010. Designation and safety classification of refrigerants. Standard, American Society of Heating". In: *Refrigeration, and Air-Conditioning Engineers, Inc., Atlanta, GA* (2010) (cit. on pp. 1, 17).

[2] James M Calm. "The next generation of refrigerants–Historical review, considerations, and outlook". In: *international Journal of Refrigeration* 31.7 (2008), pp. 1123–1133 (cit. on pp. 1–3, 7).

[3] Jacob Perkins. "Apparatus for producing ice and cooling fluids". In: *UK Patent* 6662 (1834), p. 1834 (cit. on p. 1).

[4] Thomas Midgley Jr and Albert L Henne. "Organic Fluorides as Refrigerants1". In: *Industrial & Engineering Chemistry* 22.5 (1930), pp. 542–545 (cit. on p. 2).

[5] R Downing. "Development of chlorofluorocarbon refrigerants". In: *ASHRAE transactions* 90.2 (1984), pp. 481–491 (cit. on p. 2).

[6] Montreal Protocol. "Montreal protocol on substances that deplete the ozone layer". In: *Washington, DC: US Government Printing Office* 26 (1987), pp. 128–136 (cit. on pp. 2, 6).

[7] United Nations Environmental Programme (UNEP). *Report of the 19th Meeting of the Parties to the Montreal Protocol on Substances that Deplete the Ozone Layer*. 2007 (cit. on p. 3).

[8] Guus JM Velders, David W Fahey, John S Daniel, Mack McFarland, and Stephen O Andersen. "The large contribution of projected HFC emissions to future climate forcing". In: *Proceedings of the National Academy of Sciences* 106.27 (2009), pp. 10949–10954 (cit. on pp. 3, 7).

[9] Kyoto Protocol. "United Nations framework convention on climate change". In: *Kyoto Protocol, Kyoto* 19 (1997) (cit. on p. 3).

[10] COP21 UNFCCC. "Paris agreement". In: *FCCCC/CP/2015/L. 9/Rev. 1* (2015) (cit. on p. 3).

[11] The European Parliament and the Council of the European Union. "Directive 2006/40/EC of the European Parliament and of the Council of 17 May 2006 relating to emissions from air-conditioning systems in motor vehicles and Amending Council Directive 70/156/EEC". In: *Official Journal of the European Union* 1 (2006) (cit. on p. 4).

[12] The European Parliament and the Council of the European Union. "Regulation (EC) No 842/2006 of the European Parliament and of the Council of 17 May 2006 on Certain Fluorinated Greenhouse Gases". In: *Official Journal of the European Union* (2006) (cit. on p. 4).

[13] The European Parliament and the Council of the European Union. "Regulation (EU) No 517/2014 of the European Parliament and of the Council of 16 April 2014 on fluorinated greenhouse gases and repealing Regulation (EC) No 842/2006". In: *Official Journal of the European Union* (2014) (cit. on pp. 4, 6, 8).

[14] Adrián Mota-Babiloni, Joaquín Navarro-Esbrí, Ángel Barragán-Cervera, Francisco Molés, and Bernardo Peris. "Analysis based on EU Regulation No 517/2014 of new HFC/HFO mixtures as alternatives of high GWP refrigerants in refrigeration and HVAC systems". In: *International journal of refrigeration* 52 (2015), pp. 21–31 (cit. on p. 4).

[15] European Commission. "Proposal for a Council Decision on the conclusion of the agreement to amend the Montreal Protocol on substances that deplete the ozone layer adopted in Kigali". In: *Brussels, Belgium* (2017) (cit. on p. 4).

[16] United Nations Environmental Programme (UNEP). "UNEP Ozone Secretariat in Twenty-Eighth Meeting of the Parties to the Montreal Protocol on Substances that Deplete the Ozone Layer (Kigali, Rwanda, 2016); document UNEP/OzL.Pro.28/CRP/10". In: *United Nations Environment Programme* (2016) (cit. on p. 4).

[17] Durwood Zaelke and Nathan Borgford-Parnell. "The importance of phasing down hydrofluorocarbons and other short-lived climate pollutants". In: *Journal of Environmental Studies and Sciences* 5.2 (2015), pp. 169–175 (cit. on p. 5).

[18] Barbara J Finlayson-Pitts and James N Pitts Jr. *Chemistry of the upper and lower atmosphere: theory, experiments, and applications*. Elsevier, 1999 (cit. on p. 5).

[19] S Solomon, M Mills, LE Heidt, WH Pollock, and AF Tuck. "On the evaluation of ozone depletion potentials". In: *Journal of Geophysical Research: Atmospheres* 97.D1 (1992), pp. 825–842 (cit. on p. 5).

[20] Susan Solomon and Daniel L Albritton. "Time-dependent ozone depletion potentials for short-and long-term forecasts". In: *Nature* 357.6373 (1992), p. 33 (cit. on p. 5).

[21] James M Calm and Glenn C Hourahan. "Physical, safety, and environmental data for current and alternative refrigerants". In: *Proceedings of 23rd International Congress of Refrigeration (ICR2011), Prague, Czech Republic, August*. 2011, pp. 21–26 (cit. on pp. 6, 8).

[22] Pavel Makhnatch and Rahmatollah Khodabandeh. "The role of environmental metrics (GWP, TEWI, LCCP) in the selection of low GWP refrigerant". In: *Energy Procedia* 61 (2014), pp. 2460–2463 (cit. on pp. 6, 7).

[23] JT Houghton, GJ Jenkins, and JJ Ephraums. *Climate Change: The IPCC Scientific Assessment. Report of the United Nations Environment Programme, Intergovernmental Panel on Climate Change (IPCC)*. 1990 (cit. on p. 6).

[24] Mark O McLinden, Andrei F Kazakov, J Steven Brown, and Piotr A Domanski. "A thermodynamic analysis of refrigerants: Possibilities and tradeoffs for Low-GWP refrigerants". In: *International Journal of Refrigeration* 38 (2014), pp. 80–92 (cit. on pp. 6, 8, 9, 15, 21).

[25] Piers Forster, Venkatachalam Ramaswamy, Paulo Artaxo, Terje Berntsen, Richard Betts, David W Fahey, James Haywood, Judith Lean, David C Lowe, Gunnar Myhre, et al. "Changes in atmospheric constituents and in radiative forcing. Chapter 2". In: *Climate Change 2007. The Physical Science Basis*. 2007 (cit. on p. 6).

[26] United Nations Environmental Programme (UNEP). *Technology and Economic Assessment Panel 2010 Progress Report: Assessment of HCFCs and Environmentally Sound Alternatives and Scoping Study on Alternatives to HCFC Refrigerants under High Ambient Temperature Conditions*. 2010 (cit. on p. 6).

[27] MO McLinden and DA Didion. "CFCs". In: *Is the sky falling* (1987), pp. 32–42 (cit. on p. 7).

[28] James M Calm and David A Didion. "Trade-offs in refrigerant selections: past, present, and future". In: *International Journal of Refrigeration* 21.4 (1998), pp. 308–321 (cit. on p. 7).

[29] BO Bolaji and Z Huan. "Ozone depletion and global warming: Case for the use of natural refrigerant–a review". In: *Renewable and Sustainable energy reviews* 18 (2013), pp. 49–54 (cit. on p. 7).

[30] Yitai Ma, Zhongyan Liu, and Hua Tian. "A review of transcritical carbon dioxide heat pump and refrigeration cycles". In: *Energy* 55 (2013), pp. 156–172 (cit. on p. 7).

[31] K Harby. "Hydrocarbons and their mixtures as alternatives to environmental unfriendly halogenated refrigerants: An updated overview". In: *Renewable and Sustainable Energy Reviews* 73 (2017), pp. 1247–1264 (cit. on p. 8).

[32] Mark O McLinden, J Steven Brown, Riccardo Brignoli, Andrei F Kazakov, and Piotr A Domanski. "Limited options for low-global-warming-potential refrigerants". In: *Nature Communications* 8 (2017), p. 14476 (cit. on pp. 8, 9, 15, 21).

[33] Piotr A Domanski, Riccardo Brignoli, J Steven Brown, Andrei F Kazakov, and Mark O McLinden. "Low-GWP refrigerants for medium and high-pressure applications". In: *International Journal of Refrigeration* 84 (2017), pp. 198–209 (cit. on pp. 8, 9, 15, 21).

[34] Ryo Akasaka. "Thermodynamic property models for the difluoromethane (R-32)+ trans-1, 3, 3, 3-tetrafluoropropene (R-1234ze (E)) and difluoromethane+ 2, 3, 3, 3-tetrafluoropropene (R-1234yf) mixtures". In: *Fluid Phase Equilibria* 358 (2013), pp. 98–104 (cit. on p. 8).

[35] Joaquín Navarro-Esbrí, Juan Manuel Mendoza-Miranda, Adrián Mota-Babiloni, A Barragán-Cervera, and Juan Manuel Belman-Flores. "Experimental analysis of R1234yf as a drop-in replacement for R134a in a vapor compression system". In: *International Journal of Refrigeration* 36.3 (2013), pp. 870–880 (cit. on p. 8).

[36] Sergio Bobbo, Giovanni Di Nicola, Claudio Zilio, J Steven Brown, and Laura Fedele. "Low GWP halocarbon refrigerants: A review of thermophysical properties". In: *International Journal of Refrigeration* 90 (2018), pp. 181–201 (cit. on pp. 8, 10, 48, 86).

[37] J Steven Brown, Claudio Zilio, Riccardo Brignoli, and Alberto Cavallini. "Thermophysical properties and heat transfer and pressure drop performance potentials of hydrofluoro-olefins, hydrochlorofluoro-olefins, and their blends". In: *HVAC&R Research* 20.2 (2014), pp. 203–220 (cit. on p. 8).

[38] Shigeo Kondo, Kenji Takizawa, and Kazuaki Tokuhashi. "Effect of high humidity on flammability property of a few non-flammable refrigerants". In: *Journal of Fluorine Chemistry* 161 (2014), pp. 29–33 (cit. on p. 8).

[39] Julie Majurin, Steven J Staats, Elyse Sorenson, and William Gilles. "Material compatibility of HVAC&R system materials with low global warming potential refrigerants". In: *Science and Technology for the Built Environment* 21.5 (2015), pp. 491–501 (cit. on p. 8).

[40] T Lewandowski and KR Reid. "Risk assessment for residential heat pump systems using 2L flammable refrigerants". In: *ASHRAE/NIST Refrigerants Conference*. 2012 (cit. on p. 8).

[41] Giulia Righetti, Claudio Zilio, Simone Mancin, and Giovanni A Longo. "A review on in-tube two-phase heat transfer of hydro-fluoro-olefines refrigerants". In: *Science and Technology for the Built Environment* 22.8 (2016), pp. 1191–1225 (cit. on p. 8).

[42] Ryuichi Nagata, Chieko Kondou, and Shigeru Koyama. "Comparative assessment of condensation and pool boiling heat transfer on horizontal plain single tubes for R1234ze (E), R1234ze (Z), and R1233zd (E)". In: *International Journal of Refrigeration* 63 (2016), pp. 157–170 (cit. on p. 8).

[43] Zahid Anwar, Björn Palm, and Rahmatollah Khodabandeh. "Flow boiling heat transfer, pressure drop and dryout characteristics of R1234yf: Experimental results and predictions". In: *Experimental Thermal and Fluid Science* 66 (2015), pp. 137–149 (cit. on p. 8).

[44] Sebastian Eyerer, Fabian Dawo, Johannes Kaindl, Christoph Wieland, and Hartmut Spliethoff. "Experimental investigation of modern ORC working fluids R1224yd (Z) and R1233zd (E) as replacements for R245fa". In: *Applied energy* 240 (2019), pp. 946–963 (cit. on p. 8).

[45] Sho Fukuda, Chieko Kondou, Nobuo Takata, and Shigeru Koyama. "Low GWP refrigerants R1234ze (E) and R1234ze (Z) for high temperature heat pumps". In: *International journal of Refrigeration* 40 (2014), pp. 161–173 (cit. on p. 8).

[46] Chieko Kondou and Shigeru Koyama. "Thermodynamic assessment of high-temperature heat pumps using Low-GWP HFO refrigerants for heat recovery". In: *International Journal of Refrigeration* 53 (2015), pp. 126–141 (cit. on p. 8).

[47] Adrián Mota-Babiloni, Pavel Makhnatch, and Rahmatollah Khodabandeh. "Recent investigations in HFCs substitution with lower GWP synthetic alternatives: Focus on energetic performance and environmental impact". In: *International Journal of Refrigeration* 82 (2017), pp. 288–301 (cit. on pp. 8, 9).

[48] Bernhard Platzer, Gerd Maurer, and Axel Polt. "Thermophysical properties of refrigerants". In: (1990) (cit. on pp. 9, 10).

[49] ASHRAE. *2005 ASHRAE Handbook: Fundamentals*. ASHRAE, 2005 (cit. on p. 9).

[50] U Westhaus, T Dröge, and R Sass. "DETHERM® – a thermophysical property database". In: *Fluid phase equilibria* 158 (1999), pp. 429–435 (cit. on pp. 9, 10, 51–53).

[51] W Vincent Wilding, Richard L Rowley, and John L Oscarson. "DIPPR® Project 801 evaluated process design data". In: *Fluid phase equilibria* 150 (1998), pp. 413–420 (cit. on pp. 9, 10, 15, 17, 51–53, 55, 72, 74, 75, 160).

[52] Bruce E Poling, John M Prausnitz, John P O'connell, et al. *The properties of gases and liquids*. Vol. 5. Mcgraw-hill New York, 2001 (cit. on pp. 9, 11, 12, 16, 18, 20, 22–25, 29, 35, 69–71).

[53] IU Westhaus and R Sass. "From raw physical data to reliable thermodynamic model parameters through DECHEMA Data Preparation Package". In: *Fluid phase equilibria* 222 (2004), pp. 49–54 (cit. on pp. 10, 51–53).

[54] John M Prausnitz, Rudiger N Lichtenthaler, and Edmundo Gomes de Azevedo. *Molecular thermodynamics of fluid-phase equilibria*. Pearson Education, 1998 (cit. on pp. 11, 12, 28, 29, 32–35).

[55] J Richard Elliott and Carl T Lira. *Introductory chemical engineering thermodynamics*. Vol. 184. Prentice Hall PTR Upper Saddle River, NJ, 1999 (cit. on pp. 11, 28, 29).

[56] Georgios M Kontogeorgis and Georgios K Folas. *Thermodynamic models for industrial applications: from classical and advanced mixing rules to association theories*. John Wiley & Sons, 2009 (cit. on pp. 11, 22, 32–35).

[57] Kenneth S Pitzer. "Corresponding states for perfect liquids". In: *The Journal of Chemical Physics* 7.8 (1939), pp. 583–590 (cit. on p. 12).

[58] Jan V Sengers, RF Kayser, CJ Peters, and HJ White. *Equations of state for fluids and fluid mixtures*. Vol. 5. Elsevier, 2000 (cit. on pp. 12, 13, 22–28, 32).

[59] A Yokozeki, H Sato, and K Watanabe. "Ideal-gas heat capacities and virial coefficients of HFC refrigerants". In: *International journal of thermophysics* 19.1 (1998), pp. 89–127 (cit. on p. 12).

[60] Giovanni Di Nicola, Gianluca Coccia, Mariano Pierantozzi, and Matteo Falone. "A semi-empirical correlation for the estimation of the second virial coefficients of refrigerants". In: *International Journal of Refrigeration* 68 (2016), pp. 242–251 (cit. on pp. 12, 21, 22).

[61] Viorel Feroiu and Dan Geanã. "Volumetric and thermodynamic properties for pure refrigerants and refrigerant mixtures from cubic equations of state". In: *Fluid Phase Equilibria* 207.1-2 (2003), pp. 283–300 (cit. on p. 12).

[62] Graham Morrison and Mark O MacLinden. *Applications of a Hard Sphere Equation of State to Refrigerants and Refrigerant Mixtures*. National Bureau of Standards, 1986 (cit. on p. 12).

[63] Eric W Lemmon, Marcia L Huber, and Mark O McLinden. "NIST reference fluid thermodynamic and transport properties–REFPROP". In: *NIST standard reference database* 23 (2002), p. v7 (cit. on pp. 12, 26).

[64] EW Lemmon, ML Huber, and MO McLinden. "NIST Standard Reference Database 23, Reference Fluid Thermodynamic and Transport Properties (REFPROP), version 9.0, National Institute of Standards and Technology". In: *NIST standard reference database* 22 (2010), p. 2010 (cit. on pp. 12, 17, 26, 31, 38, 107, 125, 155, 156).

[65] EW Lemmon, Ian H Bell, ML Huber, and MO McLinden. "NIST Standard Reference Database 23: Reference Fluid Thermodynamic and Transport Properties-REFPROP, Version 10.0, National Institute of Standards and Technology." In: *NIST standard reference database* (2018) (cit. on pp. 12, 13, 17, 26, 70, 81, 84, 107, 109, 125).

[66] Richard T Jacobsen and Richard B Stewart. "Thermodynamic properties of nitrogen including liquid and vapor phases from 63K to 2000K with pressures to 10,000 bar". In: *Journal of Physical and Chemical Reference Data* 2.4 (1973), pp. 757–922 (cit. on pp. 13, 26).

[67] Ian H Bell and Eric W Lemmon. "Automatic fitting of binary interaction parameters for multi-fluid Helmholtz-energy-explicit mixture models". In: *Journal of Chemical & Engineering Data* 61.11 (2016), pp. 3752–3760 (cit. on pp. 13, 26).

[68] Mark O McLinden, Sanford A Klein, and Richard A Perkins. "An extended corresponding states model for the thermal conductivity of refrigerants and refrigerant mixtures". In: *International Journal of Refrigeration* 23.1 (2000), pp. 43–63 (cit. on p. 13).

[69] Giovanni Di Nicola, Eleonora Ciarrocchi, Gianluca Coccia, and Mariano Pierantozzi. "Correlations of thermal conductivity for liquid refrigerants at atmospheric pressure or near saturation". In: *International journal of refrigeration* 45 (2014), pp. 168–176 (cit. on pp. 13, 72, 81, 84).

[70] Sanfort A Klein, Mark O McLinden, and A Laesecke. "An improved extended corresponding states method for estimation of viscosity of pure refrigerants and mixtures". In: *International Journal of Refrigeration* 20.3 (1997), pp. 208–217 (cit. on p. 13).

[71] Isidro Cachadiña, Angel Mulero, and Jianxiang Tian. "Surface Tension of Refrigerants – Selection of Data and Recommended Correlations". In: *Journal of Physical and Chemical Reference Data* 44.2 (2015), p. 023104 (cit. on pp. 13, 49, 50).

[72] Giovanni Di Nicola, Cristiano Di Nicola, and Matteo Moglie. "A new surface tension equation for refrigerants". In: *International Journal of Thermophysics* 34.12 (2013), pp. 2243–2260 (cit. on pp. 13, 48, 49).

[73] A Chouai, S Laugier, and D Richon. "Modeling of thermodynamic properties using neural networks: Application to refrigerants". In: *Fluid Phase Equilibria* 199.1-2 (2002), pp. 53–62 (cit. on p. 13).

[74] Ángel Mulero, Isidro Cachadiña, and José O Valderrama. "Artificial neural network for the correlation and prediction of surface tension of refrigerants". In: *Fluid Phase Equilibria* 451 (2017), pp. 60–67 (cit. on pp. 13, 50).

[75] Mariano Pierantozzi and Giulio Petrucci. "Modeling thermal conductivity in refrigerants through neural networks". In: *Fluid Phase Equilibria* 460 (2018), pp. 36–44 (cit. on p. 13).

[76] Chris M Bishop. "Neural networks and their applications". In: *Review of Scientific Instruments* 65.6 (1994), pp. 1803–1832 (cit. on p. 13).

[77] World Meteorological Organization. "Scientific Assessment of Ozone Depletion: 2018". In: *Global Ozone Research and Monitoring Project — Report No. 58, 588 pp., Geneva, Switzerland* (2018) (cit. on pp. 15, 17).

[78] Ryo Akasaka, Masato Fukushima, and Eric W Lemmon. "A Helmholtz Energy Equation of State for Trifluoroethylene (R-1123)". In: *International Refrigeration and Air Conditioning Conference at Purdue, West Lafayette, IN, USA* Paper 1698 (2016) (cit. on p. 17).

[79] Yukihiro Higashi and Ryo Akasaka. "Measurements of Thermodynamic Properties for R1123 and R1123+ R32 Mixture". In: *Proceedings of the 16th International Refrigeration and Air Conditioning Conference at Purdue* West Lafayette, IN, USA (2016) (cit. on pp. 17, 31).

[80] Sidney B Lang and Helen LW Chan. *Frontiers of ferroelectricity: a special issue of the journal of materials science*. Springer Science & Business Media, 2007 (cit. on p. 17).

[81] Giovanni Di Nicola, Gianluca Coccia, Mariano Pierantozzi, and Sebastiano Tomassetti. "Equations for the surface tension of low GWP halogenated alkene refrigerants and their blends". In: *International Journal of Refrigeration* 86 (2018), pp. 410–421 (cit. on pp. 17, 48).

[82] Gabriele Raabe. "Molecular Simulation Studies on the Vapor–Liquid Equilibria of the cis-and trans-HCFO-1233zd and the cis-and trans-HFO-1336mzz". In: *Journal of Chemical & Engineering Data* 60.8 (2015), pp. 2412–2419 (cit. on p. 17).

[83] Maria E Mondejar, Mark O McLinden, and Eric W Lemmon. "Thermodynamic properties of trans-1-chloro-3, 3, 3-trifluoropropene (R1233zd (E)): Vapor pressure,(p, ρ, T) behavior, and speed of sound measurements, and equation of state". In: *Journal of Chemical & Engineering Data* 60.8 (2015), pp. 2477–2489 (cit. on pp. 17, 31).

[84] Philipp Petr and Gabriele Raabe. "Evaluation of R-1234ze (Z) as drop-in replacement for R-245fa in Organic Rankine Cycles–From thermophysical properties to cycle performance". In: *Energy* 93 (2015), pp. 266–274 (cit. on p. 17).

[85] Zhi-qiang Yang, Lian-gang Kou, Jing Lu, Wei Zhang, Wei Mao, and Jian Lu. "Isothermal vapor–liquid equilibria measurements for binary systems of 2, 3, 3, 3-tetrafluoropropene (HFO-1234yf)+ 2-chloro-3, 3, 3-trifluoropropene (HCFO-1233xf) and 2-chloro-3, 3, 3-trifluoropropene (HCFO-1233xf)+ 2-chloro-1, 1, 1, 2-tetrafluoropropane (HCFC-244bb)". In: *Fluid Phase Equilibria* 414 (2016), pp. 143–148 (cit. on pp. 17, 38).

[86] Laura Fedele, Giovanni Di Nicola, J Steven Brown, Laura Colla, and Sergio Bobbo. "Saturated pressure measurements of cis-pentafluoroprop-1-ene (R1225ye (Z))". In: *International Journal of Refrigeration* 69 (2016), pp. 243–250 (cit. on pp. 17, 31).

[87] JM Smith, HC Van Ness, and MM Abbott. *Introduction to Chemical Engineering Thermodynamics, (2001) and 7th ed.(2005)* (cit. on p. 16).

[88] Milo D Koretsky. *Engineering and chemical thermodynamics*. John Wiley & Sons, 2012 (cit. on pp. 16, 28).

[89] Stanley M Walas. *Phase equilibria in chemical engineering*. Butterworth - Heinemann, 1985 (cit. on pp. 18, 19, 22).

[90] E. A. Mason and T. H. Spurling. *The virial equation of state*. 2nd ed. Pergamon, 1969 (cit. on p. 19).

[91] Constantine Tsonopoulos. "An empirical correlation of second virial coefficients". In: *AIChE Journal* 20.2 (1974), pp. 263–272 (cit. on p. 19).

[92] Kenneth S Pitzer and RF Curl Jr. "The volumetric and thermodynamic properties of fluids. III. Empirical equation for the second virial coefficient". In: *Journal of the American Chemical Society* 79.10 (1957), pp. 2369–2370 (cit. on p. 19).

[93] LA Weber. "Estimating the virial coefficients of small polar molecules". In: *International Journal of Thermophysics* 15.3 (1994), pp. 461–482 (cit. on p. 20).

[94] Usha Virendra, A Rajiah, and DHL Prasad. "Dependence of the second virial coefficient on temperature". In: *The Chemical Engineering Journal and The Biochemical Engineering Journal* 56.2 (1995), pp. 73–76 (cit. on p. 20).

[95] G. A. Iglesias-Silva and K. R. Hall. "An equation for prediction and/or correlation of second virial coefficients". In: *Industrial & Engineering Chemistry Research* 40.8 (2001), pp. 1968–1974 (cit. on p. 20).

[96] M. Ramos-Estrada, R. Tellez-Morales, G. A. Iglesias-Silva, and KR Hall. "A generalized correlation for the second virial coefficient based upon the Stockmayer potential". In: *Latin American Applied Research* 34.1 (2004), pp. 41–47 (cit. on p. 21).

[97] Farhad Gharagheizi, Ali Eslamimanesh, Mehdi Sattari, Amir H Mohammadi, and Dominique Richon. "Computation of the second virial coefficient of chemical compounds using a corresponding states based method". In: *Advances in Chemistry Research* 24 (2015) (cit. on p. 21).

[98] S Oreški. "Comparison of Neural Network and Empirical Models for Prediction of Second Virial Coefficients for Gases". In: *Procedia Engineering* 42 (2012), pp. 303–312 (cit. on p. 21).

[99] L. E. de Souza and S. Canuto. "Efficient estimation of second virial coefficients of fused hard-sphere molecules by an artificial neural network." In: *Physical Chemistry Chemical Physics* (2001) (cit. on p. 21).

[100] Giovanni Di Nicola, Gianluca Coccia, Mariano Pierantozzi, Sebastiano Tomassetti, and Roberta Cocci Grifoni. "Artificial neural network for the second virial coefficient of organic and inorganic compounds: An ANN for B of organic and inorganic compounds". In: *Chemical Engineering Communications* 205.8 (2018), pp. 1077–1095 (cit. on p. 21).

[101] G Schmidt and H Wenzel. "A modified van der Waals type equation of state". In: *Chemical Engineering Science* 35.7 (1980), pp. 1503–1512 (cit. on p. 22).

[102] Giorgio Soave. "Equilibrium constants from a modified Redlich-Kwong equation of state". In: *Chemical engineering science* 27.6 (1972), pp. 1197–1203 (cit. on pp. 22–24, 30).

[103] Ding-Yu Peng and Donald B Robinson. "A new two-constant equation of state". In: *Industrial & Engineering Chemistry Fundamentals* 15.1 (1976), pp. 59–64 (cit. on pp. 22, 24, 30, 44, 107, 125).

[104] Juan Sebastian Lopez-Echeverry, Simon Reif-Acherman, and Eduard Araujo-Lopez. "Peng-Robinson equation of state: 40 years through cubics". In: *Fluid Phase Equilibria* 447 (2017), pp. 39–71 (cit. on p. 22).

[105] R Stryjek. "Correlation and Critical-Evaluation of Vle data for Nitrogen+ argon, nitrogen+ Methane, and Argon+ Methane Mixtures". In: *Bulletin of The Polish Academy of Sciences-Chemistry* 39.4 (1991), pp. 353–361 (cit. on pp. 23, 24, 30, 32, 107).

[106] R Stryjek. "ON THE PREDICTION OF THE GAS-LIQUID CRITICAL LOCUS WITH CUBIC EQUATIONS OF STATE". In: *Bulletin of The Polish Academy of Sciences-Chemistry* 40.3 (1992), pp. 211–220 (cit. on pp. 23, 24, 30, 32, 107).

[107] IH Bell, J Welliquet, ME Mondejar, A Bazyleva, Sylvain Quoilin, and F Haglind. "Application of the group contribution volume translated Peng-Robinson equation of state to new commercial refrigerant mixtures". In: *International Journal of Refrigeration* (2019) (cit. on p. 24).

[108] Joseph J Martin. "Cubic equations of state-which?" In: *Industrial & Engineering Chemistry Fundamentals* 18.2 (1979), pp. 81–97 (cit. on p. 24).

[109] Norman F Carnahan and Kenneth E Starling. "Equation of state for nonattracting rigid spheres". In: *The Journal of chemical physics* 51.2 (1969), pp. 635–636 (cit. on p. 24).

[110] R De Santis, F Gironi, and L Marrelli. "Vapor-liquid equilibrium from a hard-sphere equation of state". In: *Industrial & Engineering Chemistry Fundamentals* 15.3 (1976), pp. 183–189 (cit. on pp. 25, 27, 28, 44, 107, 164).

[111] Graham Morrison and Mark O McLinden. "Application of the Carnahan - Starling - DeSantis equation of state to mixtures of refrigerants". In: *Winter Annual Meeting*. 1986 (cit. on p. 25).

[112] MO McLinden. "NIST thermodynamic and transport properties of refrigerants and refrigerant mixtures-REFPROP". In: *NIST Standard Reference Database* 23 (1998) (cit. on p. 25).

[113] Sergio Bobbo, Roberto Camporese, and Roman Stryjek. "Vapor- Liquid Equilibria for Difluoromethane (R32)+ and Pentafluoroethane (R125)+ 1, 1, 1, 3, 3, 3-Hexafluoropropane (R236fa) at 303.2 and 323.3 K". In: *Journal of Chemical & Engineering Data* 44.2 (1999), pp. 349–352 (cit. on p. 25).

[114] Marie-José Huron and Jean Vidal. "New mixing rules in simple equations of state for representing vapour-liquid equilibria of strongly non-ideal mixtures". In: *Fluid Phase Equilibria* 3.4 (1979), pp. 255–271 (cit. on pp. 28, 38).

[115] David Shan Hill Wong and Stanley I Sandler. "A theoretically correct mixing rule for cubic equations of state". In: *AIChE Journal* 38.5 (1992), pp. 671–680 (cit. on pp. 28, 38).

[116] G. Di Nicola, G. Coccia, M. Pierantozzi, S. Tomassetti, and Stryjek R. "Analysis of vapor pressure and VLE of HFOs, HCFOs, and their blends with cubic equations of state". In: *1st IIR International Conference on the Application of HFO Refrigerants, Birmingham*. 2018 (cit. on pp. 29, 35).

[117] Yukihiro Higashi, Naoya Sakoda, Md Amirul Islam, Yasuyuki Takata, Shigeru Koyama, and Ryo Akasaka. "Measurements of saturation pressures for trifluoroethene (R1123) and 3, 3, 3-trifluoropropene (R1243zf)". In: *Journal of Chemical & Engineering Data* 63.2 (2018), pp. 417–421 (cit. on p. 31).

[118] Giovanni Di Nicola, Fabio Polonara, and Giulio Santori. "Saturated pressure measurements of 2, 3, 3, 3-tetrafluoroprop-1-ene (HFO-1234yf)". In: *Journal of Chemical & Engineering Data* 55.1 (2009), pp. 201–204 (cit. on p. 31).

[119] Laura Fedele, Sergio Bobbo, Fabio Groppo, J Steven Brown, and Claudio Zilio. "Saturated pressure measurements of 2, 3, 3, 3-tetrafluoroprop-1-ene (R1234yf) for reduced temperatures ranging from 0.67 to 0.93". In: *Journal of Chemical & Engineering Data* 56.5 (2011), pp. 2608–2612 (cit. on p. 31).

[120] Markus Richter, Mark O McLinden, and Eric W Lemmon. "Thermodynamic Properties of 2, 3, 3, 3-Tetrafluoroprop-1-ene (R1234yf): Vapor Pressure and p–ρ–T Measurements and an Equation of State". In: *Journal of Chemical & Engineering Data* 56.7 (2011), pp. 3254–3264 (cit. on p. 31).

[121] Katsuyuki Tanaka and Yukihiro Higashi. "Thermodynamic properties of HFO-1234yf (2, 3, 3, 3-tetrafluoropropene)". In: *International journal of refrigeration* 33.3 (2010), pp. 474–479 (cit. on pp. 31, 53).

[122] J Steven Brown, Giovanni Di Nicola, Laura Fedele, Sergio Bobbo, and Claudio Zilio. "Saturated pressure measurements of 3, 3, 3-trifluoroprop-1-ene (R1243zf) for reduced temperatures ranging from 0.62 to 0.98". In: *Fluid Phase Equilibria* 351 (2013), pp. 48–52 (cit. on p. 31).

[123] Giovanni Di Nicola, J Steven Brown, Laura Fedele, Sergio Bobbo, and Claudio Zilio. "Saturated pressure measurements of trans-1, 3, 3, 3-tetrafluoroprop-1-ene (R1234ze (E)) for reduced temperatures ranging from 0.58 to 0.92". In: *Journal of Chemical & Engineering Data* 57.8 (2012), pp. 2197–2202 (cit. on p. 31).

[124] Maoqiong Gong, Haiyang Zhang, Huiya Li, Quan Zhong, Xueqiang Dong, Jun Shen, and Jianfeng Wu. "Vapor pressures and saturated liquid densities of HFO1234ze (E) at temperatures from 253.343 to 293.318 K". In: *International Journal of Refrigeration* 64 (2016), pp. 168–175 (cit. on p. 31).

[125] Mark J O McLinden, Monika Thol, and Eric W Lemmon. "Thermodynamic properties of trans-1, 3, 3, 3-tetrafluoropropene [R1234ze (E)]: measurements of density and vapor pressure and a comprehensive equation of state". In: (2010) (cit. on p. 31).

[126] Tanaka Katsuyuki. "Measurements of vapor pressure and saturated liquid density for HFO–1234ze (E) and HFO–1234ze (Z)". In: *Journal of Chemical & Engineering Data* 61.4 (2016), pp. 1645–1648 (cit. on p. 31).

[127] Katsuyuki Tanaka, Gen Takahashi, and Yukihiro Higashi. "Measurements of the vapor pressures and p ρ T properties for trans-1, 3, 3, 3-tetrafluoropropene (HFO-1234ze (E))". In: *Journal of Chemical & Engineering Data* 55.6 (2010), pp. 2169–2172 (cit. on p. 31).

[128] Jianguo Yin, Yong Zhou, Guanjia Zhao, and Suxia Ma. "Measurements of vapor pressure and gaseous pvT property for trans-1, 3, 3, 3-tetrafluoropropene (HFO-1234ze (E))". In: *Fluid Phase Equilibria* 460 (2018), pp. 69–74 (cit. on p. 31).

[129] Laura Fedele, Giovanni Di Nicola, J Steven Brown, Sergio Bobbo, and Claudio Zilio. "Measurements and correlations of cis-1, 3, 3, 3-tetrafluoroprop-1-ene (R1234ze (Z)) saturation pressure". In: *International Journal of Thermophysics* 35.1 (2014), pp. 1–12 (cit. on p. 31).

[130] Yukihiro Higashi, Shugo Hayasaka, Chihiro Shirai, and Ryo Akasaka. "Measurements of PρT properties, vapor pressures, saturated densities, and critical parameters for R 1234ze (Z) and R 245fa". In: *International Journal of Refrigeration* 52 (2015), pp. 100–108 (cit. on p. 31).

[131] Naoya Sakoda, Jiang Shiheng, Masamichi Kohno, Shigeru Koyama, Yukihiro Higashi, and Yasuyuki Takata. "Gaseous PVT property measurements of cis-1, 3, 3, 3-tetrafluoropropene". In: *Journal of Chemical & Engineering Data* 62.7 (2017), pp. 2178–2182 (cit. on p. 31).

[132] Ryan J Hulse, Rajat S Basu, Rajiv R Singh, and Raymond HP Thomas. "Physical properties of HCFO-1233zd (E)". In: *Journal of Chemical & Engineering Data* 57.12 (2012), pp. 3581–3586 (cit. on pp. 31, 32, 53).

[133] Giovanni Di Nicola, Laura Fedele, J Steven Brown, Sergio Bobbo, and Gianluca Coccia. "Saturated Pressure Measurements of trans-1-Chloro-3, 3, 3-trifluoroprop-1-ene (R1233zd (E))". In: *Journal of Chemical & Engineering Data* 62.9 (2017), pp. 2496–2500 (cit. on p. 31).

[134] Katsuyuki Tanaka, Ryo Akasaka, Eiichi Sakaue, Junichi Ishikawa, and Konstantinos Kostas Kontomaris. "Thermodynamic properties of cis-1, 1, 1, 4, 4, 4-hexafluoro-2-butene (HFO-1336mzz (Z)): measurements of the pρT property and determinations of vapor pressures, saturated liquid and vapor densities, and critical parameters". In: *Journal of Chemical & Engineering Data* 61.7 (2016), pp. 2467–2473 (cit. on p. 31).

[135] Katsuyuki Tanaka, Junichi Ishikawa, and Konstantinos Kostas Kontomaris. "Thermodynamic properties of HFO-1336mzz (E)(trans-1, 1, 1, 4, 4, 4-hexafluoro-2-butene) at saturation conditions". In: *International Journal of Refrigeration* 82 (2017), pp. 283–287 (cit. on p. 31).

[136] Yi-Dong Fu, Li-Zhong Han, and Ming-Shan Zhu. "PVT properties, vapor pressures and critical parameters of HFC-32". In: *Fluid Phase Equilibria* 111.2 (1995), pp. 273–286 (cit. on p. 32).

[137] PF Malbrunot, PA Meunier, Georges M Scatena, Whitney H Mears, Kevin Paul Murphy, and Joseph V Sinka. "Pressure-volume-temperature behavior of difluoromethane". In: *Journal of Chemical & Engineering Data* 13.1 (1968), pp. 16–21 (cit. on p. 32).

[138] Stanley I Sandler. *Chemical, biochemical, and engineering thermodynamics*. John Wiley & Sons, 2017 (cit. on p. 35).

[139] Giovanni Di Nicola, Gianluca Coccia, Mariano Pierantozzi, and Sebastiano Tomassetti. "Vapor-liquid equilibrium of binary systems containing low GWP refrigerants with cubic equations of state". In: *Energy Procedia* 148 (2018), pp. 1246–1253 (cit. on p. 35).

[140] G Di Nicola, G Giuliani, G Passerini, F Polonara, and R Stryjek. "Vapor–Liquid-Equilibrium (VLE) properties of R-32+ R-134a system derived from isochoric measurements". In: *Fluid phase equilibria* 153.1 (1998), pp. 143–165 (cit. on pp. 35, 39).

[141] Giovanni Di Nicola, Giuliano Giuliani, Fabio Polonara, and Roman Stryjek. "Solid- Liquid Equilibria for the CO2+ R125 and N2O+ R125 Systems: A New Apparatus". In: *Journal of Chemical & Engineering Data* 51.6 (2006), pp. 2209–2214 (cit. on pp. 35, 151, 154).

[142] Giovanni Di Nicola, Matteo Moglie, Giulio Santori, and Roman Stryjek. "Solid–Liquid Equilibria for the CO 2+ R143a and N 2 O+ R143a Systems". In: *International Journal of Thermophysics* 30.4 (2009), pp. 1155–1164 (cit. on pp. 35, 151).

[143] Iw Schröder. "Über die Abhängigkeit der Löslichkeit eines festen Körpers von seiner Schmelztemperatur". In: *Zeitschrift für Physikalische Chemie* 11.1 (1893), pp. 449–465 (cit. on pp. 36, 150, 160).

[144] John A Nelder and Roger Mead. "A simplex method for function minimization". In: *The computer journal* 7.4 (1965), pp. 308–313 (cit. on pp. 36, 44).

[145] Peng Hu, Long-Xiang Chen, Wan-Bao Zhu, Lei Jia, and Ze-Shao Chen. "Isothermal VLE measurements for the binary mixture of 2, 3, 3, 3-tetrafluoroprop-1-ene (HFO-1234yf)+ 1, 1-difluoroethane (HFC-152a)". In: *Fluid Phase Equilibria* 373 (2014), pp. 80–83 (cit. on p. 38).

[146] Peng Hu, Long-Xiang Chen, Wan-Bao Zhu, Lei Jia, and Ze-Shao Chen. "Vapor-liquid equilibria for the binary system of 2, 3, 3, 3-tetrafluoroprop-1-ene (HFO-1234yf)+ 1, 1, 1, 2, 3, 3, 3-heptafluoropropane (HFC-227ea)". In: *Fluid Phase Equilibria* 379 (2014), pp. 59–61 (cit. on p. 38).

[147] Zhi-qiang Yang, Lian-gang Kou, Sheng Han, Chen Li, Zhi-jun Hao, Wei Mao, Wei Zhang, and Jian Lu. "Vapor-liquid equilibria of 2, 3, 3, 3-tetrafluoropropene (HFO-1234yf)+ 1, 1, 1, 2, 2-pentafluoropropane (HFC-245cb) system". In: *Fluid Phase Equilibria* 427 (2016), pp. 390–393 (cit. on p. 38).

[148] Zhi-qiang Yang, Lian-gang Kou, Wei Mao, Jing Lu, Wei Zhang, and Jian Lu. "Isothermal Vapor–Liquid Equilibrium for the Binary System of 2, 3, 3, 3-Tetrafluoropropene and 2-Chloro-1, 1, 1, 2-tetrafluoropropane". In: *Journal of Chemical & Engineering Data* 60.4 (2015), pp. 1153–1156 (cit. on p. 38).

[149] Quan Zhong, Xueqiang Dong, Yanxing Zhao, Huiya Li, Haiyang Zhang, Hao Guo, and Maoqiong Gong. "Measurements of isothermal vapour–liquid equilibrium for the 2, 3, 3, 3-tetrafluoroprop-1-ene+ propane system at temperatures from 253.150 to 293.150 K". In: *International Journal of Refrigeration* 81 (2017), pp. 26–32 (cit. on p. 38).

[150] Peng Hu, Long-Xiang Chen, and Ze-Shao Chen. "Vapor–liquid equilibria for binary system of 2, 3, 3, 3-tetrafluoroprop-1-ene (HFO-1234yf)+ isobutane (HC-600a)". In: *Fluid Phase Equilibria* 365 (2014), pp. 1–4 (cit. on pp. 38, 87, 88).

[151] Xueqiang Dong, Maoqiong Gong, Jun Shen, and Jianfeng Wu. "Experimental measurement of vapor–liquid equilibrium for (trans-1, 3, 3, 3-tetrafluoropropene (R1234ze (E))+ propane (R290))". In: *International journal of refrigeration* 34.5 (2011), pp. 1238–1243 (cit. on p. 38).

[152] Xueqiang Dong, Maoqiong Gong, Jun Shen, and Jianfeng Wu. "Vapor–liquid equilibria of the trans-1, 3, 3, 3-tetrafluoropropene (R1234ze (E))+ isobutane (R600a) system at various temperatures from (258.150 to 288.150) K". In: *Journal of Chemical & Engineering Data* 57.2 (2011), pp. 541–544 (cit. on pp. 38, 87, 88).

[153] Takumi Kamiaka, Chaobin Dang, and Eiji Hihara. "Vapor-liquid equilibrium measurements for binary mixtures of R1234yf with R32, R125, and R134a". In: *International Journal of Refrigeration* 36.3 (2013), pp. 965–971 (cit. on pp. 38, 87, 88, 115, 122).

[154] Xueqiang Dong, Hao Guo, Maoqiong Gong, Zhi Yang, and Jianfeng Wu. "Measurements of isothermal (vapour+ liquid) equilibria data for {1, 1, 2, 2-Tetrafluoroethane (R134)+ trans-1, 3, 3, 3-tetrafluoropropene (R1234ze (E))} at T=(258.150 to 288.150) K". In: *The Journal of Chemical Thermodynamics* 60 (2013), pp. 25–28 (cit. on p. 38).

[155] Xuedong Zhang, Xueqiang Dong, Hao Guo, Yanxing Zhao, Haiyang Zhang, Maoqiong Gong, and Jun Shen. "Measurements of isothermal (vapour+ liquid) equilibrium for the 1, 1, 2, 2-1, 1, 2, 2-tetrafluoroethane (R134)+ cis-1, 3, 3, 3-tetrafluoropropene (R1234ze (Z)) system at temperatures from (303.150 to 343.150) K". In: *The Journal of Chemical Thermodynamics* 111 (2017), pp. 20–26 (cit. on p. 38).

[156] Hao Guo, Maoqiong Gong, Xueqiang Dong, and Jianfeng Wu. "(Vapour+ liquid) equilibrium data for the binary system of {trifluoroiodomethane (R13I1)+ trans-1, 3, 3, 3-tetrafluoropropene (R1234ze (E))} at various temperatures from (258.150 to 298.150) K". In: *The Journal of Chemical Thermodynamics* 47 (2012), pp. 397–401 (cit. on p. 38).

[157] Peng Hu, Long-Xiang Chen, and Ze-Shao Chen. "Vapor–liquid equilibria for the 1, 1, 1, 2-tetrafluoroethane (HFC-134a)+ 1, 1, 1, 2, 3, 3, 3-heptafluoropropane (HFC-227ea) and 1, 1, 1-trifluoroethane (HFC-143a)+ 2, 3, 3, 3-tetrafluoroprop-1-ene (HFO-1234yf) systems". In: *Fluid Phase Equilibria* 360 (2013), pp. 293–297 (cit. on p. 38).

[158] Zhi Yang, Maoqiong Gong, Hao Guo, Xueqiang Dong, and Jianfeng Wu. "Phase equilibrium for the binary mixture of {1, 1-difluoroethane (R152a)+ trans-1, 3, 3, 3-tetrafluoropropene (R1234ze (E))} at various temperatures from 258.150 to 288.150 K". In: *Fluid Phase Equilibria* 355 (2013), pp. 99–103 (cit. on p. 38).

[159] Xiaozhen Hu, Tao Yang, Xianyang Meng, Shengshan Bi, and Jiangtao Wu. "Vapor liquid equilibrium measurements for difluoromethane (R32)+ 2, 3, 3, 3-tetrafluoroprop-1-ene (R1234yf) and fluoroethane (R161)+ 2, 3, 3, 3-tetrafluoroprop-1-ene (R1234yf)". In: *Fluid Phase Equilibria* 438 (2017), pp. 10–17 (cit. on pp. 38, 87, 88, 115, 122, 123).

[160] Long-Xiang Chen, Peng Hu, Wan-Bao Zhu, Lei Jia, and Ze-Shao Chen. "Vapor–liquid equilibria of fluoroethane (HFC-161)+ 2, 3, 3, 3-tetrafluoroprop-1-ene (HFO-1234yf)". In: *Fluid Phase Equilibria* 392 (2015), pp. 19–23 (cit. on p. 38).

[161] TM Kochenburger, D Gomse, I Tratschitt, A Zimmermann, and S Grohmann. "Vapor-liquid and vapor-liquid-liquid equilibrium measurements and correlation of the binary mixtures 2, 3, 3, 3-tetrafluoroprop-1-ene (R1234yf)+ (tetrafluoromethane (R14), trifluoromethane (R23), octafluoropropane (R218), nitrogen (R728) and argon (R740)) and ethane (R170)+ trifluoromethane (R23)". In: *Fluid Phase Equilibria* 450 (2017), pp. 13–23 (cit. on p. 38).

[162] Maoqiong Gong, Yanxing Zhao, Xueqiang Dong, Hao Guo, Jun Shen, and Jianfeng Wu. "Measurements of isothermal (vapor+ liquid) equilibrium for the (propane+ cis-1, 3, 3, 3-tetrafluoropropene) system at temperatures from (253.150 to 293.150) K". In: *The Journal of Chemical Thermodynamics* 98 (2016), pp. 319–323 (cit. on p. 38).

[163] Xiaozhen Hu, Tao Yang, Xianyang Meng, and Jiangtao Wu. "Isothermal vapor liquid equilibrium measurements for difluoromethane (R32)+ fluoroethane (R161)+ trans-1, 3, 3, 3-tetrafluoropropene (R1234ze (E)) ternary mixtures". In: *International Journal of Refrigeration* 79 (2017), pp. 49–56 (cit. on pp. 38, 87, 88, 115, 123).

[164] Xuedong Zhang, Xueqiang Dong, Hao Guo, Maoqiong Gong, Jun Shen, and Jianfeng Wu. "Measurements and correlations of isothermal (vapour+ liquid) equilibrium for the {isobutane (R600a)+ cis-1, 3, 3, 3-tetrafluoropropene (R1234ze (Z))} system at temperatures from (303.150 to 353.150) K". In: *The Journal of Chemical Thermodynamics* 103 (2016), pp. 349–354 (cit. on pp. 38, 87, 88).

[165] Yanxing Zhao, Xueqiang Dong, Quan Zhong, Huiya Li, Haiyang Zhang, Maoqiong Gong, and Jun Shen. "The experimental investigation of the vapour liquid phase equilibrium for (ammonia+ 2, 3, 3, 3-tetrafluoroprop-1-ene) system". In: *The Journal of Chemical Thermodynamics* 113 (2017), pp. 257–262 (cit. on p. 38).

[166] Georgios M Kontogeorgis and Soren Kiil. *Introduction to applied colloid and surface chemistry*. Wiley Online Library, 2016 (cit. on p. 47).

[167] Giovanni Di Nicola and Mariano Pierantozzi. "Surface tension of alcohols: a scaled equation and an artificial neural network". In: *Fluid Phase Equilibria* 389 (2015), pp. 16–27 (cit. on pp. 48, 55).

[168] Giovanni Di Nicola and Mariano Pierantozzi. "A new scaled equation to calculate the surface tension of ketones". In: *Journal of Thermal Analysis and Calorimetry* 116.1 (2014), pp. 129–134 (cit. on pp. 48, 55).

[169] Giovanni Di Nicola, Gianluca Coccia, and Mariano Pierantozzi. "A new equation for the surface tension of carboxylic acids". In: *Fluid Phase Equilibria* 417 (2016), pp. 229–236 (cit. on pp. 48, 55).

[170] Giovanni Di Nicola, Gianluca Coccia, and Mariano Pierantozzi. "Surface tension of silanes: A new equation". In: *Fluid Phase Equilibria* 418 (2016), pp. 88–93 (cit. on pp. 48, 55).

[171] Giovanni Di Nicola and Matteo Moglie. "A generalized equation for the surface tension of refrigerants". In: *International Journal of Refrigeration* 34.4 (June 2011), pp. 1098–1108 (cit. on pp. 48, 49).

[172] Hans-Georg Beyer and Hans-Paul Schwefel. "Evolution strategies–A comprehensive introduction". In: *Natural computing* 1.1 (2002), pp. 3–52 (cit. on p. 49).

[173] Isidro Cachadiña, Jianxiang Tian, and Angel Mulero. "New corresponding-states correlation model for the surface tension of refrigerants". In: *The Journal of Chemical Thermodynamics* 110 (2017), pp. 201–210 (cit. on p. 49).

[174] I Cachadiña, A Mulero, and Jianxiang Tian. "Surface tension of refrigerants: A new correlation using the boiling point as reference". In: *Fluid Phase Equilibria* 442 (2017), pp. 68–80 (cit. on pp. 49, 50).

[175] Milad Nabipour and Peyman Keshavarz. "Modeling surface tension of pure refrigerants using feed-forward back-propagation neural networks". In: *International Journal of Refrigeration* 75 (2017), pp. 217–227 (cit. on p. 50).

[176] G Heyen. "Liquid and vapor properties from a cubic equation of state". In: *2nd International Conference on Phase Equilibria and Fluid Properties in the Chemical Industry, Berlin*. 1980 (cit. on pp. 50, 71).

[177] Shahin Khosharay, Masoumeh Seyfi Mazraeno, and Farshad Varaminian. "Modeling the surface tension of refrigerant mixtures with linear gradient theory". In: *International Journal of Refrigeration* 36.8 (2013), pp. 2223–2232 (cit. on pp. 50, 64).

[178] Shahin Khosharay, Masoumeh Seyfi Mazraeno, Farshad Varaminian, and Ahmad Bagheri. "A proposed combination model for predicting surface tension and surface properties of binary refrigerant mixtures". In: *international journal of refrigeration* 40 (2014), pp. 347–361 (cit. on p. 50).

[179] Giovanni Di Nicola and Mariano Pierantozzi. "Surface tension prediction for refrigerant binary systems". In: *International Journal of Refrigeration* 36.2 (2013), pp. 562–566 (cit. on pp. 50, 56).

[180] Chieko Kondou. "Private communications". In: (2017) (cit. on pp. 51–54, 87).

[181] Chieko Kondou, Ryuichi Nagata, Noriko Nii, Shigeru Koyama, and Yukihiro Higashi. "Surface tension of low GWP refrigerants R1243zf, R1234ze (Z), and R1233zd (E)". In: *International Journal of Refrigeration* 53 (2015), pp. 80–89 (cit. on pp. 51, 53).

[182] Guanjia Zhao, Shengshan Bi, Andreas Paul Froba, and Jiangtao Wu. "Liquid viscosity and surface tension of R1234yf and R1234ze under saturation conditions by surface light scattering". In: *Journal of Chemical & Engineering Data* 59.4 (2014), pp. 1366–1371 (cit. on p. 53).

[183] Katsuyuki Tanaka and Yukihiro Higashi. "Surface tensions of trans-1, 3, 3, 3-tetrafluoropropene and trans-1, 3, 3, 3-tetrafluoropropene+ difluoromethane mixture". In: *Journal of Chemical Engineering of Japan* 46.6 (2013), pp. 371–375 (cit. on pp. 53, 54, 87).

[184] Shengshan Bi, Junwei Cui, Guanjia Zhao, and Jiangtao Wu. "Surface tension and liquid viscosity measurement for binary mixtures of R134a with R1234yf and R1234ze (E)". In: *Fluid Phase Equilibria* 414 (2016), pp. 60–64 (cit. on p. 54).

[185] Junwei Cui, Shengshan Bi, Xianyang Meng, and Jiangtao Wu. "Surface tension and liquid viscosity of R32+ R1234yf and R32+ R1234ze". In: *Journal of Chemical & Engineering Data* 61.2 (2016), pp. 950–957 (cit. on pp. 54, 87).

[186] Sigrún Andradóttir. "An overview of simulation optimization via random search". In: *Handbooks in operations research and management science* 13 (2006), pp. 617–631 (cit. on p. 55).

[187] Sydney Chapman. "XII. The kinetic theory of a gas constituted of spherically symmetrical molecules". In: *Philosophical Transactions of the Royal Society of London. Series A, Containing Papers of a Mathematical or Physical Character* 211.471-483 (1912), pp. 433–483 (cit. on p. 69).

[188] FB Pidduck. "The kinetic theory of a special type of rigid molecule". In: *Proceedings of the Royal Society of London. Series A, Containing Papers of a Mathematical and Physical Character* 101.708 (1922), pp. 101–112 (cit. on p. 69).

[189] Nikolai Valerianovich Tsederberg and Robert D Cess. *Thermal conductivity of gases and liquids*. Vol. 229. MIT press Cambridge, Massachusetts, 1965 (cit. on p. 69).

[190] Farhad Gharagheizi, Ali Eslamimanesh, Mehdi Sattari, Behnam Tirandazi, Amir H Mohammadi, and Dominique Richon. "Evaluation of thermal conductivity of gases at atmospheric pressure through a corresponding states method". In: *Industrial & Engineering Chemistry Research* 51.9 (2012), pp. 3844–3849 (cit. on p. 69).

[191] HF Weber. "The thermal conductivity of liquids". In: *Rep Phys* 22 (1886), pp. 116–122 (cit. on p. 69).

[192] MF Dick and DW McCready. "The thermal conductivities of some organic liquids". In: *Trans. ASME* 76 (1954), p. 831 (cit. on p. 69).

[193] Percy Williams Bridgman. "The thermal conductivity of liquids under pressure". In: *Proceedings of the American Academy of Arts and Sciences*. Vol. 59. 7. JSTOR. 1923, pp. 141–169 (cit. on p. 69).

[194] A Kardos. "Theorie der Wärmeleitung von Flüssigkeiten". In: *Forschung im Ingenieurwesen* 5.1 (1934), pp. 14–24 (cit. on pp. 70, 81, 84).

[195] NB Vargaftik. "Thermal conductivities of compressed gases and steam at high pressures". In: *Izv. Vses. Teplotekh. Inst, Moscow Energetics Institute* (1951) (cit. on p. 70).

[196] Byron C Sakiadis and Jesse Coates. "Studies of thermal conductivity of liquids. Part I". In: *AIChE Journal* 1.3 (1955), pp. 275–288 (cit. on p. 70).

[197] Byron C Sakiadis and Jesse Coates. "Studies of thermal conductivity of liquids: Part III". In: *AIChE Journal* 3.1 (1957), pp. 121–126 (cit. on p. 70).

[198] Giovanni Di Nicola, Gianluca Coccia, and Sebastiano Tomassetti. "A modified Kardos equation for the thermal conductivity of refrigerants". In: *Journal of Theoretical and Computational Chemistry* 17.02 (2018), p. 1850012 (cit. on p. 70).

[199] Shahin Khosharay, Khashayar Khosharay, Giovanni Di Nicola, and Mariano Pierantozzi. "Modelling investigation on the thermal conductivity of pure liquid, vapour, and supercritical refrigerants and their mixtures by using Heyen EOS". In: *Physics and Chemistry of Liquids* 56.1 (2018), pp. 124–140 (cit. on pp. 71, 81, 84).

[200] Robert C Reid, John M Prausnitz, and Bruce E Poling. "The properties of gases and liquids". In: (1987) (cit. on pp. 71, 81).

[201] WJ Scheffy and EF Johnson. "Thermal Conductivities of Liquids at High Temperatures." In: *Journal of Chemical and Engineering Data* 6.2 (1961), pp. 245–249 (cit. on pp. 71, 81, 84).

[202] Giovanni Latini and Marco Sotte. "Thermal conductivity of refrigerants in the liquid state: A comparison of estimation methods". In: *International Journal of Refrigeration* 35.5 (2012), pp. 1377–1383 (cit. on pp. 71, 81, 84).

[203] Farhad Gharagheizi, Poorandokht Ilani-Kashkouli, Mehdi Sattari, Amir H Mohammadi, Deresh Ramjugernath, and Dominique Richon. "Development of a quantitative structure–liquid thermal conductivity relationship for pure chemical compounds". In: *Fluid Phase Equilibria* 355 (2013), pp. 52–80 (cit. on pp. 71, 81).

[204] Candida Ferreira. "Gene expression programming: a new adaptive algorithm for solving problems". In: *arXiv preprint cs/0102027* (2001) (cit. on p. 71).

[205] Refrigerating American Society of Heating and Inc Air-Conditioning Engineers. *2013 ASHRAE Handbook: Fundamentals*. American Society of heating, refrigerating and air-conditioning engineers, 2013 (cit. on pp. 72, 75).

[206] Andrew J Stuper, William E Brügger, and Peter C Jurs. *Computer assisted studies of chemical structure and biological function*. Wiley New York, 1979 (cit. on pp. 72, 74).

[207] Donald W Marquardt. "An algorithm for least-squares estimation of nonlinear parameters". In: *Journal of the Society for Industrial & Applied Mathematics* 11.2 (1963), pp. 431–441 (cit. on p. 74).

[208] J Steven Brown, Gianluca Coccia, Sebastiano Tomassetti, Mariano Pierantozzi, and Giovanni Di Nicola. "Vapor Phase PνTx Measurements of Binary Blends of 2, 3, 3, 3-Tetrafluoroprop-1-ene+ Isobutane and trans-1, 3, 3, 3-Tetrafluoroprop-1-ene+ Isobutane". In: *Journal of Chemical & Engineering Data* 62.10 (2017), pp. 3577–3584 (cit. on p. 86).

[209] J Steven Brown, Gianluca Coccia, Sebastiano Tomassetti, Mariano Pierantozzi, and Giovanni Di Nicola. "Vapor Phase PvTx measurements of binary blends of trans-1-chloro-3, 3, 3-trifluoroprop-1-ene+ isobutane and cis-1, 3, 3, 3-tetrafluoroprop-1-ene+ isobutane". In: *Journal of Chemical & Engineering Data* 63.1 (2017), pp. 169–177 (cit. on p. 86).

[210] Sebastiano Tomassetti, Mariano Pierantozzi, Giovanni Di Nicola, Fabio Polonara, and J Steven Brown. "Vapor-Phase PvTx Measurements of Binary Blends of cis-1, 2, 3, 3, 3-Pentafluoroprop-1-ene+ Isobutane and 3, 3, 3-Trifluoropropene+ Isobutane". In: *Journal of Chemical & Engineering Data* 64.2 (2019), pp. 688–695 (cit. on p. 86).

[211] Sebastiano Tomassetti, Gianluca Coccia, Mariano Pierantozzi, Giovanni Di Nicola, and J Steven Brown. "Vapor phase and two-phase PvTz measurements of difluoromethane+ 2, 3, 3, 3-tetrafluoroprop-1-ene". In: *The Journal of Chemical Thermodynamics* 141 (2020), p. 105966 (cit. on p. 86).

[212] Haiyang Zhang, Huiya Li, Bo Gao, Quan Zhong, Wei Wu, Wenjing Liu, Xueqiang Dong, Maoqiong Gong, and Ercang Luo. "Gaseous densities of 2, 3, 3, 3-tetrafluoroprop-1-ene (R1234yf) and isobutane (R600a) binary system: Measurements and a preliminary Helmholtz equation of state". In: *International Journal of Refrigeration* 95 (2018), pp. 28–37 (cit. on pp. 87, 88, 128, 147).

[213] Ryo Akasaka, Katsuyuki Tanaka, and Yukihiro Higashi. "Measurements of saturated densities and critical parameters for the binary mixture of 2, 3, 3, 3-tetrafluoropropene (R-1234yf)+ difluoromethane (R-32)". In: *International Journal of Refrigeration* 36.4 (2013), pp. 1341–1346 (cit. on pp. 87, 88).

[214] Y. Kayukawa. "PVTx property measurements for the low GWP refrigerant R1234yf and its mixture". In: *In: Proceedings of the JSRAE Annual Conference. Tokyo (Paper ID: C134)*. 2011 (cit. on pp. 87, 88).

[215] Xu-Dong Cai, Nan Zhang, Long-Xiang Chen, Peng Hu, Gang Zhao, and Ming-Hou Liu. "Gaseous PvTx measurements of HFO-1234yf+ HFC-32 binary mixture by single-sinker magnetic suspension densimeter". In: *Fluid Phase Equilibria* 460 (2018), pp. 119–125 (cit. on pp. 87, 88, 128, 149).

[216] Jian Yang, Xinyue Jia, and Jiangtao Wu. "Vapor phase pvTx measurements of binary mixtures of difluoromethane (R32) and 2, 3, 3, 3-tetrafluoroprop-1-ene (R1234yf)". In: *The Journal of Chemical Thermodynamics* 134 (2019), pp. 41–51 (cit. on pp. 87, 88, 128, 149).

[217] Katsuyuki Tanaka, Kohei Takahashi, Keizo Kobayashi, and Yukihiro Higashi. "Surface tension of low GWP refrigerant mixtures". In: *5th Asian Conference on Refrigeration and Air Conditioning-Green Breeze from Asia: Frontiers of Refrigerants, Heat Transfer and System, ACRA 2010*. Japan Society of Refrigeration and Air Conditioning Engineering (JSRAE). 2010 (cit. on p. 87).

[218] Yoshiaki Arakawa, Hong-Seok Kim, Takumi Kamiaka, Chaobin Dang, and Eiji Hihara. "Thermophysical property measurement of HFO-1234yf+ HFC-32 mixtures". In: *2010 International Symposium on Next-generation Air-Conditioning and Refrigeration Technology, Tokyo, Japan*. 2010 (cit. on p. 87).

[219] Yagu Dang, Takumi Kamiaka, Chaobin Dang, and Eiji Hihara. "Liquid viscosity of low-GWP refrigerant mixtures (R32+ R1234yf) and (R125+ R1234yf)". In: *The Journal of Chemical Thermodynamics* 89 (2015), pp. 183–188 (cit. on p. 87).

[220] Yagu Dang, Hong Seok Kim, Chaobin Dang, and Eiji Hihara. "Measurement of vapor viscosity of R1234yf and its binary mixtures with R32, R125". In: *International Journal of Refrigeration* 58 (2015), pp. 131–136 (cit. on p. 87).

[221] Shigeru Koyama, Yoshimi Matsuo, S Fukuda, and R Akasaka. "Measurement of vapor-liquid equilibrium of HFO-1234ze (E)/HFC-32". In: *Proc. 2010 JSRAE Annual Conf., Kanazawa, Japan*. 2010, B111 (cit. on pp. 87, 88).

[222] Liangang Kou, Zhiqiang Yang, Xiaobo Tang, Wei Zhang, and Jian Lu. "Experimental measurements and correlation of isothermal vapor-liquid equilibria for HFC-32+ HFO-1234ze (E) and HFC-134a+ HFO-1234ze (E) binary systems". In: *The Journal of Chemical Thermodynamics* (2019) (cit. on pp. 87, 88, 115, 123).

[223] Rui Cao, Yingxia Qi, and Rishuai Chen. "pVTx properties of binary R1234ze (E)/R600a system". In: *The Journal of Chemical Thermodynamics* 111 (2017), pp. 191–198 (cit. on pp. 87, 88, 128, 148).

[224] Tao Jia, Shengshan Bi, Xiaozhen Hu, Xianyang Meng, and Jiangtao Wu. "Volumetric properties of binary mixtures of {difluoromethane (R32)+ trans-1, 3, 3, 3-tetrafluoropropene (R1234ze (E))} at temperatures from 283.15 K to 363.15 K and pressures up to 100 MPa". In: *The Journal of Chemical Thermodynamics* 101 (2016), pp. 54–63 (cit. on pp. 87, 88).

[225] K Tanaka, R Akasaka, and Y Higashi. "Measurements of density and isobaric specific heat capacity for HFO-1234ze (E)+ HFC-32 mixtures". In: *Trans. JSRAE* 28 (2011), pp. 427–434 (cit. on pp. 87, 88).

[226] Keizo Kobayashi, Katsuyuki Tanaka, and Yukihiro Higashi. "Measurement of PρTx properties of HFO-1234ze (E) + HFC-32 mixed refrigerant". In: *Proceedings of the Japan Society of Refrigerating and Air Conditioning Engineers*. Vol. 28. 4. Japan Society of Refrigerating and Air Conditioning Engineers, Dec. 2011, pp. 415–426 (cit. on pp. 87, 88, 128).

[227] Akio Miyara, Koutaro Tsubaki, and Nobuki Sato. "Thermal conductivity of HFO-1234ze (E)+ HFC-32 mixture". In: *International Symposium on Next-generation Air Conditioning and Refrigeration Technology*. 2010 (cit. on p. 87).

[228] Keizo Kobayashi, Katsuyuki Tanaka, and Yukihiro Higashi. "Pressure-volume-temperature relationship for HFO-1234ze (E)+ HFC-32 mixture". In: *Proc. 2010 Int. Symposium on Next-generation Air Conditioning and Refrigeration Technology* (2010) (cit. on p. 87).

[229] K Yamaya, A Matsuguchi, and N Kagawa. "Study on the isochoric specific heat capacity of a R32+ R1234ze (E) mixture in the liquid phase". In: *The 23rd IIR International Congress of Refrigeration. Prague, Czech Republic*. 2011 (cit. on p. 87).

[230] G Giuliani, S Kumar, and F Polonara. "A constant volume apparatus for vapour pressure and gas phase P-ν-T measurements: validation with data for R22 and R134a". In: *Fluid phase equilibria* 109.2 (1995), pp. 265–279 (cit. on pp. 89, 92).

[231] Giovanni Di Nicola, Fabio Polonara, Renato Ricci, and Roman Stryjek. "PVTx measurements for the R116+ CO2 and R41+ CO2 systems. New isochoric apparatus". In: *Journal of Chemical & Engineering Data* 50.2 (2005), pp. 312–318 (cit. on pp. 89, 92).

[232] JW Magee. "Molar heat capacity (CV) for saturated and compressed liquid and vapor nitrogen from 65 to 300 K at pressures to 35 MPa". In: *Journal of research of the National Institute of Standards and Technology* 96.6 (1991), p. 725 (cit. on p. 150).

[233] M Shafiur Rahman. *Food properties handbook*. CRC press, 2009 (cit. on p. 150).

[234] Arnold Weissberger. "Technique of organic chemistry". In: (1945) (cit. on p. 150).

[235] HAJ Oonk. *Measurement of Thermodynamic Properties of Multiple Phases, Experimental Thermodynamics vol VII ed RD Weir and TW de Loos*. 2005 (cit. on p. 150).

[236] Giovanni Di Nicola, Alessia Arteconi, Giorgia Nardini, and Roman Stryjek. "Solid–liquid equilibria measurements of the carbon dioxide+ 2, 3, 3, 3-tetrafluoroprop-1-ene and carbon dioxide+ trans-1, 3, 3, 3-tetrafluoropropene mixtures". In: *Fluid Phase Equilibria* 354 (2013), pp. 54–58 (cit. on pp. 150, 154).

[237] Giovanni Di Nicola, Caterina Brandoni, Cristiano Di Nicola, and Giuliano Giuliani. "Triple point measurements for alternative refrigerants". In: *Journal of thermal analysis and calorimetry* 108.2 (2011), pp. 627–631 (cit. on pp. 150, 151, 155, 156).

[238] Sebastiano Tomassetti, Gianluca Coccia, Mariano Pierantozzi, Giorgio Passerini, and Giovanni Di Nicola. "Solid–liquid equilibria for the R32+ R1234ze (E) binary system". In: *International Journal of Refrigeration* 107 (2019), pp. 128–134 (cit. on p. 150).

[239] CD Holcomb, JW Magee, JR Scott, SL Outcalt, and WM Haynes. "NIST Technical Note 1397". In: *NIST: Gaithersburg, December* (1997) (cit. on pp. 155, 156).

[240] TO Lüddecke and JW Magee. "Molar heat capacity at constant volume of difluoromethane (R32) and pentafluoroethane (R125) from the triple-point temperature to 345 K at pressures to 35 MPa". In: *International journal of thermophysics* 17.4 (1996), pp. 823–849 (cit. on pp. 155, 156, 160).

[241] Joe W Magee. "Molar heat capacity at constant volume of 1, 1-difluoroethane (R152a) and 1, 1, 1-trifluoroethane (R143a) from the triple-point temperature to 345 K at pressures to 35 MPa". In: *International journal of thermophysics* 19.5 (1998), pp. 1397–1420 (cit. on pp. 155, 156).

[242] Evald L Skau. "The Purification and Physical Properties of Organic Compounds I. The Interpretation of Time-Temperature Curves in Freezing Point Determinations and as a Criterion of Purity". In: *Proceedings of the American Academy of Arts and Sciences*. Vol. 67. 12. JSTOR. 1933, pp. 551–576 (cit. on p. 155).

[243] James S Chickos, C Marie Braton, Donald G Hesse, and Joel F Liebman. "Estimating entropies and enthalpies of fusion of organic compounds". In: *The Journal of Organic Chemistry* 56.3 (1991), pp. 927–938 (cit. on p. 160).

List of publications

Papers on International Journals

1. J. Steven Brown, Gianluca Coccia, Sebastiano Tomassetti, Mariano Pierantozzi, and Giovanni Di Nicola. "Vapor Phase PvTx Measurements of Binary Blends of 2, 3, 3, 3-Tetrafluoroprop-1-ene+ Isobutane and trans-1, 3, 3, 3-Tetrafluoroprop-1-ene+ Isobutane." In: *Journal of Chemical & Engineering Data* 62, no. 10 (2017): 3577-3584.

2. Gianluca Coccia, Giovanni Di Nicola, Mariano Pierantozzi, Sebastiano Tomassetti, and Alessia Aquilanti. "Design, manufacturing, and test of a high concentration ratio solar box cooker with multiple reflectors." In: *Solar Energy* 155 (2017): 781-792.

3. Giovanni Di Nicola, Gianluca Coccia, Mariano Pierantozzi, and Sebastiano Tomassetti. "Equations for the surface tension of low GWP halogenated alkene refrigerants and their blends." In: *International Journal of Refrigeration* 86 (2018): 410-421.

4. J. Steven Brown, Gianluca Coccia, Sebastiano Tomassetti, Mariano Pierantozzi, and Giovanni Di Nicola. "Vapor Phase PvTx measurements of binary blends of trans-1-chloro-3, 3, 3-trifluoroprop-1-ene+ isobutane and cis-1, 3, 3, 3-tetrafluoroprop-1-ene+ isobutane." In: *Journal of Chemical & Engineering Data* 63, no. 1 (2017): 169-177.

5. Giovanni Di Nicola, Mariano Pierantozzi, Sebastiano Tomassetti, and Gianluca Coccia. "Surface tension calculation from liquid viscosity data of silanes." In: *Fluid Phase Equilibria* 463 (2018): 11-17.

6. Giovanni Di Nicola, Gianluca Coccia, and Sebastiano Tomassetti. "A modified Kardos equation for the thermal conductivity of refrigerants." In: *Journal of Theoretical and Computational Chemistry* 17, no. 02 (2018): 1850012.

7. Giovanni Di Nicola, Gianluca Coccia, Mariano Pierantozzi, Sebastiano Tomassetti, and Roberta Cocci Grifoni. "Artificial neural network for the second virial coefficient of organic and inorganic compounds: An ANN for B of organic and inorganic compounds." In: *Chemical Engineering Communications* 205, no. 8 (2018): 1077-1095.

8. Gianluca Coccia, Giovanni Di Nicola, Sebastiano Tomassetti, Mariano Pierantozzi, Manila Chieruzzi, and Luigi Torre. "Experimental validation of a high-temperature solar box cooker with a solar-salt-based thermal storage unit." In: *Solar Energy* 170 (2018): 1016-1025.

9. Sebastiano Tomassetti, Mariano Pierantozzi, Giovanni Di Nicola, Fabio Polonara, and J. Steven Brown. "Vapor-Phase PvTx Measurements of Binary Blends of cis-1, 2, 3, 3, 3-Pentafluoroprop-1-ene+ Isobutane and 3, 3, 3-Trifluoropropene+ Isobutane." In: *Journal of Chemical & Engineering Data* 64, no. 2 (2019): 688-695.

10. Gianluca Coccia, Giovanni Di Nicola, Sebastiano Tomassetti, Mariano Pierantozzi, and Giorgio Passerini. "Determination of the Boyle temperature of pure gases using artificial neural networks." In: *Fluid Phase Equilibria* 493 (2019): 36-42.

11. Sebastiano Tomassetti, Gianluca Coccia, Mariano Pierantozzi, Giorgio Passerini, and Giovanni Di Nicola. "Solid-liquid equilibria for the R32+ R1234ze (E) binary system." In: *International Journal of Refrigeration* 107 (2019): 128-134.

12. Sebastiano Tomassetti, Gianluca Coccia, Mariano Pierantozzi, Giovanni Di Nicola, and J. Steven Brown. "Vapor phase and two-phase PvTz measurements of difluoromethane+ 2, 3, 3, 3-tetrafluoroprop-1-ene." In: *The Journal of Chemical Thermodynamics* 141 (2020): 105966.

13. Sebastiano Tomassetti, Giovanni Di Nicola, and Giulio Santori. "Identification of UNIQUAC binary interaction parameters in liquid-liquid equilibrium." In: *Fluid Phase Equilibria* (2020): 112483.

Conference papers

1. G. Latini, G. Di Nicola, M. Pierantozzi, G. Coccia, and S. Tomassetti. "Artificial neural network modeling of liquid thermal conductivity for alkanes, ketones and silanes." In: *Journal of Physics Conference Series*, vol. 923, no. 1. 2017.

2. G. Coccia, G. Di Nicola, S. Tomassetti, G. Gabrielli, M. Chieruzzi, and M. Pierantozzi. "Experimental characterization of a solar cooker with thermal energy storage based on solar salt." In: *Journal of Physics Conference Series*, vol. 923, no. 1, p. 012048. IOP Publishing, 2017.

3. Giovanni Di Nicola, Gianluca Coccia, and Sebastiano Tomassetti. "A modified Kardos equation for the thermal conductivity of refrigerants." In: *Journal of Theoretical and Computational Chemistry* 17, no. 02 (2018): 1850012.

4. Giovanni Di Nicola, Gianluca Coccia, Mariano Pierantozzi, and Sebastiano Tomassetti. "Vapor-liquid equilibrium of binary systems containing low GWP refrigerants with cubic equations of state." In: *Energy Procedia* 148 (2018): 1246-1253.

5. G. Di Nicola, G. Coccia, M. Pierantozzi, S. Tomassetti, and R. Stryjek. "Analysis of vapor pressure and VLE of HFOs, HCFOs, and their blends with cubic equations of state." In: *1st IIR International Conference of the Application of HFO Refrigerants, Birmingham.* 2018.